Factors determining the cytotoxic nature of pathogenic amyloid proteins

Devkee. M. Vadukul

A thesis submitted for the degree of Doctor of Philosophy

The University of Sussex

April 2018

Declaration

I declare this thesis has not been and will not be submitted in whole or in part to another University for the award of any other degree.

Signature: _____

Acknowledgements

My first ‘thank you!’ goes to my incredible supervisor, Louise. The support, guidance and reassurance I have received, has been more than I could have ever wished for. Ever since meeting you, I have been in awe of your knowledge and expertise - you are the Amyloid Queen! There are too many things to thank you for here, but I am extremely appreciative of everything you have done for me throughout my PhD, from giving me the opportunity to grow as a scientist to stepping in whenever I was totally lost. I will be forever grateful to you for this roller-coaster journey as a PhD student and feel incredibly proud to have had you as my Supervisor. Particularly, your passion to promote women in science has had a huge impact on me and is something I will never forget. The biggest thank you, of course, for providing us with cute kittens (and what seems like an unlimited supply of cake)!

Karen, a huge thank you for mentoring me day to day throughout my PhD. I hope I have made you proud! The skills I have learnt from you are invaluable and I cannot thank you enough for all the help and guidance you have given me. You are not only a mentor I look up to and respect, but one my closest friends and I look forward to all our future adventures- from camping to I Love Techno festivals, I’m in!

To Luca (Panda), Saskia, Ana, Mahmoud and Youssra- you have made our group the best group to work with. Your willingness to help and friendship have meant the world to me. Kate, thank you for being you and always being there to point out my unreasonable moments. You have kept me sane! I will miss you all very much.

I would also like to thank Julian Thorpe, Roger Philips and Pascale Schellenberger for their help with microscopy, as well as project students Oyinkan and Astrid who were a pleasure to work with.

Finally, a huge thank you to my family for their support, patience and excellent cooking. Ba, Ma and Papa thank you for trying to fatten me up, my love to you all. Ma and Papa, your attempts to try and understand what I do, which is a world away from your professions, has been hugely entertaining and appreciated. Tori, I am sorry I made you read my thesis a hundred times, but I guess that is part of your job as my sister and best friend. Sam, there are too many things to thank you for, but I could not

have asked for a more understanding and supportive partner in crime, my love to you too. Lastly, to my Didi (Nina Rajarani, MBE), you are an inspirational role model for women and your support and love have meant everything to me.

Abbreviations

ACN	Acetonitrile
AD	Alzheimer's disease
AFM	Atomic Force Microscopy
APP	Amyloid Precursor Protein
Aβ	β-amyloid
Aβ40	β-amyloid 1-40
Aβ42	β-amyloid 1-42
Aβ42-1	β-amyloid 42-1 (reversed sequence)
AβF	Fibrillar β-amyloid 1-42
AβO	Oligomeric β-amyloid 1-42
AβS	β-amyloid scrambled
AβSon	Sonicated Fibrillar β-amyloid 1-42
BACE	β-Site Amyloid Precursor Protein Cleaving Enzyme
BBB	Blood Brain Barrier
CD	Circular Dichroism
Cryo-EM	Cryo-Electron Microscopy
CTF	C-Terminal Fragment
DIC	Differential Interference Contrast
DMSO	Dimethyl Sulfoxide
F9	FEFKFEFKK
FTIR	Fourier-Transform Infrared
HFIP	1,1,1,3,3,3-Hexafluoro-2-propanol
hIAPP	Human Islet Amyloid Polypeptide
HSP	Heat Shock Protein
kDa	kilodalton
LD	Linear Dichroism
NMR	Nuclear Magnetic Resonance

SDS PAGE	Sodium Dodecyl Sulphate Polyacrylamide Gel Electrophoresis
SEM	Scanning Electron Microscopy
SPR	SURFACE PLASMON RESONANCE
ssNMR	Solid State Nuclear Magnetic Resonance
TEM	Transmission Electron Microscopy
TFA	Trifluoroacetic Acid
ThT	Thioflavin T
UPS	Ubiquitin-Proteasome System
UV	Ultra-Violet
vAβ42	Variant β-amyloid 1-42 (F19S and G37D substitutions)
XRFD	X-Ray Fibre Diffraction

List of Figures

List of Tables

Abstract

Amyloid proteins feature in neurodegenerative diseases and functionally throughout many organisms. Furthermore, due to their structural properties, amyloid proteins have been developed as materials in biotechnology. This raises the question of what makes disease-related amyloid proteins toxic. β-amyloid 1-42 (Aβ42) is a self-assembling protein that goes through many structural changes before forming the extracellular plaques characteristic of Alzheimer's disease. We have studied the conformational changes of the Aβ42 peptide over time by combining a range of biophysical approaches including circular dichroism, and Thioflavin T fluorescence with Transmission Electron Microscopy. Aβ42 assembly is compared to a novel, rationally-designed, assembly- resistant Aβ42 peptide variant (vAβ42), as well as the two main Aβ42 controls, Aβ reversed (Aβ42-1) and Aβ scrambled (AβS). The vAβ42 differs in sequence by only two amino acids, however, does not self-assemble or form β-sheet structures, unlike Aβ42-1 and AβS which both display a high propensity to form amyloid. All three variants of Aβ42 were non-toxic in primary hippocampal cultures, highlighting the importance of primary sequence in determining the toxic nature of an amyloid protein. Furthermore, the structure and toxicity of the naturally functional amyloid protein, GNNQQNY, and the designed functional amyloid peptide, FEFKFEFKK (F9), have also been characterised. These show immediate assembly into mature fibrils, do not form intermediary species and are not cytotoxic. Together, this data suggests the ability to form oligomers and the time spent in this conformation is a requirement of amyloid toxicity. To further investigate the link between size, conformation and toxicity, we compared the cytotoxicity and internalisation of oligomeric, fibrillar and sonicated fibres of Aβ42 in primary hippocampal neurons using immunolabelling and live cell imaging. As expected, the oligomeric Aβ42 was highly neurotoxic in hippocampal cultures, however fibrillar and sonicated fibrils did not have the same effect. Finally, the necessity of internalisation in mediating cytotoxicity was investigated and showed a certain threshold of intracellular accumulation must be met to induce cytotoxicity. Overall, our data suggests primary sequence, the resultant self-assembly and intermediary species formed, and intracellular accumulation are vital in determining the pathogenic properties of amyloid proteins.

Table of Contents

Chapter 1: Introduction

1.1 Protein Folding, Chaperones and Proteostasis

1.1.1 Folding and misfolding

The way in which genetic information has been described to 'flow' from DNA to RNA and gene encoded proteins has been known for almost 60 years and is now referred to as the central dogma of molecular biology (Crick, 1970; Crick, 1958). It was already known by this time that amino acids condense into long polypeptide chains formed by covalent links whilst being translated on the ribosome. Crick proposed that subsequent folding is simply a result of the order of the amino acids. More in depth structural work by Pauling and Corey revealed the three-dimensional structure formed from the folding of these polypeptide chains was vital in the ability of the protein to perform its function. The three-dimensional shape is formed via α-helices and β-sheet secondary structures which are metastable (Pauling et al., 1951; Pauling & Corey, 1951). In 1961, Anfinsen and colleagues reported that bovine pancreatic ribonuclease could be reduced to an unfolded, randomly coiled polypeptide chain made up of eight cysteine residues, which under optimal conditions could completely reform the disulphide bonds. This led to the conclusion, supporting Crick, that information of the native secondary and tertiary structure is contained within the amino acid sequence itself (Anfinsen et al., 1961) and no external factors are required. Furthermore, Anfinsen suggested the idea that the final fold of the protein would be one that was the most thermodynamically stable. This is known as the thermodynamic hypothesis (Anfinsen, 1973).

In 1968, Levinthal put forward that there were simply far too many structural options for a protein to search for within a short time frame and that the folding process must be directed. This has become known as Levinthal's paradox and although he stated it would be logical to suggest the protein would fold to a final state of lowest free energy and highest stability, this is not always the case. The paradox has since been addressed and it has been established that the folding process does not require a number of fixed steps of specific partially folded states, but instead an unpredictable search of the conformations available to the polypeptide backbone. As there are various conformations reached by

partially folded proteins, different residues within the primary amino acid sequence can interact. Of importance, due to native interactions between the amino acids being more stable than the non-native interactions, only a very small number of conformational possibilities are explored before the correct one is reached. This concept is known as the 'new view' of protein folding which also ventures into the idea of energy landscapes and funnels. These have been used to describe the free energy for the polypeptide backbone and its conformational properties; as the polypeptide gets closer to reaching its natively folded state, there are fewer conformational possibilities. Essentially, this means that there is a decrease in the degree of disorder and entropy as the folding of the protein progresses (Hartl & Hayer-Hartl, 2009).

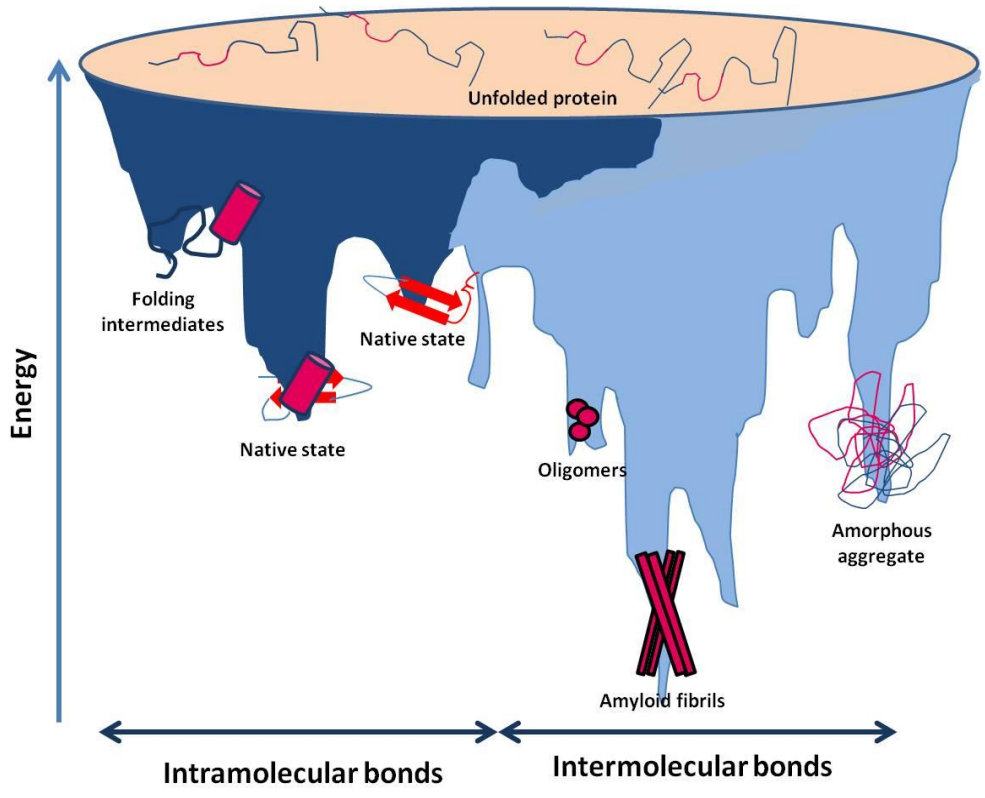

Figure 1.1. Energy landscape of protein folding and misfolding. The left hand sided (dark blue) shows the conformations 'funnelling' to the native state via intramolecular bonds. The right hand side (light blue) shows the conformations leading to amyloid fibrils via intermolecular bonds. Adapted from (Hartl & Hayer-Hartl, 2009)

As proteins are in a dynamic equilibrium between unfolded and partially folded states, and there being more than one route to reaching the native state, the energy landscape has unsystematic fluctuations as various conformations are sampled. As well as folding into their native states, proteins can also misfold. This misfolding results in the protein adopting a non-native state and can be due to a number of factors (e.g. pH, temperature). Figure 1.1 is a representation of the energy funnel of protein folding and misfolding.

The aggregates formed during misfolding will be discussed in detail in the 'Amyloid proteins' sections. Briefly, proteins can misfold and adopt a specific structure termed amyloid. This is a highly ordered and stable structure made from polymeric assemblies of normally soluble proteins. Amyloid proteins form rod-like fibrils which display a characteristic cross-β structure pattern by X-ray fibre diffraction (Serpell, 2000). Intermediary species formed on the way to these fibrils include oligomers and protofibrils (Eliezer, 2012).

It is thought that protein folding is a product of nucleation-condensation where a small number of essential residues form a 'folding nucleus' and the remainder of the structure can then condense around this (Nolting et al., 1997). This has been the conclusion drawn from many studies exploring mechanisms by which proteins fold; there is first the collapse of the hydrophobic regions into the centre of the molecule which then leads to the formation of stable secondary structures. These regions can then guide subsequent folding leading to a three-dimensional structure stabilised by covalent bonds. The process of folding is rate limited by intermediates with a strong secondary structure but lack a defined tertiary structure. These motifs are formed during the later stages of folding where intermediates are in equilibrium with fully unfolded proteins and can only very slowly be converted to their native conformation (Gething & Sambrook, 1992).

Although in vitro studies have provided fundamental understandings of protein folding, in vivo, the process of protein folding is more complicated. In vivo assays developed to monitor the formation of disulphide bonds in secretory proteins as a measure of protein folding, found that these disulphide bonds can begin to form before the synthesis of the polypeptide chain is fully complete. This suggests

that disulphide bond formation occurs at a faster rate than can be achieved in vitro and the folding is occurring in a more favourable condition (Freedman et al., 1984). As the folding of proteins in cells is a highly controlled process, it is not surprising that a number of molecular chaperones work together to ensure various stages of folding are completed successfully. These chaperones do not speed up the process of folding but rather increase the efficiency by which it occurs; for example by protecting exposed regions of partially folded proteins against inappropriate interactions in the highly crowded environment of the cell (Ellis, 2001). There are also folding enzymes present in the cell which catalyse the formation of disulphide bonds or proline *cis-trans* isomerisation (Braakman & Hebert, 2013). Peptidylprolyl isomerases are important examples of catalysts increasing the rate of isomerisation involving proline residues (Dobson, 2004).

1.1.2 Molecular chaperones and proteostasis

Molecular chaperones have a key role in ensuring that proteins do not misfold; increased levels of these chaperones have been detected during cell stress (Jolly & Morimoto, 2000), highlighting their importance. A molecular chaperone is defined as any protein involved in interacting or stabilising another protein in order to reach its functionally active conformation (Hartl et al., 2011). Molecular chaperones are often referred to as stress proteins or heat shock proteins (HSP) which are categorised according to size (e.g. HSP70, HSP90 etc). These proteins facilitate protein folding via ATP- and cofactor-regulated binding release cycles (Hartl et al., 2011). There is also a 'quality control' mechanism involving a number of glycosylation and deglycosylation steps in the endoplasmic reticulum to prevent proteins from misfolding. Finally, folded and unfolded proteins can be recognised and targeted for degradation by the ubiquitin-proteasome system (UPS) pathway (Kaufman, 2002). These numerous pathways of ensuring correct protein folding maintains the optimal homeostasis within a cell and is known as proteostasis. This is shown in Figure 1.2 where chaperone pathways, UPS system and autophagy, an intracellular degradation system (Mizushima, 2007), are integrated into a proteostasis network (Hartl et al., 2011).

Despite the process of protein folding in cells being highly controlled and efficient there is a possibility of proteins folding into a non-native state, giving rise to what are known as protein misfolding diseases.

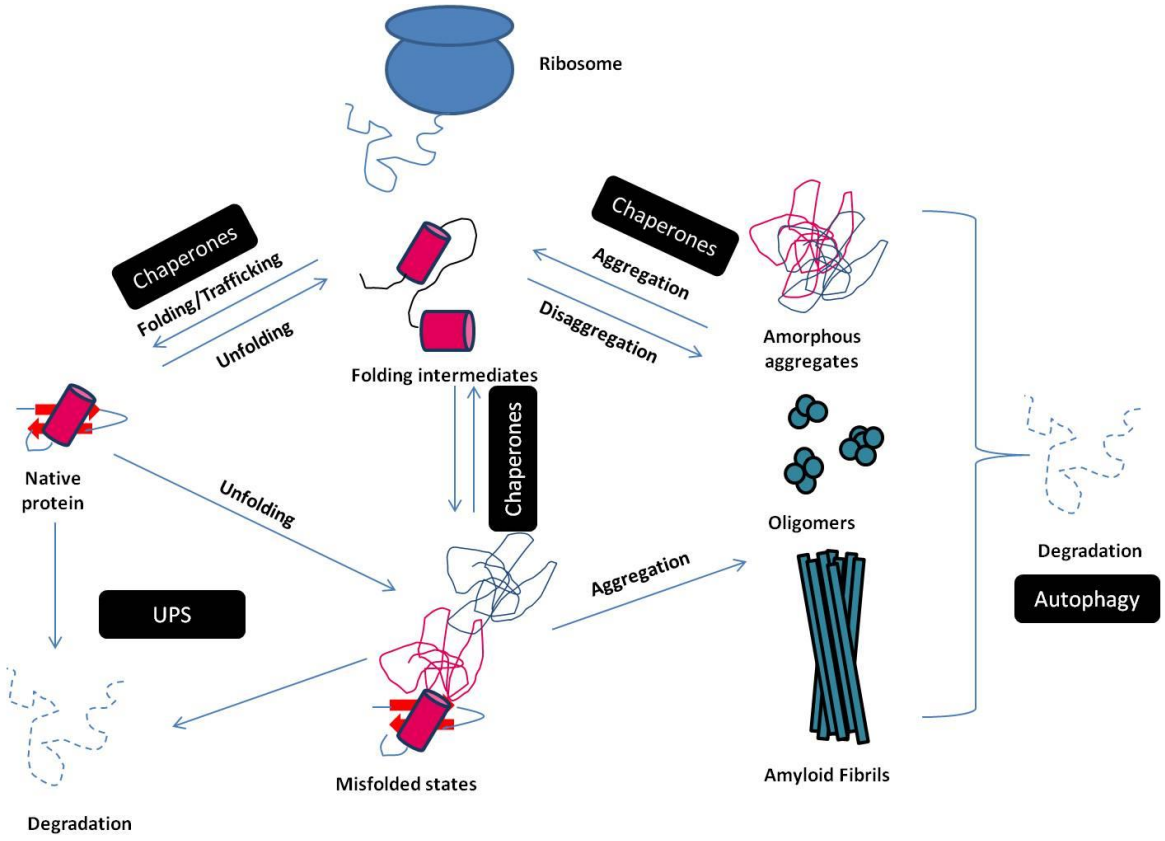

Figure 1.2. Proteostasis network. This is the integration of chaperones involved in the folding of new proteins and the remodelling of misfolded protein states and disaggregation. The UPS and autophagy systems are responsible for protein degradation. Adapted from Hartl and Hayer-Hartl, 2011.

The pathological hallmarks of several of these diseases involves the deposition of insoluble amyloid fibrils which are formed from proteins that would under normal conditions be soluble. It had been thought for many years that only a select few proteins with sequence specific motifs for the amyloid core could form these fibrils. However, it is now clear that the ability to form amyloid it is most likely a generic feature common to all polypeptide chains (Chiti et al., 1999) and under the right conditions, almost all proteins can form amyloid (Dobson, 2003).

As all amyloid fibrils share very similar morphology, despite having different precursor peptide or proteins, it is thought that the formation of amyloid fibrils is driven by the destabilisation of the native structure into a partially unfolded conformation. This may allow for interactions that would otherwise not be possible in the tightly packed tertiary structure of the protein. Intrinsically disordered proteins, which are natively unfolded (e.g. alpha-synuclein), are thought to fibrillise by first stabilising a partially folded conformation. It can therefore be argued that the structural transition of a natively folded protein into amyloid fibrils requires a partially folded conformation as a prerequisite (Uversky & Fink, 2004). As partially and unfolded proteins often exist in equilibrium with the native state under normal physiological condition, this could act as a pool of proteins that can facilitate the misfolding of proteins into amyloid (Soldi et al., 2005). As with proteins in their native state, there are many interactions that govern the formation of amyloid. These include hydrophobic, aromatic and electrostatic interactions as well as hydrogen bonding (Marshall et al., 2011). Unlike the native state where hydrophobic regions are buried within the folded protein, in misfolded proteins these are often exposed, leading to aggregation (Hartl & Hayer-Hartl, 2009) and formation of amyloid fibrils. The core of amyloid fibrils are stabilised by interactions with the main polypeptide backbone chain and as this main chain is common to all polypeptides, it is not surprising that the morphology of fibrils formed from varying amino acids are so similar (Dobson, 2004). Furthermore, these amyloid fibrils are thought to be kinetically trapped and at the lowest energy conformation (Chiti & Dobson, 2006).

In the last 20 years, advances have been made in understanding the folding process of proteins of differing sizes; small proteins (less than 100 amino acids) fold in a cooperative two state transition where only the native and denatured states are highly populated, and larger proteins (with more than 100 amino acids) fold via intermediate states that can act as stepping stones to the native state (Brockwell & Radford, 2007). It is interesting that many misfolded proteins form intermediates such as oligomers in the assembly process to amyloid fibrils, similar to those seen in native state folding (Jahn & Radford, 2005).

The mechanisms of protein folding and misfolding has been important in helping us understand basic cellular functioning as well as a providing an insight into how dysregulation of this can lead to

disease-related misfolded proteins. It has also provided a new therapeutic approach in these diseases; facilitating the folding of proteins to their native state (targeting molecular chaperones for example) could reduce the number of misfolded proteins to either slow or stop the progression of disease pathology (Cohen & Kelly, 2003).

1.2 Amyloid proteins

1.2.1 Structure and definition

The term amyloid, derived from the Latin *amylum* meaning starch, was first coined in 1854 by Rudolph Virchow to describe the lardaceous waxy deposits in brain tissue that exhibited positive staining following addition of iodine and sulphuric acid (Riek & Eisenberg, 2016). From this observation, Virchow concluded these inclusions to be primarily composed of carbohydrates. It was Friedreich and Kekule that later, in 1959, demonstrated the high nitrogen content of these amyloid deposits and began to think of these as proteins rather than carbohydrates. They concluded that the positive staining of iodine seen by Virchow was due to proteoglycans (Sipe & Cohen, 2000).

In 1959 Cohen and Clakins showed that amyloid was fibrillar in structure by transmission electron microscopy (TEM) (Cohen & Calkins, 1959). Our understanding of amyloid structure has since greatly evolved with advancing technology. Tinctorial properties of amyloid proteins, suggestive of a fibrillary structure, includes the specific binding to Congo Red (Puchtler & Sweat, 1965) which produces an apple green birefringence when visualised between cross polarisers using a light microscope (Rambaran & Serpell, 2008). Fluorescence in the presence of Thioflavin T (ThT) dye is also characteristic of amyloid proteins and suggests fibrillogenesis (Vassar & Culling, 1959). Low atomic resolution techniques including electron microscopy (EM) and atomic force microscopy (AFM) have revealed amyloid fibres to be generally between 60-120Å long, often twisted and unbranched (Petkova et al., 2006; Rambaran & Serpell, 2008; Sumner Makin & Serpell, 2004).

As amyloid proteins are inherently ordered and highly repetitive, it is possible to use X-ray fibre diffraction (XRFD) in order to gain insight into the molecular structure. XRFD reveals a cross-β pattern arising from hydrogen-bonded β-strands running perpendicular to the fibre axis and forming

β-sheet ribbons which extend along the fibre axis (Morris & Serpell, 2012). This gives rise to two characteristic diffraction signals; a sharp reflection on the meridian at 4.7-4.8 Å and a signal on the equator at approximately 10Å (Jahn et al., 2010). This pattern was first pioneered by William Astbury who obtained a XRFD pattern from a poached egg white.

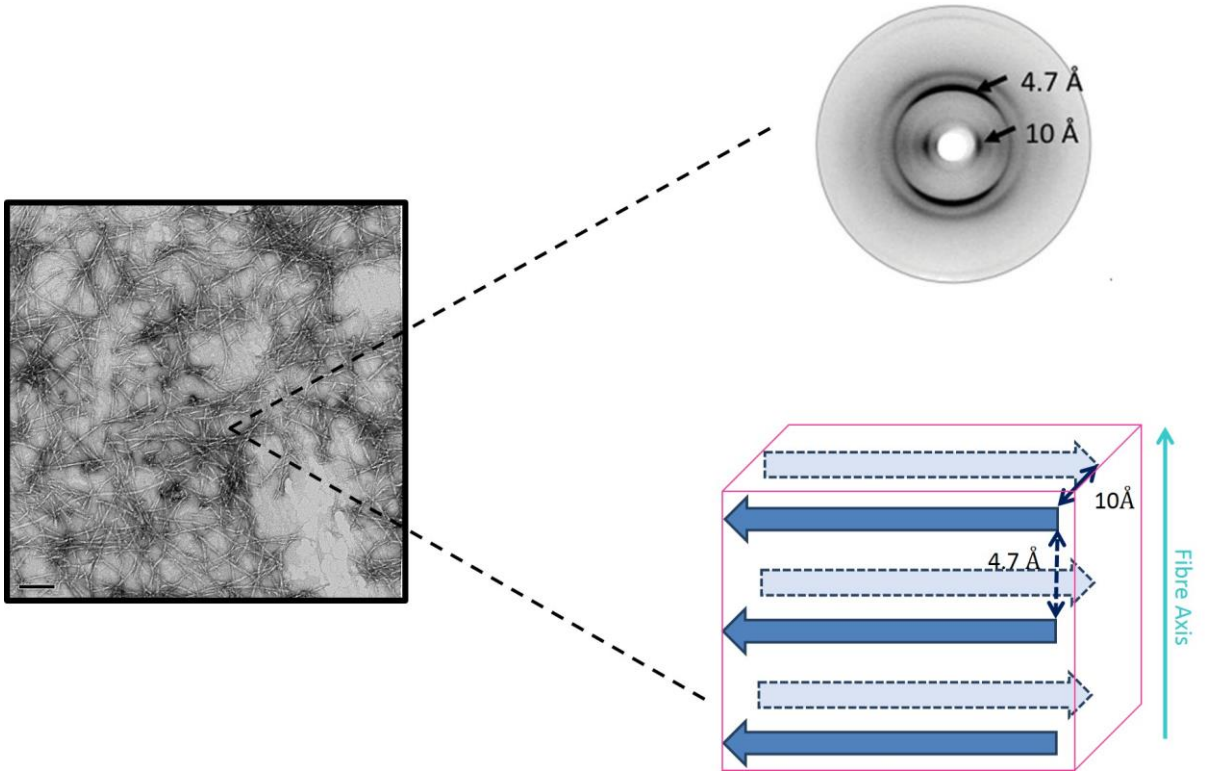

Figure 1. 3. Cross-β structure of Aβ42 fibrils (50μM incubated for 3 days, prepared in 20mM phosphate buffer pH 7.4) Scale bar shown at 0.5μm. X-ray Fibre diffraction pattern taken from (Serpell et al., 1999). The fibres display a sharp reflection on the meridian at 4.7-4.8 Å and a signal on the equator at approximately 10Å characteristic of amyloid proteins.

This cross-β structure is common to both disease-related and functional amyloids and is responsible for the highly stable nature of amyloid proteins (Figure 1.3).

Cryo-electron microscopy (cryo-EM) and single particle processing of amyloid fibres have also revealed that a single mature fibre is composed of protofilament subunits. For example, fibrils made up of the SH3 domain of phosphatidylinositol-3'-kinase, are comprised of four protofilaments around the central core (Fowler et al., 2006). The number, orientation and substructure of protofilaments respective to the central core can differ within the same precursor protein (Fandrich et al., 2009)

giving rise to a number of structures formed by one protein. This is known as amyloid polymorphism and has been shown in a number amyloidogenic proteins using techniques including cryo-EM, AFM and solid state nuclear magnetic resonance (ssNMR). One example is the 20-29 fragment and amyloidogenic core of the 37aa human islet amyloid polypeptide (hIAPP) known as amylin. ssNMR has revealed amylin can simultaneously assemble into two categories of fibres distinguishable by the alignment of the β-strands in either an anti-parallel or parallel configuration (Madine et al., 2008). It has been suggested that the number and orientation of the protofilaments within an amyloid fibre is guided by the packing of the regions of the polypeptide chain that are not involved with the formation of the cross-β core. A non- disease related example is the Pme117 repeat domain of melanosomes which act as templates for the deposition of melanin. Pme117 is polymorphic suggesting functionality does not necessarily mean one unique structure (Hu et al., 2011).

The cross-β sheet motif is made up of two tightly packed repetitive β-sheets adhered by interdigitation of the side chains; this is known as the 'steric zipper' (Nelson et al., 2005). Cross-β structures can be separated into various categories dependent on the orientation and surface interactions of these β-sheets; they can be parallel, anti-parallel, packed face-to-face or face-to-back, both sheets facing the 'up' direction or opposite 'up-down' directions. These various possibilities have given rise to eight classes of steric zippers (Sawaya et al., 2007). This structural information has been possible to uncover due to a combination of X-ray diffraction (Morris & Serpell, 2012) and advances in ssNMR where amyloid proteins containing isoptically labelled amino acids are recombinantly expressed and once fibrils are formed, resonances can be detected.

In a parallel arrangement of β-sheets, the strands can be either in-register or out-of-register. In most amyloid proteins, including β-amyloid (Aβ), the β-strands are generally in register (Landreh et al., 2016). In-register β-sheets are stacked directly on top of each other, forming hydrogen bonds to adjacent strands. In an out-of-register arrangement, β-strands either wrap around an axis to form a β-helix or a β-sandwich (Wasmer et al., 2008).

One way in which the cross-β structure provides such stability, is through the parallel N-H· · ·O=C hydrogen bonds formed between the backbone amide groups. These point up and down the β-sheets due to the polar nature of the hydrogen bonds (Riek & Eisenberg, 2016). These hydrogen bonds polarise one another and as a result, reach a cooperative energy of formation (Tsemekhman et al., 2007). van der Waals forces, increase in entropy from the release of water molecules (Gazit, 2002) and interactions between the side chains also all contribute to the stability of the fibrils. For example, the aromatic side chain Tyr, associates with the β-sheets via π-π stacking (Marshall & Serpell, 2009). It has been suggested that this π -stacking is largely driven by entropy; as ordered water molecules are released from the aromatic rings during intermolecular interactions, the overall entropy of the thermodynamic structure is increased. Other side chains, including Asn, Gln and Ser, can form hydrogen bonds called ladders also adding an additional level of stability to the fibre (Kurt et al., 2017; Tsai et al., 2006).

The insolubility and heterogeneity of amyloids has meant it is extremely difficult to achieve crystallisation which would otherwise provide structural information of high atomic resolution. Additionally, the twisted architecture of amyloid fibrils further complicates this. To overcome this problem, the shortest fragments retaining the amyloidogenicity of full length proteins were sought out. This was first achieved in the Sup35 yeast prion protein with the sequence GNNQQNY and it was confirmed this domain assembled into structures meeting all criteria for an amyloid protein. Furthermore, based on the dehydrated β-sheets observed, it was suggested that amyloid forming units may be short segments of full length proteins that are exposed by partial unfolding (Balbirnie et al., 2001).

Another example of a solved amyloid crystal structure is the 99 residue β2-microglobulin, which makes up the non-covalently linked light chain of class 1 human leukocyte antigen. It is a disease-related amyloid, where the deposition of fibrils in the musculoskeletal system leads to the development of dialysis related amyloidosis. Three segments of the sequence are found to form amyloid fibrils in isolation; Ser20 to Lys41, Asp59 to Thr71, Pro72 to Met99. However in depth studies have revealed that it is the NHVTLSQ heptapeptide of the sequence that is a significant

determinant of amyloid formation (Ivanova et al., 2004) Crystallisation studies have determined this fragment to serve as a hinge loop that folds into a two stranded antiparallel β-sheet (Domanska et al., 2011). Interestingly, there have been over 80 different solved crystal structures displaying a seven-stranded β-sandwich fold that is typical to IgG superfamilies (Berman et al., 2000; Trinh et al., 2002).

There are now over 100 atomic resolution solved structures related to 15 disease associated amyloid proteins, based on short segments of the full length protein (Eisenberg & Sawaya, 2017). All presented a steric zipper structure. Although the information provided from these crystal structures have helped progress our understanding of amyloid proteins, and in some cases provide us with some insight into the misfolding mechanism, it is also limited. As no crystal structure has been solved for a fragment longer than seven residues and not the full length of proteins, it is entirely possible that the structures represent the spines of a single polymorph.

The definition of an amyloid, or the criteria required for a protein to be classified as an amyloid, is a debated topic. In 2014, it was put forward that a protein must be deposited as insoluble ridged fibrils (roughly 10nm in diameter) in the extracellular space of organs as a result of protein misfolding to be defined as an amyloid. There are however, intracellular deposits observed e.g. α-synuclein Lewy bodies (Serpell et al., 2000). Furthermore, the fibril must bind to Congo red and display green birefringence when viewed by polarised light as well as exhibit a cross-β diffraction pattern by XRFD when isolated from tissues (Sipe et al., 2014). Due to advances in solid phase protein synthesis, it is possible to use synthetic peptides that have been previously termed to be ‘amyloid-like’. Here, we will only use the term amyloid, and not amyloid-like, to describe even synthetic proteins that fit the above criteria.

1.2.2 Amyloid assembly

The ability of form amyloid fibrils under suitable conditions is conserved amongst many peptides and proteins. This is despite differences in primary sequences and has been attributed to an inherent property of the polypeptide backbone chain (Dobson, 2003). Techniques such as XRFD and NMR spectroscopy have been essential in determining the structure and morphology of mature amyloid fibrils. There has been a considerable effort made to understand the assembly process of amyloid proteins. This is especially due to the identification of the oligomeric species, which are formed on the pathway to amyloid fibrils, as being neurotoxic in many neurodegenerative diseases (Gadad et al., 2011).

The way in which proteins can misfold to form amyloid has been discussed in Protein folding and misfolding (Section 1.1.1); briefly, there is the unfolding of the native form into a partially folded state that allows for interactions that would otherwise be unable to occur due to the tightly packed three-dimensional native conformation (Uversky & Fink, 2004). The inherent flexibility of the partially unfolded intermediate is crucial in forming the core cross-β structure characteristic of amyloid. It is believed that unfolded/partially folded monomers leads first to the assembly of small nuclei which then assemble into pre-fibrillar species (protofibrils) and mature into fibres (Serpell, 2000).

The mechanism of amyloid assembly is thought to be via nucleated polymerisation (Ferrone, 1999). There is first the nucleation phase where the monomer precursor is either in an unfolded, partially folded or natively folded state and undergoes usually unfavourable self-association (Roychaudhuri et al., 2009). For amyloid formation, this nucleus has to template the bonding pattern of the fibre spine. The nuclei formed are thought to be in a pre-equilibrium with monomers and once formed, can either disassemble back into monomers or proceed to the next series of events leading fibril formation (Wetzel, 2006). The fate of the nuclei is concentration dependent; it has been suggested that at least three to four molecules of the monomeric protein must simultaneously expose their amyloidogenic regions for templating of the fibrillar structure to occur (Nelson et al., 2005). Once the critical nucleus

has been formed, there is a very rapid formation of fibrils by the addition of monomers. This is known as the elongation phase. Fibril formation in this way is known as primary nucleation. There are also, secondary nucleation pathways that also lead to the formation of fibrils. Monomers can bind to pre-formed aggregates to form a new nuclei for fibril formation (Knowles et al., 2014) in a mechanism called surface catalysed secondary nucleation (Knowles et al., 2014). This is shown by Figure 1.4.

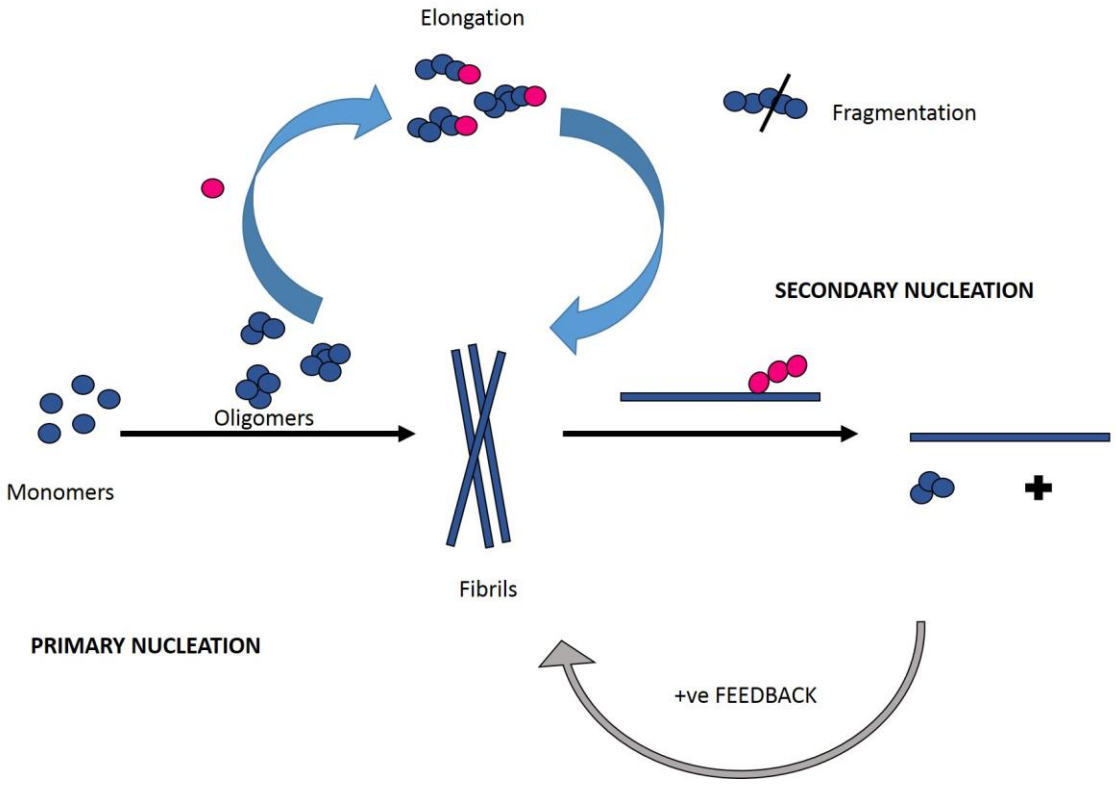

Figure 1. 4. Schematic representation of fibril formation by primary and secondary pathways. In primary nucleation, soluble monomeric forms of protein generate oligomers which have the potential to form amyloid fibrils. Secondary nucleation greatly enhances fibril formation where aggregates are able to grow by further addition of the protein. Secondary nucleation also includes fragmentation, where new fibril ends serve as elongation sites. The surface of fibrils can also facilitate fibril generation via surface catalysed nucleation.

The formation of amyloid fibrils can be monitored by ThT dye fluorescence, which displays a sigmoidal growth curve (Figure 1.5). There is a lag phase, which correlates to the time it takes to reach critical concentration of nuclei to elongate; growth phase where the conversion of peptides into amyloid fibres is at its greatest; and finally a plateau where the concentration of soluble protein for

elongation has been depleted or reached an equilibrium (Arosio et al., 2015). Addition of fragmented preformed fibrils results in the lag phase being entirely or partially bypassed, serving as evidence of secondary nucleation pathways (Xue et al., 2008).

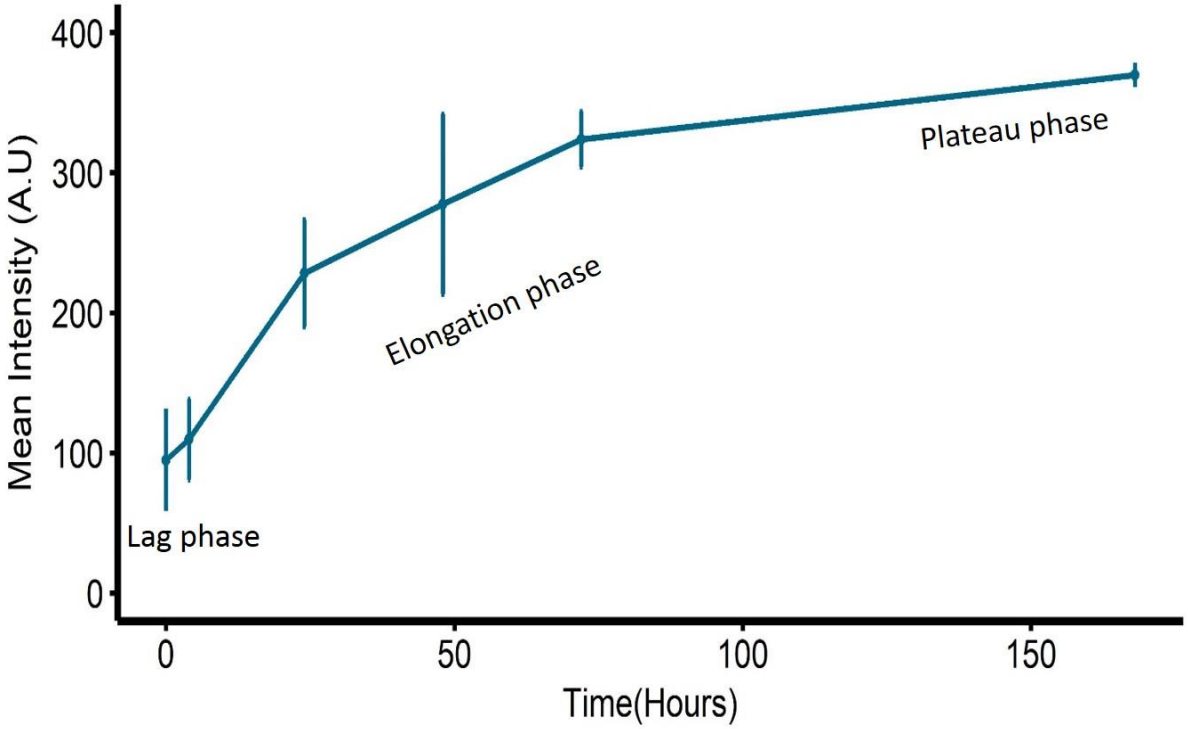

Figure 1. 5. Sigmoidal ThT aggregation curve of Aβ42 (50 µM prepared in 10mM HEPES buffer pH 7.4). In the lag phase, there is generation of nuclei which are needed for the rapid elongation phases where amyloid fibril generation is occurring. Finally, there is a plateau reached and conversion of soluble protein into insoluble amyloid fibrils has reached an equilibrium or saturated.

1.3 Disease-related amyloid proteins

1.3.1 Amyloid in disease

The deposition of amyloid fibrils in the body related to disease is known as amyloidosis. Although not all misfolded protein diseases are related to amyloid deposition, cystic fibrosis for example (Fraser-Pitt & O'Neil, 2015), there are a number of diseases that present amyloidosis. The presence of amyloid proteins in disease is not limited to one type of disease; this is seen in neurodegenerative diseases such as Alzheimer's disease (AD), Spongiform encephalopathies and Parkinson's disease, as well as non-neuropathic localised diseases such as Type II diabetes and pituitary prolactinoma.

Amyloid deposition is also seen in systemic amyloidosis. In this class of disease, amyloid is deposited in tissues as insoluble structures that can sometimes replace cells. For example, in lysozyme amyloidosis a majority of the kidney is replaced by amyloid deposits (Marshall et al., 2014).

Table 1.1 provides some examples of amyloid related diseases (Chiti & Dobson, 2006).

In vitro, it is possible for almost any native protein to misfold into amyloid under suitable conditions, although these may not be physiologically relevant (e.g. low pH or high concentrations) (Dobson, 2003). Within cells, however, there are many regulatory mechanisms that maintain correct protein folding. When there are incidences of misfolding proteins, the cell attempts to maintain normal homeostasis and prevent toxicity. For example, it has been shown that the promyelocytic leukaemia (PML) protein and the small ubiquitin-like modifier (SUMO) dependent ubiquitin ligase RNF4, bind together to identify and degrade misfolded proteins. The PML identifies misfolded proteins via a substrate recognition site which in turn conjugates the protein with SUMO ligases. The misfolded proteins are then ubiquinated by the RNF4 ligase (Guo et al., 2014). When the cell is overwhelmed by the amount of misfolded protein or can no longer sufficiently clear the accumulation of misfold protein, there is often cell death (Marshall et al., 2004).

Amyloid proteins are known to be both disease-related as well a functional; there are over 40 identified amyloidogenic proteins associated with various diseases as well as at least 12 non-pathogenic amyloid proteins that are exploited for their strength and resistance to degradation (Riek & Eisenberg, 2016). This raises the question of 'what makes an amyloid protein toxic?' In order to investigate this, the disease-related model being used is β-amyloid 1-42 (Aβ42), the deposition of which is a characteristic hallmark of Alzheimer's disease.

Disease	**Misfolded protein**	**Precursor Native structure**
Neurodegenerative disease		
Alzheimer's disease	Amyloid β	Unfolded
Parkinson's disease	α-synuclein	Unfolded
Amyotrophic lateral sclerosis	Superoxide dismutase 1 TDP 43 FUS	All-β Unfolded
#Familial British Dementia	ABri	Unfolded
Familial Danish Dementia	Adan	Unfolded
Systemic amyloidosis		
AL amyloidosis	Immunoglobulin light chains or fragments	All-β
AA amyloidosis	Serum amyloid A protein	Mostly β
Haemodialysis-related amyloidosis	β2-microglobulin	All-β
Localised diseases		
Type II diabetes	Islet amyloid polypeptide	Unfolded
Atrial amyloidosis	Atrial natriuretic factor	Unfolded
Pulmonary alveolar amyloidosis	Lung surfactant protein C	Unknown

Table 1. 1 Some human diseases associated with amyloid deposition. Adapted from Chiti and Dobson, 2006.

1.3.2 Misfolded Aβ and Alzheimer's disease: The amyloid cascade hypothesis

AD is a post developmental neurodegenerative disease characterised by a progressive decline in cognitive ability (McKhann et al., 2011). There are two broad types of AD; familial AD which approximately 5% of all cases, and sporadic AD cases which account for the remaining 95% of all AD cases (Kepp, 2017). Pathological hallmarks of the disease include extracellular plaques and intracellular neurofibrillary tangles, the components of which are Aβ and tau respectively (Hardy & Higgins, 1992). These pathological hallmarks were first identified by Alois Alzheimer over a century ago and are still used as the basis of post mortem diagnosis (Sommer, 2002).

There has been a strong correlation seen between the degree of tauopathy and cognitive decline seen in AD patients. A significant, but much weaker and inconsistent correlation is seen between the level of cognitive decline and deposition of Aβ (Wilcock & Esiri, 1982). Despite this, as Aβ was first sequenced from the meningeal blood vessels of AD and Downs's syndrome patients and was identified as the main component of neuritic plaques, this deposition was postulated to be the first pathogenic event in AD (Hardy & Selkoe, 2002). The identification and cloning of the Amyloid Precursor Protein (APP) found on chromosome 21, the trisomy of which is a causative factor for Down's syndrome (Roper & Reeves, 2006), has been instrumental in understanding the production of Aβ. There are several lengths of Aβ produced from the processing of APP, with Aβ42 identified as being the major species found in amyloid plaques deposited in AD.

Due to this, a major focus has been put on Aβ for the role it plays in AD. There are however, normal physiological roles that have been suggested for this protein when it is not misfolded. Soluble Aβ, predominantly Aβ1-40, has been reported to be involved in the modulation of synaptic function, neuronal growth and survival as well as protection against oxidative stress (Bishop & Robinson, 2004). Furthermore, clearance, transport and degradation of Aβ maintains the non-toxic, physiological Aβ concentration. It is therefore only when there is an overwhelming accumulation of misfolded protein that toxicity is induced (Marshall et al., 2004).

The last two decades have heavily focused on the Amyloid Cascade Hypothesis. This presumes Aβ deposition, particularly the oligomeric species formed on the pathway to amyloid fibrils (McLean et al., 1999), to be the causative factor of neurodegeneration.

Mutations found in the presenilin (PSEN) 1, 2 and APP genes, all of which are heavily involved in the elevated production of Aβ, have been the most compelling argument for the amyloid cascade hypothesis. Additionally, the ε4 allele of the apoplioprotein E (APOE) has been identified as strongest genetic risk factor of both early and late onset AD and is implicated in Aβ metabolism (Carter, 2005; Corder et al., 1993; Farrer et al., 1997). As a consequence of elevated Aβ production and deposition, a cascade of events is initiated, including tau pathology and synaptic dysfunction which lead to eventual neuronal loss (De Strooper & Karran, 2016)

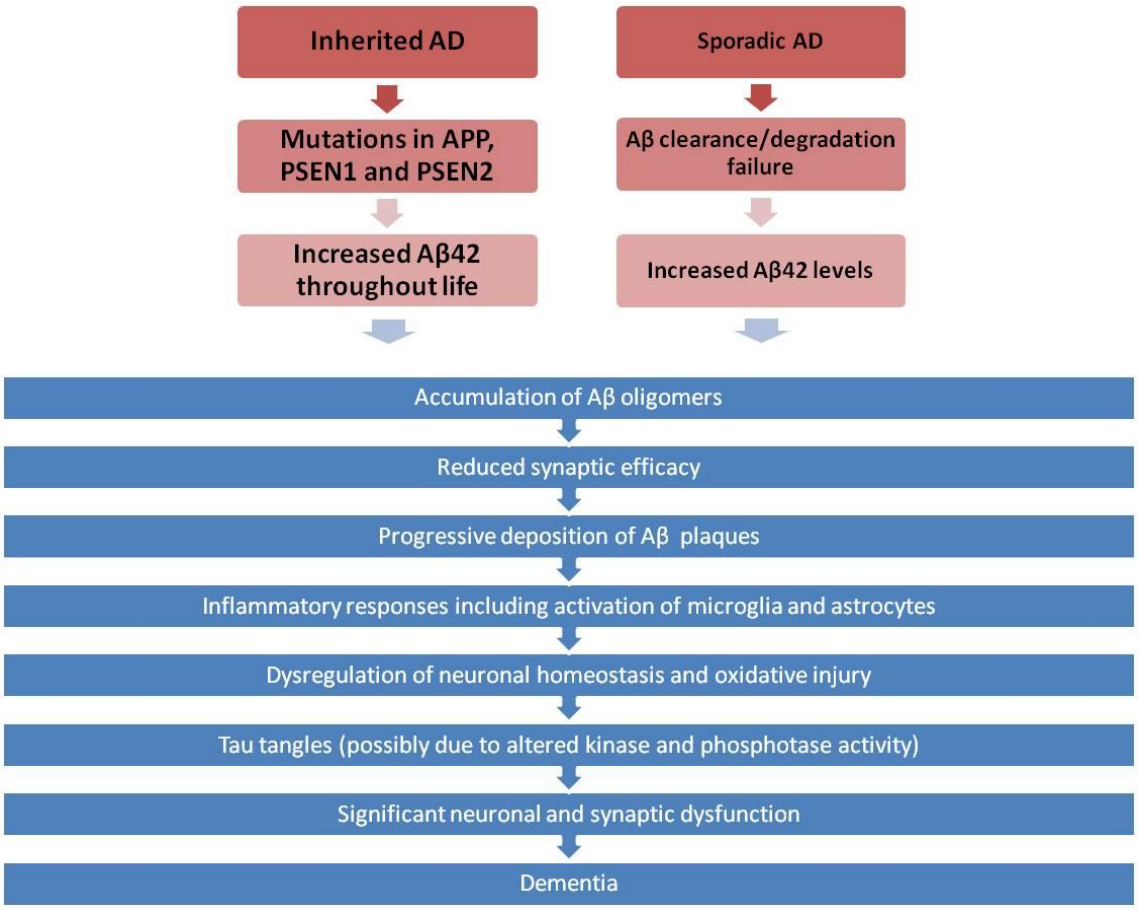

Figure 1. 6. The updated Amyloid Cascade Hypothesis which considers the importance of oligomers in neurodegeneration

There are, however, a number of arguments raised against this hypothesis which have led to questioning the importance of Aβ in AD. Figure 1.6 is a summary of the updated amyloid cascade hypothesis, trying to address some of these criticisms. Firstly, there is a low correlation seen with the amount of amyloid deposition and cognitive decline seen in AD patients. However, a strong correlation is seen with the elevated levels of soluble Aβ and the level of neurodegeneration (McLean et al., 1999). It has also been argued that the hypothesis is too neuro-centric and does not consider the other cell types that are involved in the pathogenic process. For example, it has been reported that the binding and activation of the formyl peptide receptor-like 1 (FPRL-1) receptor by Aβ could be responsible for the accumulation and activation of microglia resulting in an inflammatory response. Interestingly, the same study reported that Aβ formed a fibril forming complex with FPRL-1 following prolonged exposure and the internalisation of this complex was rapid (Cui et al., 2002). Aβ also binds to the receptor for advanced glycation end products (RAGE) which allows for transport across the blood brain barrier (BBB). The interaction of Aβ with RAGE induces oxidative stress, the activation of microglia and subsequent cell death (Chen et al., 2007; Deane et al., 2003; Yan et al., 2009).

It is becoming apparent that the linearity of the cascade is a simplification of the reality by which Aβ can facilitate eventual neuronal death. Furthermore, the cascade is quantitative, suggesting that targeting Aβ quantity should slow down or halt the progression of disease. However, therapeutic agents developed to lower the levels of Aβ produced, such as Semagacestat which is a gamma secretase inhibitor, have not been successful (Karran et al., 2011). This may be explained by the findings that mutations found in presenilin-1 component of the gamma secretase complex, do not increase the amount of Aβ produced, but promotes cleavage of APP to release longer length (>42 aa), more hydrophobic fragments. This is attributed to the destabilisation of the gamma secretase complex (Chavez-Gutierrez et al., 2012). Although the levels of shorter Aβ produced may be reduced, the production of these more amyloidogenic fragments could be a nucleation point and seed further the production of misfolded Aβ. Therefore, the mutations in AD are more related to the quality of the Aβ produced rather than the quantity (De Strooper & Karran, 2016).

Another criticism of the amyloid cascade hypothesis is the relationship between Aβ and tau. The two are found in different locations within the brain and follow a different progression in the brain, suggesting the two pathologies are independent of each other (Braak & Braak, 1995). However, it is possible that the oxidative stress caused by Aβ may initiate tau translocation and downstream deleterious events. This effect is not specific to Aβ and has also been seen to be induced by glutamate demonstrating tau can respond in this way to any oxidative stress inducing event (Alavi Naini & Soussi-Yanicostas, 2015). Furthermore, tau tangles have been found to be common in both AD and non-AD brains and are already present in early life (Braak & Del Tredici, 2011b).

Despite the controversy surrounding the amyloid cascade hypothesis, Aβ undoubtedly plays an important role in AD. The mechanisms by which Aβ leads to toxicity have been extensively studied and it is widely accepted that the oligomeric species is the primary neurotoxic culprit (McLean et al., 1999; Stroud et al., 2012; Walsh et al., 2002a). There are number of proposed mechanisms of Aβ oligomer toxicity. These include receptor mediated toxicity, cell membrane disruption related toxicity and intracellular accumulation mediated toxicity. It is likely that Aβ oligomers can mediate their effects in an array of pathways and that once downstream effects have been triggered, there is neurotoxicity.

1.3.3 An alternative to the amyloid cascade hypothesis: The three phases of AD

Recently it has been suggested that there are three phases of AD; the biochemical, cellular and clinical phase (Figure 1.7). This has been explained in depth by De Strooper and Karran (De Strooper & Karran, 2016). Briefly, during the biochemical phases there is the abnormal aggregation of Aβ, tau hyperphosphorylation and the generation of oligomeric species of both these proteins. There is also the propagation and transmission of these proteins as well as the interaction with a several other proteins and membranes leading to disruption of normal cell signalling and functioning. The order of these events is not yet understood; it is possible that impaired proteostasis leads to misfolding of proteins or vice versa. These events are not thought to be irreversible or overwhelming, however when the compensating mechanisms become chronic and irreversible (e.g. inflammatory response)

there is progression to the cellular phase. The cellular phase is extremely complex and spans over two decades which may explain the 'silent' phase of AD. It is during this phase that the compensation mechanisms become irreversible mechanisms and disrupt brain homeostasis. This phase is not specific only to neurons; a failing neurovascular system, astroglia, microglia and oligodendrocytes are all involved. When there is no longer the ability to maintain normal homeostasis in the brain, the clinical phase is initiated. These three phases are thought to be in a feedback/feedforward mechanism between cells which eventually leads to dementia (De Strooper & Karran, 2016).

This view not only provides explanations for gaps found in the amyloid cascade hypothesis, but also appreciates that there are numerous cell types that must also be involved in the pathogenic process. Although an emphasis is placed on the inflammatory response and irreversible compensatory mechanisms within the cellular phase of AD, Aβ is suggested to be the trigger for subsequent cell death in the biochemical phase.

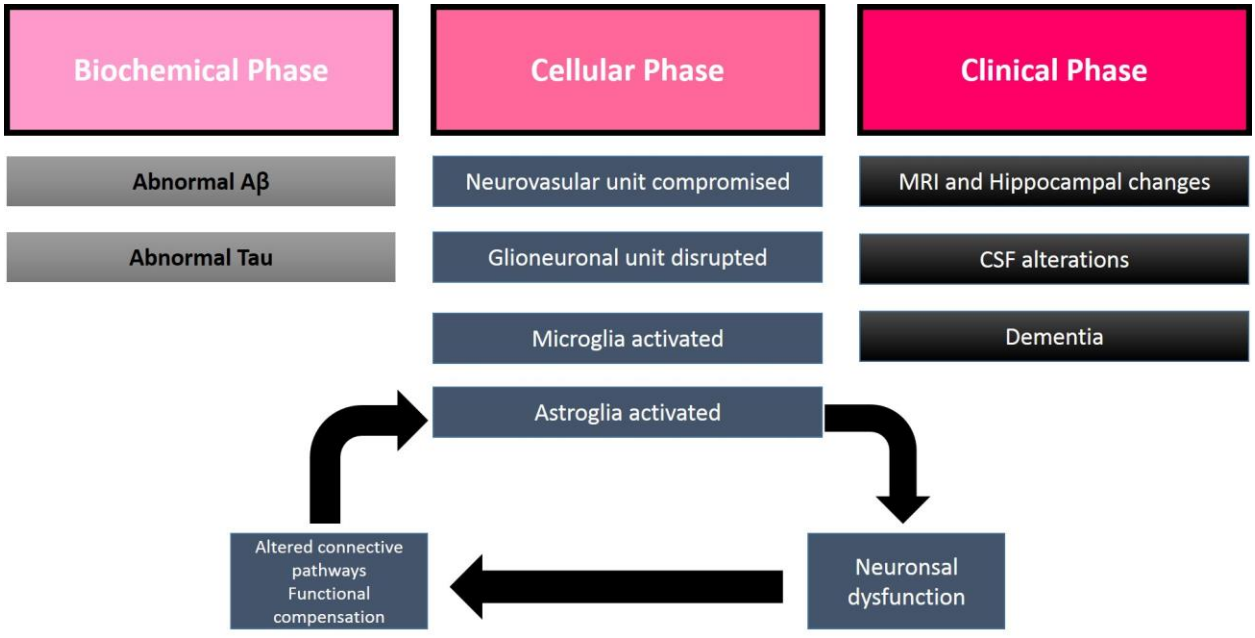

Figure 1. 7. The three phases of AD as put forward by the De Strooper group. Adapted from De Strooper & Karran, 2016

1.4 Amyloid Precursor Protein (APP) and Aβ production

1.4.1 APP structure

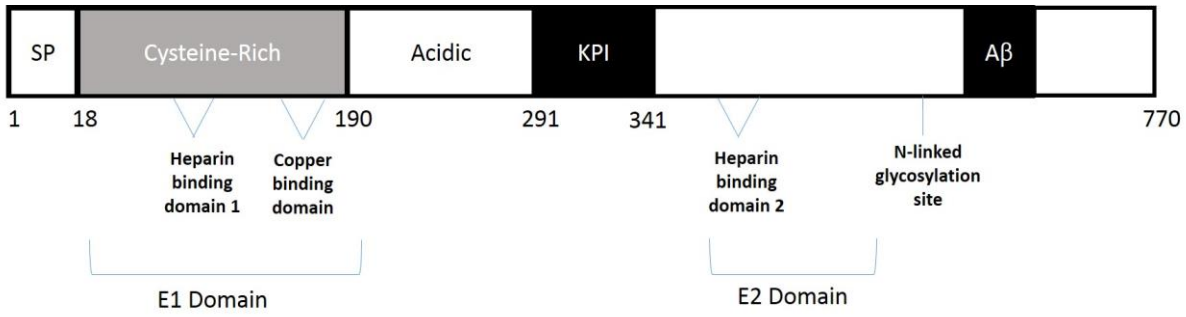

Figure 1. 8. APP structure. There is a N-terminal Signal Protein (SP) after which the E1 domain is found. This is comprised of the heparin binding domain 1 and a copper binding domain. The Kunitz protease inhibitor is found in the APP751 and APP770 only. The E2 domain also has a heparin binding domain as well as two glycosylation sites before the Aβ region.

The APP protein was first cloned and identified as the precursor to Aβ, 30 years ago (Kang et al., 1987). Located on chromosome 21, APP is a member of a family of conserved type I transmembrane proteins that also includes APP-like proteins (APLPs) 1 and 2 (Zheng & Koo, 2011). Although all three proteins share a vastly similar structure with a large extracellular domain linked via a single pass transmembrane domain to a smaller cytoplasmic region, only APP contains the domain encoding Aβ (Muller et al., 2017). Undergoing extensive differential splicing at exons 7, 8 and 15, APP has at least eight different isoforms which vary by 400 amino acids in length (Sandbrink et al., 1996). The isoform most abundant in neuronal cells is APP695, with APP751 and APP770 (named according to their amino acid length) being highly expressed in most tissue (Kang & Muller-Hill, 1990) and have almost 90% more expression in glial cells rather than neurons (Rohan de Silva et al., 1997). Figure 1.8 shows the structure of APP770 (adapted from (Dawkins & Small, 2014)). It is therefore accepted that APP expression is regulated by cell-specific transcription (Menendez-Gonzalez et al., 2005). APP751 and APP770 isoforms contain the Kunitz Protease Inhibitor (KPI) domain which is lacking from the APP695 isoform. This KPI domain is 56 amino acids long and is homologous to the Kunitz family of

serine protease inhibitors which have the function of inhibiting peptidases. The role of the KPI domain has been reviewed (Menendez-Gonzalez et al., 2005) and is involved with forming stable enzyme complexes with trypsin (Oltersdorf et al., 1989), regulation of neuronal connections (Kido et al., 1990) and also in learning and memory (Conboy et al., 2005). Furthermore, the levels of APP containing this KPI domain has been shown to be increased in AD patients (Preece et al., 2004) suggesting either a role or consequence of disease progression.

The structure of APP has been extensively studied and several possible physiological functions of this protein have come to light as a result. As mentioned above, APP has a large extracellular domain with a cysteine-rich growth factor like domain after which there is a zinc binding domain. Together these are referred to as the E1 domain. Next, an acid rich domain which contains aspartic and glutamic acids, followed by the KPI rich region for APP751 and APP770. There is then the region termed E2, consisting of another cysteine-rich growth factor like domain, zinc and copper binding domains and finally a carbohydrate domain where the N-glycosylation site can be found (Coulson et al., 2000). The crystal structures of both E1 and E2 domains have been solved (Dahms et al., 2010; Wang & Ha, 2004) and this has provided considerable detail regarding the interactions occurring at or between the different domains. Briefly, on the cell surface, this structure of APP allows it to form homo/heterodimers. Heparin binding in particular is thought to heavily influence dimerization (Xue et al., 2011). These interactions occur in the E1 region by the N terminal cysteine-rich growth factor as well as the copper binding domain (Soba et al., 2005). Disulphide bridges forming a loop in this region have been shown to be critical for the stability of the homodimer at residues 91-111 (Kaden et al., 2008). This N-terminal dependent dimerization has been shown to be both critical and sufficient whereas the C-terminal does not seem to be initially required for this process. However, although the N-terminal is a prerequisite to dimer formation, the C-terminal domain is needed to link two APP dimers together and form larger oligomeric species (Scheuermann et al., 2001).

Independently, *cis-dimerisation,* that is dimerisation between two monomers of APP within the same membrane of a single cell, is facilitated through the juxtamembrane/transmembrane (JT/TM) via cross linking disulphide bridges. This ability suggests a close proximity of the JTs between two APP

molecules. In this JT/TM region, there are three glycine (GxxxG) motifs, one of which is within the Aβ domain. There is also the presence of a GxxxA motif in the APP TM domain (but on a different interface) and as there have been observations that glycine shows compatibility with α-helices in lipid bilayers, it is possible that dimersation of APP where GxxxG/GxxxA motifs mediated by two different interfaces could regulate cleavage of APP (Khalifa et al., 2010). Mutations introduced into APP to alter the glycine motifs to alanine residues have resulted in less APP dimerization, and less APP processing resulting in a reduced Aβ42 production (Munter et al., 2007). On the other hand, studies have reported an increase in APP dimerization by introducing cysteines at the JT/TM which has led to the increase in amyloid formation. (Scheuermann et al., 2001). Therefore, *cis*- dimerization is thought to affect APP functioning (Eggert et al., 2009) although it is not yet entirely understood.

Trans-dimerisation, between monomers in the plasma membrane of different cells, can occur with not only two APP monomers but also with APP-APLP1/2 monomers. This is possible due to the E2 region of APP being able to dimerise in an antiparallel orientation and interestingly, this dimerization is reversible suggesting that once APP reaches the cell surface, the cis dimers may be able to dissociate and re-associate as trans dimers with APP on the surface of nearby cells and thus facilitating cell-cell adhesion (Wang & Ha, 2004). This has been shown to be particularly important in synaptic function (Soba et al., 2005).

1.4.2 APP Processing

APP can be processed in either the amyloidogenic or non-amyloidogenic pathways (Figure 1.9); a deciding factor is the co-localisation of APP with various secretases which in turn, is dependent on the distribution of APP. Full length APP is synthesised and dimerises in the endoplasmic reticulum (Scheuermann et al., 2001) and is then subject to a number of post translational modifications as it is transported by the Golgi/trans-Golgi network. As APP matures through a constitutive secretory pathway, it acquires a tyrosine sulphate and a phosphate as well as N- and O-linked carbohydrates (Weidemann et al., 1989). APP can be transported to the cell surface in trans-Golgi network derived secretory vesicles which have been distinguished from synaptic vesicles by the use of synaptosin

(Groemer et al., 2011). However, the majority of APP is found in the Golgi network. The production of Aβ occurs in several intracellular organelles and as such, the increased delivery of APP to the cell surface favours the non-amyloidogenic pathway. APP residing in acidic compartments such as the endosomes favours the amyloidogenic processing pathway and thereby the increased levels of Aβ (Muller et al., 2017).

APP is first cleaved either by α-secretase in the non-amyloidogenic pathway, or by β-secretase in the amyloidogenic pathway. In the non-amyloidogenic pathway, this leads to the release of sAPPα which is essentially a large ectodomain of APP as well as a membrane-associated C-terminal fragment (CTF) consisting of 83 amino acids (C83). In the amyloidogenic pathway, it is APP cleavage by the β-secretases at the N-terminal of Aβ that begins the release of Aβ. The two products of this β-secretase processing are sAPPβ and a CTF consisting of 99 amino acids (C99). The excision of Aβ from APP, however, requires the sequential cleavage by both β- and γ-secretase.

γ-secretase acts in both the amyloidogenic and non-amyloidogenic pathways by cleaving the membrane-tethered CTFs. The C83 and C99 fragments are cleaved by γ-secretase in a number of steps beginning with an endolytic cut at the ε site which frees the C terminal APP intercellular domain (AICD). In the non-amyloidogenic pathway, there is the release of the non-toxic p3 peptide whereas in the amyloidogenic pathway, the C99 fragment is internalised and further processed by γ-secretases at several sites to produce fragments of Aβ of varying length (Chen et al., 2017). This sequential cleavage has been shown to take place every three residues along the α-helical face of the transmembrane domain of APP (Takami et al., 2009). The Aβ39-42 peptides released as a result of amyloidogenic cleavage contain 28 residues of the extracellular domain and 11-15 residues of the transmembrane domain of APP. A schematic representation of APP processing in both pathways is shown in Figure 1.9.

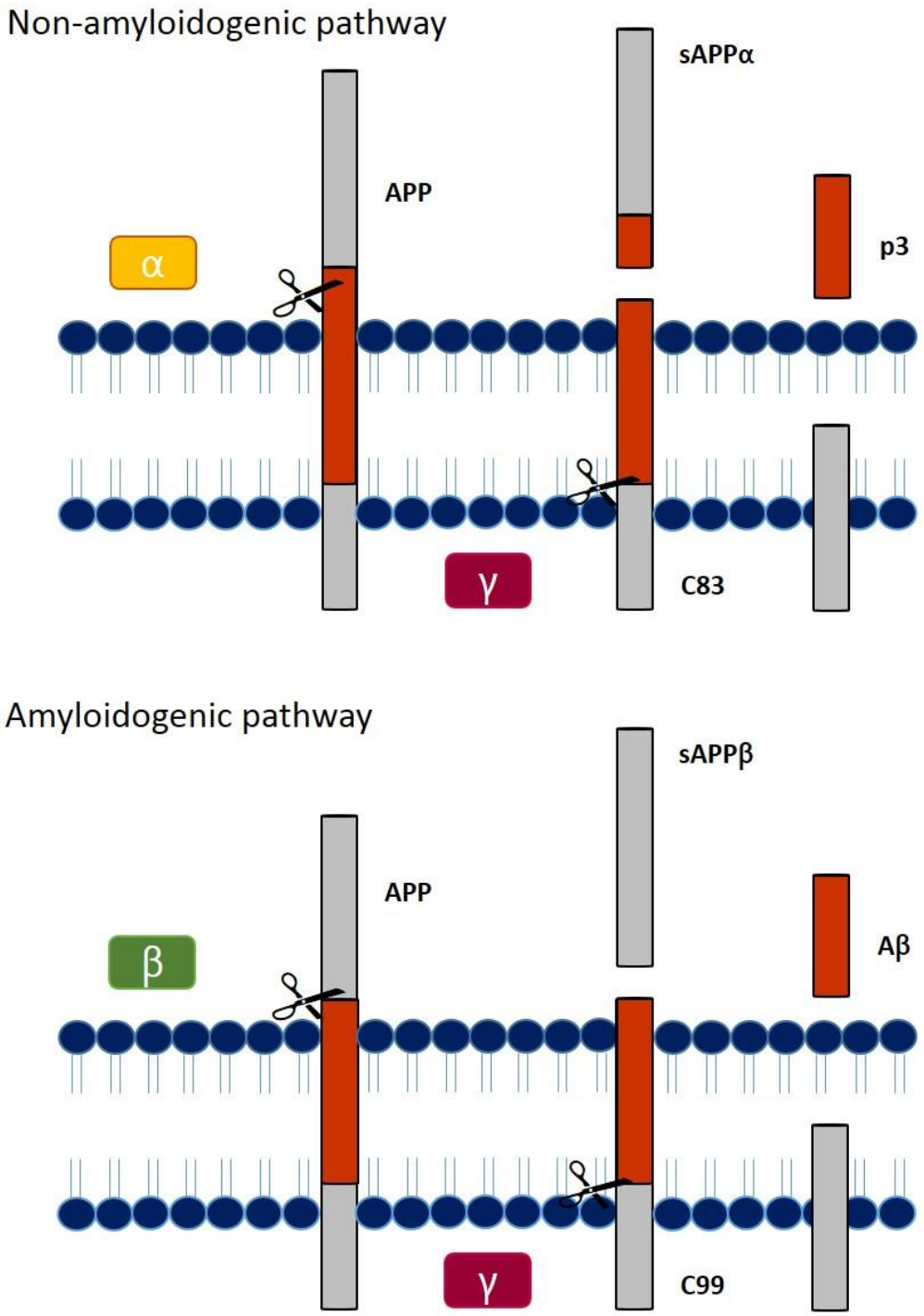

Figure 1. 9. APP processing. In the Non-Amyloidogenic pathway, APP is first cleaved by α-secretase within the Aβ sequence releasing sAPPα. This is then cleaved by γ-secretase which releases the p3 fragment. In the Amyloidogenic pathway, β-secretase cleavage of APP at the Aβ terminus releases sAPPβ. Cleavage by γ-secretase after this results in the release of Aβ. Adapted De Strooper et al, 2010.

1.4.3 α-secretases

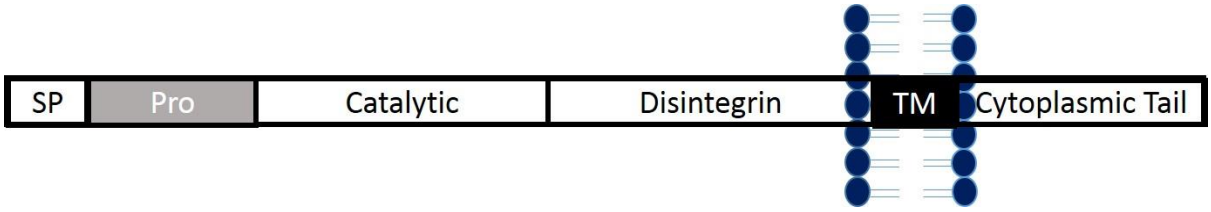

Figure 1. 10. α-secretase structure. Non-Amyloidogenic APP processing is mediated by a number of proteases, mainly from the ADAM family. These are membrane bound consisting of several extracellular domains.

There has been extensive research into each of the secretases in order to better understand their modes of action and develop therapeutics against them with the overall aim of decreasing Aβ production. This approach would address the mechanism of disease pathogenesis rather than target downstream effects of pathogenesis. α-secretase (Figure 1.10) processing of APP is mediated by members of the A disintegrin and metalloproteinase domain proteins (ADAM) and of these, ADAM 9, 10, 17 and 19 are the enzymes most likely to be involved (Asai et al., 2003), particularly ADAM10. The cleavage site of α-secretases is within the Aβ domain at Lys16-Leu17 bond. As this processing of APP does not result in the production of toxic Aβ, it has been less focused on as a therapeutic target in AD. However, enhancing the non-amyloidogenic pathway of APP processing is now becoming more popular due to the combination of the physiological benefits of the sAPPα (Habib et al., 2017; Mockett et al., 2017) as well as the disappointing results of targeting secretases in the amyloidogenic pathway.

1.4.4 β-secretases

The β-secretases (Figure 1.11), which are aspartic proteases, involved in the production of Aβ are BACE (beta-site amyloid precursor protein cleaving enzyme 1 and -2 (BACE1 and BACE2). BACE1 is the major β-secretase in the brain and acts at the β-site, whereas BACE2 acts within the Aβ domain making it a competitor to α-secretase cleavage. However, it is not thought to be a major contributor to APP processing. Both are produced as precursor proteins in the endoplasmic reticulum and have almost identical structural organisation, with BACE1 comprised of 501 amino acids and BACE2

made up of 518 amino acids. As β-secretases are aspartic proteases, their prodomain which aids in protein folding, is removed by furin-like proprotein convertases in the Golgi compartments and thereby producing active enzymes (Yan, 2017). From the Golgi, BACE1 is transported to endosomes where the acidic environment favours the processing of APP in the amyloidogenic pathway. The transportation is due to the interactions of BACE1 with Golgi localised ϒ-ear-containing ADP ribosylation factors (ARF) binding proteins, known as GGA protein (von Einem et al., 2015) . The interaction occurs between the C-terminal DXXLL motif on BACE1 and the VHL domain of the CGA proteins (Kandalepas & Vassar, 2014). Intracellularly, the localisation of BACE1 can also be regulated by Ritculon/Nogo family members; these negatively regulate BACE1 translocation to the endosome. Overexpression of reticulon proteins has been shown to keep BACE1 in the endoplasmic reticulum and therefore decrease the amount of Aβ produced (Shi et al., 2017). Other examples of BACE1 trafficking regulatory proteins include sorting nexin 6 (Okada et al., 2010) and sortilin (Finan et al., 2011).

The docking of BACE1 into the lipid bilayer has been suggested to be a crucial step for APP processing and this is facilitated by the S-palmitoylation on four Cys residues found on the junction of the transmembrane and cytosolic domains. This leads to increased activity of the enzyme (Cordy et al., 2003). However, there is also evidence suggesting that this lipid localisation and palmitoylation does not increase the activity of the β-secretase (Vetrivel et al., 2009) suggesting that BACE1 processes APP in both lipid raft and non-lipid raft environments.

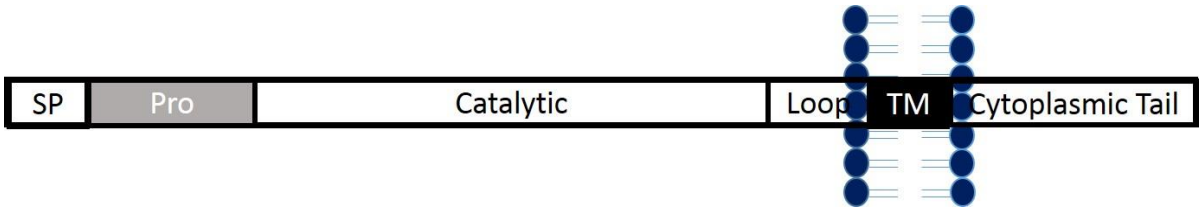

Figure 1. 11. β-secretase structure. BACE1 is a membrane bound enzyme responsible for cleaving APP at the β-site.

BACE1 plays an essential role in, and is the rate limiting factor in Aβ production and therefore it has been the focus of many therapeutic approaches in AD. The catalytic mechanism of BACE1 is

dependent on the luminal orientation of the BACE1 active site which is correctly positioned to cleave APP, and this is highly sequence specific (Cole & Vassar, 2007). The aspartates hydrolyse peptide bonds following a general acid-base mechanism where the Asp228 is the base activating a bridging catalytic water molecule, and the Asp32 is the acid protonating the carbonyl group on the substrate (Ellis et al., 2016). The activated water molecule nucleophilically attacks the scissile-bond carbonyl and the resultant intermediate is stabilised by hydrogen bonds. There is then the decomposition of the scissile C-N bond with which there is a proton transfer from the Asp32. On top of this catalytic site is the Tyr68-Glu77 β-hairpin loop which acts as the 'flap' controlling substrate exposure and solved crystal structure suggest that this flap can change from open to closed conformation at room temperature (Shimizu et al., 2008).

Overexpression (Lee et al., 2003) or downregulation (Cai et al., 2001) of BACE1 activity results in increased or decreased APP processing and Aβ production respectively. The cleavage sites of BACE1 on APP are between Met671 and Asp672 (β-site) and between Thy681 and Gln682 (β'site). Cleavage at the β-site generates the C99 fragment and cleavage at the alternative site results in the C89 fragment, both of which are then cleaved by γ-secretase to produce Aβ11-XX or Aβ1-XX respectively. A recent study has emphasised the importance of BACE1 cleavage site selection in the production of Aβ and subsequent pathogenesis (Zhang et al., 2017). A mutation of APP that causes recessively inherited AD, A673V, which occurs at position 2 of Aβ has been shown to shift the BACE1 cleavage from Glu11 to Asp1 which resulted in the increased levels of C99 and Aβ production. Furthermore, the Aβ produced seems to be more aggregation prone than the wild type (Zhang et al., 2017). The dimerisation of the mutant and wild type APP was also seen as was the increased lysosomal degradation of the mutant APP and inhibition of γ-secretase cleavage. Of note, other mutations in this site reduced C99 production and were shown to be protective e.g. Icelandic A673T mutation. Together the results suggest A673 is involved in APP processing and could be a possible therapeutic target in some cases of AD. More importantly, this study highlights the fact that BACE1 cleavage site selection is crucial in the production of Aβ. Furthermore, it has been observed that the mRNA of BACE1 is increased in both AD patients and animal models of the disease

(Coulson et al., 2010). Due to the crucial role BACE1 plays in the production of Aβ, several BACE1 inhibitors have been developed and entered clinical trials with the hope of decreasing the amount of Aβ produced in the amyloidogenic pathway and the subsequent pathology that follows.

1.4.5 γ secretase

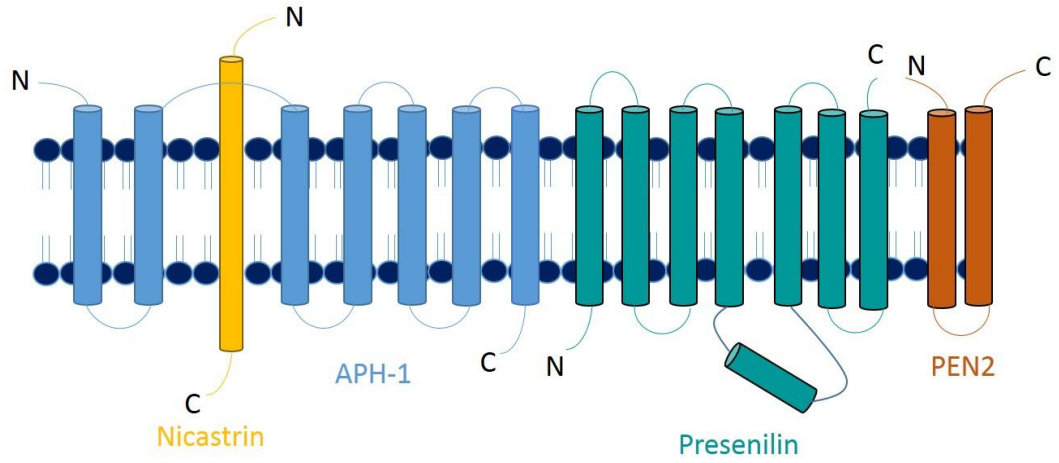

Figure 1. 12. γ-secretase structure. This secretase is made up of four proteins; nicastrin, APH-1, Presenilin and PEN2. Together these form a complex with Presenilin thought to form the catalytic core.

Following β-secretase, the subsequent cleavage of APP is by γ secretase (Figure 1.12). This is an aspartyl protease comprised of four subunits; a catalytic domain comprised of presenilin-1 and presenilin-2 (PS1/2), the substrate receptor nicastrin, PEN2 which acts as an enhancer of activity and finally anterior pharynx defective (APH-1) which is thought to be the stabilising subunit (De Strooper et al., 2012). Mutations in PS1 are well documented in familial AD. Although the crystal structure of the complex has not yet been solved, PS1 is known to have nine transmembrane (TM) helices with the aspartyl residues needed for autoproteolysis found in TM6 and TM7. This autoproteolyic cleavage is a result of full complex formation and occurs within the cytosolic loop domain between these two TM domains to generate N- and C-terminal fragments which results in the active form of γ-secretase being released. It has been known for over ten years that the active site of γ-secretase resides in a catalytic pore that is filled with water (Sato et al., 2006a). TM1, 6, 7 and 9 are thought to make up this core and face the hydrophilic environment of the catalytic pore. Studies investigating the spatial arrangement

of PS1 have shown that distance between the cytosolic sides of TM4 and 7 correlates with Aβ42 production in particular; cross-linking experiments altering this distance by manipulating the flexibility of TM4 to make it shorter resulted in lowered Aβ42 levels and increasing this distance leads to the increased amount of Aβ production (Tominaga et al., 2016). The substrate binding model demonstrates that TM2 and 6 are close to TM9 and involved in forming the substrate binding site. This displays the conformational flexibility that would be expected of 'gate doors' for substrates to reach the catalytic pore. The hinge region of this pore has been identified as loop1 (position of which is between aa 106-131) which cooperates with the C-terminus of PS1 in order to regulate substrate gating and recognition (Somavarapu & Kepp, 2016). Cryo-EM has also provided insights into the importance of the interactions between the other subunits forming the full γ-secretase complex; the nicastrin subunit has been shown to be important as a substrate recruiter. Once a substrate has been bound, the subunit has been speculated to align the nicastrin pocket and the catalytic pore of PS1 and thus facilitating the cleavage of the substrate (Zoltowska & Berezovska, 2017), in this instance the C99 fragment of APP. PS1 cleavage is between the Leu40 and Val50 which leads to an array of Aβ peptides of varying length, all spaced by three amino acids, indicating two different α-helices on C99 from which Aβ49,46,43 and 40 (one subset) and Aβ48,45,42 and 38 (second subset) are produced (Olsson et al., 2014). Together, this demonstrates that the structure and conformation of the γ-secretase complex strongly dictates the type of Aβ produced. Over a 150 AD linked mutations have been identified in the genes encoding PS1/2, which shift the ratio of Aβ produced in favour of Aβ42 by altering the overall biochemical quality of the γ-secretase complex and its interaction with APP (De Strooper et al., 2012). Considering this, γ-secretase has also been the focus of much therapeutic development for treatment of AD.

1.4.6 Therapies targeting secretases

Although these secretases provide a good starting point as therapeutic targets in developing drugs for AD patients, there have been many hurdles encountered which have not yet been resolved. Firstly, both BACE1 and PS1 have other substrates aside from their respective APP fragments and the processing of these are necessary in normal functioning and physiology. For example, BACE1 is

involved in the cleavage of neuregulin-1 is necessary for regulating myelination (Willem et al., 2006) and γ-secretase cleavage of the Notch receptor is critical in the maintenance of stem cells (Yu et al., 2008). Many inhibitors targeting γ-secretases have been unsuccessful when it comes to clinical trials due to side effect related incidences of skin cancer and a decline in cognitive functioning e.g. Semagacestat (Doody et al., 2013) (Eli Lilly) and Avagacestat (Coric et al., 2015) (Bristol-Myers-Squibb). BACE1 inhibitors are showing to be slightly more promising, however, BACE null mice showed impaired neuronal phenotypes (Hu et al., 2010), complete BACE1 inhibition can lead to severe side effects and as such there needs to be a threshold established beyond which the BACE1 inhibition levels cannot pass. Aside from the side effects, there is also the issue of therapeutics that can cross both the BBB and cell membranes. There is a vast amount of literature investigating the successes and failures of secretase inhibitors as therapeutics. These have been reviewed extensively (Bachurin et al., 2017; Cummings et al., 2017; Evin, 2016; Extance, 2010; Karran & Hardy, 2014; Mangialasche et al., 2010; Selkoe, 1994; Selkoe & Hardy, 2016).

1.5 Mechanisms of oligomer toxicity

Although the link between oligomers and toxicity has been established for many years, the mechanism for this toxicity is still unclear. One reason oligomers are thought to be cytotoxic is due to their exposed hydrophobic region, which under normal conditions would be buried, being able to interact with cellular components and exert cell dysfunction (Cheon et al., 2007).

Oligomers are formed by numerous disease-related amyloid proteins including Aβ42 and α-synuclein, which suggests a similar structural feature. This was consolidated by the development of the conformation specific A11 antibody, which binds to all oligomers regardless of the precursor protein (Kayed et al., 2003). It has therefore been proposed that these similar structures must also share commonality in mechanisms of cytotoxicity.

As this thesis focuses heavily on the disease-related Aβ42 protein, the proposed mechanisms of Aβ42 oligomer cytotoxicity will be discussed.

1.5.1 Receptor-mediated Aβ toxicity

A number of receptors have been implicated in Aβ mediated toxicity. This is then thought to lead to downstream synaptic dysregulation and eventual neurodegeneration. Figure 1.13 (De Strooper & Karran, 2016) summarises the many proposed receptor mediated mechanisms of Aβ oligomer toxicity.

The evidence for the involvement of each of these receptors has been somewhat confusing. For example, Aβ oligomers have been suggested to induce nerve growth factor (NGF) receptor mediated neuronal death via the p75 neurotropin receptor (p75NTR). This was shown to be true for Aβ-derived diffusible ligands (ADDLs) which are a class of oligomers, and that neuronal death is mediated by a death domain found in the cytoplasmic portion of the receptor (Bothwell, 1996; Yamamoto et al., 2007). Another study, however, showed that this same receptor promotes cell survival in the presence of Aβ oligomers and in fact, toxicity was independent of the p75TR receptor altogether (Costantini et al., 2005)

There has also been extensive research into the N-methyl-D-aspartate receptor (NMDAR) dependent Aβ disruption of long term potentiation. This is thought to affect several downstream pathways of the NMDA receptor which have been extensively reviewed (Yamin, 2009).

Disruption of the Wnt signally pathway is also thought to be a mechanism of Aβ toxicity. Oligomers have been shown to bind to the Frizzled cysteine-rich domain in the Wnt-binding site and thereby inhibit Wnt signalling altogether. As this is critical for cell-cell communication, disruption by oligomers in this way is detrimental to the cell (Magdesian et al., 2008). Recent studies, however, have suggested that this disruption can be overcome (Shruster et al., 2011)

The cellular prion protein has also been put forward as a receptor of Aβ oligomers (Salazar & Strittmatter, 2017). The specific binding of Aβ oligomers to cellular prion proteins has been identified in human COS cells as well as primary neurons and mutations to remove these prion proteins was able to restore synaptic long term potentiation in acute brain slices (Salazar & Strittmatter, 2017). Similar

recovery has also been shown in mouse models (Gimbel et al., 2010). Therefore, it seems extremely likely that at least some oligomer toxicity is mediated by binding to cellular prion proteins.

A brief overview has been given of the vast literature surrounding receptor-mediated toxicity of oligomers. It is most likely that oligomers are extremely promiscuous and bind to several receptors to disrupt downstream pathways. As oligomers are formed in several proteins on the process to forming amyloid fibres, it seems the structure of these oligomers plays a role in their promiscuity.

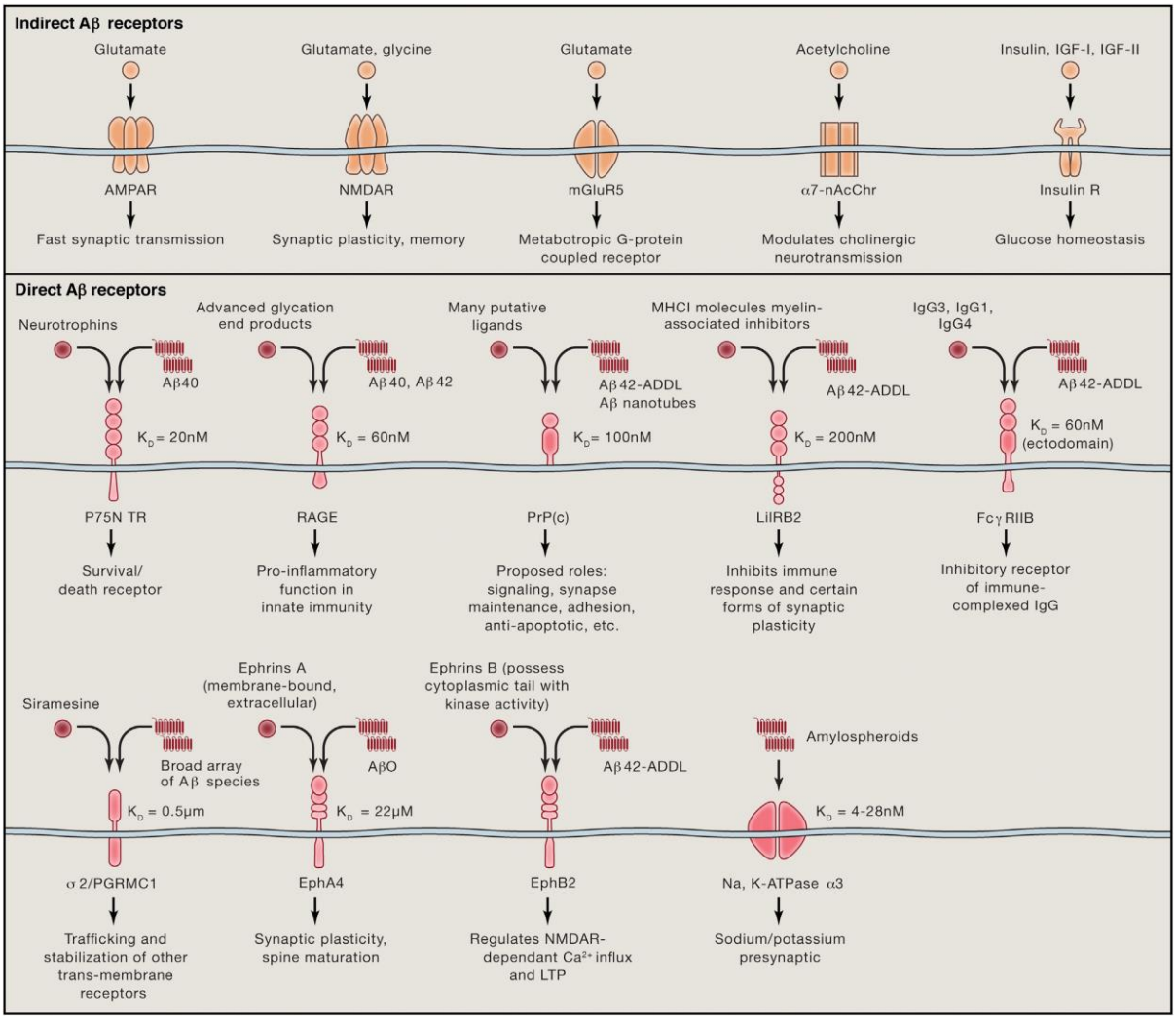

Figure 1. 13. Receptor mediated Aβ oligomer toxicity, taken from De Strooper and Karran, 2016

1.5.2 Cellular membrane disruption by oligomers

One of the more prominent mechanisms for Aβ oligomer induced neurodegeneration, is channel formation and disrupted calcium homeostasis (Glabe & Kayed, 2006). This is known as the 'channel hypothesis'. The formation of channels into lipid bilayers by oligomers, referred to as amyloid pores, has been shown by several groups (Bode et al., 2017; Meleleo et al., 2013; Serra-Batiste et al., 2016). As a result of this, elevated calcium levels were monitored in the cytosol. There is a strong suggestion that Aβ incorporated into the membrane to form pores, leads to subsequent aggregated Aβ accumulating on the membrane (Williams & Serpell, 2011). It is also entirely possible Aβ shares toxicity mechanisms similar to those displayed by antimicrobial or antifungal peptides; free radical formation is an example of how channel formation can lead to cell disruption (Kayed & Lasagna-Reeves, 2013).

More recently, it has been proposed that this 'channel hypothesis' is not responsible for cellular membrane mediated oligomer toxicity. It is more to do with membrane permeabilisation caused by oligomers which is independent of channel formation; the oligomers increase the permeability of the membrane and penetrate the cell resulting in leakage of calcium (Bucciantini et al., 2004). It has also been shown that oligomers, regardless of primary sequence, increase the conductance of the cell membrane and thereby leads to the depolarisation of the plasma membrane with detrimental effects (Kayed et al., 2004) . Increased conductance in this way can lead to ion homeostasis dysfunction as well as signal disruption. One way in which the integrity of the bilayer is disrupted by oligomers, is thought to be the spreading apart of the lipid head groups and therefore thinning of the bilayer and lowering the permeability (Kayed & Lasagna-Reeves, 2013).

1.5.3 Accumulation of intracellular oligomers

In AD, Aβ is deposited extracellularly as plaques which are made up of amyloid fibrils. There is however, Aβ accumulation intracellularly and this is thought to precede the formation of extracellular deposits (Skovronsky et al., 1998). The internalisation of Aβ will be discussed in a later chapter (Chapter 5), however as with the mechanisms of toxicity, there are several ways by which oligomers

are thought to internalise into the cell. For example, the scavenger receptor for advanced glycation end products (RAGE) is thought to be one method of internalisation in both neurons and microglia. This interaction between RAGE and Aβ can cause oxidative stress as well as the activation of the nuclear factor-κ B thereby inducing the macrophage colony-stimulating factor (Verdier & Penke, 2004; Yan et al., 1998).

Not all intracellular Aβ is accumulated by internalisation. Cell themselves produce Aβ and it is not yet understood if part of the intracellular accumulation is due to Aβ not being secreted after generation or if secreted Aβ is simply taken back up into the cell. Assembly of oligomers from intracellular monomers remains unclear, however one hypothesis is that this could be result of Aβ interactions with other intracellular proteins. For example, the accumulation of GM1 in early endosomes supports the notion that this ganglioside could induce Aβ oligomerisation (Yuyama et al., 2008). There is also the action of molecular chaperones; for example, the chaperone prefoldin which captures and delivers denatured proteins to another chaperone, chaperonin. This interaction between Aβ oligomers and prefoldin may prevent further aggregation by stabilising the oligomer (Sakono & Zako, 2010).

A fundamental understanding of mechanisms leading to toxicity is still lacking. One mechanism is thought to be by inhibiting the normal function of the proteasome and de-ubiquinating enzymes (Almeida et al., 2006). Accumulation of oligomers in mitochondria has also been related to disrupted enzyme activity of the respiratory chain complexes III and IV resulting in reduced oxygen consumption and cellular dysfunction (Caspersen et al., 2005). There is also substantial evidence to suggest intracellular accumulation of Aβ leads to synaptic dysfunction (Bayer & Wirths, 2010).

The mechanisms by which oligomers exert their toxicity is likely to be vast and far reaching. Amyloid oligomers show a high level of affinity and interactions with numerous proteins and receptors which lead to cellular dysfunction. The clearance of these misfolded proteins has been previously discussed and it seems that oligomer toxicity occurs when this clearance or degradation becomes inefficient. This could be due to several reasons such as oligomers inhibiting or disrupting the action of molecular

chaperones, or simply that the cell cannot cope with the level of protein aggregation insult accumulating over time.

A key point to take from this, however, is that the effects of the oligomeric species are not specific to primary sequence and therefore indicate structure and/or size as a mediator of toxicity.

1.6 Non-pathogenic amyloid proteins

1.6.1 Functional amyloid proteins in living organisms

Although a large focus of amyloid research has centred on disease-related proteins, there are a number of amyloid proteins identified as being non-pathogenic and functional. These functional amyloid proteins are found in a range of organisms from humans to bacteria (Table 1.2).

In humans, functional amyloid has been found to be involved in a number of physiological processes. Proteins can exploit the ability to form amyloid in order to perform function. For example it has been found that peptide hormone storage (Maji et al., 2009), pigmentation (Fowler et al., 2006) and cell responses to stress (Audas et al., 2016) all heavily involve amyloid proteins.

Peptide hormones are stored in an amyloid conformation within secretory granules, these amyloid fibrils then dissociate upon release when exposed to the correct pH (Maji et al., 2009). This reversible amyloidogenicity is tightly controlled and allows for the peptide hormones to be stored at high concentrations before being released as functional monomers (Maji et al., 2009).

Pmel17 is the glycoprotein essential in the biogenesis of melanosomes, which are the organelles of pigment cells where melanins are synthesised and stored. These organelles have been found to be loaded with fibrillar amyloid (Fowler et al., 2006). Pmel17 is known to lyse into two fragments during the biogenesis of melanosomes; one of which is the Mα fragment whilst the other, Mβ, is rapidly degraded. It is the Mα fragment that self-assembles into fibres and forms the core the mature melanosomes. The assembly process of Mα has been highly characterised (Fowler, 2006) and has been found to be extremely rapid. This suggests forming fibrils rapidly sequesters any intermediary species, thus preventing toxicity (Bissig et al., 2016; Fowler et al., 2006).

Upon severe environmental insult such a heat shock or acidosis in cells, there is the expression of A-bodies. These have been defined as rIGSRNA-seeded nuclear foci which contain proteins possessing the characteristic properties of amyloid. These A-bodies act as stores for proteins until the stressors are removed, after which they disassemble. Many proteins have been identified as being able to form A-bodies, including those involved in cell cycle progression and DNA synthesis. This allows the cells to enter a dormant state and survive the stressors being placed on the cell (Audas et al., 2016).

Functional amyloid proteins are also found in other organisms. For example, the propagation of the amyloid HET-S prion protein has been postulated to be an important factor in fungi signal transduction (Daskalov et al., 2015). In Saccharomyces cerevisiae, a type of yeast, a Sup35p fragment (GNNQQNY) is a translation termination factor that ensures the cessation of protein synthesis at nonsense (stop) codons (Kushnirov et al., 2000). Sup35p formation of amyloid prevents translation termination and thereby results in stop codon read through as well a C-terminal extension. This is critical in generating phenotypic diversity which is most likely due to an altered proteome (Bertram et al., 2001; Fowler et al., 2007). The Sup35p amyloid formation is prion-like and allows for the transmission of genetic information; the cytoplasmic amyloid is reversible and heritable leading to a particular phenotype being passed from mother to daughter cells upon division (Fowler et al., 2007) in an epigenetic, non-Mendlian manner.

More recently, the formation of hydrogels has been identified in nuclear pore complexes. One example is the hydrogel formed from the ‘amyloid-like’ β-sheet rich FG repeat domain of the nucleoporin NSp1 protein. This hydrogel has sieve like permeability to allow the entry of nuclear transport receptor but exclude the entry of large, inert macromolecules (Ader et al., 2010). The study further highlighted the importance of β-sheet structures maintaining the permeability barrier of nuclear pores.

Understanding how these proteins form amyloid in a rapid, reversible and non-toxic manner will provide us with indications as to what makes an amyloid protein toxic. As fibrils are the natural fold

of functional amyloid proteins, using lessons learnt from their assembly process, we may establish 'rules' that determine how to avoid the toxic nature of disease-related amyloid proteins.

Bacteria	**Protein**	**Reference**
Gram negative bacteria	Curli	(Chapman et al., 2002)
Streptomyces coelicolor	Chaplins	(Wasmer et al., 2008)
Staphylococcus aureus	Bap Modulin	(Taglialegna et al., 2016) (Zheng et al., 2017)
Klebsiella pneumoniae	Microcin E492	(Arranz et al., 2012)
Fungi	**Protein**	
Saccharomyces cerevisiae	Sup35	(Balbirnie et al., 2001)
Podospora anserine	HET-s	(Maddelein et al., 2002)
Candida albicans	Als adhesin	(Otoo et al., 2008)
Fungi spp.	Hydrophobins	(Morris & Sunde, 2013)
Plants	**Protein**	
Algae spp.	Macroalgal adhesive	(Mostaert et al., 2006)
Hevea brasiliensis	Rubber Elongation Factor	(Berthelot et al., 2016)
Animal- Mammals and insects	**Protein**	
Human	Pmel 17 Protegrin-1 Human defensin 6	(Fowler et al., 2006) (Jang et al., 2011) (Chu et al., 2012)
Spider	Spidroin	(Slotta et al., 2007)
Mice	CPEB3	(Fioriti et al., 2015)

Table 1. 2. Some examples of functional, non-toxic amyloid proteins across a range of organisms.

In general, functional amyloid proteins are thought to be non-toxic, however, there are a few rare instances where this is not the case. Examples of this include antimicrobial peptides, including Protegrin-1 found in humans, where cytotoxicity is induced by membrane disruption through channel formation (Jang et al., 2011). Interestingly, Aβ has been shown to be an antimicrobial peptide in its functional amyloid form (Soscia et al., 2010). Another example is the human defensin which is found at the gut mucosa and binds with a high affinity to the surface of bacteria to 'trap' them in a net-like structure thereby stopping further invasion (Chu et al., 2012). These examples illustrate the tight regulation displayed by functional amyloid proteins which exploit their cytotoxic nature only when necessary. This is not the case for disease-related amyloid proteins where pathology is linked to protein misfolding and no regulation of toxicity.

1.6.2 Regulation of toxicity

There are several ways in which functional amyloid proteins regulate their (lack of) toxicity. The rapid nature in which amyloid is formed by these proteins often means the formation of the intermediary oligomeric species is either by-passed or the kinetics of assembly are rapid enough, so toxicity is minimised. (Fowler et al., 2006). Examples of this are seen with Pmel 17 (Fowler et al., 2006) as well as the Sup35 yeast prion protein (Wang et al., 2007). This is also seen with the amyloid silk spidroin protein, produced in spiders, which rapidly forms insoluble amyloid in response finely controlled series of pH drop, salt gradients finalised by spinning (Kenney et al., 2002). Furthermore, Curli, formed by bacteria, encodes its own protective mechanism within in the CsgA subunit, to prevent the formation of oligomeric species. This is achieved by inhibition of aggregation propensities (Wang et al., 2010). The ability to form oligomers and the time spent in this aggregation state, may be a determinant of toxicity and this is minimised in functional amyloid proteins.

The location of functional amyloid proteins may also play a part in toxicity regulation. Functional amyloid proteins are often confined to specific compartments (Berson et al., 2003) and are therefore separated from other cellular compartments. In other cases, amyloid is formed outside of the cell or on

the membrane surface (Swasthi & Mukhopadhyay, 2017). Controlling the temporal location of amyloid proteins in this way, may protect other parts of the cell from cytotoxicity.

Finally, the use of molecular chaperones to inhibit the formation of amyloid may prevent toxicity. Molecular chaperones are essential for maintaining normal cell proteostasis, it is therefore unsurprising they play a role in regulating amyloid toxicity. For example HSPs are involved in binding to hydrophobic regions and transiently blocking aggregation (Hartl et al., 2011). Furthermore, the HSP70 and HSP40 have been shown to break down amyloid into 'seeds' to accelerate the formation of fibrils and avoid oligomer formation (Rikhvanov et al., 2007).

1.7 Exploiting amyloid: Nanomaterials

Amyloid proteins can be thought of as a natural nanomaterial due to their unique properties. Firstly, under suitable conditions, almost any peptide has the ability to form amyloid (Dobson, 2004). Secondly, amyloid proteins are highly stable and have high mechanical strength (Smith et al., 2006). In fact, the stability and strength of amyloid fibrils is comparable to that of steel and silk (Smith et al., 2006). The nucleation dependent polymerisation and ability to accelerate amyloid formation using seeds (Xue et al., 2009) also makes amyloid proteins extremely attractive as bionanomaterials. Amyloid properties can also easily be manipulated by altering primary sequences and functional groups can be conjugated to amino acid side chains (Mankar et al., 2011). Furthermore, amyloid proteins can also form complex networks of gels and films. (Aggeli et al., 1997). Therefore, amyloid has been exploited as a bionanomaterial for applications discussed below.

1.7.1 Applications in biotechnology – Cell culture scaffolds

One of the recent exploitations of amyloid proteins is the formation of hydrogels. Hydrogels are formed from amyloid fibrils which, above a critical gelation concentration, entangle and associate to from three-dimensional networks with the ability to trap water (Elsawy et al., 2016). These provide excellent matrixes for neuronal cell attachments, differentiation and neurite growth. This was first established by developing self-complementary β-sheet peptides using L-amino acids, alternating in positive and negative charges (Caplan et al., 2002). Moreover, it is possible to design these scaffolds

with functionalised motifs. For example, the hydrogel made from the β-sheet rich osteogenic growth peptide ALK, promoted the proliferation and osteogenic differentiation of mouse MC3T3-E1 cells (Horii et al., 2007). Similar results were seen with the β-sheet rich KLD-12 hydrogel providing an excellent scaffold for chondrocyte cartilage like extracellular matrix (Kisiday et al., 2002; Mankar et al., 2011). Although these examples are of self-assembling, β-sheet rich structures, XRFD is needed to confirm both peptides form amyloid.

1.7.2 Applications in biotechnology – overview of other applications

Table 1.3 provides some examples of applications of amyloid proteins in nanotechnology aside from cell culture scaffolds (Mankar et al., 2011).

Amyloid Protein	Applications	Reference
Transthyretin	Functionalised amyloid proteins for cell adhesion	(Gras et al., 2008)
GnRH	Depot formulation of long acting drugs	(Maji et al., 2008)
Killer peptide	Auto-delivery of therapeutic peptides	(Magliani et al., 2011)
α-Synuclein	Hydrogel to trap enzymes	(Bhak et al., 2010)
Sup35p NM domain	Nanowires	(Yin et al., 2011)
Hen egg white lysozyme amyloid fibrils	Thin films	(Knowles et al., 2010)
β2-Microglobulin	Nanoporous Matrix	(Ahn et al., 2010)
L-Diphenylalanine	Hollow nanotubes for drug delivery	(Silva et al., 2013)

Table 1. 3. Examples of amyloid proteins in nanotechnology

From the table, it is apparent to see there are several applications of amyloid proteins that do not display toxicity. Therefore, amyloid proteins serve as an extremely useful tool in developing novel biotechnological applications.

1.8 Research Objectives

The ability to form amyloid proteins under suitable conditions is an inherent property of all proteins and peptides (Dobson, 2004). Although much research has been focused on the structure and assembly process of amyloid proteins, little is understood about the factors determining the toxic nature of amyloid proteins.

The oligomeric species has been identified as being neurotoxic in disease (Glabe & Kayed, 2006; Kayed et al., 2003; Kayed & Lasagna-Reeves, 2013; McLean et al., 1999) , however, we are still unclear as to what specifically determines oligomers to be toxic. This raises questions such as, 'is it the ability to form oligomers?', 'is toxicity related to size or conformation?' and 'is internalisation required for amyloid toxicity?' Addressing these questions, combined with lessons learnt from non-toxic functional amyloid proteins, will help us determine 'rules' that govern amyloid toxicity.

To address these questions in the following chapters, we use models of disease-related and functional amyloid proteins to better understand their assembly process and relate this to cytotoxicity. By assessing factors such as primary sequence, size and conformation, we will gain a better understanding into what makes an amyloid protein toxic.

Chapter 2: Methods

2.1 Biophysical characterisation of amyloid proteins

2.1.1 Introduction

The structure of amyloid proteins has been extensively researched; we know amyloid proteins are insoluble fibrillar species which display a cross-β structure. This cross-β structure is attributed to the orientation of the β-strands which are perpendicular to the fibre axis with pairs of β-sheets being tightly bonded by interdigitating amino acid side chains (Serpell, 2000).

In pathology, oligomers have been identified as the neurotoxic species (McLean et al., 1999). The structure of this toxic species has been difficult to characterise due to its transient nature. Despite this, much effort has been made to establish the structure of the oligomeric species.

2.1.2 Techniques for amyloid structural characterisation

Mounting structural information regarding amyloid fibrils has been established due to advances in biophysical techniques. There are now a number of techniques employed to elucidate the structure of amyloid proteins. For example, electron microscopy allows for the direct visualisation of amyloid morphology. This has long been considered a low resolution method, however with the development of cryo-EM, resolution is greatly improved (Langkilde & Vestergaard, 2009).

Small angle neutron or X-ray scattering (SANS/SAXS) offers the advantage of medium resolution visualisation of any nanoscale particle. High resolution information can be obtained by X-ray diffraction patterns of crystals where the electron density provides a 'map' of all atom thereby provide structural information at atomic resolution. This can often prove difficult with amyloid proteins as crystallisation is a necessity for this technique and requires homogeneity of solution (Langkilde & Vestergaard, 2009). To obtain crystal structures of amyloid proteins, short amyloidogenic segments from the full length protein are used (Sawaya et al., 2007). Therefore, often the information obtained from this technique is usually taken to be a 'snapshot' of protein structure; in reality, the protein solution will always be in a dynamic equilibrium of several structural states. Furthermore, this may

not be the most appropriate method for structural determination since some fibres and crystals formed from the same peptide may differ in structure (Marshall et al., 2010). Nevertheless, atomic resolution structural information obtained from X-ray diffraction is invaluable to understanding fibrillar amyloid structures.

ssNMR has also been extremely useful in gaining an understanding of amyloid fibrils. This technique determines information regarding the identity and backbone conformations of (non) β-strand segments, the supramolecular organisation of β-sheets and interactions/contacts between amino acid side chains. ssNMR also provides an overall arrangement and symmetry of cross-β protofilaments (Tycko, 2011). Often combined with electron microscopy, ssNMR can be used to develop molecular models of amyloid.

As following the assembly process of amyloid proteins is a major aspect of this thesis, we use three main biophysical techniques to probe for structural changes over time. These include transmission electron microscopy (TEM), circular dichroism (CD) and Thioflavin T (ThT) fluorescence. X-ray Fibre Diffraction (XRFD) is also used to detect for the characteristic cross-β structure of amyloid proteins. These techniques are also complemented with dot/western blotting and immunocytochemistry.

2.1.3 Transmission Electron Microscopy

Electron microscopy can be separated into two broad categories (Figure 2.1); transmission electron microscopy (TEM) and scanning electron microscopy (SEM). In TEM, electrons are projected through the sample to produce a two-dimensional image. SEM, produces a three-dimensional image by using a 2-3nm spot of electrons to scan the surface of the sample to generate secondary electrons from the samples itself. These are then detected by a sensor. A third category of electron microscopy combining both TEM and SEM is known as scanning transmission electron microscopy (STEM) and is often used for analytical purposes.

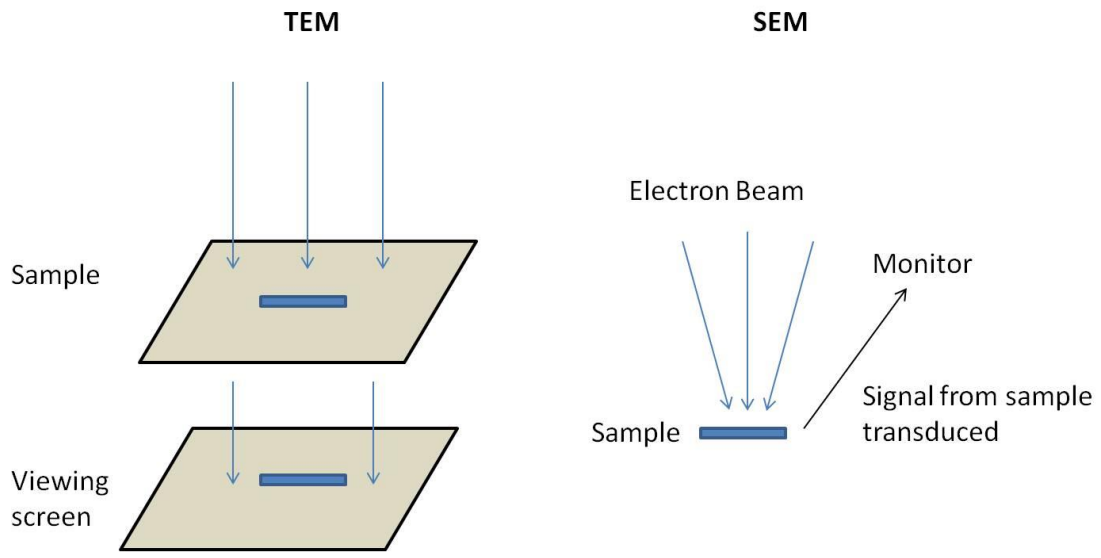

Figure 2. 1. Schematic representation of Transmission Electron Microscopy (TEM) and Scanning Emission Microscopy (SEM). In TEM, electrons are passed through the sample and provides a two-dimensional 'shadow' image. SEM produces a three-dimensional image detected by a sensor.

TEM has been used to visualise amyloid proteins for many years. It has the advantage of providing better resolution (Winey et al., 2014) than light microscopes as well as simple sample preparation for imaging, makes it a highly attractive and useful tool (Gras et al., 2011) .

In TEM, electromagnetic lenses focus electrons into a thin beam which is then passed through the specimen. Depending on the density of the material present, some electrons are scattered and disappear. The un-scattered electrons hit a fluorescent screen at the bottom of the microscope which gives rise to what is known as a 'shadow image'.

TEM is extremely useful for visualising the morphology of amyloid fibrils (e.g. ribbon-like fibrils or curved fibrils) as well as quantifying data such as fibril length. In order to achieve a good contrast and protect the specimen from radiation damage, samples are typically negatively stained using a heavy metal (Bremer et al., 1992). One of the most commonly used negative stains is uranyl acetate which forms a radiation-stable, electron dense coat over the sample. As the beam of electrons passes through the sample, electrons are absorbed by the stain and therefore the sample appears light and surrounding areas (or 'outline') appears dark (Gras et al., 2011).

Visualising the assembly of amyloid proteins using TEM is an excellent tool in monitoring species formed during the assembly process and will also enable us to link structural morphology to cytotoxicity.

2.1.4 Circular Dichroism (CD)

CD is often used to probe for the secondary structure of a protein. The way in which this is achieved is through differential absorption of circularly polarised light by an optically active molecule, either to the left or right.

As a beam of UV light has time dependent electric and magnetic fields, this beam is polarised by passing through prisms/filters, its electric field will oscillate sinusoidally in a single plane. These waves can be visualised as circles which rotate clockwise (R) or anticlockwise (L) and are 90 degrees out of phase with each other (Bulheller & Hirst, 2009). Asymmetric molecules absorb right- and left-handed circularly polarised light to different extents, as well diffract the waves by different indices. This results in a rotated plane of the light wave and the R and L vectors trace an ellipse. The light is therefore said to elliptically polarised (Greenfield, 2006).

As a protein folds into its secondary structure, the chromophores of amides in the polypeptide backbone are specifically arranged and their optical transitions are shifted as a result of exciton interactions (Sreerama & Woody, 2004). This means each secondary structure has its own characteristic spectra. Table 2.1 provides the signal wavelength for each secondary conformation (Martin & Schilstra, 2008).

Conformation	**Minima (nm)**	**Maxima (nm)**
Random Coil	-195 to -200	
α-helical	-222 -208	+193
β-sheet	-218	+195

Table 2. 1. CD minima and maxima of each secondary structure conformation (Greenfield, 2006)

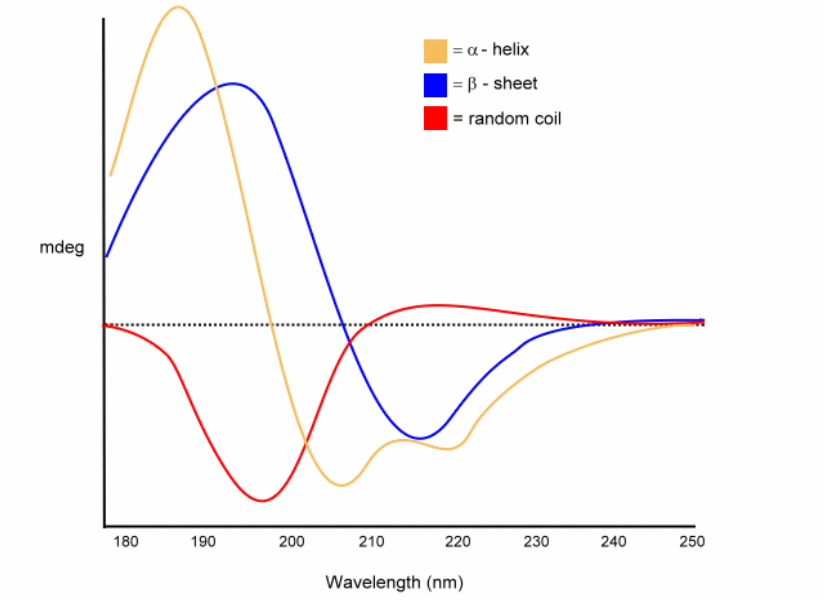

Figure 2. 2. CD spectra for α-helix, β-sheet and random coil secondary structure conformation. Taken from www.proteinchemist.com

Usually, the secondary structure of proteins is measured in the far-UV region, (180-250nm), where the peptide bonds are measured. Near-UV CD of proteins (310-255nm) reflect the tertiary structure of proteins due to Trp, Tyr, Phe and Cys residues. However, a number of amino acid side chains absorb in the far-UV regions too, including Try, Trp, Phe, His and Met (Martin & Schilstra, 2008) .

The α-helix -222nm arises from the n →π* and the -208nm and +195nm is due to the splitting of the π →π* transition where the 208nm represents the polarised component parallel to the helix and the 195nm represents the perpendicular component. The positive and negative peaks for the β-sheet signal arise from the π →π* and n →π* transition respectively (Bulheller & Hirst, 2009). The n →π* transition is of lower energy and intensity and is polarised along the carbonyl bond. The π →π* transition has a higher energy and intensity and is polarised between the oxygen and nitrogen (Figure 2.2).

2.1.5 Thioflavin T (ThT) fluorescence

Thioflavin T is an amyloid binding dye first identified in 1959 (Vassar & Culling, 1959). Much characterisation of ThT specificity for amyloid has been carried out and the significant increase in

fluorescence is attributed to the red shift upon binding to amyloid (Groenning, 2010). A strong ThT fluorescence signal at ~483nm is seen when excited at 450nm (Xue et al., 2017).

The mechanism of ThT fluorescence is thought to be due to the central C-C bond connecting the benzothiazole and benzylamine rings (Xue et al., 2017). A vast amount of evidence suggests that ThT behaves as a 'molecular rotor'; the C-C bonds allow the ThT benzothiazole and benzylamine rings to rotate freely (Biancalana et al., 2009) which quenches excited states causing low fluorescence. Binding to amyloid 'locks' the dye and immobilizes the rotation of the benzothiazole and benzylamine rings. This keeps ThT in its excited state and results in an increased fluorescence (Biancalana et al., 2009).

The binding mechanism of ThT still remains unclear, however as the dye binds to amyloid fibrils of differing primary sequence, it is a structural feature that is most likely recognised by ThT. Conformationally, it is thought that unbound ThT preferentially remains in a non-planar conformation. There are two proposed conformations of ThT when bound to amyloid; it is thought to remain planar (Krebs et al., 2005; Lindgren et al., 2005) or significantly twisted (Biancalana et al., 2009; Dzwolak & Pecul, 2005).

The cross-β structure of amyloid fibrils gives rise to cross-strand ladder arrangement of side chains. These side chains have been shown to from channel-like motifs in which linear dyes, such as ThT, could bind (Biancalana et al., 2009). Using polarised fluorescence microscopy, it has been observed that the long axis of ThT is aligned in a parallel orientation to the fibre axis (Krebs et al., 2005). Another suggested mechanism for ThT binding to amyloid, is via hydrophobic interactions with ThT micelles formed at concentration higher than 4μM in water (Khurana et al., 2005). Building on this, ThT may bind to large hydrophobic regions on amyloid proteins as excited dimers, termed as 'excimers' (Groenning et al., 2007). Both these theories, however, do not take into account the preferential parallel binding along the fibre axis.

2.2 Methods relating to chapters 3-6

Unless stated otherwise, data presented in the results chapters are the average of three independent repeats.

2.2.1 Identification of amyloidogenic regions

The WALTZ algorithm (http://waltz.switchlab.org) was used to identify amyloidogenic regions for Aβ42, Aβ42-1 and AβS peptides. The primary sequence of each peptide was input in FASTA format into the WALTZ algorithm at pH 7. Data was output as a text file and replotted using R Studio. The algorithm was also used to explore the effects of amino acid substitutions within the two amyloidogenic regions of Aβ42 sequence, in order to abolish amyloidogenicity. There were several substitutions identified at positions 19 and 37 as reducing amyloidogenicity and two were selected based on previous assembly studies; F19S and G37D. This variant Aβ42 sequence will be referred to as vAβ42.

2.2.2 Preparation of Aβ42 and primary sequence variant peptides

Recombinant Aβ42 was purchased from rPeptide as 1,1,1,3,3,3-Hexafluoro-2-propanol (HFIP) films. Aβ42-1 and AβS were purchased from Bachem in powder form and vAβ was purchased from JPT. 0.2mg aliquots of peptide were solubilised in 200µl HFIP (Sigma-Aldrich) to disaggregate any preformed aggregates. The solution was then vortexed for 1 minute and sonicated in a 50/60Hz bath sonicator for 5 minutes. The HFIP was then dried off using a steady flow of nitrogen gas. 200µl of anhydrous dimethyl sulfoxide (DMSO) (Sigma-Aldrich) was then added and vortexed for 1 minute. The solution was then sonicated for 1 minute and then put through a buffer equilibrated 7K MWCO Zeba buffer-exchange column (Thermo Scientific) at 4°C. The protein solution was then kept on ice whilst the absorbance at 280nm was measured using a NanoDrop spectrophotometer. The concentration was calculated using the molecular coefficient of 1490 $M^{-1}cm^{-1}$; (A280/1490) x1000 x 1000. Solutions were immediately diluted to 50µM in buffer and this was taken to be the new working stock. The solution was incubated at room temperature for 2 hours for AβO and incubated at room

temperature for 48 hours for AβF. For AβSon, the solution was incubated at room temperature for 48 hours and then sonicated for 10 minutes on ice.

Solutions were prepared in either HEPES buffer (10mM HEPES, 50mM NaCl, 1.6mM KCl, 2mM MgCl and 3.5mM CaCl2) or in 20mM Phosphate buffer (200mM Na_2HPO_4, 200mM NaH_2PO_4, diluted to 20mM with ddH_2O), both at pH 7.4.

2.2.3 Preparation of Alexa Fluor 488-conjugated Aβ

Aβ42 was prepared as described above (Section 2.2.2), up to the addition of DMSO. As per the manufacturer's instructions (Life Technologies), the Alexa Fluor 488 tag was prepared by adding 10µl H_2O to the Alexa Fluor TFP ester (kept on ice). This was added to the Aβ42 in DMSO with 10µl 1M sodium bicarbonate (pH 8.3), mixed for incubated at room temperature for 15 minutes. From this step onwards, the sample was protected from light using aluminium foil. After this, the usual Aβ preparation method continued with the Zeba buffer exchange column. To take into account the absorbance of the dye, the following calculation was used for the concentration of the 488-tagged Aβ42 preparation:

Protein concentration (M) = [A280 – (A494 x 0.11)]/ 1490

For 488-AβO, the preparation was incubated for 2 hours at room temperature before being added to cells. The preparation was incubated for 48 hours at room temperature for 488-AβF and for 488-AβSon, the preparation was incubated for 48 hours at room temperature and sonicated on ice for 10 minutes.

The labelling efficiency was not measured for this preparation of Alexa Fluor tagged-Aβ as it was assumed any unbound dye would be removed by the buffer exchanged column. It was also assumed that the final concentration of Aβ42 measured was all labelled with the dye. However, it would beneficial to investigate the labelling efficiency in the future to ensure the same level of labelling was being achieved in each preparation and gain a better understanding the labelling process.

The labelled peptide was only used for live cell imaging experiments. All structural characterisation, cell viability and immunocytochemistry experiments were conducted on untagged peptide.

2.2.4 Preparation of functional amyloid peptides

Both functional amyloid proteins were prepared at 1mg/ml in the appropriate buffer/ddH_2O for experimentation. Due to the amyloidogenicity of both peptides, an accurate absorbance at 280nm was not possible. Using the molecular weight of GNNQQNY (836.81 Da) a stock concentration of 1.12mM was calculated. For FEFKFEFKK (1249.47 Da) the stock concentration was calculated to be 800.33µm.

Solutions were prepared in either HEPES buffer (10mM HEPES, 50mM NaCl, 1.6mM KCl, 2mM MgCl and 3.5mM CaCl2) or in 20mM Phosphate buffer (200mM Na_2HPO_4, 200mM NaH_2PO_4, diluted to 20mM with ddH_2O), both at pH 7.4.

2.2.5 Transmission Electron Microscopy

Aliquots of peptide samples, prepared as described above, were taken at progressive time points to monitor changes in morphology. 4µl of peptide was applied on the surface of Formvar/Carbon film coated 400 mesh copper grids (Agar Scientific) and allowed to absorb for 2 minutes before being blotted dry. The grid was then washed with 4µl of milliQ-filtered water and blotted dry. The grid was negatively stained using 2% (w/v) uranyl acetate for 2 minutes blotted and dried. This was repeated once more, and the grid was left to air dry before being imaged. All grids were examined and imaged using a JEOL JEM1400-Plus TEM at 120 kV and images were captured using a Gatan OneView 4K camera (Abingdon, UK). FIJI software was used to measure the length of oligomers and sonicated fibrils; three images from three independent preparations were measured.

2.2.6 Circular Dichroism

Aliquots of peptide samples (prepared in 20mM phosphate buffer, pH 7.4) were taken at progressive time points and placed in a 1mm path length quartz cuvette (Hellma) for Aβ42, vAβ and Aβ42-1. A

0.5mm (Hellma) cuvette was used for AβS. For both GNNQQNY and FEFKFEFKK were prepared in water, a 0.1mm cuvette was used. Scans were taken between 180-280nm on a JASCO J715 Spectropolarimeter at 20°C. Three spectra were averaged for each measurement. Spectral data were converted to molar ellipticity using the following equation: Mdeg x Molecular Weight / (10 x $mg \cdot ml^{-1}$ x pathlength of cuvette x number of amino acids).

2.2.7 Thioflavin T fluorescence

As a measure of fibrillogenesis, the fluorescence of 10μM ThT in 50μM peptide was measured in a quartz 10mm cuvette. Aliquots of each peptide were taken at time points corresponding those for EM and CD. An emission scan between 460-600nm was performed in a Varian Cary Eclipse Fluorescence Spectrophotometer at a scan rate of 600nm/min and three spectra were averaged for each measurement. The sample compartment was kept at 21°C.

2.2.8 X-Ray Fibre Diffraction

X-Ray fibre diffraction (XRFD) patterns of partially aligned fibres formed by Aβ42-1 and AβS in water were obtained by Louise Serpell (Vadukul et al., 2017). XRFD patterns for aligned F9 fibres in 20mM Phosphate buffer, washed three times with water and 10 minutes centrifugation at max speed, were obtained by Youssra Al-Hilaly. Briefly, 10μl droplets of each peptide were suspended between two wax-tipped 1.2mm O.D, 0.94mm I.D borosilicate capillaries (Harvard apparatus). These were incubated for 24 hours at room temperature in a parafilm sealed petri dish. X-ray diffraction patters were obtained using a Rigaku 007HFcuKa (λ 1.5419 Å) rotating anode generator with a Saturn 944+ CCD detector. Exposure times of 10–120 seconds were used with specimen to detector distances of 50 or 100 mm. The images were displayed and examined using Mosflm.

2.2.9 NMR

NMR studies were conducted by Dr Iain Day. vAβ was prepared as described above at a concentration of 200μM in 10% v/v D_2O standard. ^1H NMR spectra were acquired every 30 minutes over a period of 66 hours (128 scans, 599.6MHz ^1H frequency). The double pulsed field gradient spin

echo method provided solvent suppression and the temperature was regulated at 25°C. The spectra were processed with 1.5Hz line broadening, base line correction and Fourier transformation (Marshall et al., 2016).

2.2.10 Dot blotting

The primary antibodies 4G8 and 6E10 were purchased from Biolegend, A11 from Thermo Fisher and NU1 was kindly gifted to us from William Klein Lab (Lambert et al., 2007). The epitopes of each antibody are shown in Table 2.2. The anti-mouse and anti-rabbit HRP conjugated secondary antibodies were purchased from Cell Signaling and Promega respectively.

Antibody	Epitope
NU1	**Conformational antibody specific to oligomers (Lambert et al., 2007)**
A11	**Conformational antibody specific to oligomers (Kayed et al., 2003)**
6E10	DA**EFRHDS**GYEVHHQKLVFFAEDVGSNKGAIIGLMVGGVVIA
4G8	DAEFRHDSGYEVHHQKL**VFFAE**DVGSNKGAIIGLMVGGVVIA

Table 2. 2. Conformation-specific and anti-Aβ antibodies and their epitopes (red)

Dot blotting was not possible for Aβ42-1, AβS, GNNQQNY and FEFKFEFKK as these do not have recognisable epitopes for our available antibodies.

5µl aliquots of Aβ42 and vAβ were taken at progressive time points over a 7-day time period and spotted onto a 0.45µm nitrocellulose membrane and allowed to dry. The membrane was boiled with PBS for three minutes twice before being incubated in blocking buffer (10% Milk in 0.1% TBS-Tween(T)) for 1 hour at room temperature. The blocking buffer was then replaced with primary antibody (NU1, 6E10 and 4G8 at a 1: 10,000 dilution. A11 at a 1:5000 dilution) and incubated overnight at 4°C. The membrane was washed three times with 0.1% TBS-T for 10 minutes per wash before being incubated with HRP conjugated secondary antibody (anti-mouse for NU1, 6E10 and 4G8

at a 1: 10,000 dilution. Anti-Rabbit for A11 at a 1:5000 dilution) for 30 minutes at room temperature. Following another set of washes, the membrane was incubated with Enhanced Chemiluminescence (ECL) substrate (Bio-Rad) for three minutes before being developed on CL-Exposure Film (Thermo Fisher).

2.2.11 Western Blotting and Immunoprecipitation

Western blotting was not possible for Aβ42-1, AβS, GNNQQNY and FEFKFEFKK as these do not have recognisable epitopes for our available antibodies.

2μg of Aβ42 and vAβ peptide in 4 x Laemelli Sample Buffer (Bio-Rad) containing 1:10 β-mercaptoethanol (BME) were loaded on a 50μl 10 well 4-20% Mini-PROTEAN TGX Stain-Free gel (Bio-Rad). The gel was run in 1X running buffer (diluted from 10X Tris/Glycine/SDS stock, Bio-Rad) at 100V. The gel was then transferred on to 0.45μm nitrocellulose membrane in 1X transfer buffer (diluted from 10X Tris/Glycine stock, Bio-Rad) for 2 hours at 25V. The membrane was incubated with blocking buffer (10% Milk in 0.1% TBS-T) at room temperature for 1 hour after which the 6E10 primary antibody (1: 10,000 dilution in blocking buffer) was applied for overnight at 4°C. The membrane was the washed three time with 0.1% TBS-T for 10 minutes per wash after which the membrane was incubated with HRP conjugated anti-mouse secondary antibody (1:10,000 dilution in blocking buffer) for 30 minutes at room temperature. The membrane was washed again three times with 0.1% TBS-T before being incubated with ECL substrate for 5 minutes. The membrane was then developed on CL-Exposure Film.

For immunoprecipitation, cells were incubated with 10μM Aβ for the required amount of time after which the media was replaced with fresh, Aβ-free media. The media removed, was kept at -80°C until ready to use. The cells were incubated for 7 days after which the new media was removed, and cells were lysed using RIPA buffer (Thermo Fisher) supplemented with phosphatase and protease inhibitors (1:100 dilution). The cell lysate was then collected in an Eppendorf tube and kept at 4°C for 20 minutes after which it was centrifuged at max speed at 4°C for 15 minutes. DynaBeads Protein G (Thermo Fisher) were coated in 4G8 antibody (10μg/ml) overnight at 4°C. The beads were then

placed on a magnet and the antibody was removed. The media removed and cell lysate samples were added to the beads and shaken at 800rpm for 45 minutes at room temperature. The samples were again placed on the magnet following this and the supernatant was discarded. The beads were washed three times with 0.025% PBS/Tween. For elution, 20µl of 50mM glycine (in H_2O) and 10µl 4x Laemelli Buffer containing 1:10 BME was added to the beads and boiled at 80°C for 10minutes. The samples were placed on to the magnets once more and everything except the beads were loaded on to the gels. Western blotting was then carried out as described above using the 4G8 primary antibody (1:10,000) and an anti-mouse HRP conjugated secondary antibody (1: 10,000).

2.2.12 Cell Culture

Rats are housed in a specialised facility under Home office guidelines and sacrificed using Schedule 1 procedures in accordance with Animals (Scientific Procedures) Act 1986, Amendment Regulations 2012. Primary hippocampal cultures were prepared from either P0 or P1 rats. Initially, the hippocampus was dissected in ice cold Hanks' Balanced Salt Solution (HBSS) containing 0.1M HEPES. It was then washed in pre-warmed Basal Medium Eagle (BME) (Gibco) containing 0.5% glucose, 2% FCS, 1mM Na-Pyruvate, 0.01M HEPES (pH 7.35), Penicillin-Streptomycin, 1% B27 supplement and 1% Glutamax. The hippocampus was then titrated using a 1ml pipette until the tissue was fully dissociated and then finally diluted further with the BME supplemented media. Approximately 40,000 cells were plated on Poly-D-Lysine (20µg·mL^{-1}) and Laminin (20µg·mL^{-1}) pre-coated coverslips and incubated at 37°C and 5% CO_2. After 3-5days incubation, the cells were treated with 3.25µM cytosine arabinoside to stop astrocyte proliferation. Cells were used for experiments, 10-14 days after plating.

2.2.13 Cell viability assay: ReadyProbes

All peptides were prepared in 10mM HEPES as described. Aβ peptides were incubated at room temperature for 2 hours before being added to rat primary hippocampal cultures at a final concentration of 10µM. GNNQQNY and FEFKFEFKK were added immediately after preparation at the same concentration. After incubation with the peptide for the required amount of time, one drop of

each Readprobes reagent (Life Technologies) was added to the wells. The NucBlue live reagent (excitation/emission at 360 and 460nm respectively) stains the nuclei of all cells. The NucGreen dead reagent (excitation/emission at 504 and 523nm respectively) stains only the nuclei of dead cells with compromised plasma membranes. Cells were incubated for 15 minutes with the reagents and then imaged using a Zeiss CO widefield microscope using the DAPI and FITC filters. 4-6 regions of interest were imaged per well and the percentage of dead cells were calculated as the number of green cells in the entire DAPI stained population. Astrocytes in the cultures were not counted. Cells were counted using the cell counter plug-in and astrocytes were excluded in the counting. The experiment was repeated 3 independent times.

To assess whether the AβO internalisation is necessary to mediate cytotoxicity, cells were treated with 10μM AβO for increasing lengths of time before being replaced with fresh, Aβ-free media. Cells were incubated for a total of 7 days before using the ReadyProbes assay to assess the measure of cytotoxicity.

2.2.14 Immunofluorescent labelling and confocal microscopy

The goat anti-mouse 488- and 555-Alexa Fluor conjugated secondary antibodies were purchased from Invitrogen.

Primary hippocampal cells were treated with the peptide as desired for the required time before removing the media and immediately fixing the cells with 2% paraformaldehyde for 15 minutes. This was then washed with wash buffer (25% Superblock (Thermo Fisher) in PBS) and cells were permeabilised with 0.3% Triton-X 100 for 10 minutes. 50μM glycine (in PBS) was then added to block unreacted aldehydes. Cells were then blocked with undiluted Superblock for 30 minutes, after which the 4G8 primary antibody (1:500 dilution in wash buffer) was incubated with the cells for 1-hour at room temperature. Following this a set of three washes for 5 minutes each using wash buffer were carried out. Alexa Fluor 555 conjugated goat anti-mouse secondary antibody (1:500 dilution in wash buffer) was incubated with the cells for 1-hour followed by another set of washes. The coverslips were mounted in ProLong Gold (Life Technologies) and cured for 2 days before imaging.

Cell were imaged using a 63x1.2NA objective on a Leica SP8 confocal microscope. Emissions were collected using a 561nm emission laser line between 555-650nm on a PMT detector. Samples were imaged in a sequential manner.

2.2.15 Live cell imaging

Aβ42 peptide was prepared with a 488 Alexa Fluor tag as described above (Section 2.2.3). Primary hippocampal neurons were plated on a PDL and Laminin coated 35mm glass bottom dish treated with 3.25μM cytosine arabinoside after 3-5days of incubation to stop astrocyte proliferation. Cells were used for experiments 10-14 days after plating. The tagged 488-Aβ peptide was added to cells and 6 regions of interest were imaged every 20 minutes for 15 hours on a Leica SP8 confocal microscope. Cells were maintained at 37°C and 5% CO_2 for the duration of imaging. Cell were imaged using a 63 x 1.2 NA oil objective and emissions were collected using a 488nm excitation laser line between 495 and 540nm on a PMT detector. The FIJI software was used to string together images from the middle of the Z-stack at each time point and produce a live cell imaging AVI video.

Chapter 3: Characterising the assembly and toxicity of the disease-related Aβ42 amyloid protein

Chapter Overview

Aβ42 deposits as extracellular plaques in Alzheimer's disease and is one of the key pathological hallmarks of the disease. The production of this amyloid protein, misfolding and subsequent self-assembly has been the focus of many studies. Using a highly reliable and reproducible method of sample preparation, this chapter presents an extensive characterisation of Aβ42 self-assembly using several biophysical techniques. These include transmission electron microscopy (TEM), circular dichroism (CD) and Thioflavin T (ThT) fluorescence. This has been combined with conformation specific and anti-Aβ antibodies to identify assemblies present over a 7-day period using dot and western blotting. The toxicity of the oligomeric species has been assessed using a ReadyProbes assay.

3.1 Introduction

The enzymatic cleavage of Aβ is normally secreted as a peptide of between 39-40 amino acids in length (Selkoe, 1994). In AD, however, there is an increase in the secretion of the longer 42 amino acids. The additional two amino acids at the C-terminal of the Aβ means a higher propensity to self-assemble into amyloid, possibly due to hydrophobicity, highlighting the importance of primary sequence in amyloidogenicity (Burdick et al., 1992). This, however, does not mean Aβ40 cannot form amyloid; extensive studies have established the formation of amyloid by Aβ40 (Lomakin et al., 1996; Schmidt et al., 2009; Villmow et al., 2016). In fact, the characteristic plaques deposited in AD are composed of both Aβ40 and Aβ42 (Fukumoto et al., 1996). The fibrillar species of Aβ42 was previously thought to be a causative factor of neurodegeneration, however, as there was a weak correlation seen with cognitive decline in relation to the amyloid plaque deposition (McLean et al., 1999), this has since been revised. There are, in fact, arguments for the protective role of Aβ42 fibrils as the formation of these sequester available oligomers from the local environment and therefore limit their toxicity (Castellani et al., 2009).

The oligomeric species of Aβ has been identified as being neurotoxic due to the strong correlation between the concentration of soluble Aβ and cognitive decline (McLean et al., 1999). The oligomers of Aβ42 have been shown to be more detrimental than Aβ40 (Bitan et al., 2003; El-Agnaf et al., 2000; Ono et al., 2009); the work presented in this chapter will solely concentrate on the structural characterisation and toxicity of Aβ42.

The assembly of Aβ42 follows a general pathway from monomers, oligomers, protofibrils and fibrils (Figure 3.1).

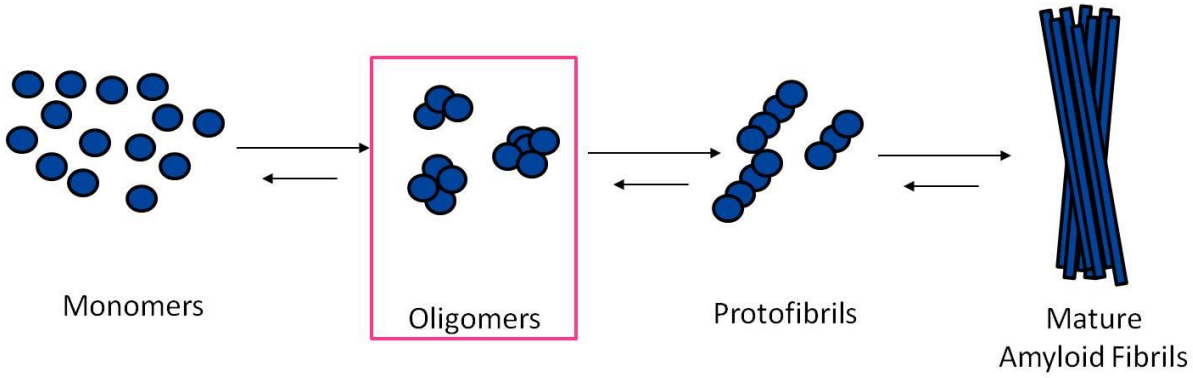

Figure 3. 1. Schematic representation of Aβ42 assembly. Aβ42 assembles from soluble monomers to oligomers (the toxic species, pink box), to protofibrils and finally insoluble mature amyloid fibrils. This is a dynamic process.

The formation of the oligomeric intermediary species in the pathway to amyloid fibrils, is nucleation dependent (Ferrone, 1999; Lomakin et al., 1996; Xue et al., 2008). The nucleation phase is the stage at which the monomer undergoes unfavourable self-association and forms a nucleus to facilitate the formation of fibrils. There is also thought to be a process of secondary nucleation whereby the surface of fibrils act as a catalyst on which monomers can bind and form new nuclei for fibril formation (Cohen et al., 2013; Linse, 2017).

The preparation of Aβ42 in vitro, differs greatly from one research group to another. This poses a problem of reproducibility, sometimes even within a research group, as different species of Aβ42 are produced. The species used in experiments are often not characterised which offers an explanation as to why there may be a lack of reproducibility and contradictory results; fibrillar Aβ42 will not exert

the same effects as Aβ42 oligomers (Kim et al., 2003). Moreover, due to the lack of a definitive definition, the term 'oligomer' covers a large range of sizes and this has led to arguments for different sizes being more or less toxic than others (Table 3.2) (Benilova et al., 2012; Larson & Lesne, 2012). Finally, as the sample population is always heterogeneous, the concentration of a particular species can vary greatly from one preparation to the next. Therefore, the oligomeric or fibrillar concentration being used in experiments may be inaccurately measured.

To overcome this problem, we have established a preparation method that allows for reproducible and reliable sample preparation. After extensive characterisation over a 7-day period, we can confidently identify the species most prevalent in the population in vitro, at each time point following preparation and confirm the oligomeric species to be deleterious to cellular function.

3.2 Aβ42 controlled assembly: overcoming factors affecting self-assembly

There are several factors that affect the assembly process of Aβ; some examples are shown in Figure 3.2. The way in which these factors affect the aggregation of Aβ are discussed below.

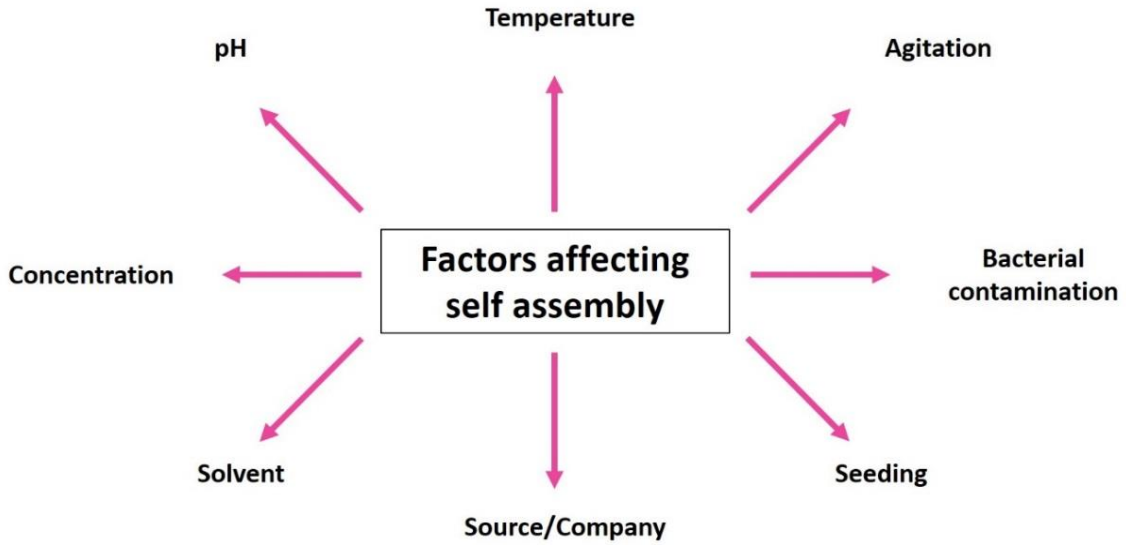

Figure 3. 2. Several factors affecting the self-assembly of amyloid proteins.

3.2.1 The effect of pH

Physiologically, Aβ has been found in low pH organelles such as late endosomes (pH 4.9-6) (Huotari & Helenius, 2011) and lysosomes (Broersen et al., 2011; Selkoe, 1994; Wood et al., 1996), and it is known that acidic pH promotes the formation of amyloid fibrils (Burdick et al., 1992; Su & Chang, 2001; Wood et al., 1996).

Studies investigating fibril formation of various Aβ fragments over the range of pH 3-10, revealed that fibril assembly and disassembly was a function of pH. Table 3.1 summarises the main findings of a study using varying lengths of the first 28 residues in the Aβ sequence, to determine the effect of pH on assembly (Fraser et al., 1991). Specific residues necessary for electrostatic and hydrophobic interactions critical for fibril formation were also identified (Fraser et al., 1991). The findings of this study reveal that fibrils are only formed between pH 3-8, suggesting the requirement of the His imidazole and the Asp/Glu carboxylic acid side chains ionisation. This is due to the pKa values of these groups in this pH range; pKa 6.6 for His imidazole and pKa 3 for the carboxyl acid side chains of Asp and Glu. Maintaining these respective positive and negative charges is optimal for fibril formation.

The same study highlighted the hydrophobic interactions between Leu17 and Ala21, therefore it was proposed during the self-assembly process, these electrostatic and hydrophobic interactions gives rise to an inter-sheet core which stabilises an anti-parallel arrangement of β-strands by residues 13-23 (Fraser et al., 1991). This was later confirmed by NMR studies which identified a hydrophobic cluster at residues 17-21 (Hilbich et al., 1991)

Truncating the first 16 residues has shown to drastically affect fibril stability (Brannstrom et al., 2017). As all three histidines of the Aβ sequence are found within this region, the importance of these residues has not been overlooked. Using Surface Plasmon Resonance (SPR) to monitor the rate at which a monomer is incorporated onto a fibril and how long it is bound for, it is possible to monitor fibril stability. Single mutations of each of the histidines for alanine, as well a variant replacing every His for Ala, showed that stability was only affected at a certain pH. Lowering the pH from 7.4 to 5.5,

resulted in a 200-fold increase in fibril stability for each alanine variant, suggesting that the histidines only play a role in fibril stability at a neutral pH (Brannstrom et al., 2017). This suggests that although histidines play an important role in fibril stability, the protonation of their side chains is not critical in enhancing fibril stability as a function of pH (Brannstrom et al., 2017). Lowering the pH, has in fact been thought to facilitate fibril stability by a gain of function allowing a more rapid addition of monomers to fibrils (Brannstrom et al., 2014).

Peptide	pH	Morphology
β(1-28)	Low (<3)	Fibril fragments
	Mid (3-7.5)	Amyloid fibrils
	High (>8)	No fibrils
β(9-28), β(11-28), β(13-28)	Low (<3)	Small fibrils
	Mid-High (3-9)	Amyloid fibrils
	High (10)	No fibrils
β(15-28)	Low (<3)	Ribbons
	Mid-High (3-9)	Ribbons and Amyloid fibrils
	High (10)	No fibrils
β(17-28)	Low (<3)	Ribbons
	Mid-High (3-9)	Ribbon fragments
	High (10)	No fibrils
β(19-28)	<3	Amyloid-like fibrils
	>3	No fibrils

Table 3. 1.Morphologies of amyloid fibres produced from various Aβ fragments at different pH. Adapted from Fraser et al, 1991.

More recent work has shown that the histidines may actually cause inhibition of fibril formation at a lower pH range due to the positively charged residues repelling each other in fibril forming structures. H6A, H13A and H14A mutants were monitored and it was revealed that while H6 does not affect fibril formation, H13 and H14 must be simultaneously protonated to inhibit fibril formation (Tiiman et al., 2015). It is likely, however, that the formation of fibrils is dependent on at least one His-Asp/Glu salt bridge (Fraser et al., 1991). This suggests that although a lower pH could result in promoting the stability of fibrils, it may not enhance the rate of fibril formation.

Although these studies are extremely important to understand the effect of pH on amyloid assembly, many did not consider the preparation of peptides (with the exception of Fraser et al, who pre-treated

fragments with trifluoroacetic acid) (Fraser et al., 1991) . The results presented may be based on pre-assembled structures rather than structures formed during assembly.

pH is also thought to play an important role in the solubility of the peptide; the pH range at which the peptide is deposited may be due to the isoelectric point when the net charge is close to zero (Burdick et al., 1992). Aβ42 is considerably insoluble at a physiological pH due to the increased length of the hydrophobic C-terminal and is even more insoluble at a lower pH of 5 (Barrow & Zagorski, 1991).

As previously mentioned, the formation of amyloid fibrils is a nucleation event which is concentration dependent. If the concentration of monomers is not high enough to form the nucleus for further addition of monomers, fibril formation does not occur. It has been shown by two groups that at a neutral pH, this critical concentration is ~100nM (Brannstrom et al., 2017; Hasegawa et al., 2002). This critical concentration is dramatically reduced, as much as 120 times, when the pH is lowered; another explanation for the formation of Aβ localised to acidic intracellular organelles such as endosomes and lysosomes (Brannstrom et al., 2017). This lowered critical concentration due to more acidic environment, also explains how there can be amyloid formation when the physiological extracellular Aβ concentration is only ~1nM (Jarrett et al., 1993).

As one of our aims is to establish a protocol allowing for a 'controlled' assembly of Aβ, an acidic environment that would promote fibril formation and stability would not be favourable. Moreover, for an Aβ42 preparation that is physiologically relevant and can be used without disrupting optimal cell culture conditions, using only buffers at pH of 7.4 was selected for our protocol.

3.2.2 Solvents and seeding

The solvent used during the preparation of Aβ42 plays a critical role in the assembly process. As Aβ is often difficult to dissolve into physiologically relevant buffers, it is often first diluted into a solvent. Some common examples include DMSO, trifluoroacetic acid (TFA) and a mixture of TFA and acetonitrile (ACN) (Shen & Murphy, 1995). The solvent is thought to contribute to the toxicity observed with Aβ; for example neuronal death was most prominent if Aβ was first dissolved in ACN,

less prominent if first dissolved in DMSO and least toxic if first dissolved in water (Busciglio et al., 1992; Shen & Murphy, 1995). This may be due to different solvents promoting different structures and aggregation states.

The effect of various solvents on Aβ aggregation has been previously demonstrated. For example, if the peptide is dissolved in DMSO, there is no β-sheet content detected (Shen & Murphy, 1995). This is thought to be due to the DMSO competing with the peptide carbonyl group for hydrogen bonding with the peptide amine groups (Shen & Murphy, 1995). In this way, DMSO destabilises the secondary structure. Although it has been shown that Aβ prepared in DMSO does form fibrillar species, it is 100-fold more toxic than Aβ prepared in water (Zagorski et al., 1999). This is thought to be due to the slower assembly of Aβ in DMSO than in water (Mattson et al., 1992).

One important reason for using solvents to dissolve Aβ, is to completely disaggregate any preformed aggregates and encourage a homogenous population of monomeric, unstructured peptide. This is due to preformed aggregates seeding further assemblies; introducing seeds can by-pass the lag phase of Aβ assembly completely by rapid secondary nucleation (Knowles et al., 2009; Xue et al., 2008). As the lag phase is an important step in the formation of the oligomeric species, it is extremely important that any seeds are removed.

HFIP is the most commonly used organic solvent for amyloid preparation; a few examples are for Aβ preparations (Hilbich et al., 1991; Snyder et al., 1994; Wood et al., 1996), prion proteins (Gasset et al., 1992; Harrison et al., 1997) and IAPP preparations (Higham et al., 2000). Alcohols are often used as solvents; alkyl alcohols (or alkanols) are more effective in denaturing proteins than those with smaller alkyl groups which indicates the importance of the hydrophobic interactions in the denaturation process. Alcohols achieve this by weakening the nonlocal hydrophobic interactions and encouraging polar interactions of proteins (Thomas & Dill, 1993). The denaturing properties of HFIP are, however, limited. For example, HFIP was not found to be effective in dissolving β2-microglobulin fibrils suggesting that although the non-polar nature of the alcohol can weaken

hydrophobic interactions, it cannot dissolve mature, rigid fibrils (Broersen et al., 2011; Hirota-Nakaoka et al., 2003).

For this reason, an Aβ42 preparation where complete disaggregation (or as near to complete as possible) is critical, an extra step after HFIP solubilisation is necessary to ensure this. For this, DMSO is often used due to its polar nature and ability to abolish hydrogen bond networks.

3.2.3 Temperature, Agitation and Concentration

Temperature is another factor affecting the self-assembly process of Aβ. It has been well understood that the Aβ aggregation kinetics are enhanced as temperature is increased (Kusumoto et al., 1998). An effect of temperature has been shown with Aβ40, Figure 3.3A (Lin et al., 2008). This shows the different rates of fibrillogenesis at temperatures ranging from 30-45°C, the rate of fibrillogenesis increases with temperature. In a protocol where we need to monitor assembly at early time points, a low temperature is essential in ensuring minimal fibril formation during the preparation process.

Concentration is another factor that can drastically affect the lag phase of the assembly process (Hellstrand et al., 2010). Figure 3.3B shows there is a decrease in the lag time as the concentration increases. This means that fibrils are formed more rapidly at higher concentrations, and at a high enough concentration could even by-pass the formation of oligomeric species. The electron micrographs in Figure 3.3C and 3.3D demonstrate the importance of concentration in fibril formation. There are very few fibrils seen after 24 hours at 30μM and abundant fibrils seen at 24 hours at a concentration of 200μM.

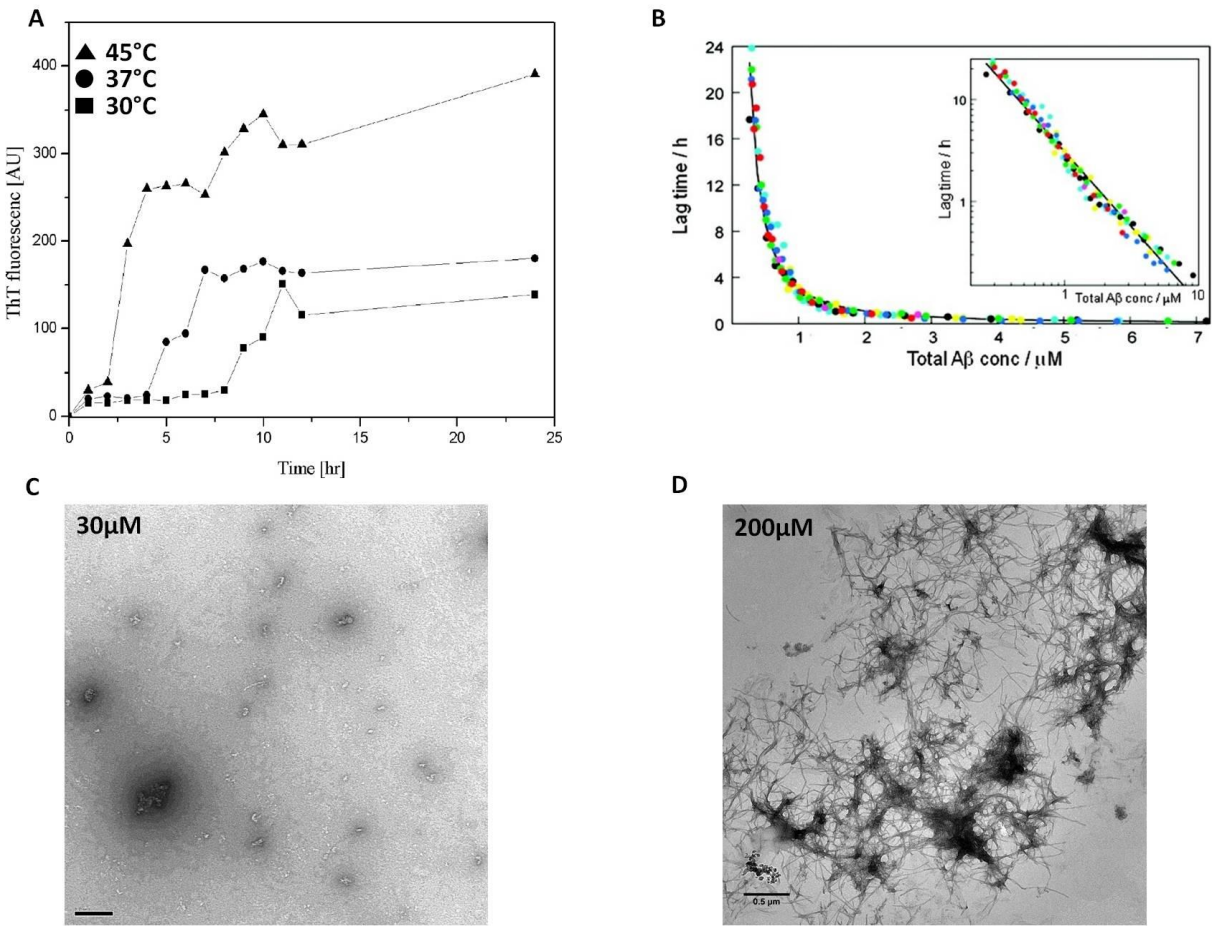

Figure 3. 3. The effects of temperature and concentration on amyloid assembly. A) The effect of temperature on the fibrillogenesis of Aβ1-40 measured by ThT fluorescence. As the temperature increases, rate of fibrillogenesis also increases and there is a reduction in the lag phase. Taken from Lin et al, 2008. B) The effect of concentration on the lag phase of Aβ. As the concentration is increased, the lag phase decreases, suggesting a more rapid formation of fibrils. Taken from Hellstrand et al, 2010. C) Electron micrograph of Aβ42 prepared at 30 µM and D) 200µM (prepared in 10mM HEPES buffer pH 7.4) at 24 hours. Few/no fibrils are seen at 30µM whereas at a higher concentration of 200µM, fibrils are abundant. Scale bar shown at 0.5µm.

It is thought that agitation also enhances aggregation due to fragmentation of existing fibrils and increasing sites for further fibril formation via secondary nucleation (Tiiman et al., 2013). It has also been suggested that agitation may lead to the formation of bubbles in the sample, which burst and can generate of hydroxyl and hydrogen radicals which induce further aggregation (Mahler et al., 2009).

These factors have all been taken into consideration in our preparation method to ensure a consistent and reliable Aβ42 sample

3.3 Results and Discussion

3.3.1 The development of a highly consistent Aβ42 preparation protocol

For reproducibility and reliability of experiments with Aβ42, it is important to characterise the species being used. As with all amyloid proteins, Aβ42 undergoes self-assembly and forms fibrils which display the characteristic cross-β structure detected by X-ray fibre diffraction (XRFD) (Serpell, 2000). The assembly process from monomer to mature fibrils (Figure 3.4) involves the formation of the toxic oligomeric intermediary species. One difficulty of working with the Aβ42 peptide has been a sample preparation that follows this assembly from monomers/oligomers into mature fibrils within a reasonable time frame. Without a protocol that controls for the several factors affecting self-assembly, every sample preparation composition in terms of the species most prevalent, will differ greatly. It would be unexpected that the results of experiments where Aβ42 is predominantly oligomeric, would be the same as that of a preparation that is predominantly fibrillar.

By controlling factors such as seeding, pH, temperature and concentration, it is possible to ensure a sample preparation that allows us to follow self-assembly within a 7-day period and also identify which species are most prevalent at each time point. Below is a summary of our optimised preparation protocol.

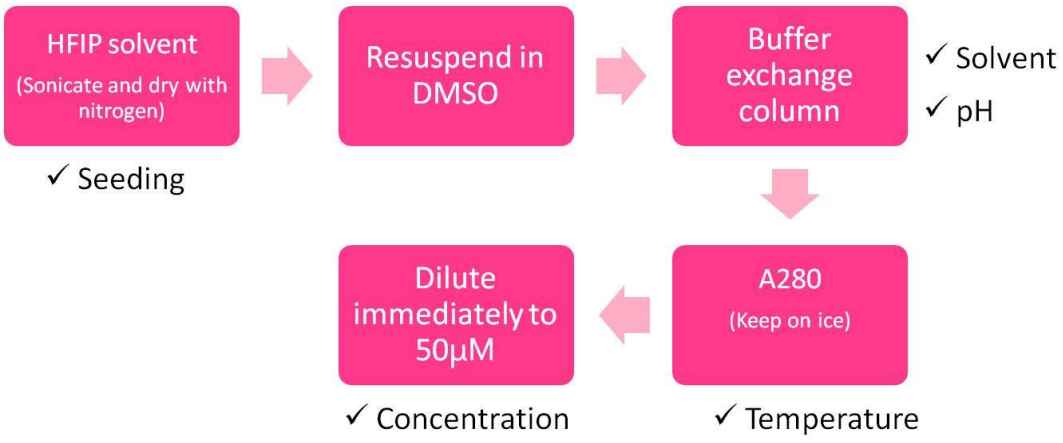

Figure 3. 4. Summary of our optimised Aβ42 preparation protocol. The factors affecting assembly which have been controlled for in this protocol have been highlighted where appropriate (✓).

The preparation method has been adapted from a previous study which validated their approach of solubilising recombinant Aβ in a sequential manner followed by removal of all chemicals to eliminate any oxidation of the peptide (Broersen et al., 2011). Samples were prepared at 1mg/ml. Firstly, HFIP is used in order to disaggregate and any preformed aggregates. Concentrated HFIP has been previously shown to be able to remove preformed aggregates (Nichols et al., 2005). The solvent ensures the sample preparation is as homogenous as possible from the beginning, and also eliminates the issue of seeding. This is vortexed and sonicated to further break up any aggregates. The HFIP is then dried using a flow of nitrogen gas. The gas used must be oxygen free due to susceptibility of Aβ42 to oxidise at Met35 (Butterfield & Boyd-Kimball, 2005). The Aβ42 peptide is then re-suspended in DMSO as a hydrogen bond acceptor to remove any water from the peptide surface through interactions of the S=O polar groups (Zheng & Ornstein, 1996). To remove the DMSO, which has been shown to affect the assembly process of Aβ in a non-physiologically relevant manner (Shen & Murphy, 1995) the peptide is put through a buffer exchange column. The centrifuge is maintained at 4°C in order to prevent the peptide from aggregating. This also retains any species larger than 7 kDa, again ensuring the final preparation is as close to monomeric as possible. Once the sample has been collected, the absorbance at 280nm (A280) is measured and using the molecular co-efficient of the peptide (Protparam) the concentration in micro-molar is calculated. This is then diluted immediately to 50μM which is taken to be the new working stock.

3.3.2 Characterising the assembly of Aβ42 from monomers to mature fibrils

After sample preparation, several imaging and biophysical techniques, including TEM, CD and ThT fluorescence, were used to monitor the assembly of Aβ42 over a 7-day period. To visualise the morphology of the structures formed over a 7-day period, TEM was used. The electron micrographs (Figure 3.6) are of un-tagged Aβ42 samples and each image is the most representative of all electron micrographs at each time point, obtained from three separate Aβ42 preparations. The electron micrographs show the presence of small spherical assemblies (blue arrows) from early time points. We identify these to be oligomers. By 2 hours, there are also some small rod-like structures which we suspect may be protofibrils (red arrows). However, using this technique, it is not possible to

confidently identify these slightly elongated structures as protofibrils; AFM measurements would be needed in order to measure the height of these and compared to what we identify to be oligomers and mature fibrils. By 24 hours, the fibrillar species (black arrows) seem to dominate the sample population which are abundant at 72 hours and 7 days. From these electron micrographs, we are able to visualise the assembly process from oligomers to protofibrils to mature fibrils. The presence of oligomers decreases as fibril formation increases suggesting these oligomers are assembling into fibrils. The presence of each of these species can be found at progressive time points due to the heterogeneity of the sample preparation as well as the dynamic nature of Aβ42 assembly. However, it is apparent that at each time point, one species predominates; oligomers are most abundant at time points earlier than 24 hours and Aβ42 forms mature fibrils at and after 24 hours.

The diameter of visible oligomers from electron micrographs from three separate Aβ42 preparations at 2 hours was measured (Figure 3.5). Although some oligomeric species are likely to be too small to be visualised by TEM, this still provides useful information regarding the average size of larger oligomers present in the sample. The diameter of these oligomers is also likely to be slightly smaller than measured due to the outline of the negative stain. The distribution shows there are a range of sizes up ~40nm with the majority measured at ~20nm. This is consistent with the previously reported diameter of oligomers (Cizas et al., 2010; Leung et al., 2017; Sakono & Zako, 2010).

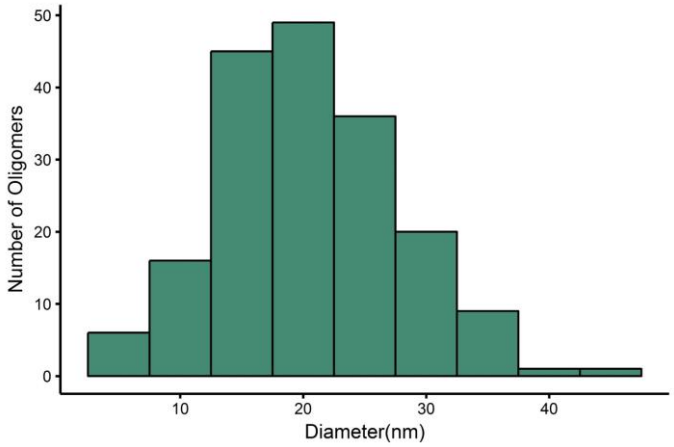

Figure 3. 5. Histogram to show the distribution of Aβ42 oligomer diameter (n=184, all oligomers counted from three separate Aβ42 preparations). The majority of oligomers were measured at ~20nm in diameter. 50μM Aβ42 was prepared in 10mM HEPES buffer pH 7.4. Oligomers were measured from electron micrographs at 2 and 4-hour time points.

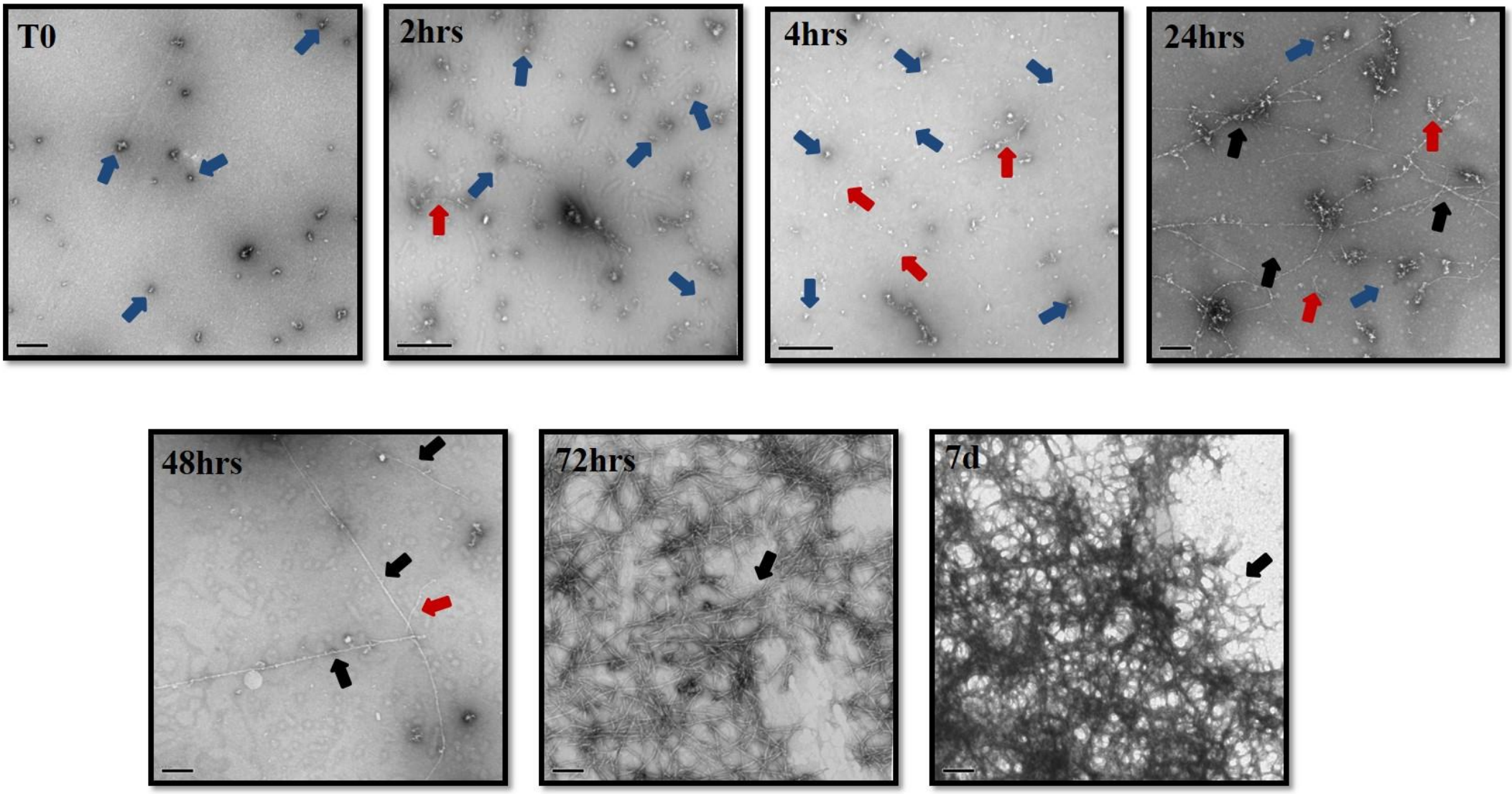

Figure 3. 6. Negative stain transmission electron microscopy images of Aβ42 over 7 days. Between T0 and 4hours, there are small spherical assemblies seen (blue arrows) which we identify to be oligomers as well structures that we suspect could be protofibrillar species (red arrows). Fibrillar species are visible by 24 hours (black arrows) which become more abundant over time. The peptide was prepared at 50µM in 10mM HEPES buffer pH 7.4, un-tagged and incubated at room temperature. Scale bar shown at 0.5µm. each image is the most representative of all electron micrographs at each time point, obtained from three separate Aβ42 preparations

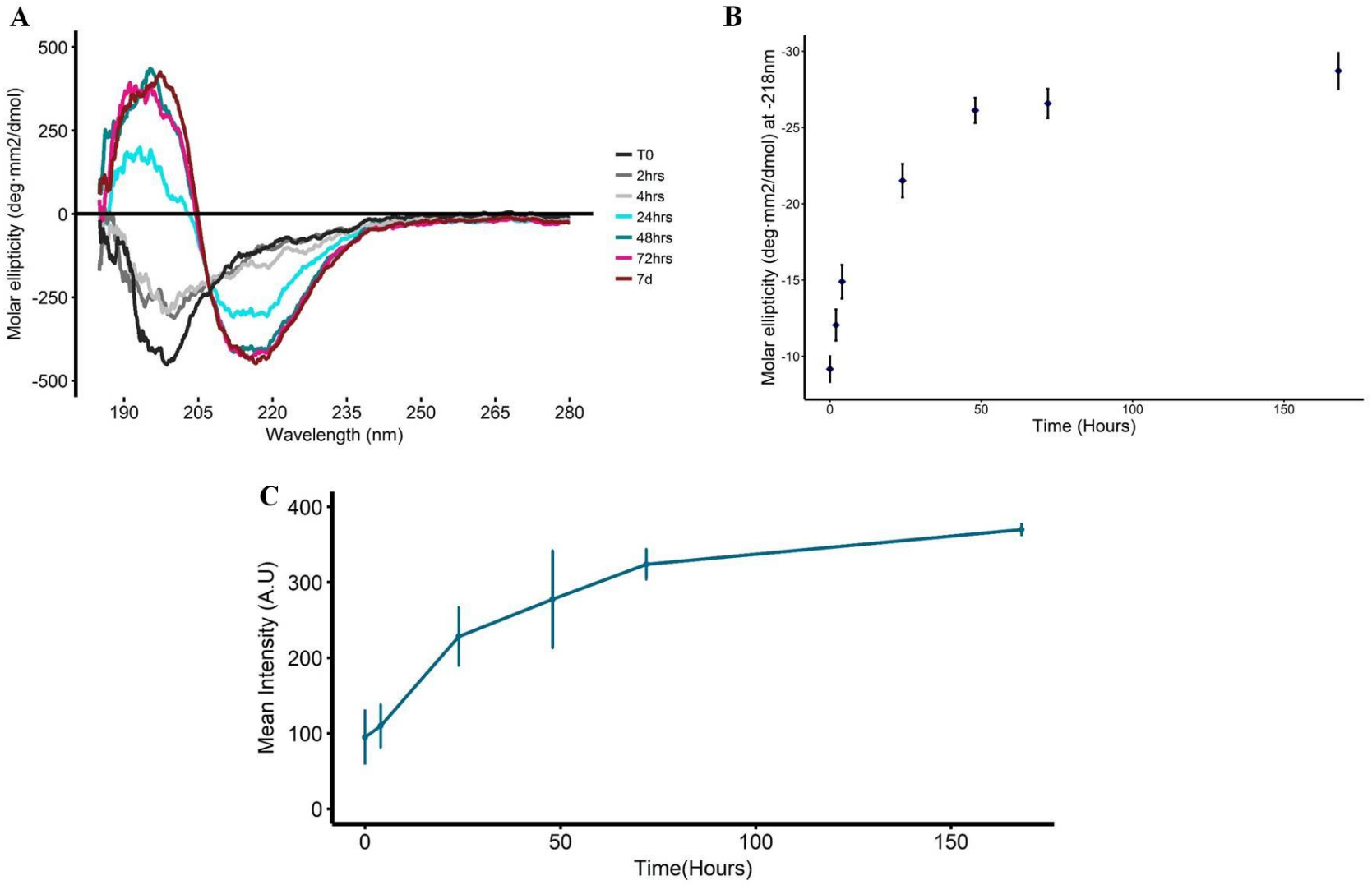

Figure 3. 7. CD and ThT fluorescence of Aβ42 over a 7 days period. A) The CD spectra of Aβ42 (using a 1mm pathway cuvette) over 7 days shows a transition from random coil to β-sheet conformation. Between T0-4h hours there is a decrease in random coil conformation and by 24 hours there is β-sheet signal, concomitant with the appearance of fibrils in the TEM (Figure 3.6). The CD spectra is for one Aβ42 sample preparation, however, is representative of what was obtained from three separate Aβ42 preparation. B) The average increase in β-sheet signal (218nm) of three separate Aβ42 preparation over time is shown.. Error bars are expressed as ±SEM C) 10µM ThT fluorescence of three separate 50µM un-tagged Aβ42 preparations over 7 days shows the typical sigmoidal curve for amyloid formation. There is a lag phase seen between T0-24hours after which there is the elongation phase followed by a plateau. 50µM Aβ42 was prepared in 20mM phosphate buffer, pH 7.4 and incubated at room temperature. Error bars are expressed as ±SEM

CD was used to monitor the secondary structure of Aβ42 at the same time points shown for EM (Figure 3.7A). The spectra shown in Figure 3.7A is from one Aβ342 sample preparation, however it is representative of the spectra obtained for three separate Aβ42 sample preparations. To show the variability within the three samples, error bars (expressed as ±SEM), have been included in Figure 3.7B which shows the average β-sheet signal from three Aβ42 preparations at each time point. There is a clear transition from random coil (minima ~200nm) to β-sheet conformation (minimum at 218nm, maximum at 195nm) over a 7 day period. At T0, there is a strong random coil conformation which reduces between 2-4 hours. This reduction in random coil signal is most likely coupled with the increase in β-sheet signal (seen clearly in Figure 3.7B) suggesting there is a heterogenous population of unfolded and folded protein, with some oligomers adopting a β-sheet structure. By 24 hours, there is a clear β-sheet signal which becomes stronger at 48 hours up to 7 days. This is concomitant with the EM, in which there is the presence of mature fibrils (β-sheet rich structures) from 24 hours onwards. This is further confirmed by Figure 3.7B which displays the increase in β-sheet signal at 218nm over 7 days; there is an increase in β-sheet signal up to 48 hours after which there is a plateau suggesting the sample population is primarily β-sheet rich. These data therefore confirm that there is a transition from disorder to order as fibril formation proceeds (Bacci et al., 2017). This order-dependent increase in β-sheet content has been previously seen by other research groups (Ono et al., 2009). Studies on Aβ40 assembly have previously shown a size and order dependent increase in β-sheet content of oligomers by CD (Ono et al., 2009). This supports the CD spectra presented in Figure 3.5 where there is a simultaneous decrease in random coil signal and increase in β-sheet signal between 2-4 hours i.e. disorder to order.

A ThT fluorescence assay was carried out to monitor fibrillogenesis over the 7 days period (Figure 3.7C). Aβ42 displays a low intensity signal even at the early time points suggesting some fibrillar species being present for dye binding. There is then a steep increase in signal intensity, concurrent with when the CD spectra display a β-sheet signal and mature fibrils are observed by TEM. The sigmoidal aggregation curve displayed by Aβ42 can be explained by the nucleation-dependent polymerisation model. The short lag phase (between 0-4 hours) can be attributed to the nucleation

phase of polymerisation where a critical concentration of misfolded protein need aggregate into a nuclei (Ferrone, 1999). The steep increase in fluorescence intensity seen from 24-72 hours represents the elongation phase, where there is a rapid growth of fibrils by monomer addition to the nuclei. The monomer 'docks' on to an aggregate reversibly and is then 'locked' in a number of steps, allowing it to become integrated onto the template for further elongation (Bacci et al., 2017; Esler et al., 2000). This is a time-dependent transition where the monomer becomes irreversibly associated with the pre-existing template or 'critical nuclei' (Figure 3.8). This irreversible association has been proposed in the mechanism of amyloid plaque deposition in AD (Cruz et al., 1997).

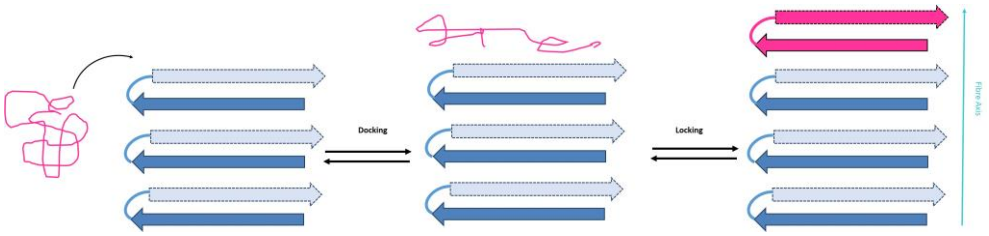

Figure 3. 8. A schematic representation of the monomeric dock-lock mechanism. The monomer added is shown in pink. Adapted from Bacci et al, 2017.

Although it would be possible to obtain the kinetics of the elongation by calculating the slope of the curve, it was not deemed necessary to do so as we are not making comparisons of elongation rates/assembly under different conditions (e.g. temperature, concentration, pH); all experiments were conducted at 50μM under the same preparation conditions. Furthermore, although several studies have used ThT fluorescence in order to calculate elongation rates (Milto et al., 2013; Platt et al., 2008), it is difficult to obtain quantitative data from this method due to the molecular binding of ThT to amyloid fibrils not being fully known. This combined with the susceptibility to bind to impurities or amorphous aggregates means that although this type of fluorescence spectroscopy is a widespread and highly utilised method to monitor fibrillogenesis, it should ideally be combined with another method to obtain fully quantitative data (Arosio et al., 2015). One example of a better method to obtain the elongation rate would be by real-time monitoring of the changes in the number of molecules in the fibrils (calculated by the variations in mass), using a quartz crystal oscillator (Knowles et al., 2007).

Studies using surface-based single fibril imaging have also been highly informative of the elongation phase. This phase occurs in a stepwise manner and alternates between a growth and arrest phase displaying a preferential direction of growth (Bacci et al., 2017; Watanabe-Nakayama et al., 2016). Little is known about the arrest phase of fibril elongation but it may relate to a 'trapped' state of fibril conformation which is not thought to require any disassembly to re-enter the growth phase (Bacci et al., 2017; Watanabe-Nakayama et al., 2016; Young et al., 2017). After the elongation phase, a plateau is reached (between 72 hours-7 days in the protocol presented in this Chapter) where fibrillisation has reached a steady state.

Together, these biophysical data present a clear assembly of Aβ42 into amyloid fibrils, allowing us to pinpoint specific stages and the appearance of different species. To further consolidate this, a series of antibodies against different conformations and epitopes of Aβ42 were used. This also ensures that any small species that are not able to be detected by these biophysical techniques are not overlooked.

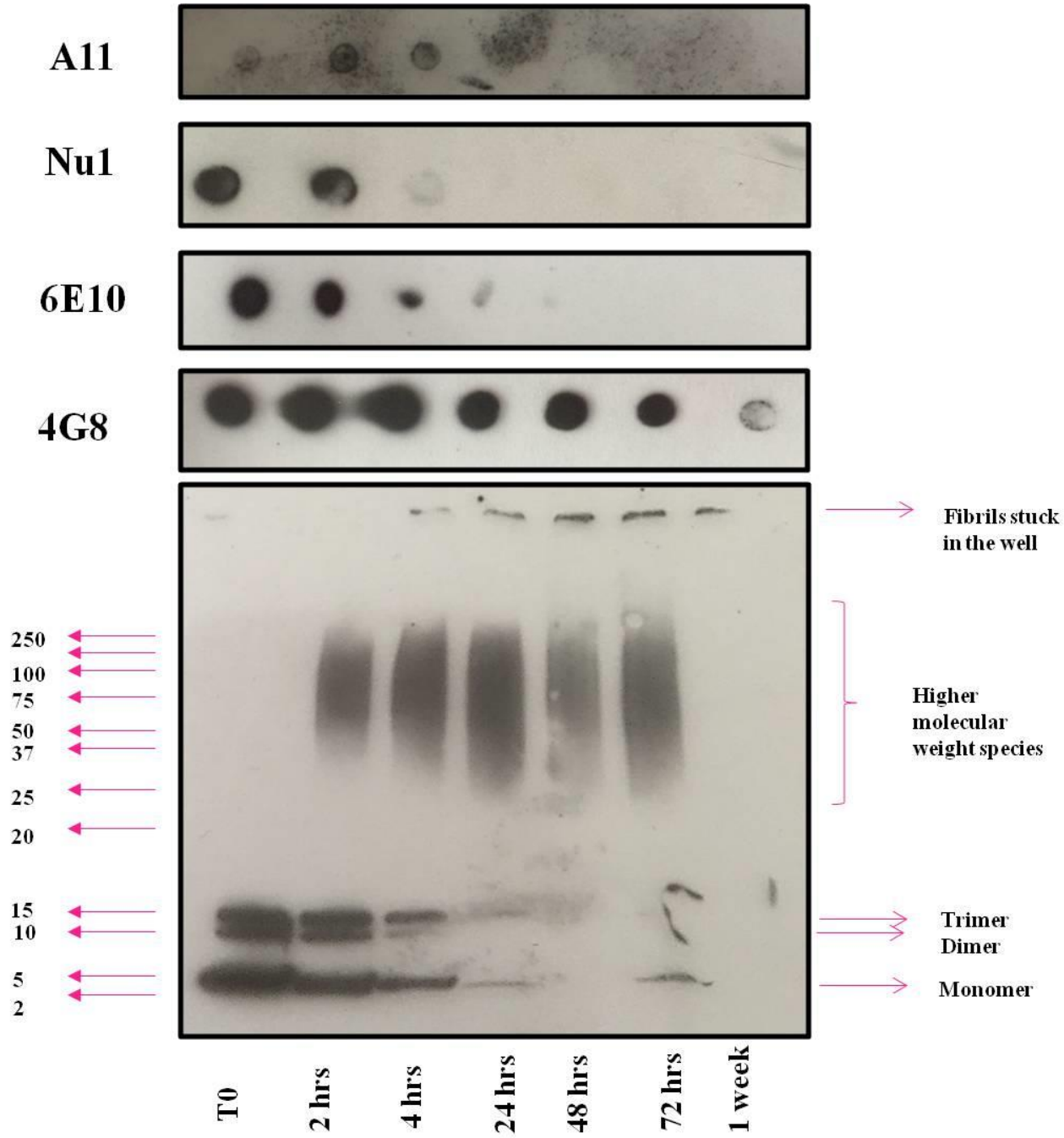

Figure 3. 9. Aβ42 dot blot and western blot. The NU1 (1:10000 dilution) and A11 (1:5000) oligomer-specific antibodies detected oligomers for up to 4 hours. The anti-Aβ 4G8 (1:10000 dilution) and 6E10 (1:10000) antibodies with epitopes at the N- and C- terminal of the sequences respectively, were used to detect for Aβ42 over 7 days; the 6E10 signal is displayed up to 24 hours suggesting the epitope is buried during assembly after this time point. The 4G8 signal is displayed at all time points confirming the presence of the protein. The 6E10 antibody (1: 10,000 dilution) was used to detect Aβ42 in the western blot, 50μM Aβ42 was prepared in 10mM HEPES buffer pH 7.4 and incubated at room temperature. Aliquots were taken for each time point. 1 and 2μg of protein were loaded for dot blotting and SDS-PAGE electrophoresis respectively. Both the dot blots and western blot was only carried out once and therefore quantification was not possible.

The dot blots shown in Figure 3.9 (top 4 panels), reveal that oligomer specific antibodies A11 (Kayed et al., 2007) and NU1 (Lambert et al., 2007) detected Aβ42 only up to 4 hours. The 6E10 antibody, which is raised against the N terminal of the Aβ42 sequence, displays a signal for up to 24 hours. This can be attributed to the epitope being 'buried' as Aβ42 continues to assemble. The 4G8 antibody is raised against the C terminal of the sequence and displays a signal at each time point over 7 days, confirming the presence of the protein.

The Aβ42 sample preparation is expected to be heterogeneous. Therefore, although dot blots provide a useful tool to assess antigenicity of Aβ42, it does not tell us about the entire population of species present in the sample. To overcome this, we ran SDS-PAGE for samples at each time point and carried out a western blot using the 6E10 antibody (Figure 3.9, bottom). It is important to remember that the dot blot and SDS-PAGE can have different results because of the denaturation of the protein in the gel. This explains the detection of Aβ42 in the western blot by the 6E10 antibody, even though the epitope for this is buried in the dot blot. The effects of SDS on Aβ have been evaluated critically due to the artificial oligomerisation it may induce (Bitan et al., 2003). Despite this, combining these data with our robust biophysical characterisation is informative of the assemblies at each time point. There is a clear increase in the presence of larger assemblies at increasing time points. At T0 the Aβ42 is mainly monomeric (4.5kDa), dimeric (9kDa) and trimeric (13.5kDa). At 2-4 hours we begin to see the presence of higher molecular weight species which migrate as a smear, still with the presence of the smaller assemblies. This can be explained by the assembly of larger oligomers as seen in Figure 3.6. At 24 hours, there is an evident decrease in the signal for monomers, dimers and trimers, with a strong signal for larger assemblies and some fibrils being stuck in the well of the gel. This trend continues at 48 and 72 hours and by 7 days there is no signal for oligomeric species with fibrils only observed in the well.

Both the dot blot and western blot were carried out once from one Aβ42 sample preparation, and therefore it was not possible to quantify the data. As a future objective, it would be beneficial to do a minimum of three repeats in order to obtain more data from the experiments. For this thesis, however,

only one repeat was carried out in order to begin to get a preliminary understanding of the range of assembly sizes present in our sample preparation at each time point.

The biophysical data combined with antibody-directed experiments confirm that using our sample preparation, Aβ42 is most oligomeric between 2-4 hours. After this time period, the sample preparation population is dominated by the fibrillar species.

3.3.3 Aβ42 oligomers are cytotoxic

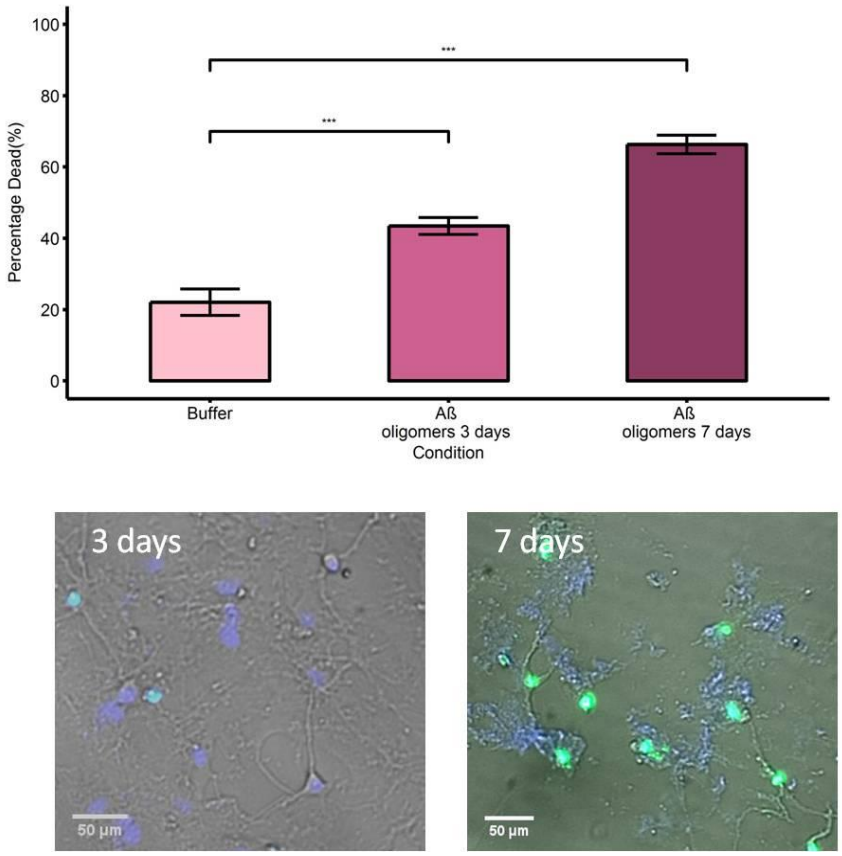

Figure 3. 10. Aβ42 oligomer ReadyProbes cell viability assay. Rat hippocampal cultures were treated with 10µM Aβ42 oligomers for 3 and 7 days. Examples of ReadyProbes for both time points have been included in the bottom panel. Cytotoxicity was measured as a percentage of dead cell in a culture and compared to buffer incubated cells. Aβ42 oligomers were significantly toxic at both 3days (43.2% ± 2.35, total number of cell =1619, number of dead cells = 703) and 7 days (66.3% ± 2.59, total number of cells = 1172, number of dead cells=777) compared to buffer incubated cells (17.8% ± 3.06, total number of cells = 1239, number of dead cells=221). One-way ANOVA with Tukey's post hoc comparison where p= < 0.01 (*), < 0.001 (**), < 0 (***). Error bars are expressed as ±SEM. Data shown here is the average of three separate Aβ42 preparations incubated with three separate hippocampal cultures. Aβ42 was prepared untagged, in 10mM HEPES buffer pH 7.4.

Having a protocol that produces a consistent preparation of Aβ42 allows us to confidently identify oligomers being most prevalent 2 hours after preparation. To confirm our oligomeric species is cytotoxic, we carried out a ReadyProbes assay in primary rat hippocampal cultures after incubation periods of 3 and 7 days with 10μM oligomeric Aβ42 (Figure 3.10). The assay labels the nuclei of all cells with a blue dye and all dead cells with a green dye. The percentage of green labelled cells of the whole neuronal population is taken as the measure of cell death. Examples of cells incubated with oligomers for both time points have been shown in the bottom panel of Figure 3.10. The average of three separate biological repeats (separate Aβ42 preparations and hippocampal cultures for each repeat) are shown in Figure 3.10. As expected, there was significant cell death seen at both these time points; ~44% (43.2% ± 2.35, total number of cell =1619, number of dead cells = 703) cell death after 3 days and ~70% (66.3% ± 2.59, total number of cells = 1172, number of dead cells=777) after 7 days compared to buffer incubated cells (17.8% ± 3.06, total number of cells = 1239, number of dead cells=221). This confirms that our oligomeric species are cytotoxic. The deleterious effects of our Aβ42 oligomers have also been verified in SHSY5Y human neuroblastoma cells (Marshall et al., 2016). Although a concentration of 10μM is not physiologically relevant, however, it allows for the accelerated effect of the peptide within a reasonable time frame and ensures that any negative results are not due to low levels of protein concentration. This concentration was chosen based on previous dose-response curve experiments conducted by other members of the lab group who assessed the cytotoxicity of Aβ42 oligomers at 1-, 5- and 10μM.

Despite confirming our preparation method produces toxic oligomers, it is important to note that the preparation consists of only one Aβ length (Aβ42). Physiologically there are many fragments of Aβ formed, all of which are likely to influence the assembly behaviour and toxicity of Aβ42. For example, it has been demonstrated that Aβ40 and Aβ42 directly interact to alter aggregation kinetics directly linked to the changes in Aβ 40/42 ratio seen in AD (Pauwels et al., 2012). Furthermore, using mass spectroscopy and ion mobility studies, it has been suggested that Aβ40 may inhibit the oligomerisation of Aβ42 (Murray et al., 2009) thereby suggesting a protective role of Aβ40. The data

presented here suggest although other assemblies of Aβ may affect Aβ42 cytotoxicity, Aβ42 oligomers alone are sufficient to cause cytotoxicity.

There are several identified Aβ42 oligomers which vary in the levels of cellular dysfunction they cause. Some examples have been summarised in Table 3.2.

Aβ42 Species	**Effect**	**References**
Dimers/Trimers	LTP impairment Little/No cytotoxicity	(Shankar et al., 2007; Shankar et al., 2008; Townsend et al., 2006)
A11 positive oligomers	Cytotoxicity in Human cortical cultures and PC12 cells	(Deshpande et al., 2006; Ladiwala et al., 2012)
Aβ*56	NMDAR-dependent synaptotoxicity	(Lesne et al., 2013)
Aβ-derived diffusible ligands	Cytotoxic in primary hippocampal cultures	(Lambert et al., 1998)

Table 3. 2. Size and cellular dysfunction induced by previously identified oligomers.

Using our protocol, we cannot specify the exact size of the toxic oligomeric species, however, we identify the toxic species to be pre-fibrillar with low ThT fluorescence, lacking significant β-sheet structure but reduced random coil signal by CD, and are A11/NU1 antibody positive.

3.4 Conclusion

Using extensive characterisation methods, we have established a reliable and reproducible protocol for the preparation of Aβ42. This allows for assembly from small monomeric/oligomer species to insoluble fibrils, to be monitored over a reasonable timeframe of 7 days. From the electron micrographs, it is possible to visualise the change in morphology of the peptide over 7 days. Small spherical species, which we identify to be oligomers, are most prevalent between 2-4 hours, whilst mature fibrils begin to dominate after 24 hours. The CD spectra shows a transition from random coil to β-sheet signal over 7 days. This data complements the appearance of fibril in the EM at 24 hours, as at time points before this the CD spectra displays a predominantly random coil signal. Finally, ThT

fluorescence monitored at the same time points, displays a typical sigmoidal curve for Aβ42 which represents the lag, elongation and steady phase of Aβ42 assembly (Xue et al., 2008). Combining this with the dots blot and western blots signals displayed at each time point, we can confidently identify our sample population to be most oligomeric between 2-4 hours. Using this information, we verified our oligomeric species, 2 hours after sample preparation, to be cytotoxic utilising the ReadyProbes assay in rat primary hippocampal cultures.

Although this chapter has provided a thorough characterisation of the assembly process and oligomers of Aβ42 produced from the sample preparation presented, there are several factors to consider in the critical evaluation of the techniques that were used and some of the conclusions reached. Firstly, the electron micrographs are representative of only 4µl of the entire sample preparation. Although the electron micrographs shown are representative of three independent Aβ42 sample preparations, it is possible the species visualised from the grids are not truly representative of the entire population. Furthermore, techniques such as cryo-EM or AFM measuring the height of the species, would provide more detailed and higher resolution information regarding the assemblies in the sample preparation. However, both these techniques were not readily available and therefore pursuing this would be a future direction for this project. The CD spectra presented in this chapter shows a transition from random coil to β-sheet signal over a 7 day period. Although the CD spectra between T0-4hours shows a reduction in random coil, there is most likely there is a simultaneous increase in β-sheet signal (shown in Figure 3.7B) that is being masked by the strength of random coil. In order to further analyse the ratio of random coil to β-sheet signal at each point, the DichroWeb online tool could be used. This would provide a better understanding the proportion of the sample preparation that is adopting a β-sheet conformation. Furthermore, CD only provides information regarding the secondary structure of the protein. Using a technique such as FTIR would provide further information regarding the anti-parallel/parallel packing of the β-sheets, again providing a better structural understanding of the assemblies in the sample preparation.

The sample preparations of Aβ42 presented in this chapter, and all subsequent chapters to follow, have been at a pH of 7.4. This was due to the fact that the Aβ42 is being exogenously added to the cells and the extracellular Aβ42 in the brain would be at this pH. Physiologically, however, it is thought that the production/accumulation of is in lysosomes/early endosomes which typically have a lower, more acidic pH. Therefore, it would have been beneficial and interesting to do similar characterisation at a more acidic pH environment to link the assembly to cytotoxicity. Based on the discussion above (Section 3.2.1), it would be reasonable to suggest that the kinetics of the assembly process would be enhanced, and the mature fibrils produced would be much more stable.

Finally, although the ReadyProbes assay is an extremely useful tool as a measure of cytotoxicity, it does not provide any information regarding any cellular dysfunction that may occur before cell death. As a further complementary technique to the ReadyProbes assay, an MTT assay to monitor any mitochondrial dysfunction would be one way in which to assess cell dysfunction before cell death. Furthermore, one of the biggest limitations of this preparation method is the inability to distinguish different categories of oligomers. Our identification of the oligomers being most prevalent at 2 hours does not specify a particular size as the main toxic species and therefore is a significant limitation of this kind of biophysical classification.

Taking into consideration the critical evaluation presented above, the data presented in this chapter is important is still important two-fold; 1) we provide a thoroughly characterised and highly consistent Aβ42 preparation method, 2) the oligomeric species from our preparation method is cytotoxic and therefore representative of a disease-related amyloid protein. Using the amyloidogenic Aβ42 as our disease-related amyloid model, we can gain a further understanding into what makes an amyloid toxic by comparing the cytotoxicity of assemblies formed from primary sequence variants of Aβ42, as well functional amyloid proteins.

Chapter 4: Model peptides to investigate the importance of primary sequence in amyloidogenicity

Chapter Overview

The ability to form amyloid is an inherent property of all proteins and peptides (Dobson, 2006). Under suitable conditions, irrelevant of primary sequence, almost all peptides can form amyloid (Dobson, 2004). There has been much research into how the amyloidogenicity of proteins is influenced by the primary sequence of peptides (Caputo et al., 1993; Frousios et al., 2009; Idicula-Thomas & Balaji, 2005). Although several factors are involved in the formation of amyloid, the amino acid sequence of the protein is ultimately responsible for determining the propensity to form amyloid (Familia et al., 2015). This chapter will address the ability of three Aβ42 primary sequence variants to self-assemble and in their cytotoxicity. This is compared to the assembly and toxicity of Aβ42 presented in the previous chapter.

4.1 Introduction

The cytotoxic effect of the Aβ42 peptide is believed to be linked to its ability to self-assemble to form oligomers and amyloid fibrils (Kayed et al., 2003). It is the oligomeric species proposed to represent the toxic species leading to neuronal dysfunction and eventual cell death (Glabe & Kayed, 2006; Kayed et al., 2003).

The lack of a suitable control peptide has been a big constraint in our fundamental understanding of Aβ42 assembly and toxicity. Many studies examining the role of Aβ42 have utilised a buffer/vehicle solution, Aβ42-1 (reversed primary sequence) or AβS (scrambled amino acid sequence) as control peptides (Izzo et al., 2014; Jean et al., 2015). These Aβ42-1 and AβS "control" peptides are chosen because they are not expected to self-assemble or to form toxic oligomeric species, despite sharing amino acid composition with Aβ42. However, the fibrillogenesis of these peptides and resulting structures has not been previously analysed in detail. Furthermore, despite being used in cellular

assays as controls, the cytotoxic nature, or lack of, has not been studied in relation to their assembly state.

A novel assembly impaired variant of the Aβ42 peptide, vAβ42, was designed to investigate the importance of primary sequence in amyloid self-assembly and cytotoxicity (Marshall et al., 2016). The effects of several amino acid substitutions within the amyloidogenic regions of wild-type Aβ42 (16-22 and 36-42) were predicted using the WALTZ algorithm (Maurer-Stroh et al., 2010). These substitutions were then ranked by their predicted ability to abolish amyloidogenicity. A double substitution of phenylalanine for serine at position 19 (F19S) and glycine with aspartic acid at position 37 (G37D) was the most promising and predicted to abolish amyloidogenicity completely. The importance of Phe19 and Gly37 as drivers of assembly has been extensively examined and is discussed below. It is therefore unsurprising that the WALTZ algorithm identified substitutions of these hydrophobic amino acids with polar, hydrophilic amino acids to abolish amyloidogenicity. This vAβ42 is presented in this chapter to serve as an additional model of primary sequence importance in amyloidogenicity and also as a more suitable experimental control for Aβ42.

In this chapter, all three models, Aβ42-1, AβS and vAβ42, with similar yet varied primary sequences have been thoroughly characterised using a range of biophysical techniques. Linking the assembly process (or lack of) to the cytotoxicity of each of these models using a cellular viability assay in rat hippocampal cultures provides useful information regarding the importance of primary sequence in the deleterious effects of amyloid proteins.

4.2 Results and Discussion

4.2.1 WALTZ identified amyloidogenic regions in Aβ42-1, AβS and vAβ42

The primary sequence of wild-type Aβ42 and the three variants are provided in Table 4.1. The vAβ42 has two amino acid substitutions at F19S and G37D. Aβ42-1 is the reversed sequence of the wild type peptide and AβS is a scrambled sequence of the amino acids.

Peptide	Sequence
Aβ42	DAEFRHDSGYEVHHQ**KLVFFA**EDVGSNKGAIIGLMV**GGVVIA**
vAβ42	DAEFRHDSGYEVHHQKLVSFAEDVGSNKGAIIGLMVDGVVIA
Aβ42-1	AIVVGGV**MLGIIA**GKNSGVAGAFFVLKQHHVEYGSDHRFEAD
AβS	AIAEGDSHVLKEGAYMEIFDVQGHVFGGKIFRVVDLGSHNVA

Table 4. 1. The primary sequence of Aβ42 and the variant peptides, vAβ42 (substitutions shown in red), Aβ42-1 and AβS. Amyloidogenic regions identified by the WALZ algorithm are shown in bold.

The sequence of AβS is dependent on the company it is purchased from. Table 4.2 presents two Aβ42 scrambled sequences available to purchase from several companies. The AβS sequence examined in this chapter has been purchased from Bachem.

Company	**AβS sequence**
rPeptide **Merck** **AmideBio**	KVKGLIDGAHIGDLVYEFMDSNSAIFREGVGAGHVHVAQVEF
AnaSpec **Bachem** **Eurogentc**	AIAEGDSHVLKEGAYMEIFDVQGHVFGGKIFRVVDLGSHNVA

Table 4. 2. AβS sequences available from different companies. The sequence presented in this chapter has been purchased from Bachem.

The WALTZ algorithm, which identifies amyloidogenic regions using a positional algorithm, was used to predict the propensity of each peptide to aggregate (Maurer-Stroh et al., 2010). The graphical trace for wild-type Aβ42 has two amyloidogenic regions with peaks at 16-22 and 37-42. In contrast,

the trace for Aβ42-1 predicts a single region from 8-13 whilst both vAβ42 and AβS were predicted to have no amyloidogenic regions (Figure 4.1).

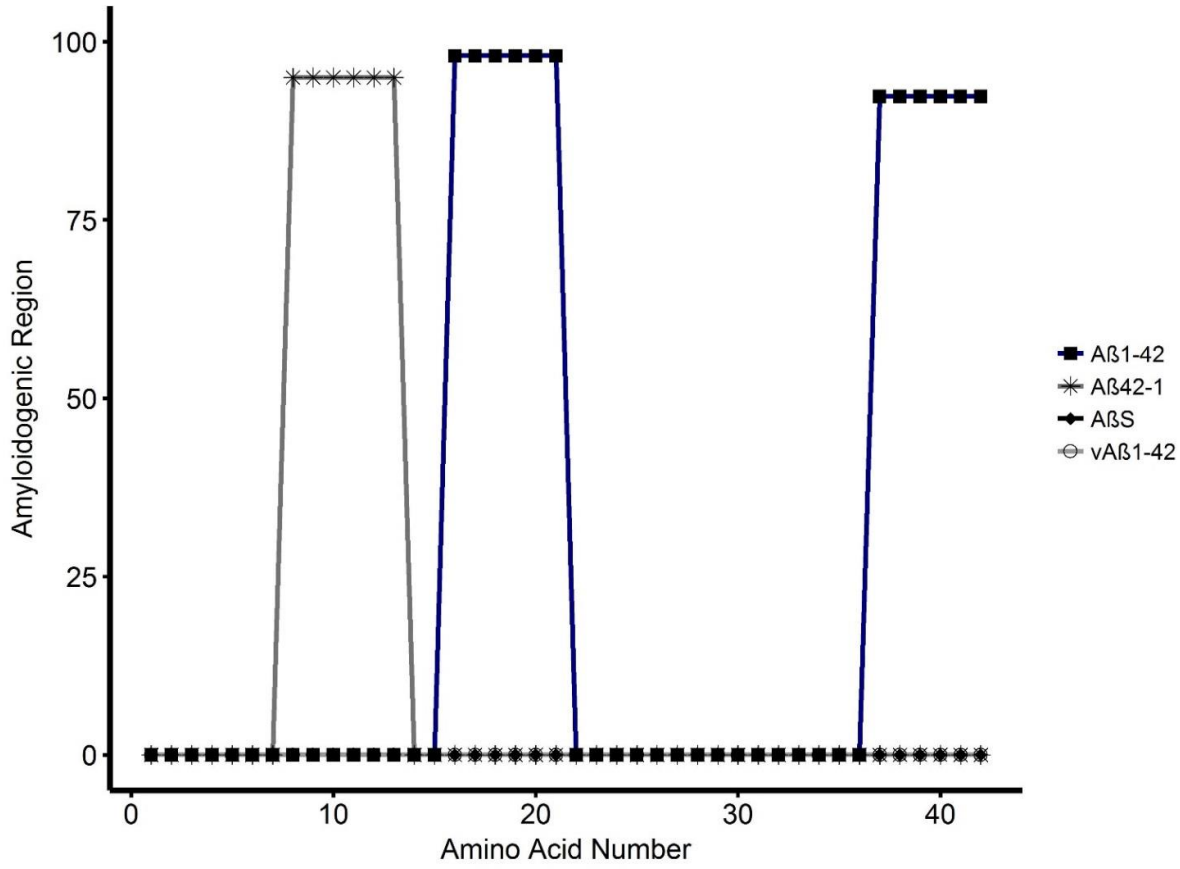

Figure 4. 1. Traces produced using the WALTZ algorithm for Aβ42 and primary sequence variants. The trace for Aβ42 (blue line, black filled squares), shows two peaks indicating two amyloidogenic regions (16-22 and 37-42). Aβ42-1 (dark grey line, asterix) shows one peak suggesting an amyloidogenic region between 8-13 and no regions were identified for both vAβ42 (light grey line, unfilled black circle) and AβS (dark grey line, black filled diamonds). Traces were obtained from www.switchlab.org and replotted in R Studio.

WALTZ is a web-based tool that uses a position specific scoring matrix to identify amyloid forming sequences. The rational of using this particular algorithm over the many others that are available is that due to the lack of extensively validated amyloid sequences, these sequence specific algorithms often cannot distinguish between β-sheet like amorphous aggregates and amyloid (Maurer-Stroh et al., 2010; Morris et al., 2013). WALTZ overcomes this issue and was developed by exploring the sequence diversity of over 200 hexapeptide amyloid proteins, allowing users the ability to explore the sequence space of amyloid proteins (Maurer-Stroh et al., 2010). WALTZ also emphasised the

importance of amino acid specific positioning in the formation of both disease and functional amyloid proteins (Maurer-Stroh et al., 2010).

The hexapeptide sequences identified as being amyloidogenic regions are **KLVFFA** (16-21) and **GGVVIA** (37-42) in Aβ42 and **MLGIIA** (8-13) of the Aβ42-1 sequence. The Eisenberg group has previously identified and crystallised the KLVFFA and GGVVIA fragments (Colletier et al., 2011) . This was accomplished using a 3D profile method which scored six residue segments on their propensity to form steric zippers based on the profile of a canonical model (Colletier et al., 2011). The KLVFFA crystallised in three forms, all of which were in an antiparallel β-sheet 'face-to-back' stacking, via hydrophobic side chains giving rise to a dry interface (Colletier et al., 2011; Sawaya et al., 2007). GGVVIA crystals display parallel β-sheets with a 'face-back' orientation (Sawaya et al., 2007).

As Aβ42-1 is not a naturally occurring peptide, there has been little/no characterisation of its primary sequence. It has previously only been used as an experimental control rather than a model to investigate the importance of primary sequence and therefore there is no literature exploring the amyloidogenicity of the MLGIIA fragment identified by WALTZ, even as a stand-alone hexapeptide. The naturally occurring, mirrored sequence of AIIGLM in the Aβ42 sequence, however, has been shown to form fibrils and crystals. This AIIGLM sequence is not identified by WALTZ in the Aβ42 sequence, but is well known to be amyloidogenic using other algorithms (e.g. AWSEM-Amylometer) (Zheng et al., 2013). This fragment forms a dry steric zipper interface with an anti-parallel β-sheet in a 'face-back' orientation. The interface packs in 'knobs-into-holes' as described by Crick in 1952 (Crick, 1952). The Ile32 and Leu34 from one β-sheet form the 'knob' that will enter the hole, created by the presence of the glycine at position 33, between the Ile31 and Met35 of the partnering β-sheet. In the reversed sequence, this type of packing maybe be unchanged as the β-sheet parallel in-register arrangement seen in Aβ42 is unlikely to be disrupted.

The WALTZ algorithm has highlighted the importance of amino acid position in amyloid propensity; almost all amino acids display a strong position dependency. Low hydrophobic residues in particular

showed the highest positional dependency (Maurer-Stroh et al., 2010). As all amino acids in the amyloidogenic regions of the Aβ42 sequence (with the exception of lysine) are highly hydrophobic, reversing the hexapeptide sequence would not drastically influence amyloid propensity solely based on this. A better explanation is offered by the positions of the residues in the hexapeptide fragments (Lopez de la Paz & Serrano, 2004). Positional mutations introduced into the STVIIE hexapeptide has provided a detailed understanding of the importance of amino acid position specificity. Table 4.3 summarises the findings of different mutations at each position inducing the formation of amyloid as described previously (Lopez de la Paz & Serrano, 2004).

Position	Amino Acid substitution
1	Gly Ala Ser Lys Arg His
2	Gln Glu Thr
3	Val Leu
4	Ile Leu Asn Phe Glu
5	Ile Phe Try
6	All amino acid substitutions resulted in amyloid except Leu and Glu

Table 4. 3. Positional amino acid substitutions within the STVVIE hexapeptide which resulted in amyloid formation. Summary of findings by Paz et al, 2004.

Despite positions 1 and 6 being able to accommodate almost any amino acid, position 5 is highly specific and restricted, with Ile, Phe and Tyr being strongly favoured (Lopez de la Paz & Serrano, 2004). The MLGIIA fragment has an Ile at position 5, making it strongly amyloidogenic. Regions 16-21 and 37-42 of the Aβ42-1 sequence are **NSGVAG** and **HRFEAD** respectively. The lack of one of three critical amino acids needed at position 5 and most likely weak positioning regarding hydrophobicity of each amino acid, are two possible reasons why these regions are not identified as being amyloidogenic despite the sequence for Aβ42-1 only being a reversal of Aβ42.

AβS purchased from Bachem has no identified regions of amyloidogenicity by the WALTZ algorithm. WALTZ was also used to predict regions for amyloidogenicity for the alternate AβS sequence (Figure 4.2). Both sequences show no regions of amyloidogenicity, despite having different scrambled primary sequences. This suggests that a very specific order of amino acids is critical for amyloidogenicity.

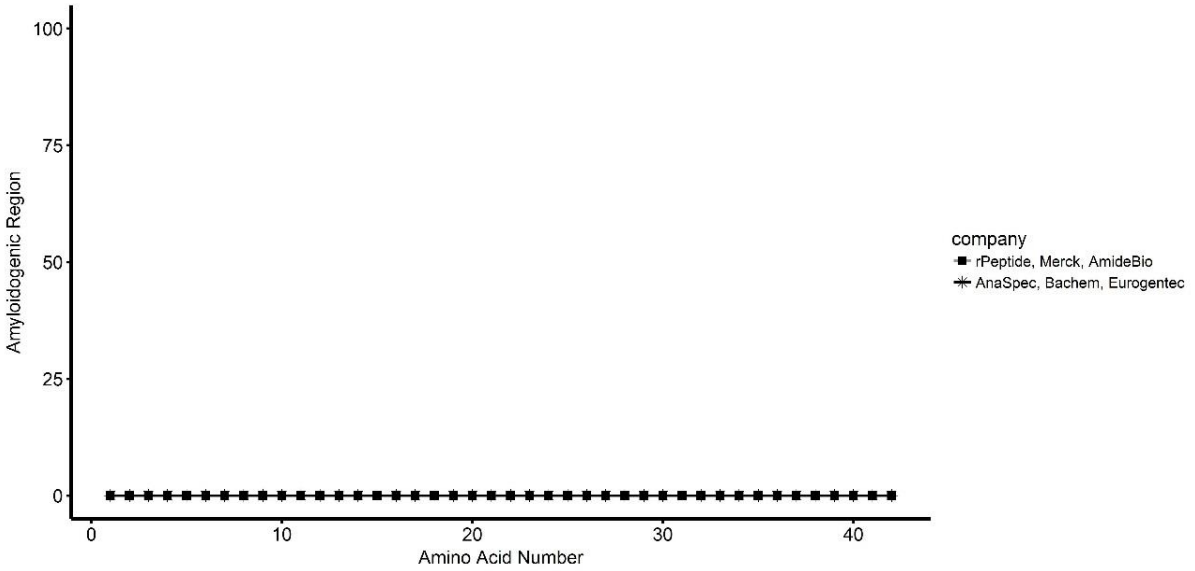

Figure 4. 2. Traces produced using the WALTZ algorithm for two AβS sequences available for purchase from various companies. No peaks are shown suggesting no amyloidogenic regions in either sequence. Traces were obtained from www.switchlab.org and replotted in R Studio.

The abolished amyloidogenic regions displayed in the vAβ42 graphical trace (Figure 4.1), is expected since WALTZ was utilised in designing the variant primary sequence (Marshall et al., 2016). Furthermore, both phenylalanine at position 19 and glycine at position 37 have been shown to be important drivers of assembly. Therefore, substitutions at these positions would likely impair assembly.

Phenylalanine is an aromatic amino acid. The presence of aromatic amino acids has been identified in several amyloidogenic fragments of disease-related amyloid proteins. Examples of this include the **FGAIL** fragment (Tenidis et al., 2000) of the Islet amyloid polypeptide associated with Type II diabetes and the **SFFSFLGEAFD** fragment of Serum amyloid A which is associated with Chronic inflammation amyloidosis (Gazit, 2002). The interactions between two planar aromatic residues are attractive and non-bonded; these interactions are referred to as π-stacking. π-stacking has been found to be important in the process of molecular recognition and self-assembly in amyloid proteins by providing two key features for self-assembly (Gazit, 2002). Firstly, π-stacking provides a thermodynamic drive towards assembly and secondly, the specificity of the direction and orientation of the stacking, which is particularly important due to the highly structured morphology of amyloid (Gazit, 2002). There are four different types of π -stacking (Figure 4.3) that can occur; 1) parallel displaced 2) T-shaped 3) parallel staggered and 4) herringbone

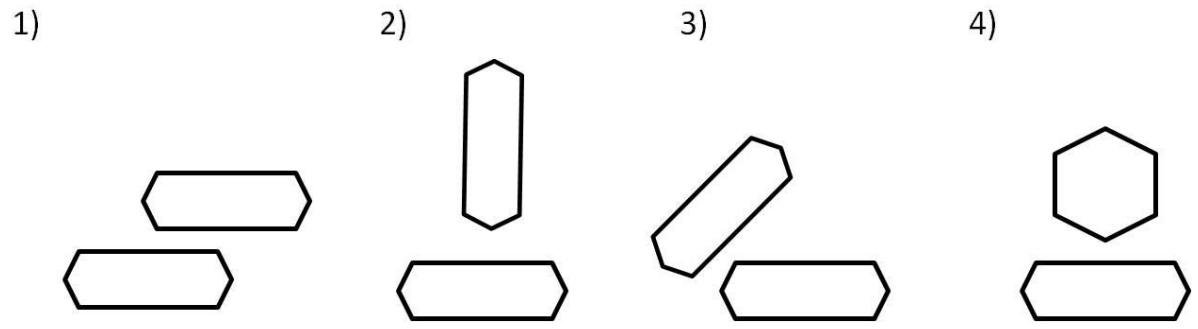

Figure 4. 3. Schematic diagram of possible π-stacking orientations. 1) Parallel displaced 2) T-shaped 3) parallel staggered 4) herringbone. Adapted from Gazit, 2002.

In amyloid fibrils, it is thought that both parallel displaced (Gazit, 2002) and T-shaped (Makin et al., 2005) are the π-stacking that occurs. The T-shaped π-stacking arises due to the phenylalanine

interactions between β-sheets and also between hydrogen bonded strands (Makin & Serpell, 2005). As monomers of protein begin to assemble into fibrils, they are restricted by the geometry of two aromatic residues forming π-stacking. This is true for all further monomers that add on to form the mature fibril and therefore the entire assembly process is being regulated and restricted by the geometries of the stacking interactions (Gazit, 2002). Figure 4.4 shows a possible model for π-stacking in a parallel and anti-parallel β-sheet arrangement.

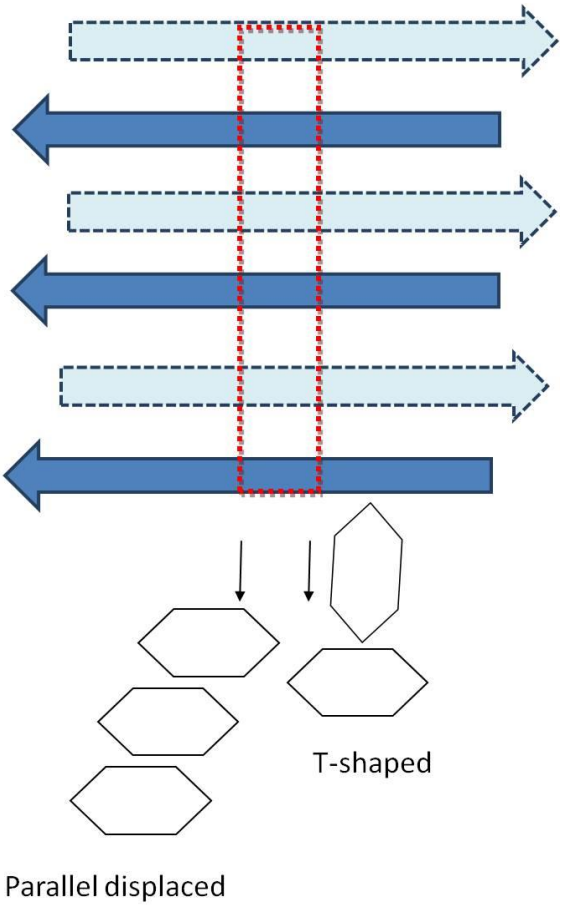

Figure 4. 4. π-stacking in Aβ42. Phenylalanine residues in parallel (Dark blue only) or anti-parallel (dark and light blue) β-sheet arrangements interact to form π-π interactions. These have postulated to be either parallel displaced or T-shaped in orientation.

The importance of the two phenylalanine residues forming π-stacking in Aβ42 has been demonstrated in experiments where short phenylalanine rich fragments bound specifically to the length of the peptide. This inhibited addition of monomers and subsequent formation of fibrils (Tjernberg et al., 1996). The two phenylalanine residues in the KLVFFA fragment provide molecular recognition

needed for formation of amyloid fibrils and place the two monomers in the correct position for subsequent hydrogen bonding that is characteristic of amyloid fibrils. Several small, aromatic compounds have been shown to interact with amyloid proteins in a similar manner and inhibit the formation of fibrils (Gazit, 2005; Porat et al., 2006). The therapeutic potential of using these compounds to inhibit the formation of amyloid fibrils can be questioned as it is the oligomeric species identified as being cytotoxic (McLean et al., 1999). It would seem unlikely that neurodegeneration could be halted simply by inhibiting the formation of fibrils, however, it may be that the loss of neurons could be slowed down by reducing the number of fibrils that can act as either a 'pool' of oligomers or a site for secondary nucleation. On the other hand, inhibiting the formation of fibrils may increase the concentration of oligomers, driving further toxicity.

Interestingly, Congo red dye (structure shown in Figure 4.5) which binds specifically to amyloid fibrils is a linear and amphiphilic molecule. There are two amino acid groups and a negatively charged sulphate group that comprise the hydrophilic part of the dye and a biphenyl group in the middle with a diazo group and two naphthalene groups (Wu et al., 2012). There is a strong presence of aromatic elements in this structure that are thought to facilitate the interaction of Congo red with amyloid fibrils by π-stacking (Gazit, 2002; Porat et al., 2006).

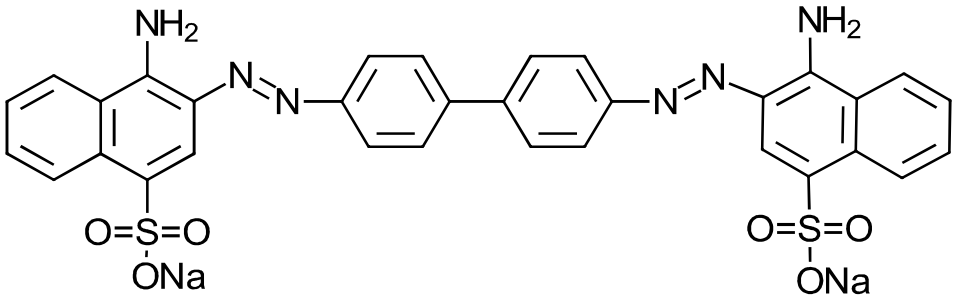

Figure 4. 5. Structure of Congo red dye. The dye has a strong presence of aromatic residues which bind to amyloid via π-stacking.

Many mutations targeting the phenylalanine residues, Phe19 in particular, has demonstrated the critical role they play in amyloidogenesis. Examples of substitutions made at position 19, all of which negatively affect amyloidogenicity, include serine (Wurth et al., 2002), leucine (Cukalevski et al., 2012), threonine (Esler et al., 1996), glycine (Hilbich et al., 1992) and isoleucine (Hilbich et al., 1992). Substitutions made at Phe20, however, have still resulted in assembly. This has been observed with leucine (Cukalevski et al., 2012) and also with tryptophan (Pachahara & Nagaraj, 2015).

One possible explanation for amyloid formation being greatly affected by mutations at F19 and not F20, is due to the role F19 has been hypothesised to play in nucleation (Cukalevski et al., 2012). Furthermore, using solid state NMR, contacts between F19 and L34 have been observed suggesting a turn conformation between this region of Aβ42 and also supports the notion that there is a hydrophobic collapse in the two most amyloidogenic regions of the sequence (Ahmed et al., 2010). Therefore, making a substitution at F19 with the polar residue serine, is expected to disrupt the normal π-stacking and fibril formation that is usually seen with wild type Aβ42 sequence. This is due to a combination of the small size of serine causing steric hinderance, and its hydrophilic properties disrupting the hydrophobic interactions usually buried within the protein.

The glycine at position 37, substituted with aspartic acid, has also been shown to be critical in Aβ42 assembly. Solid state NMR studies measuring amide exchange have identified solvent accessible turns at H13-Q15, G25-G29 and G37-G38. The β-sheet bend between G37 and G38 allows for the A42 to come into contact with the side chain of the M35 (Ahmed et al., 2010; Masuda et al., 2008). It has been suggested that this stabilizes the S-oxidized radical cation formed as a result of M35 oxidation by metal ions, by forming an S-O bond with an amide carbonyl oxygen or carboxylate anion on the A42. This has led to the assumption that there is the formation of intramolecular anti-parallel β-sheets at positions 35-42 in order to facilitate the S-O bond (Masuda et al., 2008). This results in a hydrophobic core being formed, long term oxidative stress and accelerated aggregation (Murakami et al., 2005). A model of this is shown in Figure 4.6 to highlight the importance of the Gly37.

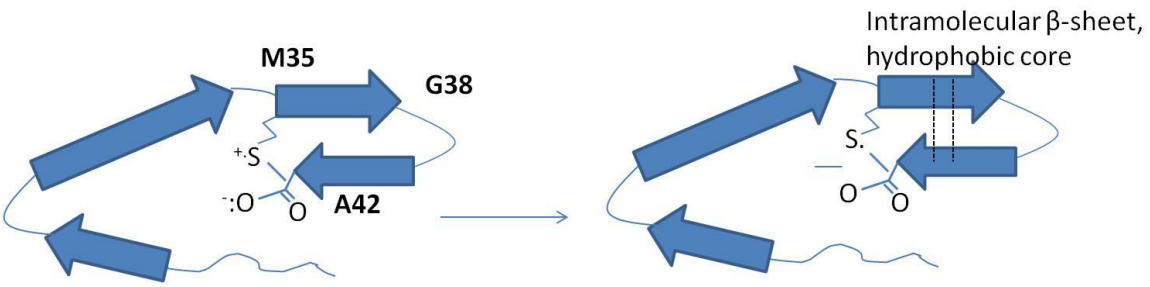

Figure 4. 6. The β-sheet bend between G37-38 in Aβ42 allows for the A42 to come into contact with the M35 side chains and stabilise radical cations which have been suggested to cause long term oxidative stress and aggregation of Aβ42 by the formation of intramolecular β-sheets.

The C terminal of Aβ42 contains a Gly-XXX-Gly-XXX-Gly motif (also discussed in APP section). This is known as a glycine zipper (Kim et al., 2005) and is often found on the transmembrane domain of several bacterial channel proteins (Kim et al., 2005). This glycine motif can drive the formation of packing between two α-helical regions of two Aβ monomers and leads to the formation of cytotoxic membrane pores (Fonte et al., 2011). Substituting the glycine residues for leucine, especially at position 37, has been shown to drastically reduce Aβ42 toxicity in cell cultures and *C.elegans* (Fonte et al., 2011; Harmeier et al., 2009; Hung et al., 2008; Kim et al., 2005). Taking into consideration the importance of glycine at position 37 in forming a solvent accessible turn, as well as the role it plays in α-helical packing of Aβ monomers, substituting G37 with a negatively charged, bulky amino acid such as aspartic acid will disrupt the turn and interactions that would usually occur in the wild type Aβ42 sequence. This is likely is due to the disruption of hydrophobic interactions and large size of aspartic acid causing steric hinderance.

4.2.2 Aβ42-1 and AβS are amyloidogenic

Using a range of biophysical techniques, the assembly and structure of the two control peptides were monitored until it was apparent that amyloid formation had reached a plateau. The peptides were prepared in an identical manner to the method developed in Chapter 3 for Aβ42 (Marshall et al., 2016). The assembly of the peptides was monitored using TEM, CD and ThT fluorescence.

TEM was used to observe the morphology of untagged peptide assemblies over time (Figure 4.7). Electron micrographs are the most representative of three independent peptide sample preparations. For Aβ42-1 at T0, there are small aggregates (black arrows) which are identified as being prefibrillar oligomers. These are similar to those seen with Aβ42 (Marshall et al., 2016) at 4 hours and also seen by other groups with Aβ40 (Sarroukh et al., 2011). By 4 hours, there are obvious large fibrillar aggregates formed. These are not as ordered as fibrillar aggregates observed with Aβ42, however the presence of fibrillar species is seen at an earlier time point that for Aβ42. It is evident that by 24 hours Aβ42-1 forms fibrillar structures, although again these are less ordered in appearance than those formed by Aβ42 and are comparable to those seen with Aβ40 (Kok et al., 2009; Qiang et al., 2012). This may due to be only one amyloidogenic region being identified within the sequence. Furthermore, in Aβ42, the β-sheet packing is in register and anti-parallel. By reversing the sequence, the hydrogen bonding in this arrangement could be affected giving rise to less stable and ordered mature fibrils.

Interestingly, AβS forms plaque-like fibrillar networks by 24 hours which are only observed with Aβ42 after 7 days (Figure 3.6 in Chapter 1) at the same concentration. As WALTZ predicted no amyloidogenic regions for AβS, this assembly was unexpected and highlights the importance of conducting experimental structural characterisation. It is possible the 200 hexapeptide used to develop WALTZ did not include sequences within the AβS sequence, however, it is more likely to be a limitation within the algorithm itself. Despite no amyloidogenic region being identified, the presence of fibrils which display similarity to Aβ42, indicates that AβS is amyloidogenic. TEM suggests that not only does AβS aggregate but does so with a higher propensity than Aβ42. This raises the question of why rearranging the same amino acids in a different order increases the propensity to self-assemble. As with Aβ42-1, AβS is not a naturally occurring peptide. However, as amyloidogenicity is an inherent property of all peptides under the correct conditions, perhaps the way in which the AβS was prepared (e.g. pH, salts in buffer, concentration) provided the optimal conditions to form amyloid. It is also possible that the arrangement of the amino acids may also lead to stronger hydrogen bonding and side chain interactions.

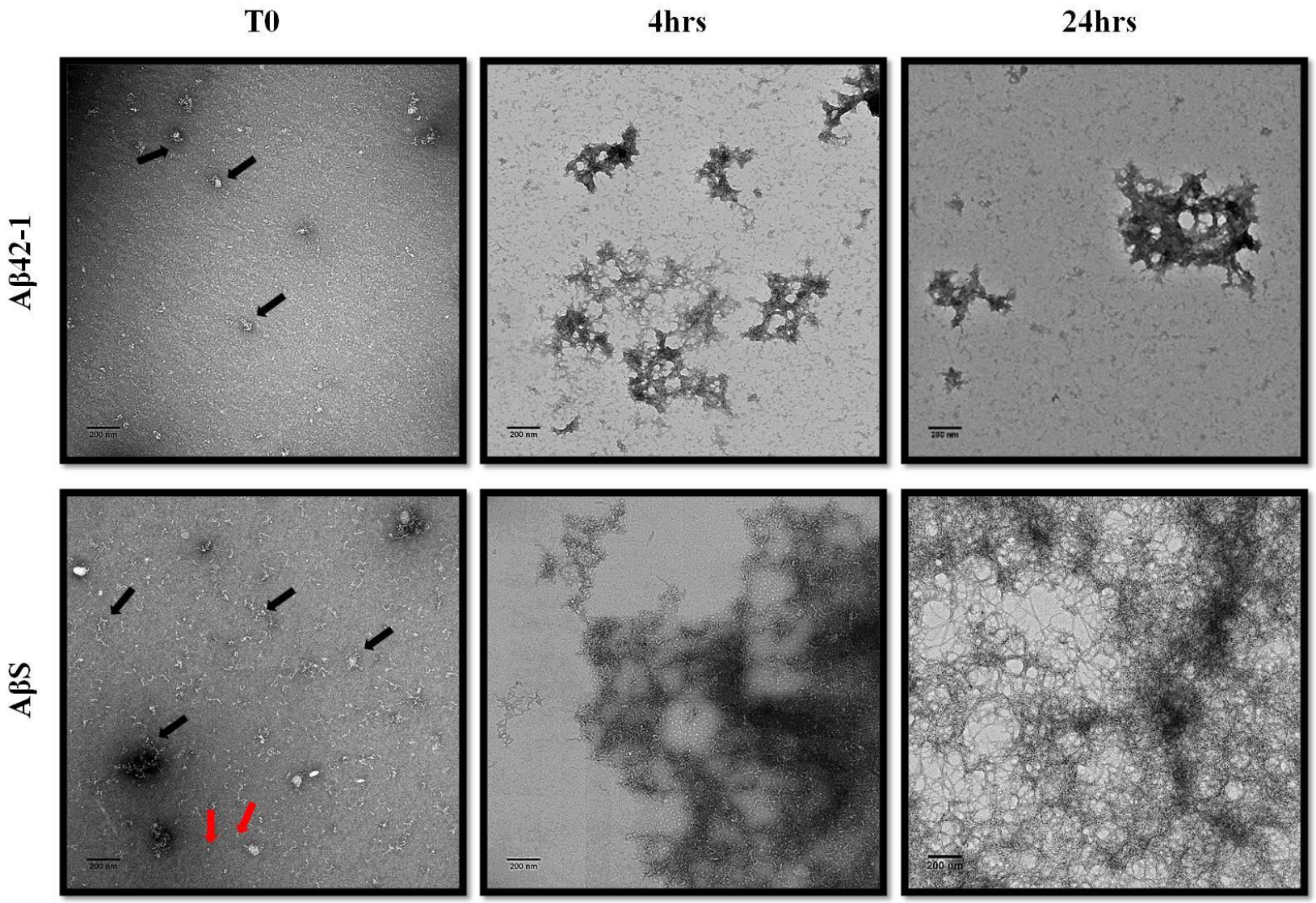

Figure 4. 7. Negatively stained electron micrographs of Aβ42-1 and AβS over 24 hours. 50μM untagged peptides were prepared in 20mM Phosphate Buffer (pH 7.4) and incubated at room temperature. Aβ42-1 shows the presence of spherical aggregates (black arrows) at T0 which form clumps fibrils by 4 hours. AβS shows small fibrillar species at T0 (black arrows) as well as some possible small oligomers (red arrows), fibrillar networks by 4 hours and these were much larger by 24 hours. Scale bars are shown at 200nm. The electron micrographs are the most representative of three independent peptide preparations.

To confirm both peptides can be classified as amyloidogenic proteins, X-ray fibre diffraction was used to confirm a cross-β molecular structure. The X-ray fibre diffraction patterns for both are shown below in Figure 4.8. The sample preparation was carried out by myself and the X-ray fibre diffraction data was collected by Louise Serpell.

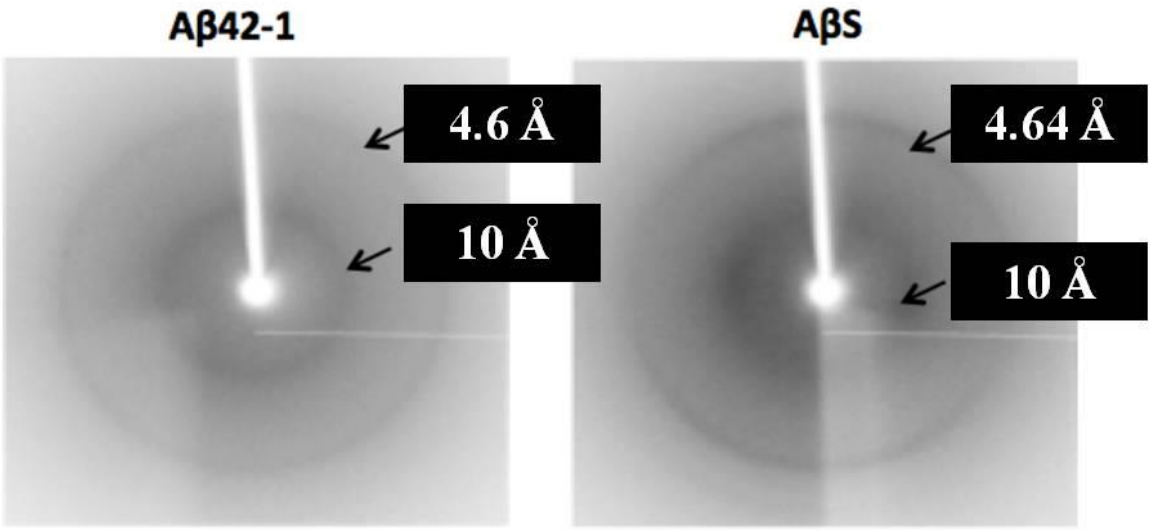

Figure 4. 8. X-ray fibre diffraction patterns for partially aligned fibrils formed by Aβ42-1 and AβS. X-ray fibre diffraction patterns revealed characteristic cross-β diffraction signals at 4.7 Å and at 10 Å. The sample preparation was carried out by myself, however, the X-ray fibre diffraction data was collected by Louise Serpell. This XRFD experiment was carried out once in order to confirm amyloid formation.

The fibril samples were not aligned enough to provide details of structural similarities compared to Aβ42, however, the X-ray fibre diffraction patterns for the partially aligned fibres of both peptides display the characteristic signals at 4.6 Å and 10 Å for a cross-β structure. This confirms that both peptides form amyloid.

4.2.3 Aβ42-1 and AβS form mature fibrils with β-sheet rich secondary structure

CD was used to investigate the secondary structure of both peptides over a 48-hour incubation time (Figure 4.9A and B). The spectra shown as the mean of three independent samples. Both control peptides show a strong β-sheet signal (minimum and maximum at 218nm and 192nm respectively) almost immediately after preparation. The spectrum for AβS is initially shifted slightly towards random coil, suggesting a mixed population, but displays a strong β-sheet signal by 24 hours. The unchanged β-sheet signal seen for Aβ42-1, together with the electron micrographs suggests the small aggregates seen at T0 have already adopted a β-sheet structure. The change in β-sheet signal (218nm) over the incubation time are also shown (Figure 4.9 A and B, insets). There is a decrease in β-sheet signal from time zero to 4 hours, however, after this there is relatively little change in the spectra at increasing time points for Aβ42-1, with the molar ellipticity remaining at ~ -250deg.mol^2/dmol up to 48 hours. The initial decrease seen in might be explained by some of the fibril falling out of solution as aggregation progresses. An increase from -180deg.mol^2/dmol at T0 to -500deg.mol^2/dmol at 48 hours is seen with AβS. Again, this could suggest a small population of random coiled conformation at early time points which quickly adopt a strong β-sheet signal. The TEM of AβS at T0 show small spherical structures (red arrows) that do not yet have a distinct appearance of a larger oligomers/protofibrils which may account for the slight shift to a random coil signal at the early time points. This is in contrast to wild-type Aβ42 which transitions from random coil to β-sheet over a 24 hours period under the conditions used. From TEM and CD, there seems to be an immediate assembly into β-sheet rich Aβ42-1 entities for Aβ42-1 and an extremely rapid assembly process including intermediary random coiled species for AβS.

Fibrillogenesis was monitored using a ThT fluorescence assay (Figure 4.9C); both control peptides show a signal at 483 nm, which indicates the presence of ThT positive structures. The ThT fluorescence of both control peptides is shown over a 48-hour period. A typical spectrum for wild-type Aβ42 (Figure 3.7C, Chapter 3) shows a lag phase before a steep increase in intensity, which then begins to plateau. This can be explained by nucleation-dependent fibrillisation; the lag phase is the period during which oligomers are generated through a primary pathway and act as

thermodynamically stable nuclei for fibril growth. Once a critical fibril concentration has been reached, secondary nucleation becomes the dominant nucleation process and the surface of these fibrils can act as a catalyst for the formation of oligomers and further proliferation into fibrils. This lag and elongation phase is not observed with either of the control peptides, consistent with the results indicating rapid assembly from TEM and CD. The lower intensity in ThT fluorescence at later time points may be attributed to the loss of peptide from solution as larger aggregates form. This is supported by the dense fibril morphology observed in the electron micrographs at 24 hours (Figure 4.7). The ThT fluorescence spectrum for Aβ42-1 showed a very shallow increase in intensity, although fibrils are visible in the electron micrographs. Different peptide systems are difficult to directly compare using ThT fluorescence due to differential binding, however, it is clear that ThT intensity increases with incubation time. This suggests the peptides self-assemble to form amyloid fibrils during the timeframe of the experiment.

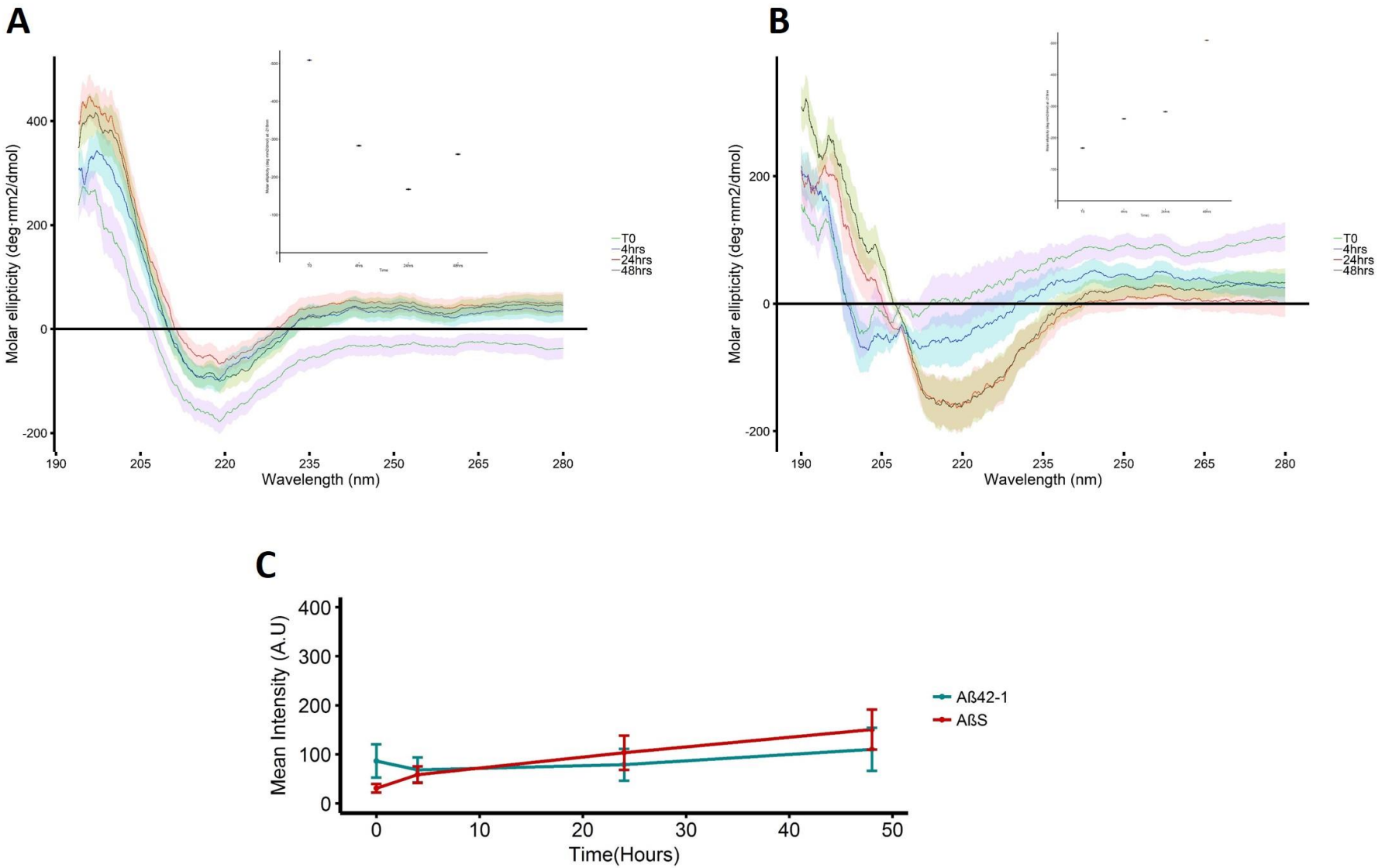

Figure 4. 9. CD spectra and ThT fluorescence of Aβ42-1 and AβS over 48 hours. A) The CD spectra for Aβ42-1 (1mm cuvette) shows a β-sheet signal from T0. B) The CD spectra for AβS (0.5mm cuvette) shows a weak β-sheet signal at early points which shifts to a stronger signal by 24 and 48 hours. This increase in β-sheet signal is more clearly seen in the graph inserted above the CD spectra showing the molar ellipticity at -218nm over time. Both CD spectra are means of the spectra obtained from three independent sample preparations. The insets show the mean increase in β-sheet intensity C) ThT fluorescence of both Aβ42-1 and AβS show a slight increase in intensity over time. The average of three independent sample preparations for each peptide is shown. Peptides were prepared untagged at 50µM in 20mM phosphate buffer pH 7.4 and incubated at room temperature.

4.2.4 vAβ42 is assembly impaired

As the vAβ42 is presented as a more appropriate, novel experimental control peptide, as well as a model to investigate the importance of primary sequence in amyloidogenicity, the characterisation was carried out over a 7-day period for a true comparison with Aβ42 (Chapter 3). This extensive biophysical characterisation is necessary to ensure that assembly for this peptide sequence is impaired, despite only a two amino acid substitution.

As with Aβ42-1 and AβS, the vAβ42 peptide was prepared in an identical manner to Aβ42. CD, ThT fluorescence and TEM were used to investigate self-assembly. From TEM (Figure 4.10), no assemblies were visualised even at 7 days. The CD spectra for vAβ42 (Figure 4.11A) confirms that there is no secondary structure reorganisation and that the peptide remains in a random coiled conformation (minimum at 198nm) from T0 to 7 days. ThT fluorescence (Figure 4.11B) confirmed a lack of fibrillogenesis within the same timeframe, displaying negligible intensity at 483nm. Together, these results suggest vAβ42 does not assemble in the same time frame as Aβ42 (Marshall et al., 2016).

To further confirm lack of assembly into insoluble amyloid, solution state NMR was utilized to monitor changes in solubility over time (Pauwels et al., 2012). Scans were taken every 30 minutes over 66 hours to monitor changes in shift positions and signal strength. Figure 4.11C. If there is a change in solubility, the signal disappears once the peptide assembles past than a certain size. Even at the high concentration of 200μM necessary for solution state NMR, the two traces at T0 and 66 hours are identical suggesting no changes in solubility (Marshall et al., 2016). The NMR trace of Aβ42 has been included as a comparison; the traces are T0 and 66hours are not identical and there is a loss of signal from the aromatic residues suggesting a change in solubility and structure. NMR results were obtained by Dr. Iain Day and the experiment was conducted once due to the high concentration and volume of the peptide needed as well as the availability of the NMR instrument.

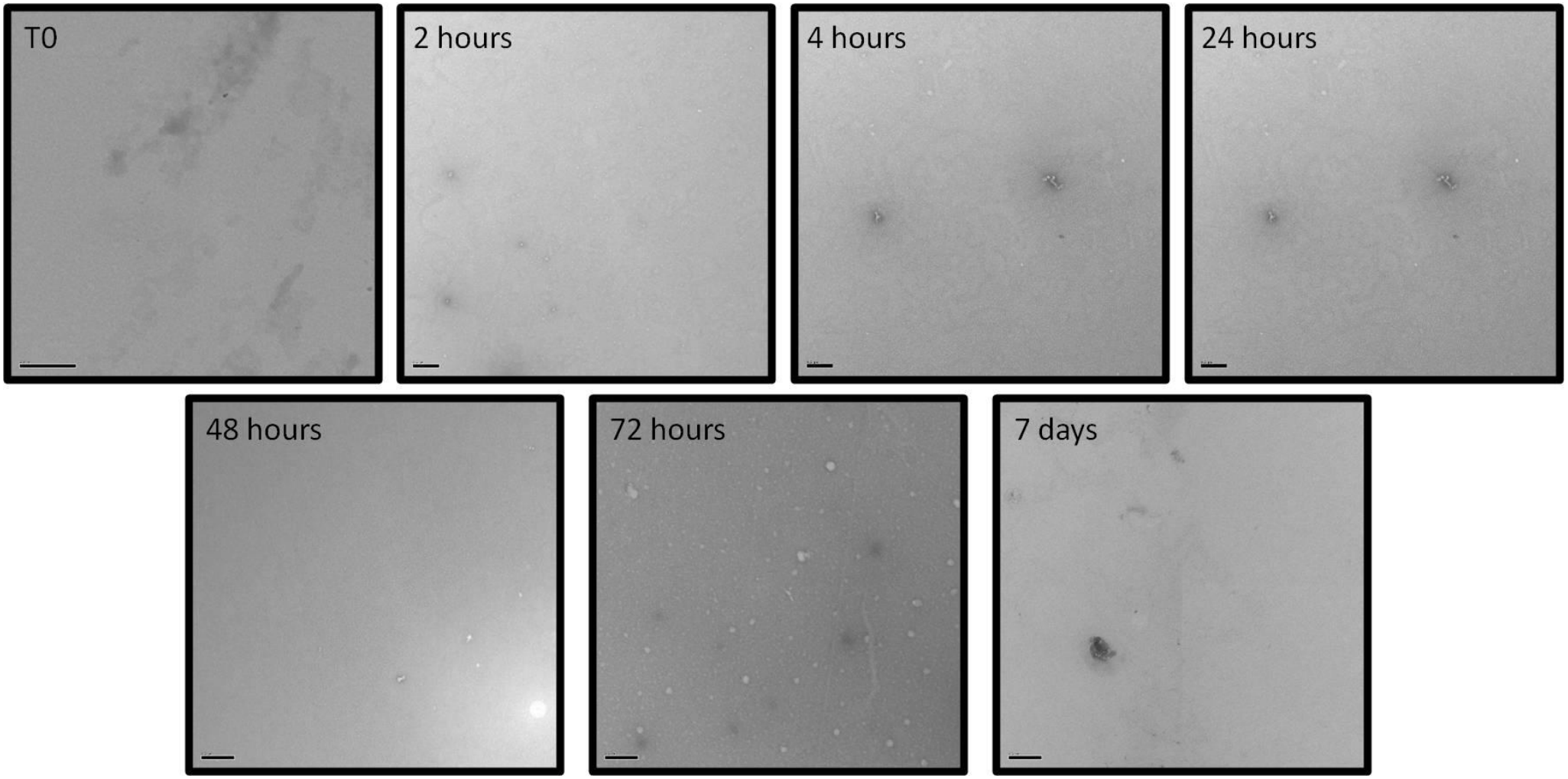

Figure 4. 10. Negatively stained electron micrographs of 50µM vAβ42 over 7 days. No assembly was seen in the time frame. Peptide was prepared in 10mM HEPES buffer pH 7.4 and incubated at room temperature. Scale bars are shown at 0.5µm. The electron micrographs are the most representative of all images obtained from three independent sample preparations.

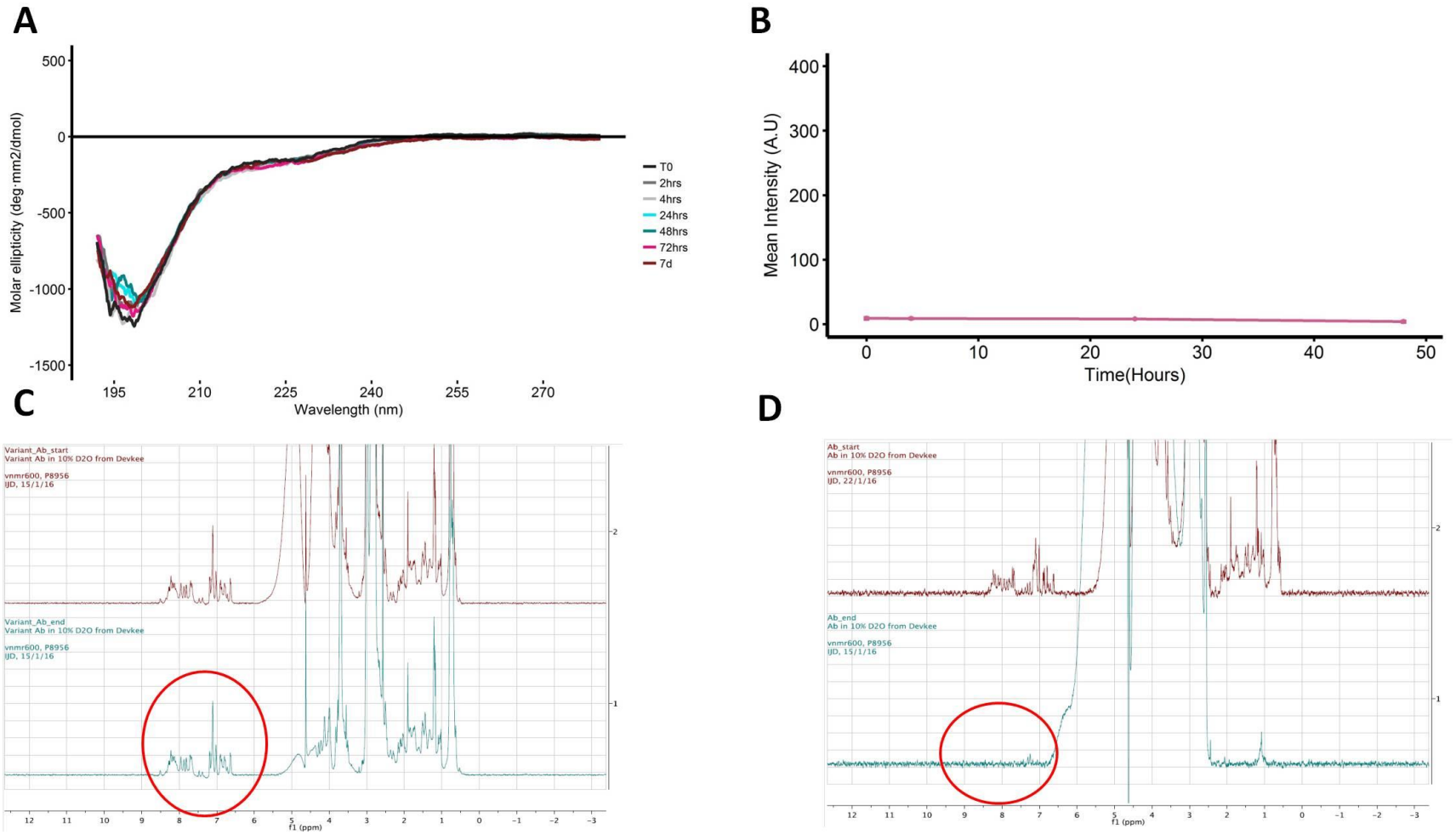

Figure 4. 11. CD, ThT fluorescence and NMR for vAβ42. A) CD spectra for vAβ42 displays a signal for random coil conformation from T0-7 days. This suggests the peptide remains unfolded and does not undergo any structural reorganisation. The spectra is representative of three spectra obtained from three separate sample preparations. B) ThT fluorescence for vAβ42 is negligible confirming a lack of fibrillogenesis. The graph is the average of three separate sample preparations. Error bars expressed as ±SEM. C) The NMR signal of vAβ42 remains unchanged over 3 days shown by the red circle on the bottom trace (T0 signal shown in the top trace, 3 day signal shown in the bottom trace) indicating that the peptide does not change structure in this time period. D) The NMR signal for the Aβ42 peptide is included for comparison and shows a loss in signal of the aromatic residues suggesting there is a structural change occurring and a change in solubility. The NMR experiment was performed by Dr. Iain Day. For CD and ThT, 50µM untagged peptide was prepared in 20mM Phosphate buffer pH 7.4. For NMR, the peptide was prepared at in water and used at the stock concentration of 200µM.

Despite the biophysical characterisation presented above indicating impaired assembly of vAβ42, it is possible there may be small species (possible oligomers) that are undetected by TEM, with β-sheet secondary structure not detectable by CD or bind ThT. To examine whether vAβ42 forms small oligomers, antibodies directed at different conformations and epitopes were used.

The anti-Aβ antibodies used in this chapter and their epitopes are shown in Table 2.2 (Chapter 2). As the epitope for the N-terminal anti-Aβ 4G8 antibody, used in Chapter 1, overlaps with the F19S substitution in the vAβ sequence (18-23), this antibody is not expected to show reactivity with vAβ42. Dot blots (Figure 4.12A) were carried out and provide useful information regarding the antigenicity of vAβ42 as well as the species in present in the sample. However, as the assembly of amyloid is dynamic, the sample population is likely to be heterogenous. Therefore, SDS-PAGE and western blotting was also used separate the sample by size and detect any assembled strucutres. Samples of vAβ42 were collected at each time point and the 6E10 antibody was used to detect the peptide (Figure 4.12B).

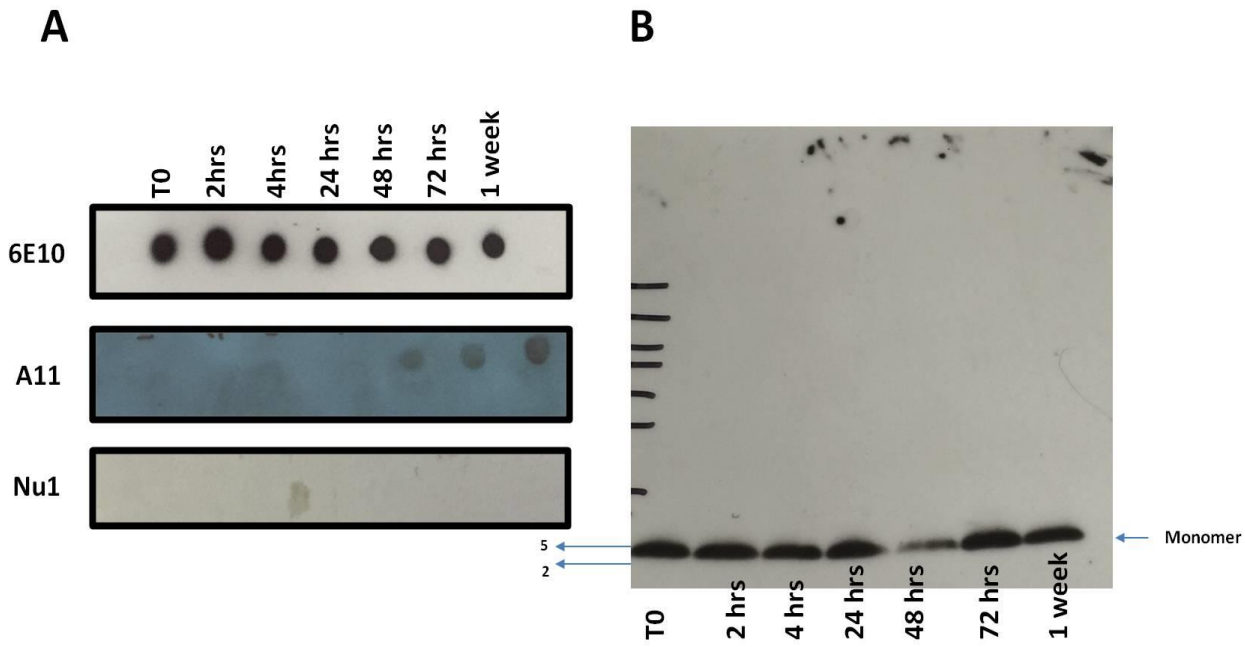

Figure 4. 12. Antigenicity of vAβ42. A) Dot blots using 6E10 (1:10,000), A11 (1:5000) and Nu1(1: 10,000) antibodies to detect for vAβ42 over 7 days. The 6E10 antibody confirms the presence of the peptide at each time point. A11 and Nu1 are oligomer specific conformational antibodies; there is a very faint signal displaced by A11 at later time points and no reactivity with Nu1 over 7 days, suggesting no oligomeric species are formed. B) Western blot using the 6E10 antibody shows that the vAβ42 runs as a monomer and does not assemble into higher molecular weight structures over 7 days. The untagged peptide was prepared at 50μM in 10mM HEPES buffer pH 7.4 and incubated at room temperature. 1 and 2ug of protein was loaded for the dot blot and western blot respectively. Both the dot blot and western blot were carried out once, therefore quantitative analysis was not possible.

One repeat of both the dot blot and western blot were carried out and therefore quantitative analysis was not possible. Additional repeats for robust quantification would be a future direction.

The dot blot (Figure 4.12A) using 6E10 antibody, the epitope for which is still conserved in the vAβ42 sequence (3-8), confirms the presence of the peptide at each time point. However, NU1 shows no reactivity and only a faint signal is seen with A11. As both these antibodies are conformation-specific for oligomers, this suggests there are no oligomeric assemblies formed over the course of 7 days. The western blot (Figure 4.12B) using 6E10 detects only monomeric vAβ42 suggesting this peptide does not assemble into higher molecular weight structures over 7 days.

The A11 antibody has been used extensively in several studies to differentiate between oligomeric and fibrillar species. As it is a conformational antibody with no specific epitope, A11 can be used to detect oligomers of a wide range of proteins including α-synuclein, HTT and SOD (Kayed et al., 2003). The binding mechanism, however, has not yet been established and it is possible that the faint signal seen in the dot blot for vAβ42 is simply an artefact. Another possibility is that vAβ42 could be forming stable dimers at later time points that cannot be seen at the resolution of TEM. However, this seems to be unlikely as SDS-PAGE electrophoresis and western blotting reveal only a monomeric size from T0 to 7 days.

Overall the biophysical and conformational specific antibody directed characterisation of vAβ42 confirm that this sequence is assembly impaired and does not form β-sheet rich structures within the same time frame as Aβ42. This makes it an ideal and more suitable experimental control for Aβ42 compared to Aβ42-1 and AβS.

4.2.5 vAβ42, Aβ42-1 and AβS are not cytotoxic

As all three peptides are both controls and models to explore the importance of primary sequence in amyloidogencity, their cytotoxic nature was investigated in rat primary hippocampal neurons. All three peptides were prepared in the same manner as Aβ42, which is most oligomeric after a 2 hour incubation period (Chapter 3). After 2 hours of incubation at room temperature, 10μM of peptide was added to cells and incubated for 7 days, after which toxicity was assessed using a ReadyProbes assay. Although this concentration is not physiologically relevant, it allows us to rule out the possibility that negative results are not due to a low peptide concentration and also ensures effects are seen within a reasonable timeframe. ReadyProbes is a live/dead assay containing two reagents, one labelling the nuclei of all cells with a blue dye and a second that labels dead cells only with a green dye. An example for each peptide added to cells is shown below (Figure 4.13).

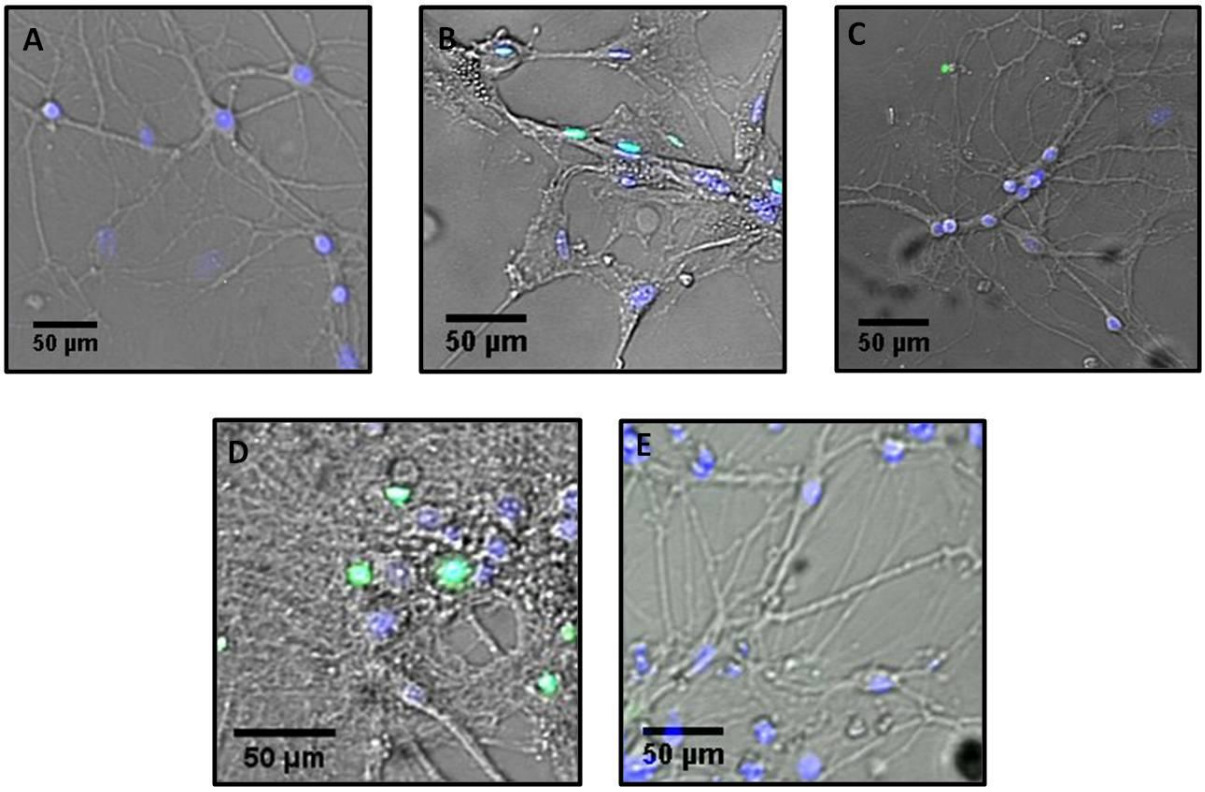

Figure 4. 13. Examples of ReadyProbes images. Zooms of images taken at 10X of hippocampal cultures incubated with 10µM (A) Buffer (B) AβS (C) Aβ42-1 (D) Aβ42 (E) vAβ42 at 7 days. Peptides were prepared at 50µM in 10mM HEPES buffer pH7.4 and incubated for 2hours before added to cells. The ReadyProbes cell viability assay was then carried out at 7 days. Scale bars shown at 50µM.

The number of green cells were calculated as a percentage of the blue cells, to quantify toxicity (Figure 4.14, top left). As the density of cells plated remained constant, imaging and counting the same number of regions for each condition of treated cells provides a valid indication of cyototxicity. Data for Aβ42 have been included as a comparison for both structure and cytotoxic effects. DIC images (Figure 4.14, bottom panel) are useful to look at the morphology of the cells, although, it is not possible to comment on the viability of cells simply using these images. From the DIC images, it is possible to see that cells treated with three variants of Aβ42 for 7 days are plentiful with their cell bodies and axons still intact. Finally, EM was used to confirm the morphology of the peptides being added to the cells (Figure 4.14, top right).

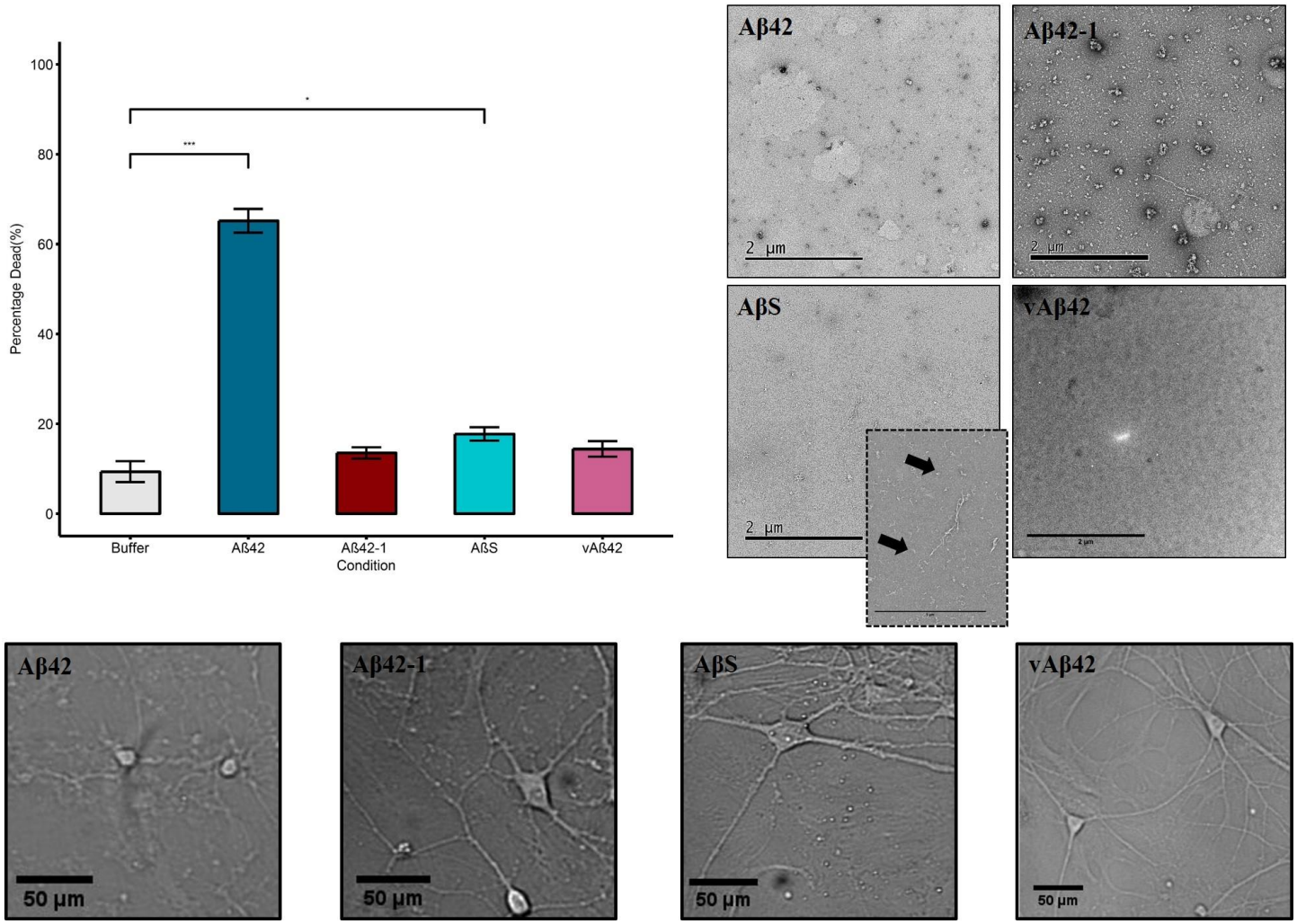

Figure 4. 14. Aβ42 variant peptides ReadyProbes cell viability assay. Rat hippocampal cultures were incubated with 10µM Aβ42, Aβ42-1, AβS and vAβ42 for 7 days, after 2 hours of peptide incubation. The average of three independent experiments (three separate Aβ42 preparations and hippocampal cultures) is shown. Cytotoxicity was measured as a percentage of dead cell in a culture and compared to buffer incubated cells (10.21% ± 2.32, total number of cells = 558, number of dead cells=52). Aβ42 oligomers were significantly toxic compared to the buffer at 7 days cell (66.3% ± 2.59, total number of cells = 1172, number of dead cells=777) as was AβS (17.19 ± 1.49, total number of cells = 1627, number of dead cells=288) Both Aβ42-1 (14.06% ± 1.26, total number of cells = 719, number of dead cells=97) and vAβ42 (12.38% ± 2.81, total number of cells = 1245, number of dead cells=179) were non-cytotoxic. Unpaired parametric student's t test where p= < 0.01 (*), < 0.001 (**), < 0 (***). Error bars are expressed as ±SEM. Electron micrographs of each peptide are shown (top, right. Scale bars at 2µm) as are the DIC images of cells incubated with each peptide after 7 days (bottom panel. Scale bars shown at 50µM).

It is important to note that although cell viability assays are widely used to investigate cytotoxicity, the relationship to AD pathology may not be closely linked due to the various pathways involved in cell death and the specificity of the assay being used. Nevertheless, as the cytotoxicity of these control peptides in hippocampal neurons is being investigated, and not a model of AD pathology, the ReadyProbes assay is a valid approach. As described previously, Aβ42 causes 65% (66.3% ± 2.59, total number of cells = 1172, number of dead cells=777 , '***') cytotoxicity after 7 days of incubation compared to the buffer only condition that showed only 10% cell death (10.21% ± 2.32, total number of cells = 558, number of dead cells=52). In comparison, AβS and Aβ42-1 demonstrated less potent toxicity than wild-type Aβ42 at the same time point and using the identical preparation conditions; 17% (17.19 ± 1.49, total number of cells = 1627, number of dead cells=288, '*') and 14% (14.06% ± 1.26, total number of cells = 719, number of dead cells=97) respectively. Previous studies have also shown that Aβ42-1 (Yatin et al., 1999) and AβS (identical sequence to AβS used here from Anachem) (Izzo et al., 2014) are inactive in cellular assays.

Electron micrographs of the peptides 2 hours after preparation offer an explanation for the difference in cytotoxicity. Aβ42 shows small spherical species, which we identify as oligomers. In contrast, electron micrographs of Aβ42-1 and AβS taken at the same time point show some larger aggregates, possible protofibrils and some fibrils. No assemblies were visible for vAβ42, which may explain its non-cytotoxic nature; all three peptides do not form visible oligomers in the same timeframe as Aβ42.

It appears that reversed and scrambled variants of Aβ42 self-assemble to form fibrillar structures more rapidly than wild-type and these are much less toxic than oligomeric Aβ42. Previous work has linked internalisation of oligomers with toxicity and therefore one hypothesis for the reduced toxic nature of these peptides is that these structures are less able to enter the neurons (Chafekar et al., 2008; Marshall et al., 2016) and cause their downstream toxic effects due to their increased size. The inability for cells to take up AβS has been previously reported (Nath et al., 2012), as has the non-apoptotic effects of Aβ42-1 (Gamba et al., 2011; Troy et al., 2000). The slightly significant cytotoxic effects of AβS may be attributed to the random coil species detected by CD (Figure 4.9C); it could be

hypothesised that some oligomeric species remains in the AβS population after 2 hours (black arrows in electron micrograph, Figure 4.8). If AβS was incubated for a shorter period of time before being added to neuronal cultures, it may exhibit slightly more toxicity due to the higher presence of oligomers.

The vAβ42 peptide displayed no significant cytotoxicity (12.38% SEM± 2.81). Previous work adopting the MTT assay to monitor the metabolic function of hippocampal treated neurons, also confirmed no deleterious effect to cellular function by this peptide (Marshall et al., 2016) . Extensive functional characterisation was also carried out to confirm that vAβ42 has no effect on hippocampal synaptic function and does not disrupt the recall of consolidated long-term memory in *Lymnaea stagnalis* (Marshall et al., 2016). Together, these data shows the vAβ42 to be non-cytotoxic. This can be again linked to internalisation, which was not seen with this peptide (Marshall et al., 2016).

Overall, the data presented on the cytotoxic nature of all three sequence variants of Aβ42, show them to be much less deleterious to cellular function than Aβ42.

4.3 Conclusions

In this chapter, we explored the importance of primary sequence in determining assembly propensity and its corresponding toxicity of Aβ42 related proteins.

By characterising assembly of each Aβ42 variant (summarised in Figure 4.15) and relating this to toxicity, our findings suggest the toxic nature of these amyloid proteins is highly related to primary sequence. It is however, extremely, important to note that this is true for the peptides presented in this chapter using our preparation method. It is possible, using a different protocol of peptide preparation may not result in the same assembly or toxicity. Therefore, without exploring other methods of peptide preparation in a similar manner and relating assembly to cytotoxicity, we can only confidently state that primary sequence highly influences cytotoxicity due to the assembly process in our specific sample preparation. The influence of primary sequence in the propensity to form amyloid has been previously established, however, linking this to cytotoxicity provides insights into ‘rules’ for amyloid

toxicity. The WALTZ algorithm predicted both control peptides to have fewer amyloidogenic regions than the wild-type; Aβ42-1 was predicted to have one amyloidogenic region, whereas AβS was predicted to have none. Despite this, both peptides show a high propensity to form amyloid with similar non-toxic behaviour in cells. Therefore, we can also make the conclusion that as a consequence of primary sequence, the ability to assemble into amyloid via oligomeric species, is an important factor influencing the cytotoxic nature of pathogenic amyloid proteins.

The vAβ42 was predicted to have no amyloidogenicity, which has been confirmed by extensive characterisation. This peptide has also been shown to be non-toxic which is suggested to be related to impaired assembly due to the primary sequence. All three sequences do not assemble to form oligomeric species within the same timeframe as Aβ42 and therefore the species of each variant peptide added to our neuronal cultures were not oligomeric and non-toxic. This supports the view that Aβ42 oligomers represent the toxic entity. Further experiments assessing cytotoxicity of Aβ42-1 and AβS after a shorter/no incubation to neuronal cultures would provide stronger evidence for this, as it would be likely some oligomeric species would be present (especially for AβS as suggested by CD). This toxicity may be related to internalisation of oligomers due to their size (discussed in-depth in Chapter 5). Furthermore, to understand better whether the process of self-assembly plays an important role in cytotoxicity the cells should be incubated with both Aβ42-1 and AβS immediately after preparation. This would allow us to add any oligomers that may be have been missed in the two-hour incubation and allow us to evaluate whether the assembly from oligomers to fibrils may mediate cytotoxicity.

It has previously been reported that the uptake of aggregating amyloid proteins is sequence specific (Couceiro et al., 2015), and the cellular response to these proteins is thought to be highly dependent on aggregation propensity, size and charge. As the sequences of both Aβ42-1 and AβS peptides result in a higher propensity to aggregate than wild-type Aβ42, confirmed by structural characterisation presented above, the reported mechanisms of internalisation, which include dynamin-mediated endocytosis (Yu et al., 2010), may not be possible with these peptides. Alternatively, the specific

order of amino acids in Aβ42-1 and AβS may affect binding to receptors or assembly into specific oligomeric species that are required for toxicity.

As a future direction, the internalisation of all three peptides should be looked at using techniques such as immunocytochemistry and live cell imaging. This would enable to gain a further understanding of whether the larger assemblies, or no assemblies in the case of the vAβ42, are not causing significant cytotoxicity due to internalisation.

Although both Aβ42-1 and AβS have been used in many studies as experimental controls for Aβ42, the data presented in this chapter suggest their validity should be questioned. If conclusions are to be made regarding the effects of amyloidogenic proteins, it is desirable for controls to be sequence related but ideally show no propensity for self-assembly. The structural characterisation presented here confirms that the F19S and G37D substitutions are able to disrupt self-assembly and thereby render the sequence to be non-toxic in primary hippocampal cultures. Therefore, the sequence-related, non-aggregating variant of Aβ42, vAβ42, serves as a more suitable control. To critically evaluate and continually develop experimental controls in this way will ultimately aid our understanding of the mechanisms involved in AD.

Overall, the Aβ42 variant models presented in this chapter provide support for the importance of primary sequence in determining amyloid toxicity. This due to the subsequent assembly process; the ability to assemble in a process allowing for the formation of intermediary oligomeric species is a factor determining amyloid toxicity.

Finally, relating this work to disease-related mutations within the Aβ sequence that affect the assembly process and relating this to cytotoxicity would be future direction of this work. For example, the Arctic FAD mutation where there is a substitution of the glutamic acid with a glycine at position 22, is thought to enhance the fibrillisation of Aβ. A similar characterisation of this sequence, including using the WALTZ algorithm to identify any shifts in the amyloidogenic regions, and

relating this to cytotoxicity in primary hippocampal cultures, would begin to relate the conclusions reached using the primary sequence models in this chapter to disease-related sequences.

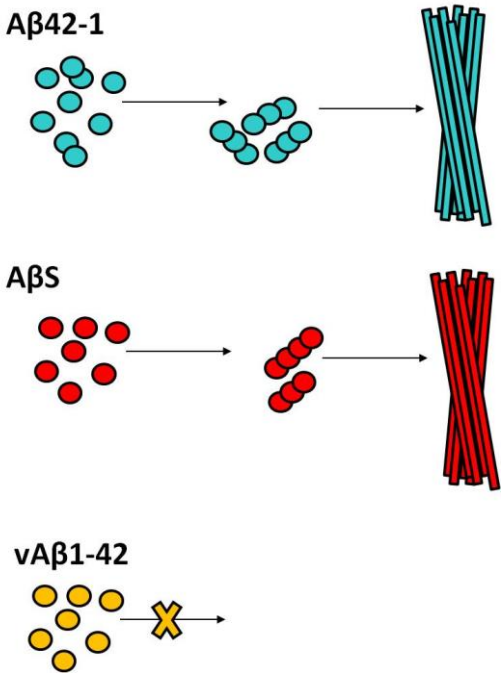

Figure 4. 15. Schematic diagram to summarise the assembly process of three Aβ42 variants. Aβ42-1 assembles from small aggregates which are β-sheet rich, into protofibrils and mature fibrils. AβS assembles rapidly from monomers/ small oligomers to fibrils and the vAβ42 is assembly impaired, remaining monomeric (at least within the time frame of our characterisation).

Chapter 5: Implications of size, conformation and internalisation in amyloid toxicity

Chapter Overview

Having established the importance of primary sequence in the role of amyloid toxicity using Aβ42 variants, we sought to determine the importance of the size and conformation of Aβ42 assemblies. The ReadyProbes cell viability assay was utilized to assess the cytotoxicity of Aβ42 oligomers (AβO), Aβ42 fibrils (AβF) and sonicated fibrils (AβSon) in rat primary hippocampal cultures. The data presented in this chapter also uses a combination of immunocytochemistry and live cell imaging to investigate the localisation and internalisation of each of these species in primary hippocampal and SHSY5Y cultures. In this way, we linked the importance of size, conformation and internalisation (or lack of) to cytotoxicity.

5.1 Introduction

The plaque deposits in AD brains are composed of cross-β sheet units arranged into amyloid fibrils of the Aβ peptide (Benilova et al., 2012). Although it has been reported that cognitive decline seen in AD patients correlates poorly with plaque deposition (McLean et al., 1999), there is mounting evidence to suggest that these may play a role in disease process due to the dystrophic neurons, activated microglia and reactive astrocytes (Bezprozvanny, 2009; Meyer-Luehmann et al., 2008) surrounding plaques areas. Plaques have also been implicated as reservoirs of oligomers which may facilitate further toxicity (Kayed et al., 2007; McLean et al., 1999; Verma et al., 2015; Walsh et al., 2002b) .

The relationship between amyloid structure and toxicity has been the focus of much research, and it is generally accepted that Aβ exerts its deleterious effects due to the self-assembly process (Broersen et al., 2010; Pike et al., 1991; Pike et al., 1993; Williams & Serpell, 2011). This is supported by the data presented in Chapter 4 where the assembly-impaired vAβ is not cytotoxic (Marshall et al., 2016).

The amyloid cascade hypothesis identifies the Aβ42 oligomeric species as the primary culprit of toxicity (Hardy & Higgins, 1992). Focus on oligomers has been heavily influenced by the correlation between cognitive decline and soluble Aβ (McLean et al., 1999). The lack of a universal definition for the term 'oligomer' and the many different preparation methods used, has led to several oligomeric species being identified as neurotoxic (Reviewed in Table 3.2). This serves as support for the theory that rather than one size or species in particular being responsible for the toxic nature of Aβ42, it is more feasible toxicity of Aβ42 is somewhat linked to conformation (Broersen et al., 2010)

5.1.1 Oligomeric and Fibrillar Aβ42

The factors affecting amyloid assembly and the variability of different preparation methods have been discussed in Chapter 1. The result of this has been the identification of several species as being cytotoxic (Benilova et al., 2012; Broersen et al., 2010).

From the data presented in Chapter 4, Aβ42 is the only primary sequence that forms intermediary species on the pathway to becoming amyloid fibrils. This was also the only peptide to exhibit cytotoxicity in rat primary hippocampal cultures (Vadukul et al., 2017) and SHSY5Y cells (Marshall et al., 2016). The toxicity is therefore, at least in part, related to the ability to form these intermediary oligomeric species. A specific understanding of why these oligomers are toxic, however, is not fully understood- is it related to size or conformation?

As there are several conformations the term ‘oligomer’ can encompass, simply stating oligomers are toxic is not sufficient to gain an understanding regarding what makes an amyloid protein toxic. There is still much debate as to which conformational changes are needed to move from one phase to the next during the assembly process of Aβ, in which there is the lag phase followed by the elongation phase (Ferrone, 1999). Generally, it is accepted that Aβ begins as a randomly coiled (unstructured) monomer which then becomes ‘activated’ as a critical nucleus for further monomer addition and elongation (Taylor et al., 2003).

The initial steps of Aβ assembly are thought to include an equilibrium of randomly coiled, α-helical and β-sheet species monomers (Bartolini et al., 2007; Benseny-Cases et al., 2007; Broersen et al., 2010). It is thought that only those species with β-sheet conformation can facilitate the elongation into fibrillar oligomers and mature fibrils (Broersen et al., 2010) (Figure 5.1)

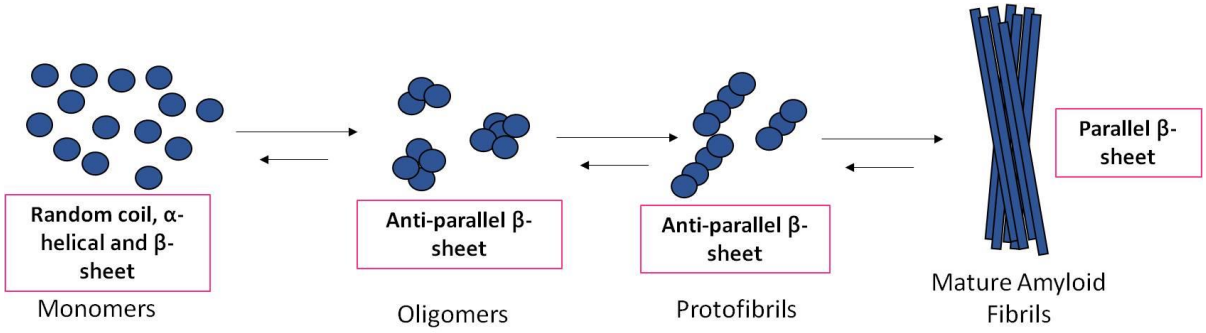

Figure 5. 1. Schematic diagram of conformational changes that occur during Aβ42 assembly. There is the equilibrium of β-sheet, random coil and alpha helix monomer which assemble into anti-parallel β-sheet oligomers and protofibrils. These then assemble into parallel β-sheet mature amyloid fibrils. Adapted from Broersen et al, 2010.

Many groups have reported the oligomeric species as being β-sheet rich structures (Cheon et al., 2007; Kayed et al., 2007; Stroud et al., 2012). Although this is in contrast to the data presented in Chapter 3 where we identify toxic oligomers to lack a significant secondary β-sheet rich structure by CD, it is likely that 1) both conformations co-exist and certain percentage of our oligomeric species is β-sheet rich with the random coil signal dominating due to the majority of the sample remaining unstructured and 2) oligomers can be both prefibrillar or fibrillar, with the β-sheet rich oligomeric species identified by other groups being the fibrillar oligomeric species. Fourier-transform infrared (FTIR) spectroscopy and NMR studies have shown pre-fibrillar Aβ42 oligomers lack a parallel β-sheet structure found in fibrillar oligomers and mature amyloid fibrils, and have an anti-parallel packing of β-sheets (Verma et al., 2015; Yu et al., 2009; Yu & Zheng, 2011). The oligomeric species can therefore be split into two broad categories; prefibrillar (anti-parallel β-sheets) and fibrillar (parallel β-sheets).

Mature Aβ amyloid fibrils possess a hairpin secondary structure with an exposed N terminal (Tycko, 2011) . A β-turn loop links two parallel β-sheet structures (Buchete & Hummer, 2007) (Figure 5.2),

which is thought to be further stabilised via a salt bridge between Asp23 and Lys 28 (Kahler et al., 2013; Roychaudhuri et al., 2009). These fibrils are highly ordered and stable with their hydrophobic surfaces buried within the fibre.

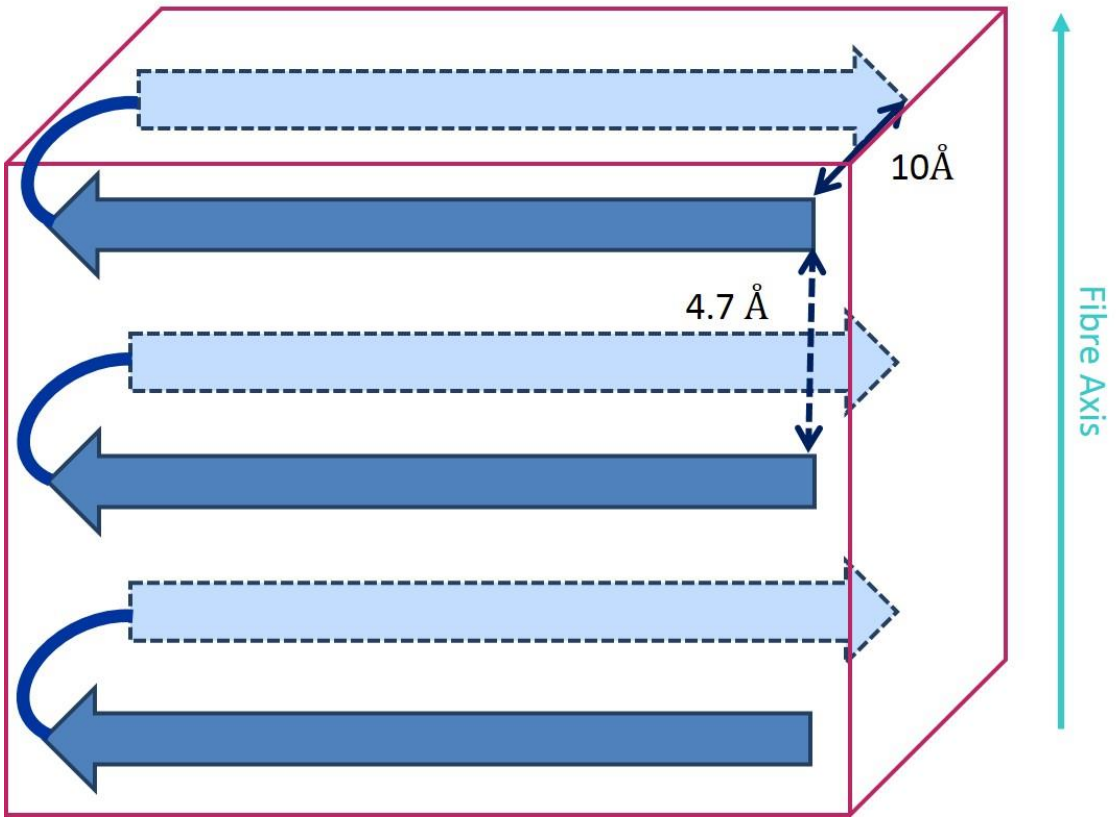

Figure 5. 2. Schematic representation of the Aβ42 β-turn loop linking two parallel β-sheet structures.

5.1.2 Conformation-specific antibodies

The ability to differentiate between different aggregation states based on conformation has been the focus of much research (Kahler et al., 2013; Kayed & Glabe, 2006; Kayed et al., 2007; O'Nuallain & Wetzel, 2002). The development of conformation specific antibodies that recognise mature fibrils and soluble fibrillar oligomers, serves as evidence for establishing the importance of conformation in amyloid toxicity (Kayed et al., 2007). For example, the OC antibody does not recognise randomly coiled monomeric or pre-fibrillar oligomers, thereby confirming oligomers do not display a conformation dependent epitope found in fibrils (Kayed et al., 2007). The ability of these

conformation specific antibodies to bind to specific fibrillar structures, despite differences in primary sequence, could be due to the steric zipper side chains. These are found in fibrils formed by large number of amyloid forming sequences and could be the recognised generic epitope (Glabe, 2008). Furthermore, the A11 antibody specific for oligomers does not bind mature fibrils, fibrillar oligomers or fragmented fibrils. This further suggests prefibrillar and fibrillar oligomers are structurally distinct (Kayed et al., 2007). Co-incubation of A11 with Aβ oligomers has been shown to suppress toxicity suggesting that although these oligomers may be different in size (and possibly shape), there could be a common feature rendering them toxic (Broersen et al., 2010).

To directly link structure (i.e. size and conformation) to amyloid toxicity, we used our highly consistent preparation of Aβ42 to obtain and assess the toxicity of the fibrillar species. This was compared to the already established cytotoxicity of AβO. To probe further into the importance of structure in amyloid toxicity, the effect of sonicated fibrils was also monitored. Sonicating the fibrils not only allows us to compare the effects of size, but also conformation. As we define our oligomers to be a pre-fibrillar species, investigating the effects of sonicated fibrils, which we presume will retain their fibril-like β-sheet rich conformation, will allow us to determine whether this is a requisite of amyloid toxicity.

5.2 Results and Discussion

5.2.1 Establishing the biophysical properties of AβO, AβF and AβSon

Before being able to determine the cytotoxicity of AβO, AβF and AβS, we first confirm their structural properties. In order to do so, we used TEM and CD in combination with western blotting. Using our highly consistent and reliable preparation of Aβ42 (Marshall et al., 2016), we confidently identify the sample to be most oligomeric 2 hours after preparation and fibrillar by 48 hours.

For sonicated fibrils, it was important to first optimise conditions so fibrils were fragmented to a size as close to oligomeric as possible. These small, fibrillar oligomers will be referred to as oligomer-like to differentiate them from oligomers assembled from soluble Aβ42. This allows us to compare similar sizes with different conformations.

Figure 5.3B-D shows the EM of fibres sonicated for 5-, 10- and 20-minutes. From this, it is apparent that sonication for longer than 10 minutes disrupts the integrity of the fibrils beyond the size of what we could classify as oligomers-like, whereas 5 minutes was not long enough for sufficient fragmentation. 10 minutes was therefore selected as the appropriate length of time for sonication. This sonication optimisation was carried out on one independent sample preparation of Aβ42 to ascertain the appropriate sonication time . From electron micrographs, the length of sonicated fibrils (n=544) were measured to assess the range of assembly sizes present (Figure 5.3E). From the histogram (Figure 5.3E), we can conclude the majority of sonicated fibrils are between 30 and 90nm in length. Fewer fibrils of increasing lengths are counted, with the longest fibril measured at ~800nm (n=1). Therefore, we are confident AβSon has been significantly fragmented.

The oligomer-like species is difficult to clearly identify in electron micrographs, however, a zoom of the AβSon electron micrograph has been included (Figure 5.3B); the black arrow points to an example of an oligomer-like structure. The ability of sonication to produce species similar to oligomers has been previously shown in hen egg white lysozyme (Harte et al., 2015) and the prion protein (Lee et al., 2011). The diameter of these oligomer-like structures was measured (n=101) (Figure 5.3F) and compared to AβO (Figure 3.5, Chapter 3), shown as a boxplot (Figure 5.3G). The median diameter size of ~20nm are similar for both oligomer and oligomer-like species formed by sonication. Sonication must be carried out on ice due to the likelihood of the fragmented fibrils driving assembly due to fragmentation or secondary nucleation (Cohen et al., 2011). It was not possible to measure the length of AβF as these were indefinite in length or quite often bundled together and therefore difficult to differentiate as individual fibres, however, these are ~12nm in diameter.

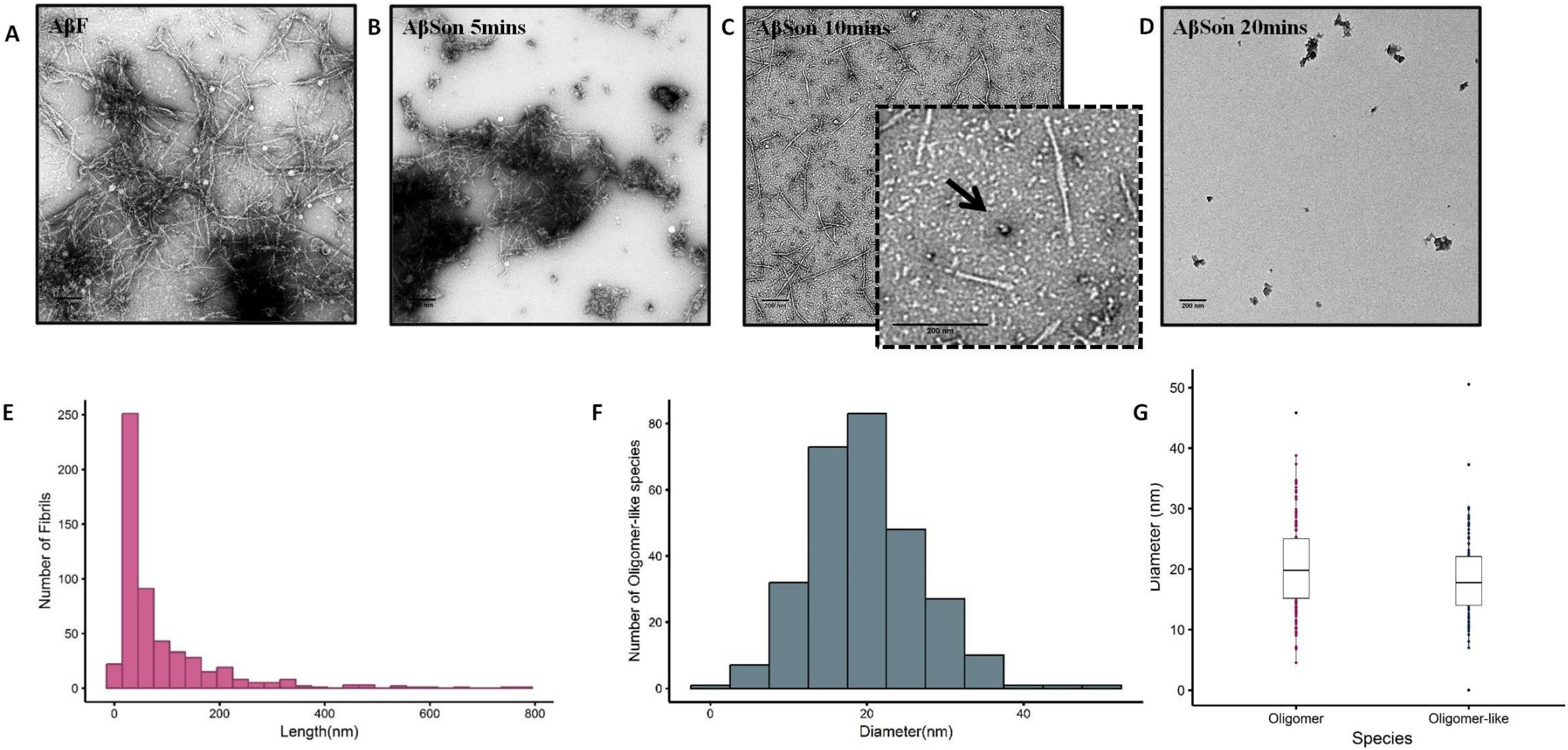

Figure 5. 3. Optimisation of Aβ42 sonicated fibrils (AβSon). Aβ42 fibres (A) were sonicated at the maximum setting for (B) 5-, (C) 10- and (D) 20 minutes on ice. Fibres were not sufficiently sonicated by 5 minutes whilst 20 minutes disrupted the integrity of fibrils beyond what could be classified as oligomer-like. 10 minutes sonication provided fibrils of varying length including those similar in size to oligomers. The optimisation was carried out on one independent sample preparation of Aβ42. Once optimised, quantification was conducted on three independent sample preparations. Quantification of Aβ42 sonicated (E) fibres (n=544) (10mins) confirm the majority of fibrils were between 30-90nm in length and (F) ~20nm in diameter (G) A boxplot to show the range of diameters in oligomer and oligomer-like species. Scale bar shown at 200nm. 50μM untagged Aβ42 was prepared in 10mM HEPES buffer pH7.4 and incubated for 48 hours at room temperature to obtain a predominantly fibrillar population before sonication.

To gain further insight into the size of each species, we carried out SDS-PAGE electrophoresis and western blotting (Figure 5.4).

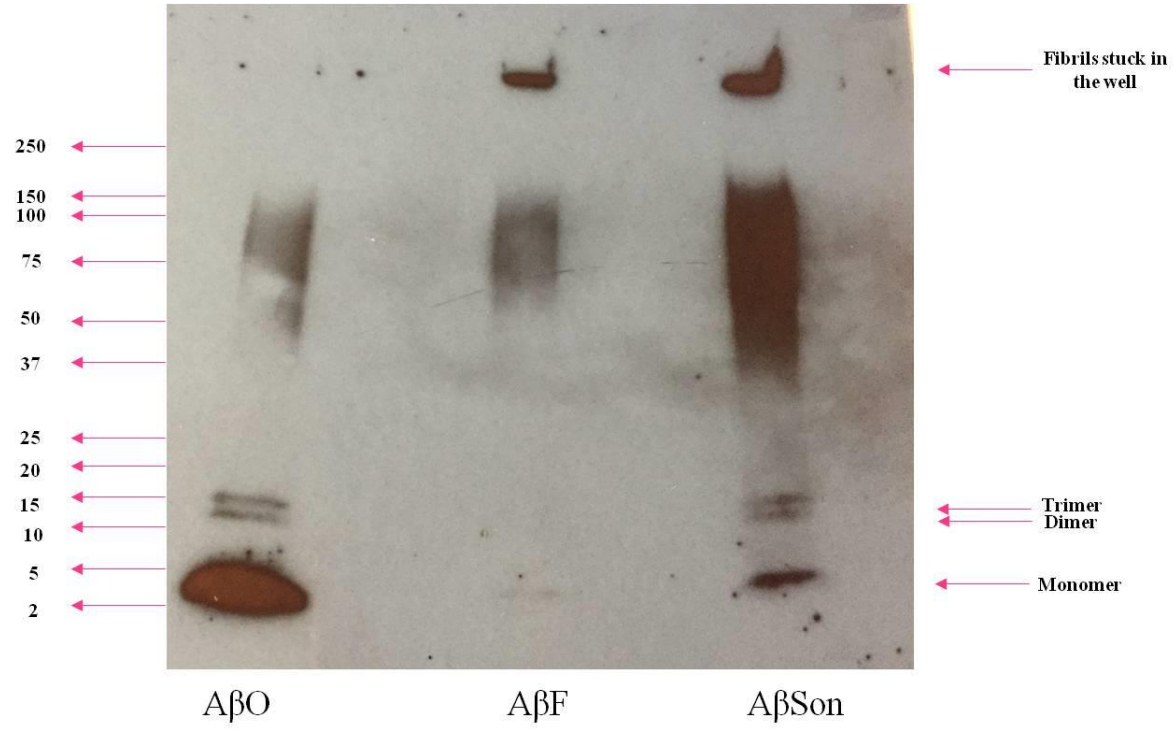

Figure 5. 4. Western blot of AβO, AβF and AβSon samples using 6E10 (1:10,000 dilution) was used to detect the size of assemblies present in each species. AβO migrate as monomers (4.5kDa), dimer/trimers (9kDa/13.5kDa) and a smear of higher molecular weight species. AβF show no lower molecular weight species with some fibrils stuck in the well of the gel. AβSon shows a mixture of all species from monomers to fibrils stuck in the well. 50µM untagged Aβ42 was prepared in 10mM HEPES buffer pH7.4 and incubated for 2 hours at room temperature for AβO, 48hours for AβF and these were sonicated on ice for 10 minutes for AβSon. As only one repeat was carried out in order to get an idea of the range of assemblies present, quantification was not possible.

The anti-Aβ monoclonal antibody 6E10 was used to detect the size of each species. As expected from our previous data, AβO displayed bands corresponding to monomeric, dimeric and trimeric species as well as higher molecular weight species which migrate as a smear (Marshall et al., 2016). AβF fibrils are stuck in the well of the gel, with the presence of some higher molecular weight species. There are no bands for lower molecular weight species, confirming that our AβF sample is larger in size than AβO. Importantly, AβSon shows bands for monomeric, dimeric, trimeric species as well as higher molecular weight species and some fibrils stuck in the well of the gel. This ensures that our AβSon

sample is indeed representative of some species similar in size to that of our oligomeric sample. Previous studies have shown a large overlap in the sizes of prefibrillar and fibrillar oligomers (Kayed et al., 2007) suggesting that distinct conformations of the same size do indeed exist. (Glabe, 2008). As only one repeat was carried out in order to get an idea of the range of assemblies present, quantification was not possible. Again, this would be a future direction as more repeats would allow for quantification and a more robust conclusion reached regarding the assemblies sizes in each of the preparations.

Next, we characterised the secondary structure of each species using CD (Figure 5.5). The average of three independent sample preparations are shown with error ribbons expressed as ±SEM.

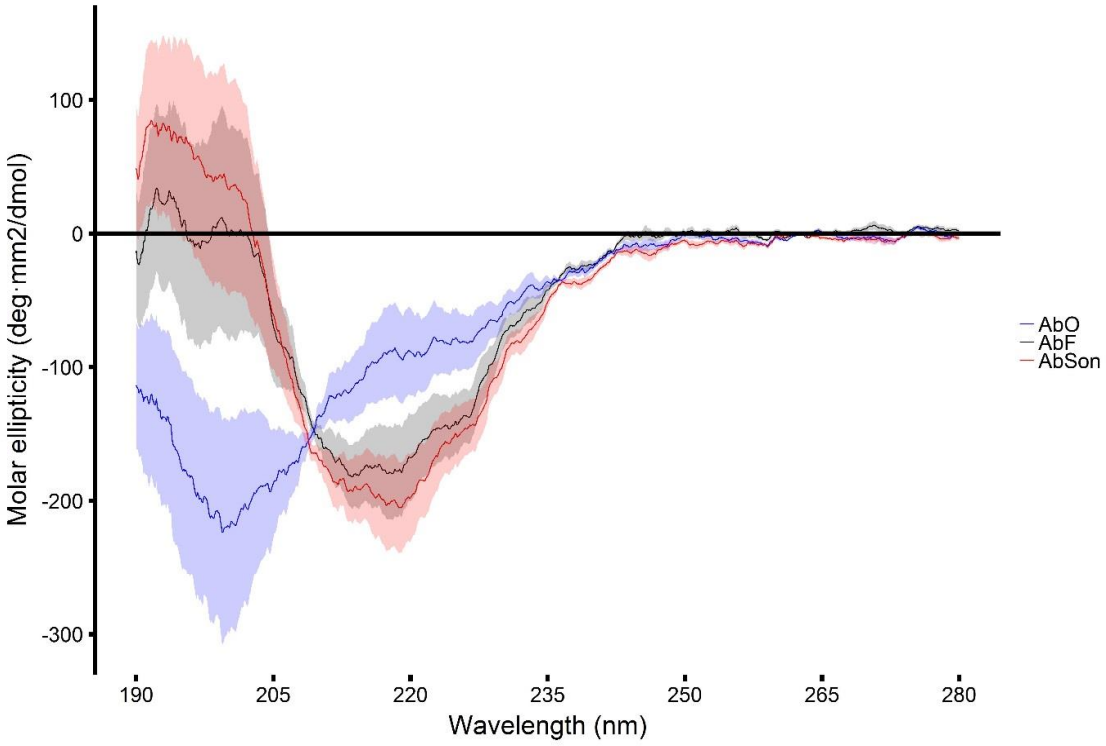

Figure 5. 5. CD spectra for 50µM AβO, AβF and AβSon. The signal for AβO shows a random coil signal (minimum at -198nm) and the signal for AβF and AβSon shows a β-sheet signal (minimum at -218nm, maximum at -198nm). Samples were prepared in 20mM Phosphate buffer pH 7.4 and measured in a 1mm pathway cuvette. Error bars expressed as ±SEM. The average of three independent sample preparations are shown.

The oligomeric species shows a dominant signal for random coil (minimum at ~198nm) whereas AβF and AβSon both display a signal for β-sheet (minimum at ~218nm, maximum at ~198nm). This confirms that at the secondary structural level, the oligomeric species is conformationally distinct from the fibrillar species. The sonicated fibrils retain their β-sheet signal despite being close to oligomeric in size. It is important to note that as previously stated, the random coil signal is most likely masking some β-sheet signal in the AβO sample. The difference in conformation between AβO and AβSon may be that of the anti-parallel/parallel β-sheet packing found in the samples. This cannot, however, be deduced from the CD spectra and would techniques such as FTIR to further investigate this.

5.2.2 AβO but not AβF or AβSon is cytotoxic

Having confirmed the structural and size differences of AβO, AβF and AβSon, we carried out a ReadyProbes live/dead assay to assess the cytotoxicity of each species. Rat primary hippocampal cultures were incubated with 10μM of each species for 3 days. It was not possible to incubate the cells with the peptides for 7 days as with our previous toxicity assays due to the fibrils growing over the cells. This made cells incubated with AβF extremely difficult to count at longer time points.

As shown in Figure 3.10 (Chapter 3), AβO displayed ~43% cell death (43.2% ± 2.35, total number of cell =1619, number of dead cells = 703). AβF and AβSon (Figure 5.6) displayed ~18% (18.1% ± 2.12, total number of cells = 783, number of dead cells=142) and ~20% (19.5% ± 2.09, total number of cells = 425, number of dead cells=83) cell death respectively compared to buffer incubated cells (17.8% ± 3.06, total number of cells = 1239, number of dead cells=221, ***). The average of three independent experiments where three separate sample preparations were incubated with three separate hippocampal cultures are shown. and an example of the ReadyProbes images for each condition is shown in the top panel. The right hand panel in Figure 5.6 shows the most representative electron micrographs of each sample from three separate sample preparations, confirming the species being added to neuronal cultures.

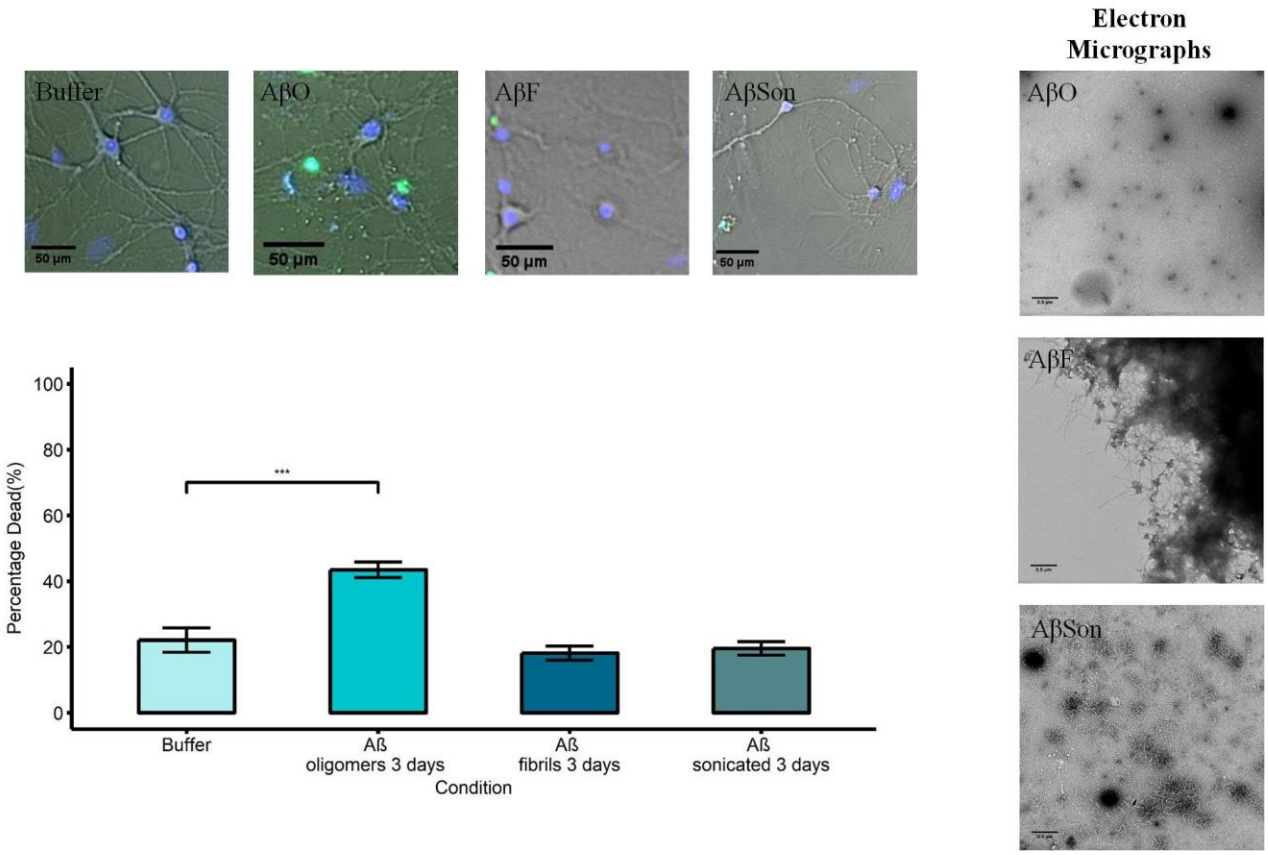

Figure 5. 6. AβO, AβF and AβSon ReadyProbes cell viability assay. An example of each Readyprobes condition is shown in the top panel. Rat hippocampal cultures were treated with untagged 10µM AβO, AβF and AβSon (prepared in 10mM HEPES buffer pH7.4) for 3 days. Cytotoxicity was measured as a percentage of dead cell in a culture and compared to buffer incubated cells. AβO were significantly toxic (43.2% ± 2.35, total number of cell =1619, number of dead cells = 703). AβF (18.1% ± 2.12, total number of cells = 783, number of dead cells=142) and AβSon (19.5% ± 2.09, total number of cells = 425, number of dead cells=83) showed no significant cytotoxicity compared to buffer incubated cells (17.8% ± 3.06, total number of cells = 1239, number of dead cells=221). Unpaired parametric student's t test where p= < 0.01 (*), < 0.001 (**), < 0 (***). The average of three independent experiments where three separate sample preparations were incubated with three separate hippocampal cultures are shown. Error bars are expressed as ±SEM. Negative stain electron micrographs for AβO, AβF and AβSon are included to ensure the correct species were added to the neuronal cultures. Scale bars shown at 0.5µm.

The difference in AβO and AβSon toxicity may be explained by the difference in conformation; AβO lacks a significant β-sheet signal and has a reduced random coil signal by CD, whereas this is not the case for sonicated fibrils. Despite AβSon being similar in size to oligomers (Figure 5.3 and 5.4), and the sample preparation covering a large range of sizes, these are non-toxic to hippocampal cultures. The AβF, which display a strong β-sheet structure, are also non-toxic and display a similar percentage of cell death as buffer incubated cells. Therefore, in this toxicity assay, AβSon and AβF have a similar

effect on the neuronal culture which can be attributed to both species being β-sheet rich. The AβO, which lacks significant β-sheet structure by CD, exerts significant toxic effects.

It is also interesting to note that these results implicate the self-assembly mechanism to be important in cytotoxicity; the oligomers self-assemble into mature fibrils and this process influences their toxicity. However, the fibrils are already fully assembled and are non-cytotoxic. As a future direction, it would be interesting to investigate whether sonicated fibrils continue to assemble to further establish the importance of the self-assembly process in cytotoxicity.

Together with the biophysical characterisation of each species, the data presented thus far are in support of conformation, and not necessarily size, as a determinant of amyloid toxicity.

5.2.3 AβO, AβF and AβSon display differing internalisation in primary hippocampal cultures

Having established that the oligomeric species, and not the fibrillar or sonicated fibrils are cytotoxic, we determined whether this was due to internalisation. The role of size in internalisation has been investigated and it has been postulated that oligomers can induce toxicity as they are small enough to be internalised (Chafekar et al., 2008; Lambert et al., 1998; Marshall et al., 2016).

We first used immunocytochemistry and confocal imaging to visualise Aβ42 in rat primary hippocampal cultures. Neurons were treated with the peptide for 30 minutes, 4 hours, 24 hours and 3 days to monitor changes in localisation and internalisation over time (Figure 5.7). The anti-Aβ 4G8 antibody, which detects all Aβ42 species, was used with an Alexa Fluor-555 secondary antibody to probe for Aβ. Zooms for each image are shown in Figure 5.8. Images shown are the middle slice taken from a Z-stack. Internalisation over time of each species has been quantified using FIJI software (Figure 5.9). All three species of Aβ bind to the neuronal projections and cell body (Figure 5.7). At 30 minutes, AβO displays a punctate staining whilst AβF and AβSon also display some ‘clumps’ which we presume are large aggregates. These are smaller in AβSon, again confirming we have successfully fragmented our Aβ fibrils at the time of adding it to the cells. There does not seem to be any (or very little) internalisation occurring at this time point in AβF and AβSon incubated cells.

At 4 hours, there is some internalisation seen with AβO (white arrows). This is not seen with AβF or AβSon, which are still bound to neurons and the cell body. Although AβSon appears to follow a similar distribution to AβF at this time point, the fluorescence is brighter than that of AβF. This could be due to there being more epitopes exposed to antibody in the AβSon sample; these could be buried in AβF (Marshall et al., 2016).

At 24 hours, it is apparent that oligomers have been internalised (white arrows). The AβF and AβSon appear much 'clumpier' which is likely due to the Aβ aggregating into larger entities. There does appear to be some internalisation seen here which can be explained by 1) the heterogeneity of the sample preparation means some oligomers will inevitably be present and 2) oligomers may shear off the ends of these fibrils (Verma et al., 2015; Walsh et al., 2002b). In inability to distinguish between oligomers and fibrils due to the limitations in resolution of confocal microscopy (~250nm) is a notable criticism of approach to investigate internalisation of different assemblies sizes/conformation. In order to overcome this, using super-resolution microscopy, which has ~20nm resolution (roughly the size of our oligomers) would be a future direction and one way in which to obtain more robust and clear data.

Finally, by 72 hours, the AβF and AβSon 'clumps' have disintegrated/degraded and are not internalised. This is specific only to the images shown in Figure 5.7 and we cannot disregard the possibility that these disintegrated fibrils may be internalised at a later time point in cells that have not yet died. This disintegration can be explained by the reported instability of amyloid fibrils at pH7.4; it has been shown that β2-microglobulin fibrils dissociate into non-toxic native monomers at this pH (Tipping et al., 2015). The oligomers also become slightly 'clumpier' and fewer cells were identified as having internalised AβO at this time point. This could be due to the fact that cells which have already died due to internalisation of oligomers (~40% according to our toxicity assay) cannot be imaged. It is also possible that the larger aggregates seen could be due to Aβ42 released into the extracellular space after cell death (Friedrich, 2010).

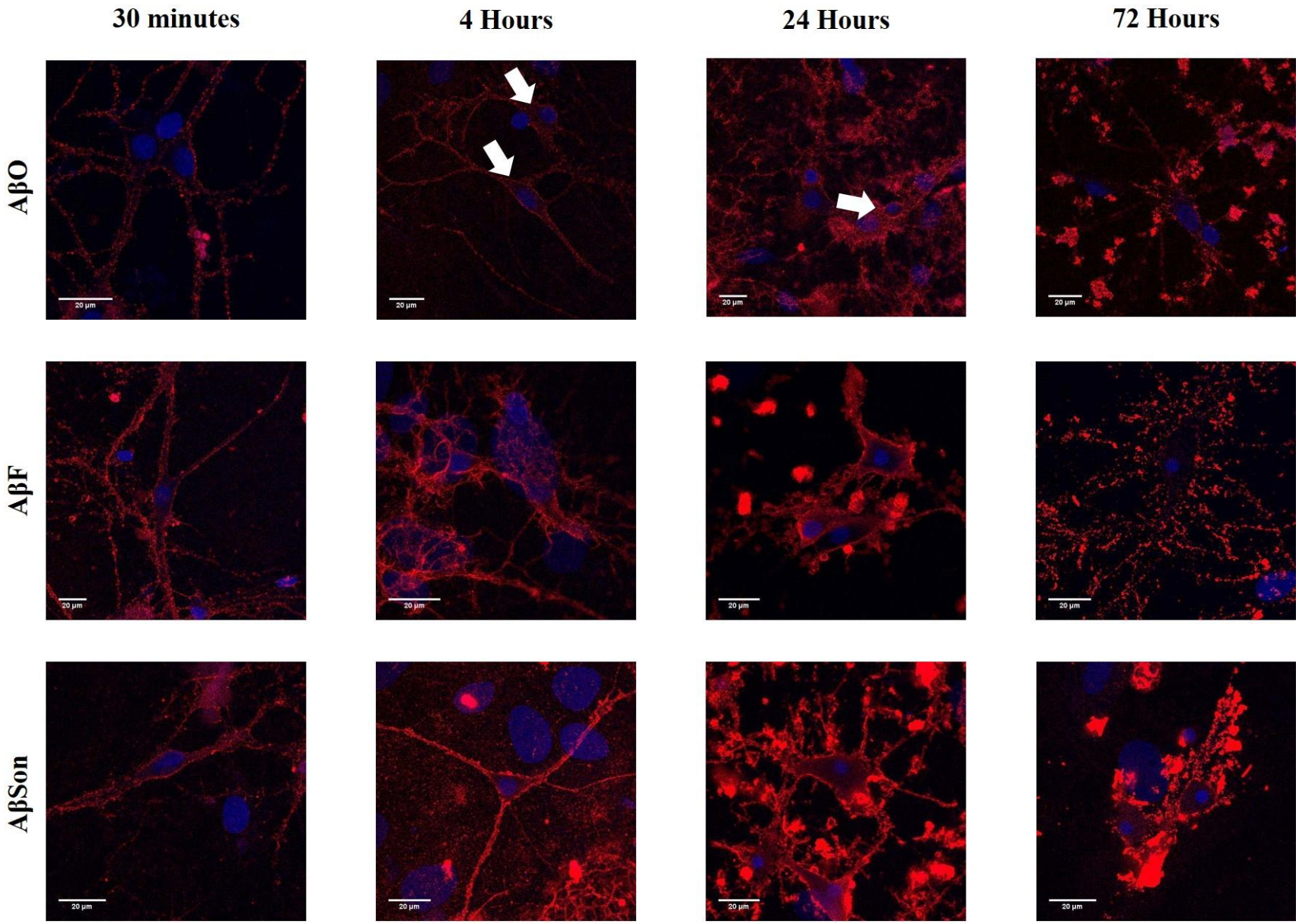

Figure 5. 7. Immunolabelled neurons incubated with 10µM untagged AβO, AβF and AβSon (prepared in 10mM HEPES buffer pH 7.4) for 30 minutes, 4-, 24- and 72- hours. Cells were fixed and labelled with 4G8 antibody (1:500) and Alexa Fluor-555 secondary antibody (1:500 dilution). White arrows point to clear AβO internalisation seen by 4 and 24hours which is seen to a lesser extent with AβF and AβSon. Scale bars are shown at 20µm. Zooms of images are shown in Figure 5.8.

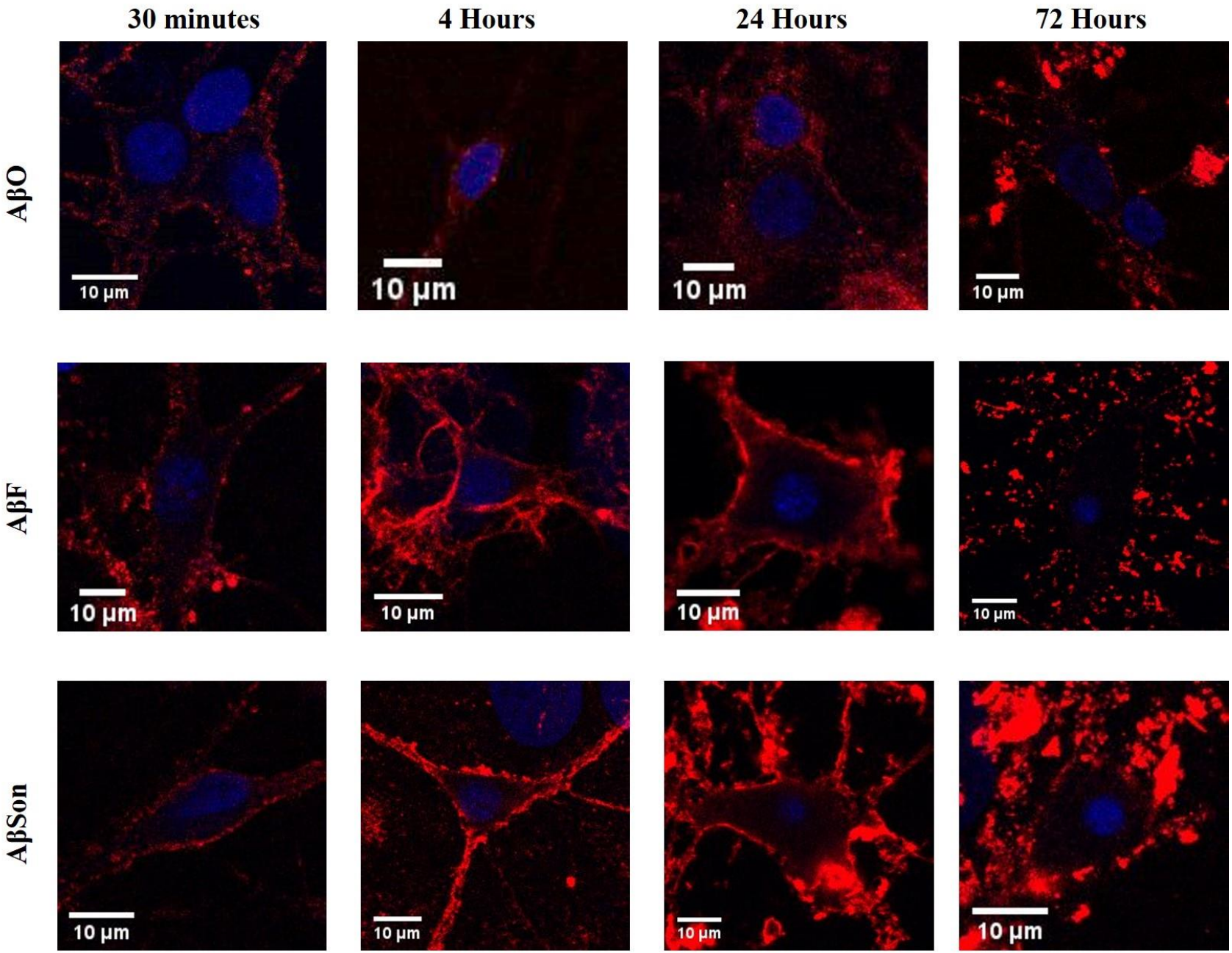

Figure 5. 8. Zooms of images in Figure 5.7. Scale bar shown at 10µm

The images shown are representative of three separate repeats (separate Aβ preparations and hippocampal cultures) at each time point. Aβ was prepared without a tag for this set of experiments.

The buffer incubated control at the longest time point of 72 hours is show in Figure 5.9. No endogenous Aβ signal was detected in buffer incubated cells, as was expected. This is likely to be due to either the 4G8 antibody unable to detect endogenously expressed Aβ or more likely, due to very low levels of Aβ expressed until 21 days, as has been reported previously (Bertrand et al., 2011). The lack of significant endogenous Aβ is beneficial to assess internalisation of Aβ species as this allows us to confidently conclude that it is the exogenously incubated with the neurons that is being internalised. It would have useful to have a secondary antibody control to ensure no non-specific binding is occurring.

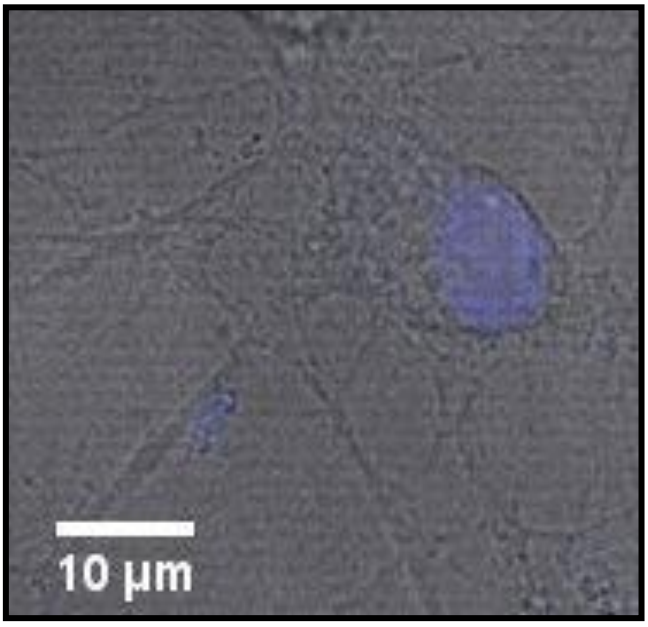

Figure 5. 9. Buffer incubated neuron at 72 hours.

Emissions from coverslips of antibody bound Aβ42 were collected using a 561nm emission laser line between 555-650nm on a PMT detector. In order to quantify internalisation, the intensity within the cell body was measured. To ensure any Aβ42 bound to the membrane of the cell was not measured as being internalised, only intensity inside on the cell membrane was measured. An example of this is shown in Figure 5.10. Although this approach seemed reasonable due to the clear visibility of the cell membrane, using a marker for the cell membrane would have been a more thorough way in which to ensure only Aβ42 inside of the cell body was quantified.

From Figure 5.10, there is a clear increase in intensity seen with time for AβO. This increase is steepest between 30 minutes to 24 hours, suggesting internalisation is most active during this time. There is little change in intensity between 30 minutes and 24 hours seen in cells incubated with AβF, however, after 24 hours there is a steep increase in intensity suggesting internalisation. This could be due to depolymerisation of fibrils to act as a source of fragmented fibrils and fibrillar oligomers (Jiang et al., 1994; Martins et al., 2008). AβSon show a steep increase in internalisation between 30 minutes and 4 hours, which decreases over time. This may be explained by sonicated fibrils driving further assembly via secondary nucleation and therefore reducing the presence of shorter fibrils/oligomer-like species that may be internalised. The ability of nanoscale fibrils produced from fragmentation to be internalised has been previously reported for β2-microglobulin (Jakhria et al., 2014), however were shown to have no cytotoxic effects. This is in line with AβF and AβSon showing some internalisation but displaying no cytotoxicity in the ReadyProbes assay (Figure 5.6).

The internalisation of AβO in 14, 16, 15 and 10 cell was quantified at 30 minutes, 4 hours, 24 hours and 72 hours respectively. For AβF, 13, 9, 8 and 11 cells were quantified at 30 minutes, 4 hours, 24 hours and 72 hours respectively. To quantify the internalisation of AβSon, 9, 6, 11 and 6 cells were measured at 30 minutes, 4 hours, 24 hours and 72 hours respectively. These were all the cells that could be quantified from three separate repeats at each time point for each of the Aβ42 species.

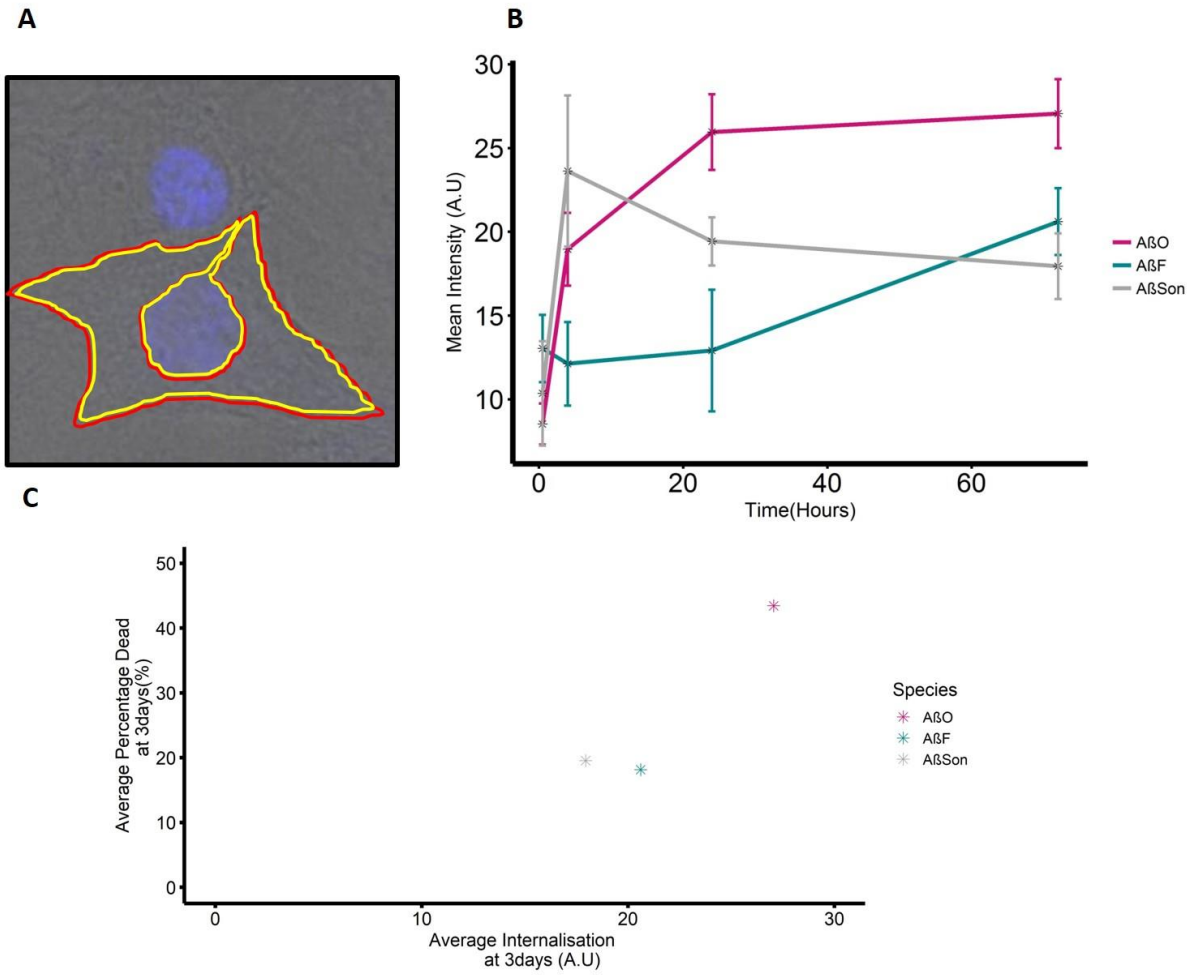

Figure 5. 10. Quantification of Aβ42 internalisation using FIJI software. . Cells were incubated with AβO, AβF and AβSon for progressive time points before being fixed and labelled for Aβ42 to visualise localisation and internalisation. Internalisation was quantified in the middle of the Z stack for all cells from three independent experiments. A) An example of how internalisation was quantified is shown by the image on the left. The red outline is on the membrane of the cell and intensity within the yellow outline was quantified. This was to ensure any Aβ42 bound to the cell membrane was not measured as internalisation. B) Quantification. There is a clear increase in internalisation seen with AβO, an initial increase in internalisation at 4 hours with AβSon, which then plateaus from 24 hours. AβF shows a slight increase in internalisation from 30 minutes to 24 hours, after which there is a steeper increase in intensity suggesting increased internalisation. Error bar are expressed as ±SEM. The internalisation of AβO in 14, 16, 15 and 10 cells were quantified at 30 minutes, 4 hours, 24 hours and 72 hours respectively. For AβF, 13, 9, 8 and 11 cells were quantified at 30 minutes, 4 hours, 24 hours and 72 hours respectively. To quantify the internalisation of AβSon, 9, 6, 11 and 6 cells were measured at 30 minutes, 4 hours, 24 hours and 72 hours respectively. C) The average percentage toxicity of three experiments plotted against the average internalisation (fluorescence) at 3 days. Both AβF and AβSon displayed similar levels of toxicity and internalisation, whereas AβO had a much higher average internalisation measured and displayed greater cytotoxicity.

In order to establish the relationship between the quantified internalisation and cytotoxicity of each of these species (Figure 5.10C), the average internalisation (i.e. the average fluorescence intensity) was plotted against the mean toxicity (shown in Figure 5.6). This was done from the fluorescence intensity quantified from the immunolabelled neurons (Figure 5.12A) at 3 days. As the ReadyProbes assay was

not used to assess cytotoxicity at any other time point, this was the only time that could be used to directly link internalisation of each of the species to toxicity and although we have AβO toxicity for 7days, the internalisation was not monitored up to this time point. From the graph we can begin to suggest that due to an increased internalisation compared to AβF and AβSon, AβO displays greater cytotoxicity. Ideally, we would have ReadyProbes for each of the time points quantified for internalisation, which would allow us to establish the link between increased internalisation and cytotoxicity over time rather than just one-time point.

In order to monitor the same cells over a 15-hour time period, live cell confocal imaging was used. As mentioned, one major limitation of using confocal microscopy to assess the internalisation of different assemblies formed from the same protein, is resolution of the microscope (~250nm). This does not allow us to distinguish between different assemblies (e.g. oligomers which are roughly 20nm). Ideally, super- resolution microscopy which has a resolution of ~20nm would allow us to begin to identify the internalisation of different assemblies with better confidence. In the following analysis of the images from the live cell imaging, we suggest the punctate staining corresponds to smaller oligomeric species whereas the larger, dense staining is most likely aggregated Aβ.

Live cell imaging over a 15-hour time frame is a reasonable time frame allowing us to maintain the cells in a healthy environment and still gain valuable information regarding the early internalisation of each Aβ species. The peptide was conjugated with an Alexa Fluor-488 tag which has been previously shown not affect assembly (Soura et al., 2012). However, this study only confirmed the ability of the tagged Aβ42 to form fibrils by EM; therefore, a thorough characterisation of the tagged peptide over time to confirm the kinetics or oligomers do not differ from the untagged peptide is still needed and would be a future set of experiments to be conducted.

Figure 5.11 show snapshots of cells incubated with each Aβ species over 15 hours; AβO are evidently internalised and there are very few large aggregates or ‘clumps’ seen. AβF incubated cultures show large Aβ aggregates from the time it is added. There is some internalisation seen, however, the punctate staining (white arrows in Figure 5.11) of this again suggests these are oligomers. Due to

experimental limitations, AβSon internalisation could only be followed for 8 hours, however, there is clear internalisation seen by this time point.

The quantification of internalisation from live cell imaging is also shown in Figure 5.11. As the experiment was only carried out once, in this instance the n number was taken to be the total number of cells quantified per condition. Quantification was carried out for every hour over 15hours by drawing within the membrane of the cell and measuring the fluorescence intensity, in the same way as shown in Figure 5.10A. 12, 3 and 1 cell(s) were quantified for AβO, AβF and AβSon respectively. There is a clear increase in internalisation with time seen with AβO, however this is not as prominent with AβF. Although this may be due to fibrils not being able to be internalised, it may also be due to fibrils being internalised at later points and therefore conclusions other than the fact that fibrils are not internalised to the same extent as AβO in this timeframe, cannot be reached. As only one cell was quantified for AβSon internalisation over 8 hours, it is not possible to comment on the amount of internalisation seen. From these preliminary data, however, it does seem as though there is an increase in internalisation over time from the cell live imaging quantification.

The time frame in which internalisations differs to that shown from the immunolabelling shown in Figure 5.9 and 5.11. However, this could be due to the Alexa Fluor tag influencing uptake properties, or perhaps the cells which internalise Aβ at these early time points have already died and therefore are not present to image at our later time points by immunolabelling. It may also be that some cells internalise Aβ with higher affinity than others (Chafekar et al., 2008) or that the Alexa Fluor tagged method is more sensitive.

Together, the confocal and live cell imaging presented here confirm AβO are internalised by primary neuronal cultures. This internalisation is not as pronounced in AβF and AβSon incubated cells (although these samples inevitably also have some oligomers present), which may be due to the difference in conformation of these structures and AβO. Notably the difference in β-sheet packing (anti-parallel/parallel) may influence uptake. Although some AβSon fibrils are similar in size to AβO, their reduced internalisation compared to that of AβO suggests that conformation is an important

factor in internalisation. Due to time constrictions, live cell imaging for each of the Aβ species was recorded only once. For this reason, each cell within the experiment was quantified and this has been expressed as the n number. Further repeats are needed in order to make reliable and concrete conclusions regarding the internalisation of Alexa Fluor-488 tagged AβO/AβF/AβSon.

It was also not possible to plot the toxicity against internalisation as shown for the immunolabelled cells (Figure 5.10C) for tagged-Aβ in neurons as this was only monitored over a 15 hour time period and cytotoxicity was not assessed at this point.

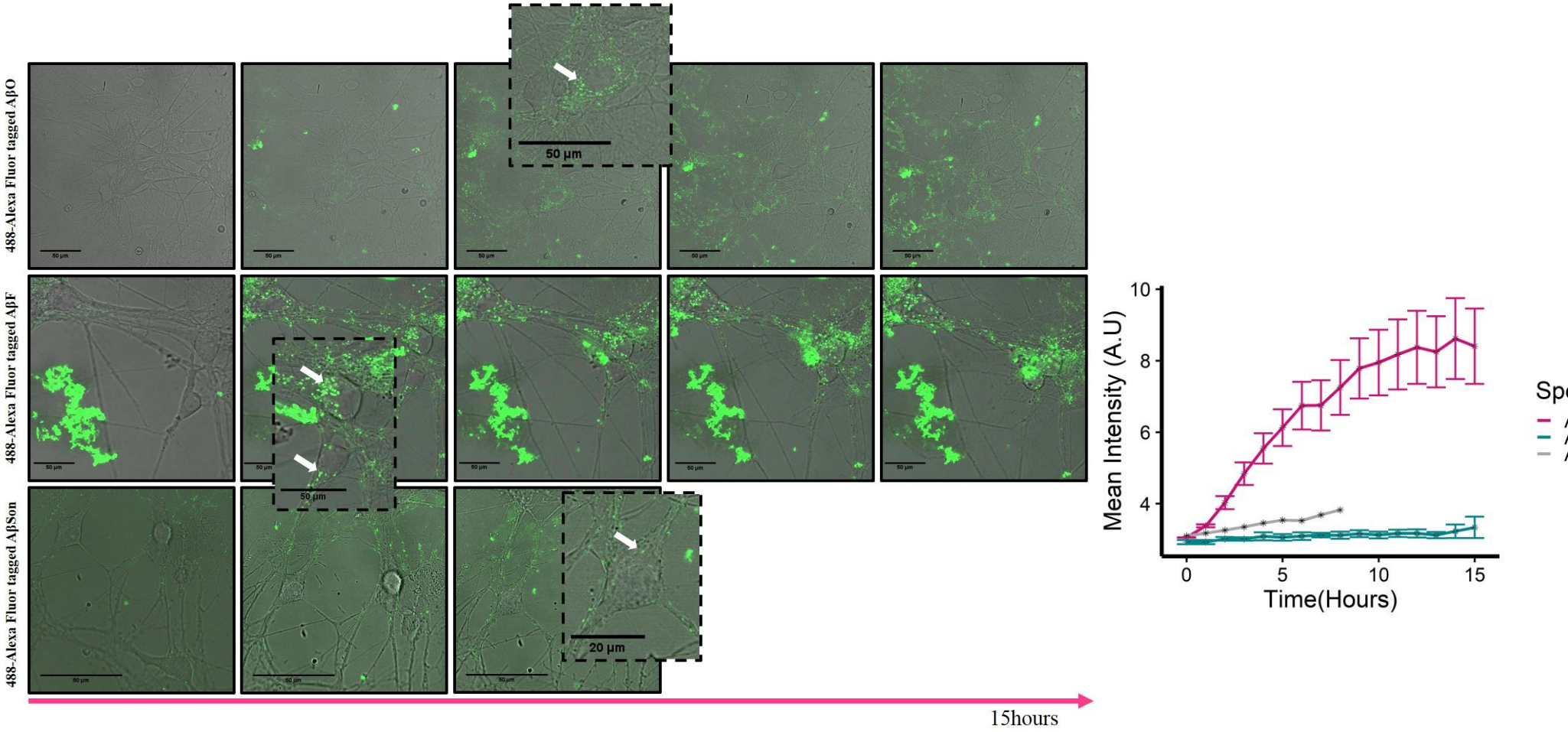

Figure 5. 11. Snapshots of live cell confocal imaging. Cells were incubated with 10µM Alexa Fluor-488 tagged AβO, AβF and AβSon and imaged every 20 minutes for 15 hours. There is evident internalisation of AβO over the course of 15 hour (suggested by the punctate staining shown by white arrow in the inset). There is less prominent internalisation seen with AβF, which due to the punctate staining, is believed to be the internalisation of oligomeric species. Live cell imaging was only possible over 8 hours for AβSon and some internalisation was seen. Scale bars shown at 50µm (AβSon zoom shown at 20µm). The quantification of internalisation at every hour over 15 hours is shown by the graph in on the right. Internalisation of oligomers was quantified from 12 cells, fibrils from 3 cells and sonicated fibrils from 1 cell. Error bars for oligomers and fibrils are expressed as ±SEM

5.2.4 Internalisation is a requirement for cytotoxicity

Having established AβO is internalised by primary hippocampal cultures, we questioned whether this was a requirement of cytotoxicity. In order to do so, we once again utilised the ReadyProbes assay as a measure of cell death after incubation with oligomers for increasing lengths of time. To remove Aβ from the culture after the required incubation period, we replaced the media with fresh, Aβ-free media. The percentage of cell death was measured after 7 days after initial addition of AβO.

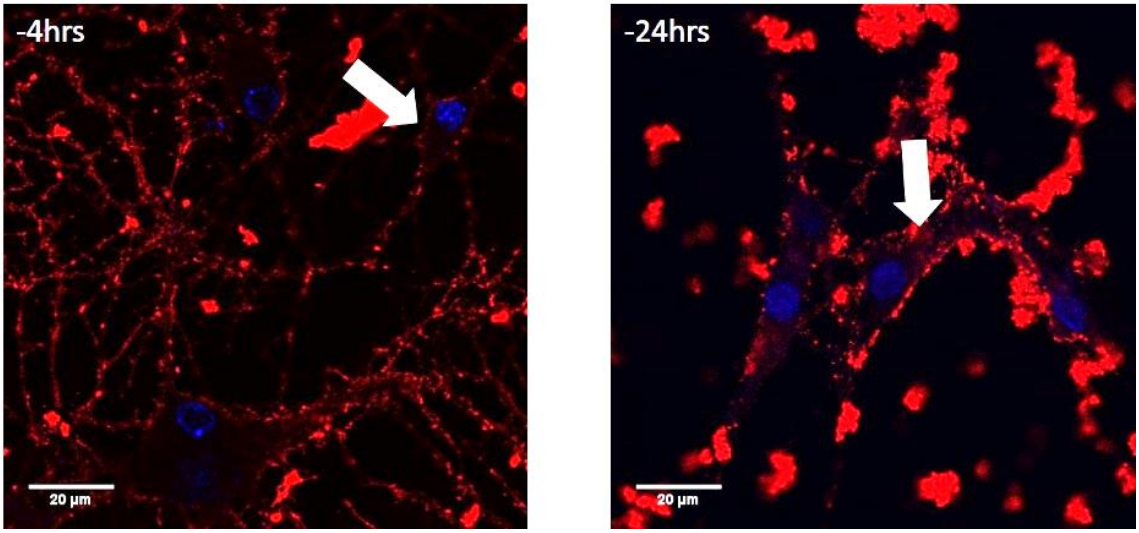

Figure 5. 12. Immunolabelled neuronal cells incubated with untagged AβO (prepared in 10mM HEPES buffer pH7.4) for 4 hours and 24 hours followed by a media change to remove soluble Aβ. Cells were fixed and labelled after the media change using the primary 4G8 antibody (1:500 dilution) and Alexa Fluor-555 secondary antibody (1:500 dilution). White arrows show internalisation at both time points, although this is more prominent at 24 hours. Scale bars shown at 20µm. This immunolabelling was only carried out once in order to establish if there was a difference seen in the staining after a media change.

We first used immunocytochemistry in order to establish whether the removal of Aβ with a media change did indeed remove extracellular AβO. Again, we used the 4G8 anti-Aβ antibody with an Alexa Fluor-555 secondary antibody (Figure 5.12). Cells were incubated with AβO for 4- and 24-hours, followed by a media change after which they were 'rested' for ~1 hour before being fixed and stained. Following media change after 4 hours of incubation (-4 hours), there is very little punctate staining in the extracellular space to indicate the presence of oligomers. The staining seen is the AβO that have bound to the cell body and neuronal projections. There is some internalisation seen,

indicating the media change only removes soluble Aβ from the extracellular space. Following media change after 24 hours of incubation (-24 hours), the majority of Aβ present is 'clumped' which is as expected; although Aβ is added as oligomers, it will continue to aggregate over time. There is also more internalisation of AβO seen at 24 hours, consistent with the data presented above. We can begin to conclude from the difference in staining at both points that by removing the media, unbound soluble (and not high molecular weight or fibrillar Aβ) is removed from the extracellular space. However, this immunolabelling was only carried out once to establish a whether a difference in staining is seen which would allow us to directly monitor the effect of AβO internalisation.

To further confirm replacing the media with fresh, Aβ-free media removes soluble Aβ from the cellular environment, we compared the amount of AβO in the media removed and lysates of treated cells. We immunoprecipitated Aβ from the media removed and cell lysate at both time points, and conducted SDS-PAGE electrophoresis, followed by western blotting using the 4G8 antibody.

From the western blot (Figure 5.13, left) we can see there is less AβO in the cell lysate than in the media removed at 24 hours. Comparing this to the amount of AβO seen after 7 days, there is an increased amount seen in the lysate than at 24 hours. There is also less AβO in the media removed at 7 days compared to 24 hours. This has been quantified and shown in Figure 5.13, right.

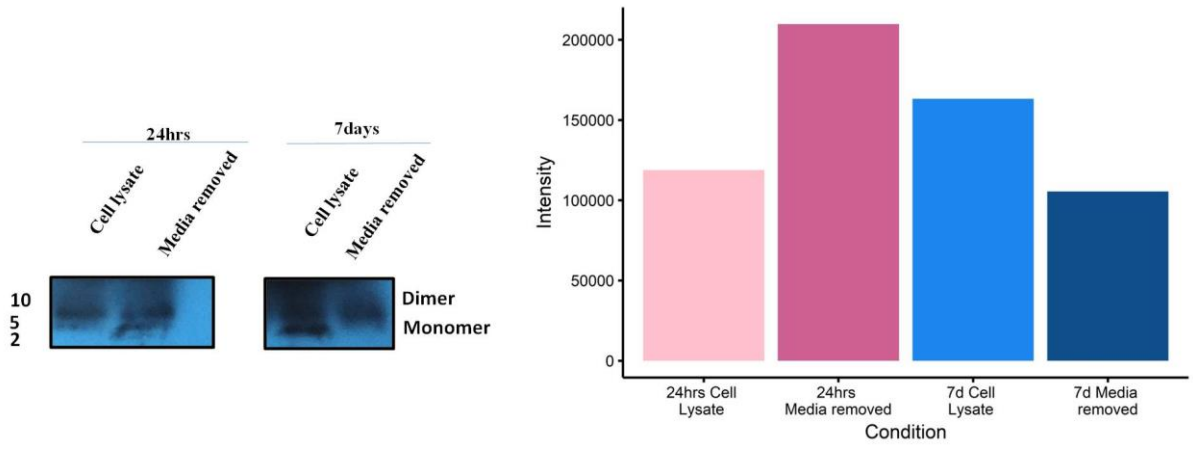

Figure 5. 13. Western blot of immunoprecipitated Aβ42 in the cell lysate and media removed at 24 hours and 7 days (left hand side), detected using 4G8 (1:10000 dilution). The amount of soluble Aβ42 was quantified (right hand side); there was more detected in the media removed than in the cell lysate at 24hours and in contrast, there was more in the cell lysate and less in the media removed at 7 days. Cells were treated with 10μM untagged AβO prepared in 10mM HEPES buffer pH7.4. This experiment was carried out once in order to gain an initial insight into the Aβ42 levels in the media and cell lysate.

This data informs us that 1) there is increased internalisation with time and 2) removing the media removes soluble Aβ from the neuronal cultures. This experiment was carried out only once due to time constraints and therefore reliable quantification was not possible. However, combined with the immunolabelling shown in Figure 5.12 these data together suggest there is the removal of extracellular AβO by a media change.

Next, we established the cytotoxicity of treating cells with AβO for increasing amounts of time before being removed from the extracellular space (Figure 5.14). The cytotoxicity of AβO at 7 days shown in Chapter 3, has been included for a comparison, ~70% (66.3% ± 2.59, total number of cell =1172, number of dead cells = 777, '***'). Cells were incubated with 10μM AβO for 2 hours, 4 hours and 24 hours before replacing the media and thereby removing Aβ from the environment. Cell viability was measured 7 days after initial incubation with AβO. Cells incubated for 2- or 4-hours with AβO before being replaced with fresh media, displayed no significant cytotoxicity (17.7% ± 2.13, total number of cells =595, number of dead cells = 105 and 25.7% ± 24.6, total number of cell =599, number of dead cells = 154 respectively) compared to buffer incubated cells, which also had a media change 15.63% ± 1.91, total number of cell =1152, number of dead cells = 180 at 7 days. Cells incubated with AβO for 24 hours before being replaced with fresh media, displayed significant toxicity at 7 days (41.3% ± 4.22, total number of cells =602, number of dead cells = 249, '***').

Combining this with internalisation, toxicity seems to be linked to the amount of AβO internalised into the cell. This is consistent with the hypothesis that cells are capable of degrading and clearing misfolded protein from their environment up to a certain point. However, once a certain threshold is reached, the cell becomes overwhelmed and can no longer cope with misfolded protein burden. (Chen et al., 2011; Valastyan & Lindquist, 2014). Our findings suggest this threshold is reached around 24hours, as at this point the cells can no longer recover from the amyloid insult. Removing AβO after 2- and 4-hours does not allow for this threshold of internalisation to be reached and therefore there is no significant toxicity seen at 7 days.

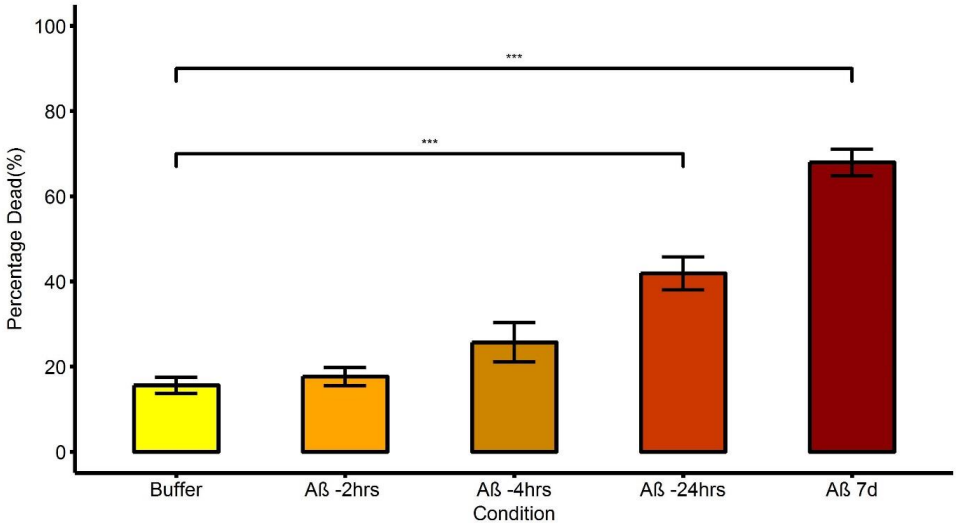

Figure 5. 14. 'Is internalisation a necessity for cytotoxicity? -ReadyProbes cell viability assay. Rat hippocampal cultures were treated with 10µM untagged AβO, (prepared in 10mM HEPES buffer pH7.4) for increasing amounts of time before being removed and replaced with Aβ-free media. Cytotoxicity was measured 7 days after initial addition of AβO. Cytotoxicity was measured as a percentage of dead cell in a culture and compared to buffer incubated cells which also had a media change (15.63% ± 1.91, total number of cell =1152, number of dead cells = 180). AβO were significantly toxic (66.3% ± 2.59, total number of cell =1172, number of dead cells = 777) at 7 days. Cells incubated with AβO for 2- (17.7% ± 2.13, total number of cells =595, number of dead cells = 105) and 4 hours (25.7% ± 24.6, total number of cell =599, number of dead cells = 154) displayed no significant cytotoxicity at 7 days. Cells incubated with AβO for 24 hours (41.3% ± 4.22, total number of cells =602, number of dead cells = 249) displayed significant cytotoxicity at 7 days. One-way ANOVA with Tukey's post hoc comparison where p= < 0.01 (*), < 0.001 (**), < 0 (***). The average of three independent experiments (three separate AβO preparations and three independent hippocampal cultures are shown in this Figure). Error bars are expressed as ±SEM.

5.3 Conclusions

Having established Aβ42 is the only primary sequence out of three variants characterised that forms intermediary oligomeric species, we sought to determine whether the toxicity mediated by these oligomers was due to size and/or conformation. Gaining an understanding of this will further aid us in deciphering the determinants of amyloid toxicity. A schematic diagram summarising the data presented in the chapter is shown in Figure 5.15.

We first thoroughly characterised the size and conformation of AβO, AβF and AβSon. Samples were prepared using our highly consistent, thoroughly characterised preparation of Aβ. AβO displayed a predominantly random coil conformation by CD, although it is likely this is masking some β-sheet content. Both AβF and AβSon displayed β-sheet conformations by CD. The sonicated fibrils,

however, did display a wide range of assemblies (detected by western blot) some of which corresponded to the size of AβO. This therefore allows us to evaluate the importance of size and conformation- the sonicated fibrils displayed a strong β-sheet conformation and were a similar size to oligomers (lacking a predominant β-sheet structure by CD).

The ReadyProbes assay used to measure the cytotoxicity of each species confirmed only AβO were significantly toxic after 3 days. AβF and AβSon showed no significant cytotoxicity; as AβSon is a similar size to AβO, we can conclude toxicity of Aβ is not mediated by size. The difference in conformation of both AβO and AβSon suggests conformation influences toxicity.

Unfortunately, the conclusions reached regarding internalisation from these data are preliminary and further repeats are necessary to reach concrete conclusions. Furthermore, due to the limitation in resolution of the microscope, it is difficult to ensure that species we believe to be internalised are indeed what we identify to be oligomers and fibrils. However, in order to begin linking the above data with internalisation, we report that AβO are internalised by 4 hours of incubation with cells. The same level of internalisation is not observed with AβF or AβSon which could be indicative of conformation-specific internalisation of Aβ42. The endocytosis of β-sheet rich structures is thought to be an important feature of several disease-related amyloid proteins, e.g. α-synuclein (Desplats et al., 2009), however, the anti-parallel arrangement of β-sheets of Aβ42 oligomers described in the literature (Cerf et al., 2009), could influence its toxic nature compared to the in register, parallel arrangement seen in fibrils. Furthermore, selective uptake of oligomers and not fibrils has been reported previously in HeLa and differentiated SK-N-SH cell lines, consistent with our data (Chafekar et al., 2008). The uptake of β2-microglobulin fragmented fibrils, has however been reported and although these were shown to be non-toxic, they did exert cellular dysfunction by disrupting lysosomal membrane protein trafficking and inhibit lysosomal protein degradation (Jakhria et al., 2014). It is therefore reasonable to hypothesise that although AβSon is not cytotoxic (Figure 5.6), it may affect normal cellular functioning. As a future direction, an MTT assay to evaluate cell metabolic activity would provide further information to make concrete conclusions on this.

Furthermore, by 72-hours, the images shown in Figure 5.7 and 5.8 show the nuclei of the cells incubated with AβF and Aβson, to be rounded. This suggests that the cells are damaged, even though AβF and AβSon are non-cytotoxic as assessed by the ReadyProbes assay (Figure 5.6). This is again in line with previously reported effects of fragmented β2-microglobuin fibrils on cell functioning (Jakhria et al., 2014). Furthermore, from the data presented in this section (Figure 5.7 and 5.8, clearly seen at 24 hours), it seems that the internalisation of AβO causes the entire cell to change in morphology and become rounded. Although internalisation is seen to a lesser extent in cells incubated with AβF and AβSon (Figure 5.10), as future work, analysis of the morphological changes induced by incubating neurons with each of the Aβ42 species (e.g. overall morphology of cell, shape of nuclei, nuclear membrane integrity etc) and linking this to internalisation, would provide useful information regarding the effect of structure/conformation on cellular dysfunction.

Similar data are presented in Figure 5.16, where the same experiments presented above were conducted in the SHSY5Y cell line. This was to ensure robust conclusions of the data presented in this Chapter and that these data are not specific to primary neuronal cultures only. Data presented in Figure 5.16 was obtained and analysed by Astrid Nardecchia (undergraduate student) and I was Astrid's laboratory supervisor for her project. We first had to determine the concentration dependent cytotoxicity of AβO in these cells (Figure 5.15, top left); 10μM was too low to see significant cytotoxicity over 7 days, however, 20μM required a large volume of AβO therefore making it uneconomical. 15μM AβO was therefore decided upon. Next, the cytotoxicity of 15μM AβO, AβF and AβSon at 3 and 7 days was established (Figure 5.15, top right). Only AβO at 7 days (69% ±SEM 3.4) displayed significant toxicity compared to buffer incubated cells, consistent with data presented in Figure 5.6. Immunolabelling was used to monitor internalisation at 3 and 7 days (Figure 5.15, bottom) and showed AβO and AβSon internalisation. AβO internalisation has been previously shown in this cell line (Soura et al., 2012). Again, this is consistent with the data presented in primary hippocampal cultures, however, a quantification of this internalisation is lacking due to the number of repeats.

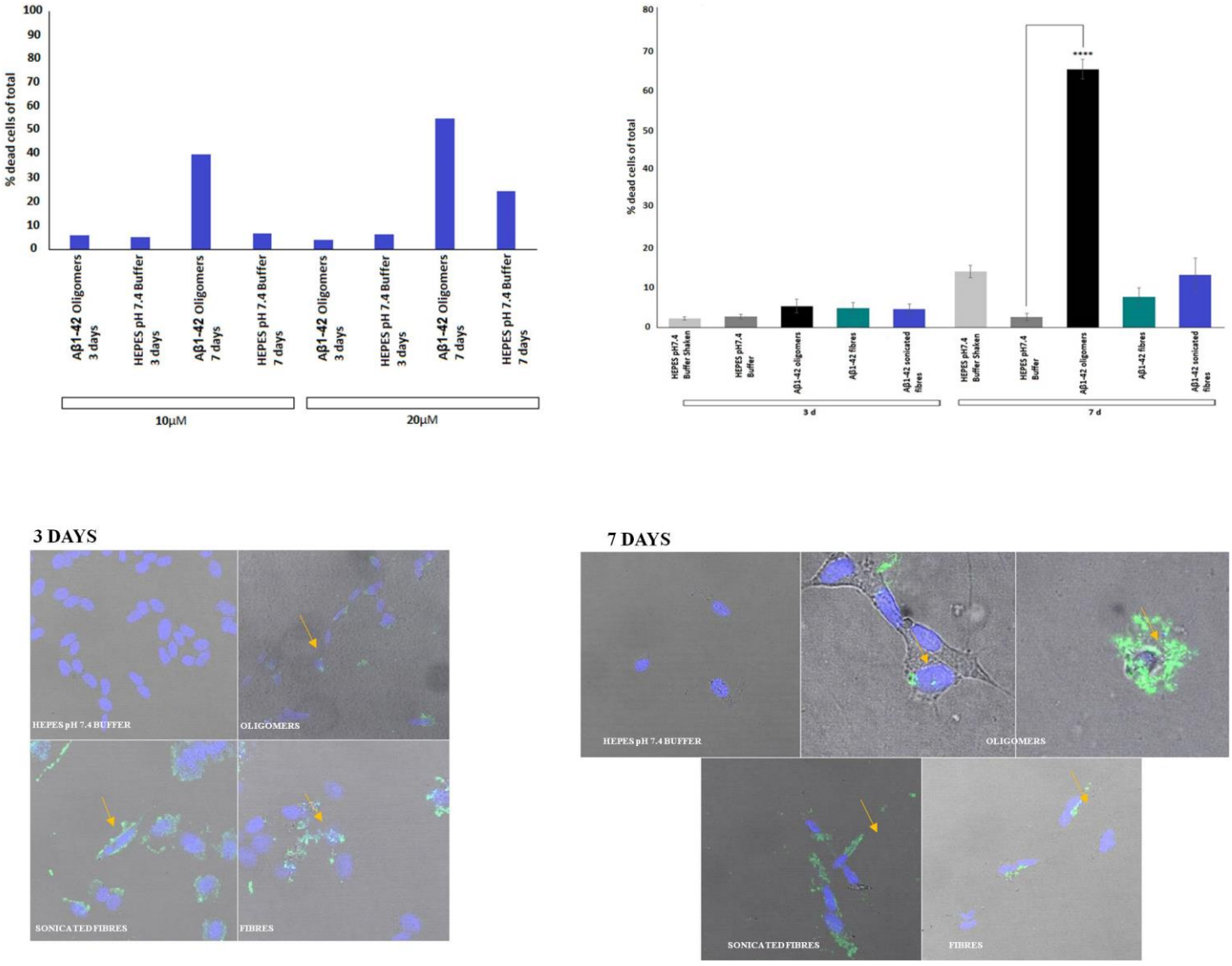

Figure 5. 15. AβO, AβF and AβSon toxicity and internalisation at 3 and 7 days in SHSY5Y cells. The concentration dependent cytotoxicity of AβO was first established (top left). This was carried out once in order to decide the concentration to use for the ReadyProbes assay and therefore statistical analysis was not possible. Cytotoxicty was assessed using the ReadyProbes assay. 15 μM AβO, AβF and AβSon were incubated with cells for 3 and 7 days Only AβO at 7 days displayed significant cytotoxicity (69%, '*') compared to buffer incubated cells. The average of three experiments are shown. One-way ANOVA with Tukey's post hoc comparison where p= < 0.01 (*), < 0.001 (**), < 0 (***). The average of three independent experiments (three separate AβO preparations and three independent hippocampal cultures are shown in this Figure). Error bars are expressed as ±SEM. Internalisation of each species was monitored at 3 and 7 days (bottom panel); AβO and AβSon show internalisation, this is not seen with AβF. Data was obtained, analysed and presented by Astrid Nardecchia.**

There are many proposed mechanisms of oligomer internalisation, some examples include clatherin and/or dynamin mediated endocytosis (Chafekar et al., 2008; Wu & Yao, 2009; Yue & Zhang, 2012),

receptor mediated e.g. LDLR and LRP1 receptors as well as RAGE (Yan et al., 1996), and lipid raft mediated internalisation (Saavedra et al., 2007). Each of these are likely to play a role in the accumulation of oligomers within neuronal cells. There is a threshold of oligomer internalisation after which the cell is unable to efficiently clear/degrade Aβ (Domert et al., 2014) and therefore no longer recover. Some mechanisms of Aβ degradation clearance are outlined in Table 5.1. All of these are thought to be affected in AD.

	Protein/Receptor	**Mechanism of clearance/degradation**	**References**
Aβ degrading proteases	**Metalloendopeptidses-** including Neprilsin (NEP), Insulin degrading enzyme (IDE) and endothelin-converting enzymes (ECE)	Degradation of monomeric Aβ, hydrolyse oligomers (NEP), acts on extracellular deposits (ECE)	(Iwata et al., 2001) (Kurochkin & Goto, 1994) (Eckman et al., 2001)
	Matrix Metalloproteinases	Degradation of both monomeric and fibrillar Aβ	(Carvalho et al., 1997)
	Lysosomal Peptidases e.g. cathepsin D	Degradation of longer Aβ into shorter, less toxic from e.g. Aβ38	(Hamazaki, 1996)
Proteasomal degradation	**Ubiquitin proteasome system**	Dose-dependent cleaving of Aβ42 by degradation mediated by the conjugation of ubiquitin and several enzymes	(Zhao & Yang, 2010)
Autophagic degradation		Clearance of Aβ fibrils	(Nixon, 2007)
Clearance by extracellular chaperones	**Apolipoprotein E**	Facilitates the intracellular trafficking of Aβ to the lysosome for degradation	(Verghese et al., 2013)
	Apolipoprotein J	Alters Aβ fibril formation ability as well as facilitates Aβ transport across the blood brain barrier through the megalin/LRP-2 receptor	(Bartl et al., 2001)
	α2-Macroglobulin	Complexes with Aβ and mediates endocytosis via LRP protein	(Lauer et al., 2001)

Table 5. 1. Mechanisms of Aβ degradation and clearance.

Together, our data strongly suggest that conformation rather than size influences AβO mediated cytotoxicity. The accumulation of intracellular oligomers must reach a certain threshold after which the cell can no longer recover, and cytotoxicity is mediated.

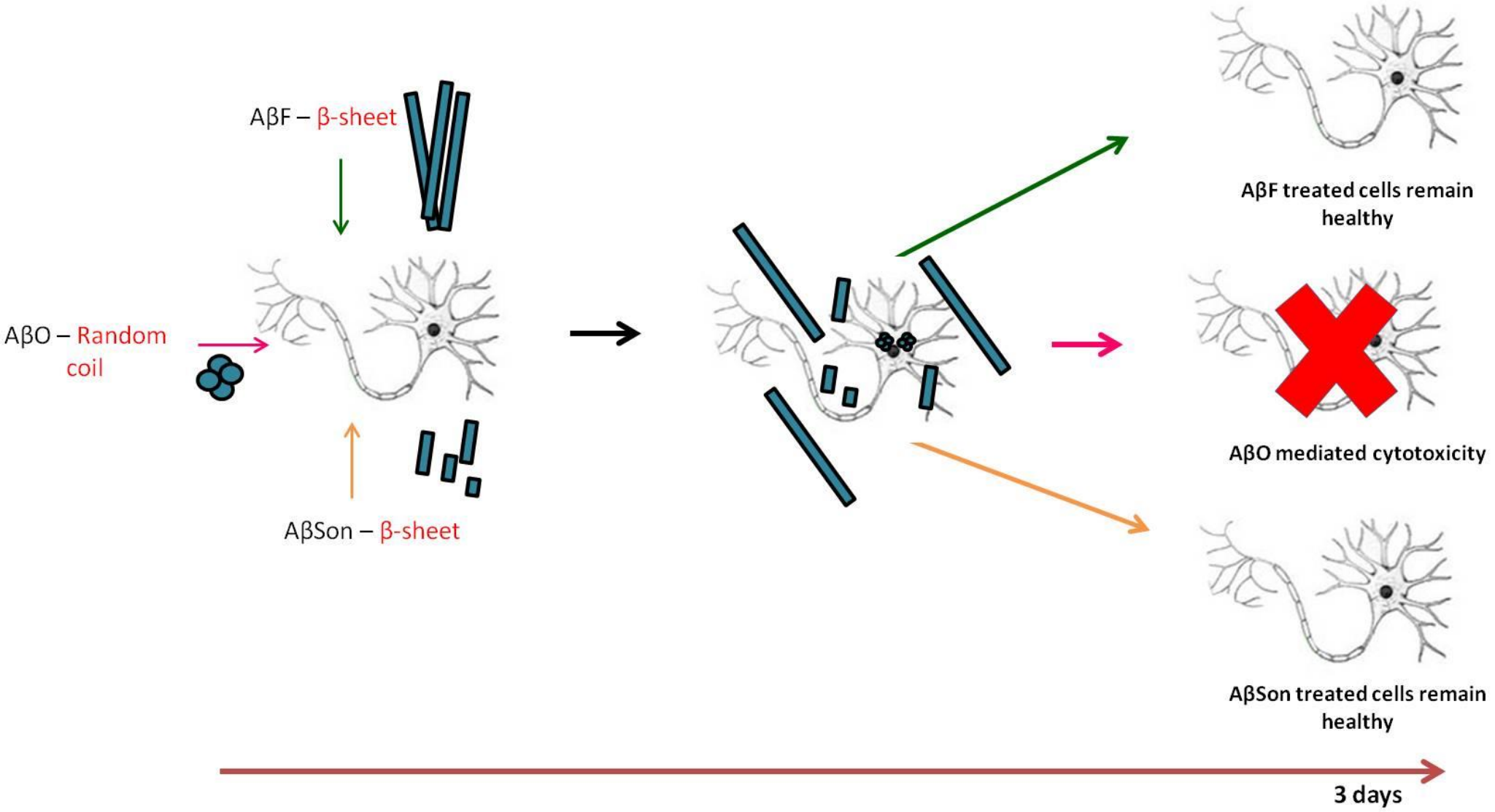

Figure 5. 16. Schematic diagram summarising the data presented in this chapter. AβO which has a random-coil conformation, are internalised and have cytotoxic effects. AβF and AβSon are β-sheet rich and do not display significant cytotoxicity.

Chapter 6: Characterising the assembly and cytotoxicity of the GNNQQNY and FEFKFEFKK functional amyloids

Chapter Overview

Functional amyloid proteins feature throughout nature and have been exploited as nanomaterials, neither of which display cytotoxicity. To better understand how these amyloid proteins avoid toxicity, the Sup35 prion protein fragment GNNQQNY and the hydrogel forming FEFKFEFKK (F9) are presented in this chapter as models of functional amyloid proteins. The assembly process of both peptides was monitored using biophysical techniques including transmission electron microscopy (TEM), circular dichroism (CD) and ThT fluorescence. The cytotoxicity of these peptides has been assessed using the ReadyProbes assay. By characterising the assembly and toxicity (or lack of) of functional amyloid proteins in this way, lessons or 'rules' can be determined to avoid amyloid toxicity.

6.1 Introduction

Functional amyloid proteins are a feature in many living organisms (Table 1.2, Chapter 1). In these examples, the amyloid state is the native fold of the protein and is critical to perform function. The Sup35p prion protein [PSI] found in *Saccaromyces cerevisiae* (yeast) plays a role in termination of mRNA translation in wild type cells. (Kushnirov et al., 2000). However, it can also behave as an amyloid forming prion [PSI+] to prevent translational termination (due to a loss of function); this allows for stop codon read-through and C-terminal extension. From this, there is phenotypic diversity created (Bertram et al., 2001). Prion proteins are self-propagating and transmissible therefore the Sup35p amyloid forming protein allows for the transmission of genetic information; the cytoplasmic amyloid is reversible and heritable leading to a particular phenotype being passed from mother to daughter cells upon division. This non-Mendelian inheritance is facilitated by cytoduction which involves the fusion of donor and acceptor cell cytoplasm, without nuclear fusion (Conde & Fink, 1976). The amyloidogenic fragment of the Sup35p protein, found in N-region prion determining domain, has been identified as the GNNQQNY sequence. It was one of the first amyloidogenic fragments to have its crystal structures solved (Nelson et al., 2005).

The use of amyloid proteins in the development of biomaterials is vast both in vitro and in vivo. They are often used as scaffolds for 3D cell cultures and tissue engineering (Szkolar et al., 2014; Tang et al., 2014; Wan et al., 2016). Hydrogels have also been used as a vehicle for localised drug delivery in regenerative medicine. The F9 peptide is a short, hydrogel forming peptide which are three-dimensional networks of entangled fibrous structures. They are able to form these structures due to non-covalent interactions in response to external factors such as pH and temperature (Morris et al., 2017). The F9 peptide is an amphipathic peptide with alternative hydrophobic and hydrophilic residues which assembles into β-sheet rich assemblies above a certain concentration. This is known as the critical gelation concentration (CGC) (Elsawy et al., 2016).

GNNQQNY and FEFKFEFKK peptides were used as models of non-toxic amyloid peptides which have a functional role in yeast and a designed bionanomaterial respectively. Their assembly was characterised using CD, ThT and TEM. ReadyProbes assay was used to assess the cytotoxicity the resulting amyloid.

6.1.2 Structure of GNNQQNY

The crystal structure of GNNQQNY was solved by the Eisenberg group (Nelson et al., 2005). This peptide was previously shown to form amyloid fibrils when dissolved in water and used at a concentration of 400μM (Balbirnie et al., 2001). At higher concentrations of 10-100mM (Balbirnie et al., 2001; Langkilde et al., 2015; Nelson et al., 2005; Sawaya et al., 2007), this peptide forms elongated microcrystals which allows for X-ray diffraction studies. Electron diffraction examination of GNNQQNY microcrystals showed three important features; firstly, the β-sheets are tightly packed with hydrogen-bonded neighbouring side chains, secondly, the β-sheets were anhydrous and finally, the β-sheets were parallel (Diaz-Avalos et al., 2003). Although this provides important information regarding the packing of the peptide, conclusion about the interactions of the side chains and backbone cannot be made. The Eisenberg group were the first to crystallise GNNQQNY (pdb code 1YJP) (Nelson et al., 2005) and established that the strands in one sheet are anti-parallel to those in the partnering sheet. Each sheet is subsequently shifted relative to its partnering sheet as the side

chains extending form a strand fit between the side chains extending from two strands of the partnering sheet (Nelson et al., 2005). The crystal structure of GNNQQNY suggests that a tight dry steric zipper between a pair of β-sheets is a fundamental feature of amyloid fibrils. This steric zipper is best described as polar side chains of the dry interface (i.e. no water molecules between two β-sheets) being tightly interdigitated with the three same polar side chains of the partnering sheet (Nelson et al., 2005). The side chains of the dry interface do not form hydrogen bonds with each other, but rather form van der Waal interactions due to their complementing shapes. This suggests the β-sheets to be the stable structural unit of the cross-β spine. Though there is a lack of hydrogen bonds within the dry interface of GNNQQNY, there are 11 hydrogen bonds formed with two neighbouring molecules in the same sheet. These 11 are made up of five backbone hydrogen bonds, four amide stacks (hydrogen bonds between pairs of Asn or Gln residues) and two hydrogen bonds between the backbone amide nitrogen to the Asn2 side chain oxygen. It is the amide stacks that force the GNNQQNY molecules to stack in a parallel and in register manner in their respective sheets. There is also a wet interface formed which is lined with water molecules, completely separating GNNQQNY molecules (~15Å).

In 2007, a second crystal structure was solved (pdb code 20MM) (Sawaya et al., 2007) which although shared similarities to the first, also displayed significant differences. The two crystals can be separated into monoclinic and orthorhombic structures. The monoclinic form has been described above. The orthorhombic form has a much less defined wet interface and the N3 and Y7 residues from one molecule interact with the Y7 and N3 on a different molecule. There is also no interaction of the tyrosine side chains in the sheet-spacing direction (Sawaya et al., 2007).

The GNNQQNY peptide is investigated in this chapter as a model of a non-toxic functional amyloid peptide.

6.1.2 Hydrogels

Historically, hydrogels were formed from high molecular weight polymers (Hirst et al., 2008), however the properties of amyloid forming peptides make them highly attractive as alternatives. Their high stability, and combination of hydrophobicity and charges residues enable them to bind to both macro and small molecules and cells (Ahmed, 2015). Low molecular weight gelators have also recently been developed and can be triggered to form gels using several triggers. An example of this are hydrogels formed using the functionalised dipeptide 2NapFF (Colquhoun et al., 2017) .

There are a number of factors that contribute to the gelation properties of peptides and these can be adapted to provide different functionalities of the hydrogel. Hydrogel scaffolds should ideally have certain characteristics including ease of handling under physiological conditions, uniformity at nano, micro and macroscopic levels as well as the possibility of being able to design gels to match the cell type. Traditionally, synthetic hydrogels were formed by covalently cross-linking polymers, however due to the toxic nature of some cross-linking reagents, their biological applications were limited. Supramolecular hydrogels can be formed without the need for cross-linking, using self-assembling peptides via number of non-covalent interactions. These include van der Waals, electrostatic and hydrophobic interactions (Dou & Feng, 2017). The weaker non-covalent interactions in supramolecular hydrogels allows for smart responses to external stimuli and thereby allowing for manipulation of characteristics such as pore size of fibrillary network as cells migrate through them.

There are four main families of self-assembling peptides used to form hydrogels; 1) short peptide derivatives; 2) α-helix/coiled-coiled; 3) amphiphilic peptides and 4) β-sheet peptides. Specific amino acids and peptide derivatives are gelators, with intermolecular hydrogen bonds between amide bonds as the gelation driving force (Bakota et al., 2013). Generally, amino acid and peptide derived gelators are often designed to have both hydrophobic and hydrophilic groups. This is due to the hydrophobic side chains shielding amide groups from water to form hydrogen bonds and hydrophobic central cores (van Bommel et al., 2004). Charge and pH are important factors in designing peptides to form hydrogels, as is the β-sheet forming ability of peptides. This is demonstrated by a peptide designed to

form flat, straight fibrils by the insertion of a diproline peptide between two β-sheet forming strands consisting of alternating lysine and valine residues. Under basic conditions, lysine has no charge which allows for its folding into a β-hairpin where one face is lined with the hydrophobic valine residues and the other with the hydrophilic lysine residues (Schneider et al., 2002). The subsequent self-assembly is due to lateral hydrogen bonding between β-hairpin and also due to hydrophobic interactions between the valine rich faces of the folded peptide (Schneider et al., 2002). When the pH was lowered to below the pKa of the lysine chains (i.e. protonating the lysine residues), intrastrand repulsion between partnering lysine residues and the unfolding of individual β-hairpins occurred. This led to hydrogel formation (Schneider et al., 2002).

Amyloidogenic sequences have also been shown to form hydrogels which have been used in number of biological applications. For example, amyloid fibrils have been shown to support cell adhesion and growth (Reynolds et al., 2014). For this reason, their application in tissue engineering in vitro and in vivo has been extensively developed. A recent example was shown in exploiting the self-recognition motif of α-synuclein to promote the differentiation of mesenchymal stem cells without the addition of growth factors. In vivo, human mesenchymal stem cells were transplanted with the hydrogel in mice. The hydrogel was shown to contain the cells at the transplant site and provided support for neuronal differentiation as well as improved survival (Das et al., 2016).

A similar effect was seen with hydrogels formed from peptides based on the aggregation of the C-terminal of Aβ42, GGVVIA, which has previously shown to form a hydrogel. (Jacob et al., 2015; Lakshmanan et al., 2013). This hydrogel was shown to be non-toxic in the SHSY5Y neuroblastoma line (Jacob et al., 2015). The KLVFF fragment of the Aβ peptide has also been shown to form a hydrogel when prepared in concentrated phosphate buffered saline. This highlights the importance of the electrostatic charges between the lysine residues and the salts in the buffer (due to the screening of the lysine side chains), which are thought to enable the aggregation of β-sheets into hydrogels (Krysmann et al., 2008). Each of these hydrogels showed recovery after disruption (e.g. by vortexing), suggesting if these should be injected as a method of drug delivery for example, any occurring damage could be rectified (Krysmann et al., 2008). The porous nature of hydrogels allows the loading

of drugs into the gel matrix and subsequent release at a diffusion rate that is dependent on the diffusion coefficient of the drug (Hoare, 2008).

The F9 peptide has been recently characterised in vivo as a therapeutically relevant self-assembling, β-sheet rich hydrogel (Morris et al., 2017). From the study, positron emission tomography and fluorescence labelling assessed the pharmacokinetics, bio-distribution and excretion of the hydrogel in healthy mice and found it to be a highly promising biomaterial for drug delivery with no toxicity of the hydrogel detected (Morris et al., 2017). This non-toxic hydrogel forming F9 peptide will be used as a second model of functional biomaterial amyloid in this chapter.

6.2 Results and Discussion

6.2.1 GNNQQNY and F9 form fibres with a high propensity

In order to confirm both peptides formed fibrils, 1mg/ml of each peptide was dissolved in water or 10mM HEPES buffer. It was necessary to confirm assemblies formed in 10mM HEPES buffer for cell viability assays. The GNNQQNY peptide (Pepceuticals) and F9 peptide (kindly provided by the Saiani group, Manchester) assembly morphologies were examined using TEM (Figure 6.1). It is evident GNNQQNY fibrils are abundant at T0 and 24 hours in both water and 10mM HEPES buffer. This is consistent with immediate fibril assembly observed over a range of concentrations from 0.5mg-10mg/ml (Marshall et al., 2010). Similar abundance of fibrillar species is seen with F9 at both time points, shown in Figure 6.2. Previous reports have demonstrated the ability of GNNQQNY to form fibrils and crystals in a concentration dependent manner (Balbirnie et al., 2001; Nelson et al., 2005). Here, we have used the relatively low concentration of 1mg/ml for GNNQQNY in an attempt to monitor the assembly process. Although we cannot visualise the gradual formation of fibrils over time, Figure 6.1D shows an example of crystals that were observed at 24 hours suggesting crystals are formed from fibrils. This is consistent with previous reports of GNNQQNY crystal formation (Marshall et al., 2010).

The cross-β structure of GNNQQNY fibrils has been previously shown (Balbirnie et al., 2001). To ensure the F9 peptide is amyloidogenic and displays the characteristic cross-β structure, XRFD was

used (Figure 6.2E) and the XRFD pattern was collected by Y. Al-Hilaly. F9 displays a XRFD pattern consistent with a cross-β structure, previously not shown. The XRFD pattern shows a 4.7 Å reflection on the meridional axis consistent with hydrogen bonded beta-strands oriented perpendicular to the fibre axis. The equatorial reflection at 10.8Å arises from the spacing between associated beta-sheets. This will be determined by the size of the side-chains and is consistent with the phenylalanine content (Fandrich & Dobson, 2002). More detailed information of the structure could not be obtained from the XRFD pattern due to the way in which the fibres entangle to form large networks.

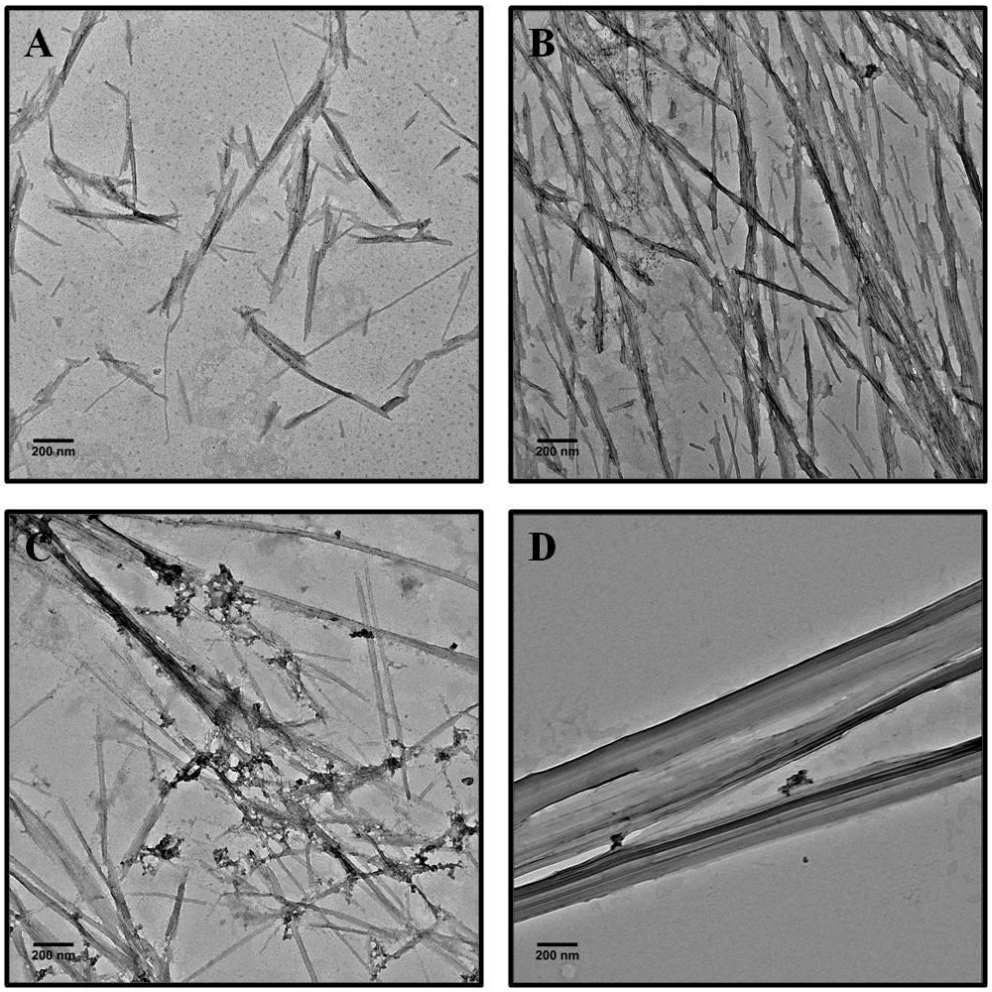

Figure 6. 1. Negatively stained electron micrographs of GNNQQNY prepared in water and 10mM HEPES buffer. Prepared in water at T0 (A) and 24 hours (B) and in 10mM HEPES buffer pH 7.4 at T0 (C) 24 hours (D) show assembly into fibrils. Scale bars shown at 200nm. Representative images from three separate sample preparations are shown at each time point.

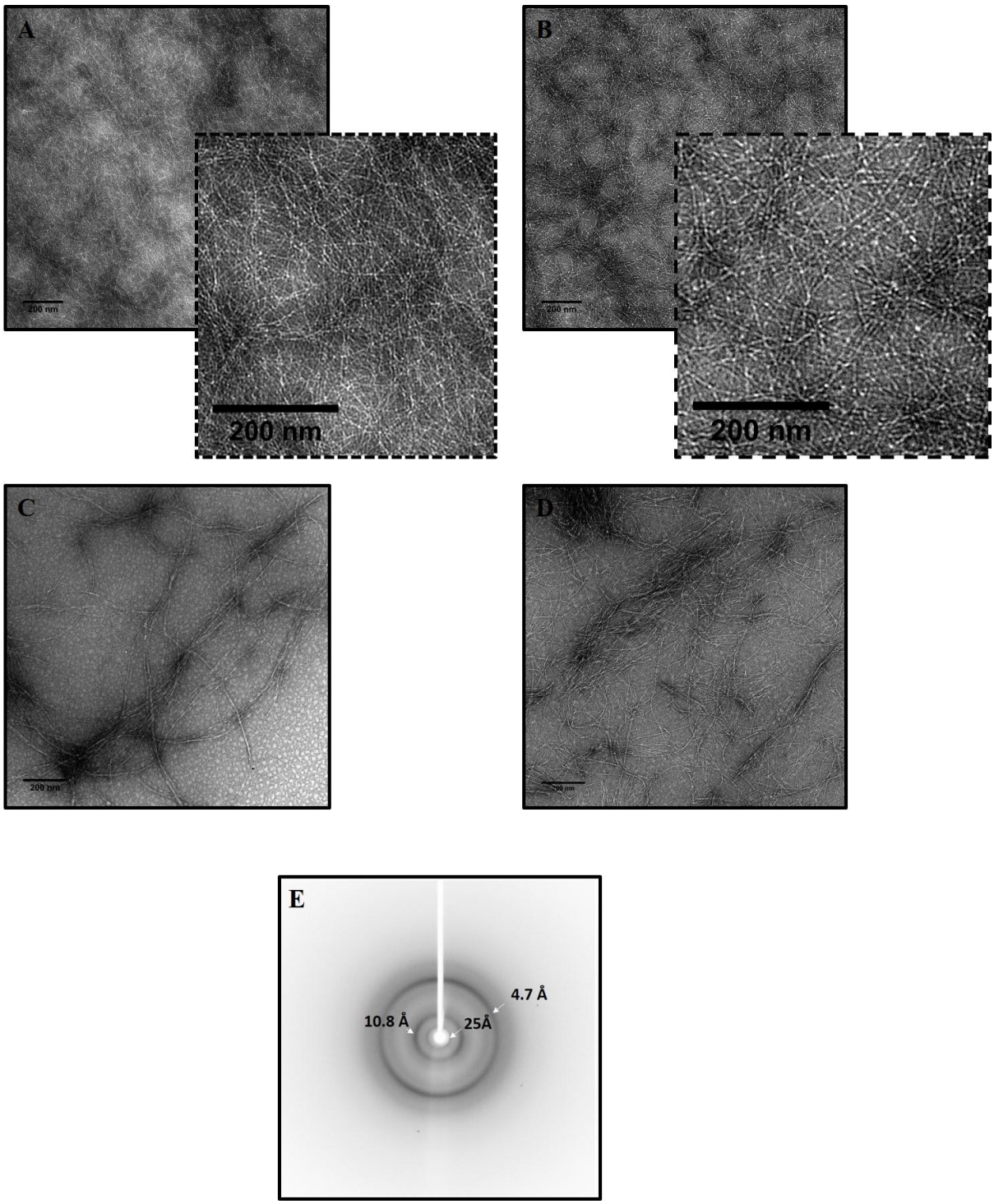

Figure 6. 2. Negatively stained electron micrographs and XRFD pattern of the F9 peptide in water and 10mM HEPES buffer. Prepared in water at T0 (A) and 24 hours (B) and in HEPES buffer (C) and (D), F9 forms abundant fibrils. Scale bars shown at 200nm. Electron micrographs are representative of three separate peptide preparations (E) The F9 XRFD pattern shows the characteristic cross-β structure typical of amyloid peptides The XRFD experiment was carried out by Y. Al-Hilaly. The diffraction pattern was obtained from fibrils from one sample preparation.

Due to the rapid formation of fibrils, an accurate concentration could not be obtained using the A280 as a result of scattering. For these peptides, the theoretical molar concentration at 1mg/ml was calculated using their molecular weight; 1.12mM for GNNQQNY and 800µM for F9.

Having confirmed both peptides form amyloid fibrils, we next prepared both using the protocol presented for Aβ42 in Chapter 3. This was done with a view to control and follow assembly of the peptides into amyloid fibrils.

Figure 6.3 below shows electron micrographs of the GNNQQNY and F9 peptide following buffer exchange spin column method. Very little assembly is shown in these electron micrographs, even after a 24-hour incubation period.

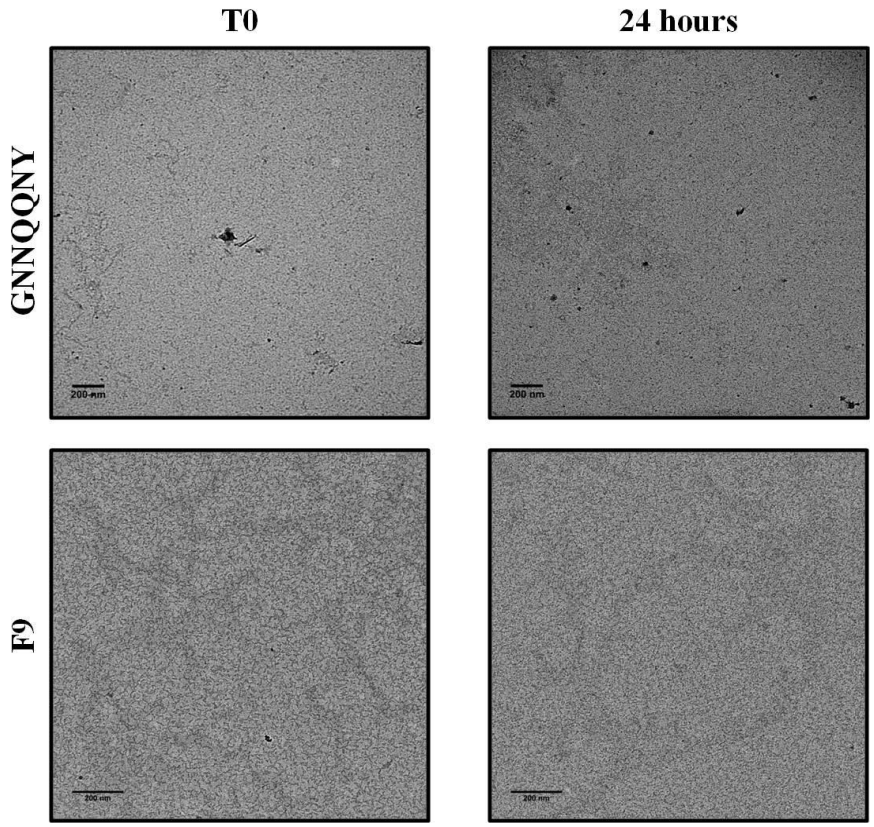

Figure 6. 3. Negatively stained electron micrographs at T0 and 24 hours of the GNNQQNY and F9 peptides prepared using the same protocol as described in Chapter 3. Little/no assembly is seen for either peptide following the buffer exchange spin column method. 1mg/ml of each peptide was dissolved in HFIP, sonicated for 5 minutes before drying the HFIP with nitrogen gas. The peptides were then resuspended in DMSO before being put through a 10mM HEPES equilibrated buffer exchange column. Scale bars shown at 200nm. This sample preparation was carried out once as it was clear this spin column method of preparation was not appropriate.

In this protocol, HFIP is used to disaggregate any preformed aggregates. As it is possible HFIP may not be having this effect, TEM was used to visualise the GNNQQNY and F9 peptide dissolved in HFIP. From Figure 6.4 it is clear that HFIP does not disaggregate GNNQQNY and F9 fibrils, and due to this the fibrils are most likely getting trapped in the spin column. This also demonstrates the unusually high stability of these fibrils.

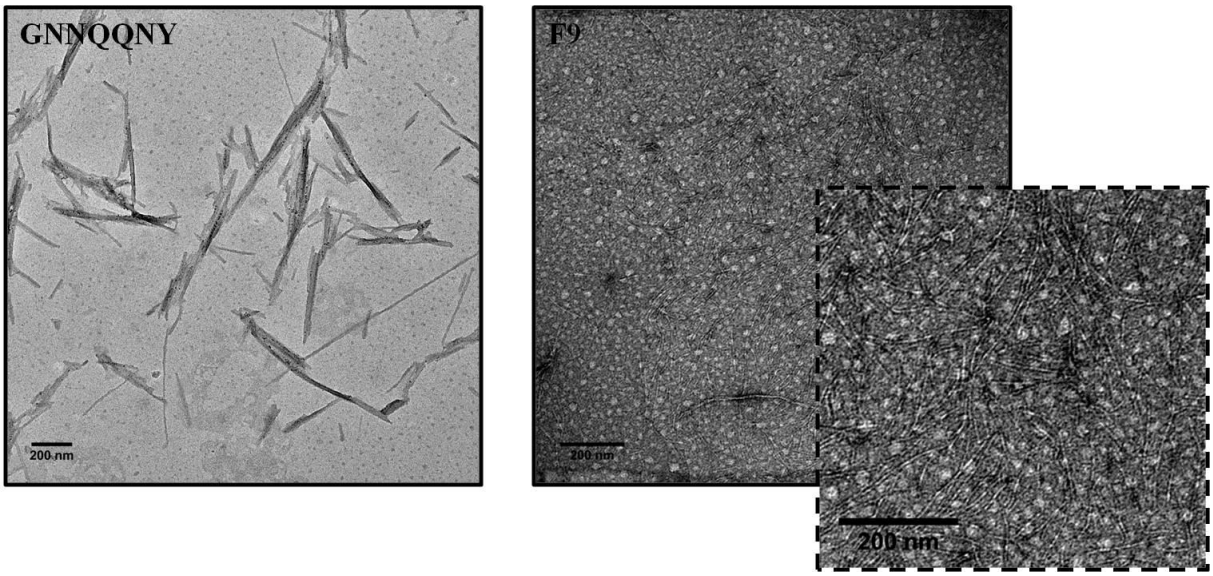

Figure 6. 4. GNNQQNY and F9 dissolved in HFIP at T0. Scale bars shown at 200nm. This was carried out once as it was apparent that HFIP does not disaggregate fibrils.

From this, we can conclude both peptides form amyloidogenic fibrils with a high stability and are resistant to solvents and due to this, the buffer exchange spin column method of peptide preparation cannot be utilised. Therefore, for all subsequent data presented in the chapter, peptides were dissolved in water or HEPES buffer as appropriate.

To determine a lag phase in which ThT negative (non-fibrillar) assemblies were present, the ThT fluorescence of both peptides was monitored. The assembly of GNNQQNY has been proposed to occur in three stages. Firstly, there is the rapid formation of parallel β-sheets by β-strands (Nelson et al., 2005) which in the second stage, slowly form pair-of-sheets structures with a characteristic dry interface. Here, there are van der Waals interactions rather than hydrogen bonding, giving rise to less

specific patterns of bonding and therefore polymorphism (Nelson et al., 2005). These can then behave as the nucleus for subsequent fibril formation. Using structure-based energetics, the Eisenberg has argued that the nucleus must be made up of ~4 GNNQQNY molecules requiring a ~3 molecule transition state complex, for subsequent fibril formation. The formation of this nucleus is likely to occur relatively slowly due to the need of amide side chains acquiring the appropriate rotamers for interdigitation with partnering β-sheets, and also due to the dehydration needed to allow for the dry amide-hydrogen bonds (Nelson et al., 2005). The decrease in entropy during this step is thought to act as a barrier to fibril formation. Physiologically, the Sup35 gene encodes the release factor 3 (eRF3). Under normal conditions the Sup35p, in the non-prion conformation [PSI^-], functions together with eRF1 to release polypeptide chains. The frequency with which there is a conformational switch from [PSI^-] to the prion [PSI^+] is proportional to the level of [PSI^-]. Once this seed has been established, the formation of fibrils occur rapidly (Liebman & Derkatch, 1999). A fourth stage of crystal formation from these fibres has been more recently proposed (Marshall et al., 2010) which may affect ThT binding.

By using ThT fluorescence, we aimed to monitor this lag-dependent cooperative formation.

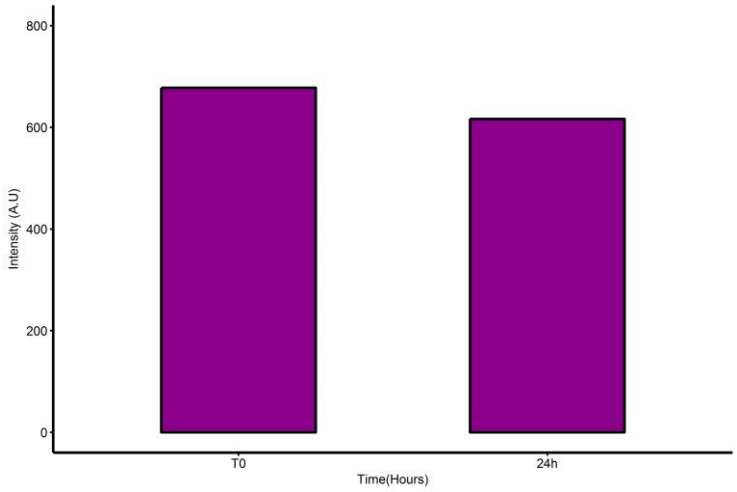

Figure 6. 5. ThT fluorescence of GNNQQNY over 24 hours show no lag or elongation phase. The peptide was incubated with 10µM ThT at 1.12mM stock concentration. This was carried out once in order to establish if there was an increase in fluorescence seen over 24 hours as this was not the case, no further repeats were carried out and statistical analysis was not possible.

From Figure 6.5, we can conclude that due to the rapid assembly of the peptide, it is not possible to monitor assembly following a lag and elongation phase using ThT fluorescence. However, this does complement the TEM data to confirm the formation of fibrils.

ThT fluorescence of F9 at stock concentration and 50µM was observed at T0. A dilution to 50µM was used as at the stock concentration of 800µM, ThT positive assemblies were already present at T0. This is consistent with the TEM (Figure 6.1). Dilution of these fibrils may allow us to monitor any assembling F9 into mature fibrils over time. However, as seen in Figure 6.6, both concentrations displayed similar fluorescence intensities at T0, in fact, a slightly higher intensity is seen with the diluted sample. This is possibly due to more binding sites being available to the dye; at higher concentrations, the characteristic fibrillar tangles may limit these binding sites. ThT fluorescence of 50µM F9 was monitored up to 24 hours (Figure 6.6B) to identify whether there was a lag phase followed by elongation phase, as is seen with Aβ42. No increase in fluorescence intensity was seen over 24 hours further suggesting immediate assembly into fibrils by the entire sample population.

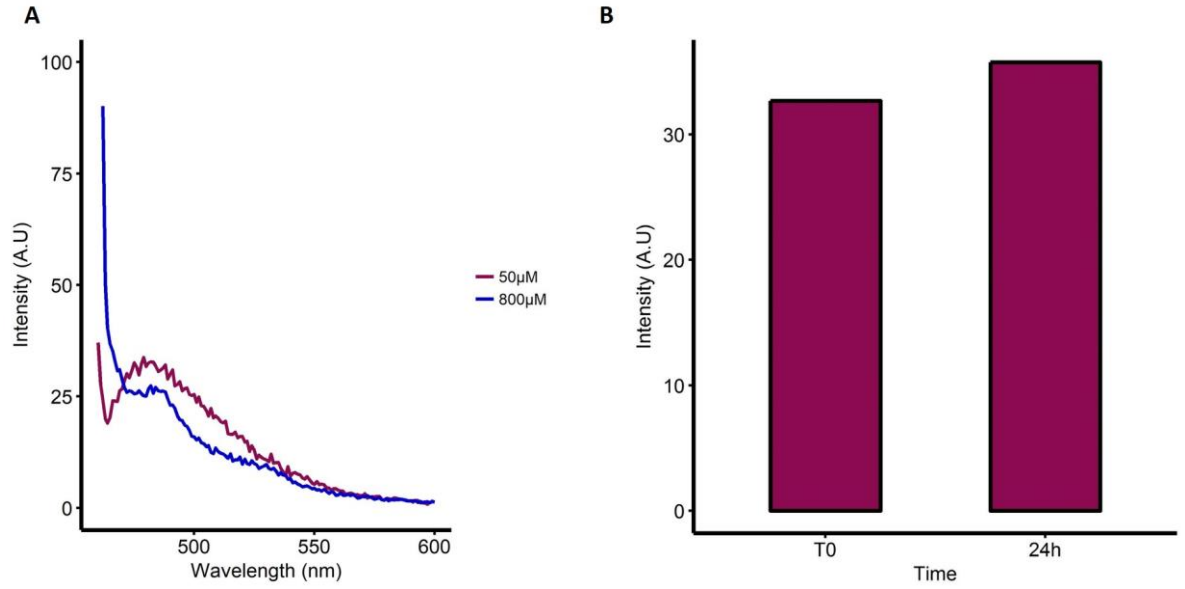

Figure 6. 6. F9 ThT Fluorescence. A) ThT fluorescence of 50µM (purple) and 800µM (blue) F9 at T0 (prepared in 10mM HEPES buffer pH 7.4, incubated at room temperature) Both display similar fluorescence (B) ThT fluorescence of 50 µM F9 over 24hours. There is no increase seen in intensity over 24 hours suggesting assembly of the peptide is immediate. This was carried out once in order to establish if there was an increase in fluorescence seen over 24 hours as this was not the case, no further repeats were carried out and statistical analysis was not possible.

The differences in ThT fluorescence intensities for GNNQQNY and F9 can again be explained by the tangled nature of the F9 peptides 'burying' sites for the dye to bind to. Combining the TEM, ThT fluorescence and CD spectra, it is evident that even at relatively low concentration both peptides assembly rapidly into β-sheet rich structures.

6.2.2 Secondary structure of GNNQQNY and F9

As with peptides presented in the previous chapters, CD was used to probe for the secondary structure of GNNQQNY and F9. From the electron micrographs for both peptides, we are confident fibrillar structures are seen at T0 and 24 hours. Therefore, the secondary structure was monitored for these times only.

Figure 6.7 displays the CD spectra for GNNQQNY.

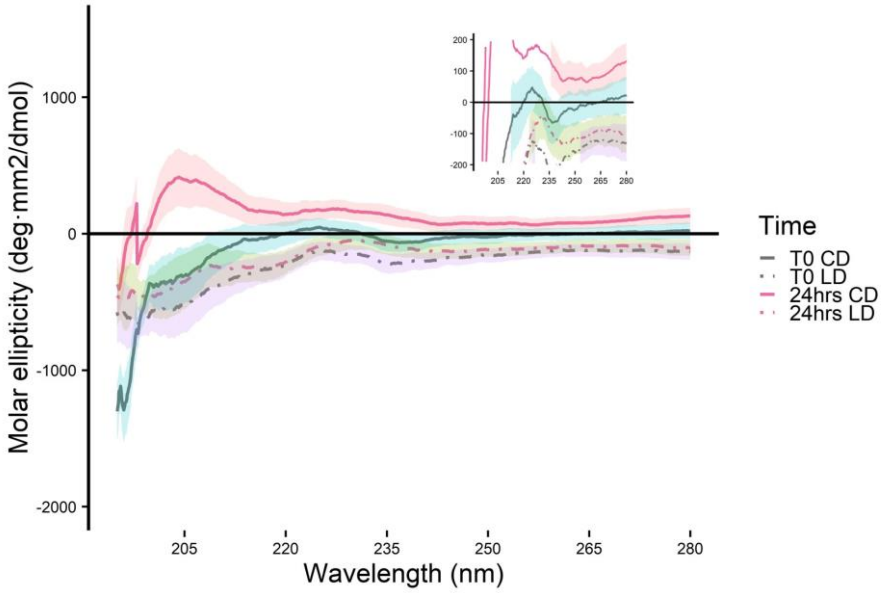

Figure 6. 7. GNNQQNY secondary structure by CD. CD (solid line) and 90° rotation (dash-dot line) spectra GNNQQNY at T0 (grey) and 24 hours (pink). Without flow and at this low concentration, it is difficult to obtain a true LD spectrum with the characteristic positive peak at 195nm, however, at 24 hours the CD and rotated spectra display different spectra, suggesting there is LD contribution. The inset shows a small peak seen at 278nm (shown in inset) in the 24 hours CD spectra, which is due to the splitting of a peak in the aromatic region of the peptide. The peptide was prepared at 1mg/ml in water and CD spectra were obtained using a 0.01mm pathlength cuvette. The spectra shown are the mean of three separate peptide preparations and each displayed a spectra indicative of LD contributions. Error bars expressed as ±SEM.

The CD spectra do not display the characteristic spectra expected for β-sheet rich structures. There is no strong signal seen at T0, which could be due to the low concentration of the peptide. From the electron micrographs, it is more likely however, that the fibrils are oriented in a manner that does not allow for the chromophores to create oscillations of circularly polarised light. As there could be contribution of Linear Dichroism (LD) due to the inherent orientation of the fibrils, the cuvette containing the GNNQQNY sample was rotated by 90° and spectra were collected at same wavelengths. In LD, it is the differential absorbance of light polarised in a parallel and perpendicular manner to an orientation axis that is measured. The signals in the subsequent spectra are due to the aligned samples showing directional dependence. Therefore it is reasonable to consider that the CD spectra obtained at 24 hours, with positive peaks seen at 204nm and 235nm, may be due to LD contributions arising from the regular and ordered arrangement of the assemblies (Bulheller et al., 2007).

The 90° rotated spectra at T0 shows a small positive signal at 235nm and a small negative signal at 204nm. This could be due to fibrils at T0 that are not fully aligned to give a definite LD signal. At 24 hours, smaller peaks are seen at the same positions as the CD spectra, confirming that there is some contribution by LD. Furthermore, the tyrosine residue in this peptide is expected to contribute significantly to the CD spectra which can be intensified due to the coupling transitions of close proximity of aromatic residues (Sreerama et al., 1999). This can be seen in the peaks arising at 235nm can be attributed to the close proximity of the tyrosine residues undergoing exciton coupling. There is also a small peak seen at 278nm (shown in inset) which is due to the splitting of a peak in the aromatic region of the peptide. The second peak is expected to be at 286nm, as has been observed in previous studies (Marshall et al., 2010). The importance of aromatic residues in the assembly of Aβ42 has been discussed (Chapter 3). Similarly, the behaviour of the aromatic tyrosine residue in the assembly process of GNNQQNY has been established (Marshall et al., 2010). Previous studies on the crystals of GNNQQNY have shown there is a strong positive LD signal at 195nm due to the $\pi \rightarrow \pi^*$ amide transition dipole moment being oriented perpendicularly to the β-strands which is consistent with the formation of cross-β structure (Marshall et al., 2010). However, in order to observe this

signal from crystals observed by 24 hours in the electron micrographs (Figure 6.1D), a Couette flow and tilt to orient the long axes of the crystals with the direction of flow, as well as high concentration of peptide, are needed. It is likely that this 195nm peak has shifted to 204nm in the CD spectra shown above due to LD, confirming the formation of cross-β structure from β-sheet rich fibrils.

The folding of GNNQQNY into β-sheet rich structures has been previously described from solved crystal structures (Nelson et al., 2005) and therefore we are convinced of the secondary β-sheet structure of the fibrils and crystals shown in the electron micrographs (Figure 6.1). The elongated morphology of fibrils (and crystals) is attributed to the hydrogen bonded addition of GNNQQNY β-strand molecules was found to occur at growing β-sheets (Nelson et al., 2005).

The F9, which also rapidly forms fibrils (Figure 6.2), posed a similar problem of an LD rather than CD spectra (Figure 6.8). As with GNNQQNY, a characteristic β-sheet spectra was not seen with the F9 peptide. At T0, the CD spectra displays a small negative signal at ~218nm and positive peak at roughly 198nm which suggests a β-sheet rich structures due to the transition of $\pi \rightarrow \pi^*$ and $n \rightarrow \pi$ respectively. There is also, however, the presence of a negative signal at roughly 198nm which is likely due to LD artefacts similar to those seen with GNNQQNY. By 24 hours, the CD spectra shows a negative peak at 222nm due to $n \rightarrow \pi^*$ transition and two positive peaks at 192 and 198nm. The 222nm negative peak in the CD spectra of F9 has been previously observed and is attributed to the aromatic phenylalanine residues (Elsawy et al., 2016). It is interesting that although there is no change in fibril morphology viewed in electron micrographs, the CD spectra changes from T0 to 24 hours. This suggests there is a change occurring within the structures. The 90° rotation LD spectra at 24 hours (dotted black line) displays a characteristic β-sheet spectrum. Although it was not possible to replicate the CD spectra, the LD spectra shown above is consistent with data previously presented by the Saiani group (Elsawy et al., 2016). This would suggest that the CD spectra is due to LD artefacts that have led to a shift in the spectra. Using the rotated spectra, we can confidently identify the F9 peptide to be β-sheet rich. This has also been previously confirmed by FTIR spectroscopy where two strong absorption peaks at 1624 and 1524 cm^{-1} were shown, corresponding to an extended β-sheet conformation (Elsawy et al., 2016).

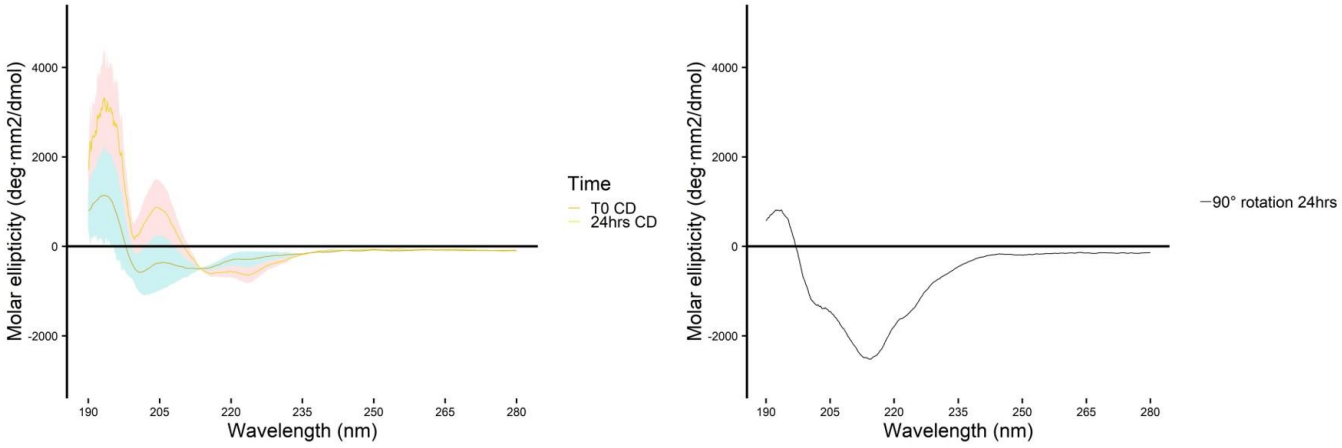

Figure 6. 8. Secondary structure of F9 by CD. CD spectra for F9 peptide at T0 and 24hours are shown in the left hand spectra. The 90° rotation spectra at 24 hours is also shown in the right hand specta. The peptide was prepared at 1mg/ml in water and spectra were obtained in a 0.01mm pathlength cuvette. The spectra shown for CD at T0 and 24hours are representative of spectra seen from three independent peptide preparations, error bars expressed as ±SEM. The β-sheet signal seen at 24hours with a 90° rotation, however, was only obtained from one sample preparation.

Due to the alternating hydrophobic and hydrophilic resides in the F9 peptide, the peptide is thought to self-assemble into anti-parallel β-sheet fibrils. These have both a hydrophobic and hydrophilic face and in order to avoid contact with water, the hydrophobic faces of β-strands pair to from β-sheet fibres with hydrophobic residue side chains buried in the core (Elsawy et al., 2016). A schematic of this is shown in Figure 6.9.

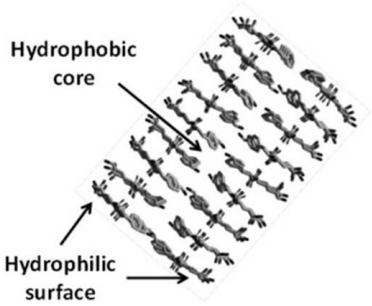

Figure 6. 9. Schematic representation of the extended β-sheet conformation of the F9 peptide. Taken from Elsawy et al, 2016

The importance of phenylalanine aromatic residues in the F9 peptide to form β-sheet structures has been demonstrated by another group (Elsawy et al., 2016). Disruption of the phenylalanine packing resulted in the loss of β-sheet structure as measured by FTIR (Elsawy et al., 2016). This further demonstrates the importance of primary sequence in amyloidogenicity; as the F9 peptide is rich is aromatic residues, this is likely a factor influencing amyloid forming propensity.

6.2.3 GNNQQNY and F9 functional amyloid peptides are non-cytotoxic

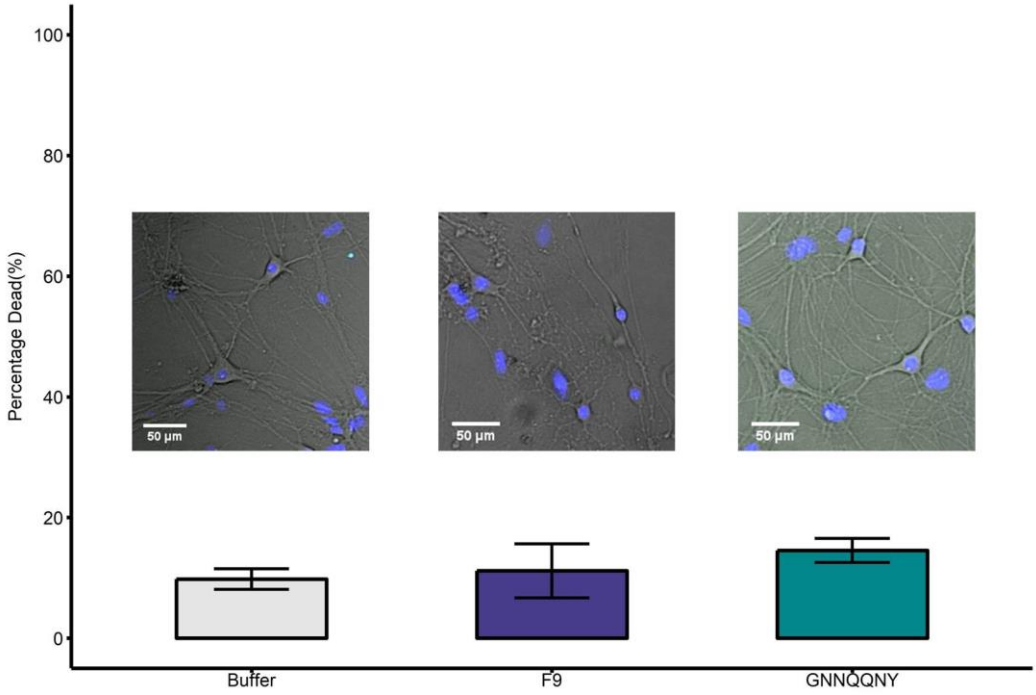

Figure 6. 10. GNNQQNY and F9 ReadyProbes cell viability assay. 10µM incubation of both GNNQQNY (14.54% ± 1.98, total number of cells =1025, number of dead cells = 149) and F9 (11.2% ± 4.4, total number of cells =215, number of dead cells = 24) peptides show no significant toxicity compared to buffer incubated neurons (9.8% ± 1.7, total number of cells =929, number of dead cells = 91) . Examples of the ReadyProbes images show the morphology of cells incubated with the peptides look healthy and similar to those incubated with buffer only with very few/no green labelled cells. Unpaired parametric student's t test where p= < 0.01 (*), < 0.001 (**), < 0 (***). Error bars are expressed as ±SEM. The averages of three separate peptide preparations in three separate hippocampal cultures are shown.

Due to their functional properties, both peptides were expected to be non-toxic. In order to investigate this, we utilised the ReadyProbes assay as a measure of cytotoxicity (Figure 6.10). Peptides were prepared in 10mM HEPES and incubated with primary hippocampal cultures at a final concentration

of 10μM. Due to the rapid assembly of the peptides, they were added to cells immediately after preparation. Cells were incubated with the peptide for 7 days, after which cytotoxicity was measured. No significant cytotoxicity was displayed by the F9 peptide (11.2% ± 4.4, total number of cells =215, number of dead cells = 24) and GNNQQNY (14.54% ± 1.98, total number of cells =1025, number of dead cells = 149) compared to buffer incubated cells (9.8% ± 1.7, total number of cells =929, number of dead cells = 91). The morphologies of the assemblies added to the cells can be seen in Figures 6.1C and 6.2C. Despite no incubation period, both peptides are added as mature fibrils due to their high propensity to aggregate. The non-toxic properties of these mature fibrils, is consistent with that of the AβF presented in Chapter 5. These data supports the hypothesis that the ability to form oligomeric species is extremely important in determining the cytotoxic properties of amyloid proteins.

The lack of cytotoxicity by the GNNQQNY and F9 peptides is unsurprising for several reasons. Firstly, as previously discussed (Chapter 5), internalisation is a likely factor influencing amyloid toxicity. From the electron micrographs (Figure 6.1 and 6.2), it seems unlikely that the GNNQQNY or F9 fibres would be internalised by hippocampal neurons due to their size. Furthermore, immediately after preparation, there are no oligomeric species detected by the biophysical techniques presented above, confirming the high efficiency with which both peptides from amyloid.

Although the absence of oligomers to mediate cytotoxicity may serve as an explanation for the non-cytotoxic behaviour seen in the ReadyProbes assay, both peptides would be expected to assemble in the characteristic nucleation-dependent pathway of amyloid formation (Xue et al., 2008). An example of functional amyloid proteins forming oligomers has been seen in acrosomes of sperm cell, which react positively with the A11 oligomer specific conformational antibody (Guyonnet et al., 2014). Furthermore, computational simulations as well as de novo [PSI+] have suggested the ability of GNNQQNY to form oligomers (Qi et al., 2012; Sharma et al., 2017; Zhang et al., 2007). These studies often do not take into account experimental procedures and data so their validity is somewhat limited. Therefore, it is possible that functional peptides do form oligomers, however spend very little time in this conformation on the pathway to forming mature fibrils. Using SAXS, a recent study has established there is no structural nucleus observed during the fibrillisation process of GNNQQNY

(Langkilde et al., 2015). They observed the presence of only two species, monomers and fibrils, in the sample solution at all time points monitored and postulate the elongation phase to proceed via monomer addition (Langkilde et al., 2015). The lack of oligomeric intermediates formed is attributed to the GNNQQNY monomers fluctuating between different conformations, some of which are extended β-like conformations and can serve as the site for fibril elongation. Therefore, in this case, an oligomeric intermediate is not needed to drive amyloid assembly (Langkilde et al., 2015; Strodel et al., 2007). This supports our hypothesis that it is the ability of an amyloidogenic protein to form oligomers that contributes to its cytotoxic properties. A possible way to reconcile this finding with that of the Eisenberg group, who have proposed a nucleus is made up of ~4 GNNQQNY molecules, is due to several segments of a monomer needed to form an intramolecular nucleus (Nelson et al., 2005).

This rapid assembly is also seen with the Aβ42-1 and AβS sequences which from larger aggregates faster than Aβ42 and display a drastically reduced cytotoxicity (Chapter 4, Figure 4.14) (Vadukul et al., 2017). Lastly, shown by a previous group, the natural amino acid composition of the F9 peptide along with its in vivo metabolic profile made it highly unlikely to be cytotoxic (Morris et al., 2017). This further highlights the importance of primary sequence in amyloid toxicity.

Cell viability assays assessing the cytotoxicity of several functional amyloid proteins have shown the ability of these proteins to cause cellular dysfunction. For example, amyloid fibrils formed from glucagon, α-helical corticotropin-releasing factor, glucagon-like peptide 2 and urocortin 3 were shown to decrease cell viability in primary neurons (Maji et al., 2009). Another example is seen with the disruption of PMEL fibril formation by a three amino acid insertion in the transmembrane domain of the glycoprotein precursor. Ordinarily, PMEL assembles into fibrils at a rate that is order of magnitudes faster than that of Aβ40 (Fowler et al., 2007). This mutation causes oligomerisation of the transmembrane domain which subsequently alters the assembly of PMEL to form toxic oligomers (Kerje et al., 2004; Watt et al., 2011). This supports the notion of oligomers being the toxic species as well as the need to reduce/'by-pass' oligomer formation by rapid fibril formation, to avoid toxicity. Lastly, it is important to note that mediating cell death could be a functional role for amyloid proteins in normal cell functioning. This is seen with amyloid fibrils formed by RIP-1 and RIP-3 kinases,

inducing regulated necrosis (Li et al., 2012). Therefore, it is only the misfolding of proteins into a fold not native to its function that mediates toxicity.

Finally, disease-related amyloid proteins are deposited as either extracellular plaques or intracellular inclusions (Sipe et al., 2016). This suggests a failure to clear or degrade the misfolded protein. This is not the case with functional amyloid. There are several examples of the disassembly of functional amyloid proteins seen at physiologically relevant pH; PMEL and hormone fibrils are disassembled into monomers and not oligomers again avoiding toxicity. This also removes the possibility of fibrillar oligomers being 'shed' from the end of mature fibrils (Tipping et al., 2015) and causing deleterious effects to the cell. The [PSI+] amyloid forming prion conformation of Sup35p, containing the GNNQQNY fragment, is thought to be in part disaggregated into monomers by the over-expression of chaperone heat shock protein 104 (Paushkin et al., 1996; Romanova & Chernoff, 2009), highlighting the importance of tightly controlled assembly and disassembly in functional amyloid proteins and avoiding cytotoxicity. The disaggregation of F9 peptide hydrogels injected into mice as method of drug delivery has been recently monitored. The hydrogel is gradually disaggregated in vivo followed by renal excretion, showing no subsequent toxicity (Morris et al., 2017)

The non-toxic nature of the two functional amyloid peptides presented in the chapter, can be linked to their rapidly forming amyloid fibril structure. In doing so, the formation/quantity of toxic oligomeric species is kept below a cytotoxic threshold. Using these lessons learnt from both functional amyloid peptides, we postulate the time spent in the oligomeric species before forming mature fibrils influences the toxic nature of amyloid proteins.

6.3 Conclusions

Using lessons learnt from the assembly of functional amyloid proteins, which do not display cytotoxicity, we can gain valuable information regarding factor determining amyloid toxicity. In this Chapter, we have used the GNNQQNY and F9 peptide as our models of functional amyloid. Using biophysical techniques such as TEM, CD and ThT fluorescence we can conclude there is extremely rapid formation of β-sheet fibrils by both peptides; no oligomeric species were detected, even at T0.

The cross-β structure of GNNQQNY has been previously reported (Nelson et al., 2005), however using XRFD, we show for the first time that the β-sheet F9 peptide also displays this characteristic feature of amyloid proteins.

Using the ReadyProbes assay, we show both peptides do not display cytotoxicity. Possible reasons for this have been discussed above, however, the most likely reason is due to the rapid formation of fibrils and therefore minimum time spent in oligomeric conformation. This does not necessarily implicate driving disease-related proteins into amyloid fibrils would sequester toxicity as disassembly of functional amyloid into monomers in normal physiology is also key in avoiding toxicity. It is therefore reasonable to conclude that avoiding the formation of oligomers during assembly and disassembly has potential to minimise cytotoxicity.

Chapter 7: Discussion

Amyloid proteins feature in several diseases (Table 1.1), have a functional role across many organisms (Table 1.2) and have also been exploited for their properties as functional materials (Table 1.3) (Gras et al., 2008). The oligomeric species of disease-related amyloid protein have been identified as neurotoxic (Glabe & Kayed, 2006), however, functional amyloid proteins do not appear to induce cellular dysfunction (Jackson & Hewitt, 2017; Pham et al., 2014). This raises the question of which factor(s) make pathogenic peptides deleterious to cellular function. In order to answer this question, the assembly process of disease-related and functional amyloidogenic peptides were thoroughly characterised and linked to cytotoxicity in primary hippocampal cultures.

Several factors such as primary sequence, amyloidogenicity, size and conformation have been investigated using a wide variety of biophysical techniques. These have been combined with molecular techniques including western blotting, dot blotting, immunolabelling and live cell imaging where possible, for robust characterisation of assemblies and to probe for localisation of peptides incubated with neurons. In order to establish the cytotoxic effect of assemblies, the live/dead ReadyProbes assay was used as a measure of cytotoxicity. The limitations of this approach has been discussed in the appropriate chapters however, despite this, using a wide variety of complementary techniques in this way has proven to be invaluable in order to the overarching aim of investigating factors that determine amyloid toxicity (Marshall et al., 2016).

Aβ42 is the amyloid protein deposited extracellularly as plaques in AD brains. The self-assembly of this peptide has been heavily researched, with several groups establishing the formation of oligomers, protofibrils and mature fibrils (Lomakin et al., 1996; Roher et al., 1996; Tjernberg et al., 1999). This assembly follows the characteristic nucleation-dependent polymerisation pathway of amyloid proteins (Xue et al., 2008). Here, we have established a consistent and reliable protocol for the preparation of recombinant Aβ42 from monomer to mature fibril (Broersen et al., 2011; Marshall et al., 2016).

This is important for two reasons. Firstly, it provides the ability to follow assembly over a reasonable time frame and identify which species is most prevalent in the population at each time point. This has

been previously lacking and often the structure and morphology of the Aβ42 species being used in experiments is not characterised. As shown in Chapter 5, the oligomeric and fibrillar species of Aβ42 display differing cytotoxicity and this therefore serves as an explanation for inconsistent results in Aβ42 experiments. It is important to note here, however, that the lack of toxicity of fibrils and sonicated fibrils has only been established within the timeframe of our experiment. It is possible that these may take longer than 7 days to exert their cytotoxic effect. To ensure reliable and comparable results regarding Aβ42 mechanisms of pathology from one research group to the next, the same preparation method should ideally be used. However, the use of different preparation methods is potentially extremely valuable in understanding how different assembly conditions affect the pathological properties of the peptide. This is particularly true for the pathogenic properties of oligomers. As the term 'oligomer' covers a wide range of sizes (Table 3.2) and possibly conformation (Kayed et al., 2010), a continued review of the preparation methods of Aβ oligomers, the size and structure of aggregates formed and their cytotoxic effects from a vast number of groups would provide a large collection of data to gain a further understanding of oligomer pathogenic properties.

This preparation method has allowed us to investigate the importance of primary sequence in amyloid toxicity. Using a range of biophysical and antibody-directed techniques, we can identify the oligomeric species to be most prevalent in population after 2 hours. We therefore have a disease-related amyloid model that assembles into a toxic species, in a time frame suitable for experimentation. Using the same preparation method, we characterised the assembly of three primary sequence variants of wild-type Aβ42 and investigated their cytotoxic nature after an initial 2-hour incubation period. The vAβ42 peptide with two amino acid substitutions showed an impaired assembly and remains monomeric for 7 days. The importance the F19S and G37D substitutions have been discussed in Chapter 3 and were identified by the WALTZ algorithm to abolish amyloidogenic regions found in the wild-type sequence (Marshall et al., 2016). Several studies have identified various amino acid substitutions that impair assembly, however, we have taken this a step further and established the effect of this on the cytotoxic nature of the peptide. The same characterisation for Aβ42-1 and AβS was carried out, which revealed both peptides assembled with a higher propensity

than the wild-type sequence. Therefore, we can conclude, using our preparation method, the propensity with which amyloid fibrils are formed relies heavily on the primary sequence of the precursor protein. All three variants did not form oligomers within the same time frame as the wild type sequence and displayed drastically reduced cytotoxicity. This indicates that it is 1) the ability to form oligomers and 2) the time spent in an oligomeric conformation that influences the pathogenic properties of amyloid proteins. It is entirely possible that this may not be the case if the peptides were prepared using a different protocol which would result in an altered/different self-assembly process. Therefore, the conclusions reached regarding the importance of primary sequence in Chapter 4, can only be made for the preparation method used here. Using this approach, the processing of APP discussed in Chapter 1 that results in several different lengths of Aβ being produced, could be structurally characterised and provide insights into the altered self-assembly process seen in disease.

The second reason our preparation method is important is due to the nucleation-dependent polymerisation mechanism of amyloid proteins. Whilst some experiments use techniques such as photo-induced cross linking of unmodified proteins (PICUP) (Ono et al., 2009) or reverse phase purification (Sato et al., 2006b) for assessing structure and cytotoxicity of Aβ, it has been shown that a crude preparation of Aβ containing a heterogeneous population of monomer and oligomer species was more toxic than purified peptide (Jan et al., 2011). This has been attributed to the critical role nucleated polymerisation plays in cytotoxicity. Oligomer/protofibrillar toxicity was abolished when the population of monomers were removed by sub-fractionation, and re-introduction of monomers recovered cytotoxicity leading to the conclusion that the interaction of monomer-oligomer was critical for toxicity (Jan et al., 2011). This implicates that it is the ability to assemble into fibrils via oligomeric and larger aggregates that renders a peptide toxic which has been supported by the data presented in Chapter 6 where both functional amyloid proteins did not form detectable oligomers on the pathway to mature fibrils.

Peptide	Fibrils seen in TEM?	ThT positive?	Initially unfolded by CD?	Cytotoxic?
Aβ1-42	✓	✓	✓	✓
vAβ1-42	✖	✖	✓	✖
Aβ42-1	✓	✓	✖	✖
AβS	✓	✓	✖	✖
GNNQQNY	✓	✓	✖	✖
F9	✓	✓	✖	✖

Table 7. 1. Summary of the biophysical and cytotoxic characterisation of each peptide presented in Chapters 3-6

Table 7.1 summarises the biophysical characterisation and cytotoxic properties of each peptide, which supports the implication that it is the ability to form oligomers that influences amyloid toxicity. From the table, we can see that it is only Aβ42 which shows cytotoxicity. It is also the only peptide that is initially unfolded by CD (Figure 3.7, Chapter 1) and also fibrils visualised by TEM. This suggests soluble protein must be present in order for nucleation-dependent polymerisation to occur and form oligomers that display cytotoxicity. The vAβ42 does not form oligomeric species and therefore the lack of cytotoxicity was expected; by introducing the F19S and G37D substitutions, we impaired the ability of the peptide to assemble into amyloid. This is further supported by the data presented in Chapter 5 where fibrillar Aβ showed no significant cytotoxicity. This fibrillar sample showed no monomeric, dimeric or trimeric species in the population (Figure 5.2, Chapter 5) and therefore very little nucleated polymerisation is expected to be occurring. The AβSon has been shown to be structurally identical to AβF but fragmented in size. Therefore, although oligomer-like sized species

are present, shown in Figure 5.2 (Chapter 5), these may at a low enough concentration to avoid the cytotoxicity as a consequence of nucleation-dependent polymerisation. In this case it is most likely secondary nucleation that is occurring (Cohen et al., 2013; Linse, 2017).

A similar explanation can be used for the non-cytotoxic effects of the two functional peptides presented in Chapter 6. From the structural characterisation, both peptides form amyloid fibrils extremely rapidly with no oligomeric species being detected. This high propensity to form fibres is likely due to the primary sequence of the peptides. Due to rapid fibre formation, only fibrillar species were incubated with the cells. Again, this lack of oligomeric species, immediate fibril formation and non-cytotoxic behaviour suggests the imperative influence the time spent in an oligomeric conformation plays in the amyloid toxicity.

During the assembly of Aβ42, there is a conformational rearrangement from randomly coiled soluble protein, anti-parallel β-sheet pre-fibrillar oligomers and parallel β-sheet mature fibrils (Figure 3.7, Chapter 1). It is important to distinguish between pre-fibrillar and fibrillar oligomers (Kayed et al., 2010) as these are most likely structurally distinct. We identify the lower molecular weight species in the AβSon to represent fibrillar oligomers. Although there is a difference in secondary structure of AβO (prefibrillar oligomers) and AβSon (fibrillar oligomers) detected by CD (Figure 5.5, Chapter 5), to get a deeper understanding of the β-sheet packing in an anti-parallel or parallel manner, FTIR spectroscopy would need to be utilised. However, as the anti-parallel β-sheet arrangement of oligomers has been extensively reported in the literature (Cerf et al., 2009; Colletier et al., 2011; Gu et al., 2014), we assume our prefibrillar oligomers to have an anti-parallel β-sheet conformation which seems to be an important determinant of amyloid toxicity.

Overall, from this structural characterisation, we can conclude that the primary sequence of peptides greatly influences the propensity with which amyloid fibrils are formed using the preparation method presented in this thesis. This significantly determines the time spent in an oligomeric conformation and therefore the subsequent toxicity displayed by the amyloid peptide.

To further investigate whether it is size, conformation or internalisation (or all three) that mediates cytotoxicity of AβO, the cytotoxicity and internalisation of AβF and AβSon were assessed. Both AβF and AβSon displayed no significant toxicity. Although this was expected for AβF, it was thought that the possible fragmentation to a size similar to that oligomers (AβSon) may cause cytotoxicity. This, however, was not the case. Analysis of species visualised by TEM combined (Figure 5.3, Chapter 5), combined with the western blot (Figure 5.5, Chapter 5) confirmed that AβSon does indeed have species similar in size to AβO. The secondary structure of AβO was shown to be randomly coiled, although some β-sheet signal is expected to be present, and AβSon showed a strong β-sheet structure. As AβSon displayed no significant cytotoxicity despite being similar in size to AβO, conformation is implicated as an important factor in amyloid toxicity. Additionally, the β-sheet packing in AβO is expected to be anti-parallel and in AβSon, parallel. This further emphasises the importance of conformation. Furthermore, Aβ42 shows a transitional change from randomly coiled to β-sheet structure after 2 hours, which again serves as evidence for the importance in nucleation dependent polymerisation from soluble to insoluble species in mediating cytotoxicity.

The data presented in Chapter 5 also supports the notion that internalisation is necessary to mediate cytotoxicity. However, the conclusions regarding internalisation of each of the Aβ species are limited due to the resolution of the microscope and the heterogeneity of the sample. Furthermore, additional repeats for quantification of internalisation at each time point are needed and it would be useful to obtain data from the ReadyProbes assay at the same time points in order to establish a relationship between internalisation and cytotoxicity. From the data obtained, however, oligomers are internalised whereas this is to a lesser extent with AβSon fibres, and little internalisation is seen with AβF. AβSon internalisation is most likely due to the smaller species present in the sample population, although internalisation of larger β2-microglobulin sonicated fibrils has been previously observed (Jakhria et al., 2014). Nevertheless, sonicated fibrils are smaller in size than mature fibrils and this therefore suggests size is important in the internalisation process of amyloid proteins. Despite some AβSon internalisation, the lack of significant cytotoxicity again suggests it is conformation that is an

important factor in amyloid toxicity and it is the anti-parallel packing of β-sheets and/or presence of random coil conformation in oligomers that mediates this.

Together, the data presented here has used several models of amyloid proteins in order to determine factors that make pathogenic amyloid deleterious to cellular function. We show that the ability to from oligomeric species and the time spent in this conformation greatly influences amyloid toxicity. Furthermore, although size influences internalisation into primary hippocampal neurons, once internalised it is conformation that is a determining factor of cytotoxicity.

Concluding Statement

'What makes pathogenic amyloid proteins deleterious to cellular function?' In answer to this question, the data presented in this thesis suggests it is the ability to form oligomers with anti-parallel β-sheet packing, the time spent in this conformation and the intraceullar accumulation of these oligomers above a certain threshold, that determines amyloid toxicity.

Future Directions

All peptide sequences characterised in this thesis have provided invaluable information regarding factors that make an amyloid protein cytotoxic. Similar characterisation of assembly and cytotoxicty of other disease-related amyloid proteins in this way, α-synuclein or tau for example, would further establish the important factors contributing to amyloid toxicity.

Establishing a high resolution structure of Aβ42 oligomers using cryo-EM would further build on the structural characterisation presented here and in the literature. A recent example of this has been shown by the cryo-EM structure of tau filaments (Fitzpatrick et al., 2017). This study provided cryo-EM maps and identified filament cores made up to two identical protofilaments adopting a combined cross-β/β-helix structure and identified this as the seed. Cryo-EM is a particularly attactive technique as it does not require crystallisation and allows for the visualisation of 3D structures at near-atomic resolution. This technique has been previously used to dissect the structure of Aβ42 fibrils (Gremer et al., 2017; Miller et al., 2010; Schmidt et al., 2015; Zhang et al., 2009). To use this technique for Aβ42 oligomers, would provide a fundamental understanding of the strucutral features that drive assembly. Furthermore a true high resolution structure of oligomers of different sizes would provide an explanation for the varying levels of cytotoxicity. Furthermore, using super-resolution microscopy it would also be extremely useful to monitor the aggregation of pathogenic amyloid peptides once internalised into cells.

Building on the data presented in Chapter 4, assessing the cytotoxicty of the Aβ42-1 and AβS peptides added to cells immediately after preparation (instead of after a 2 hour incubation period), will help confirm their reduced cytotoxicity (Figure 4.14) is due to a lack of oligomeric species. The sample prepararions at T0 may be more oligomeric than at 2 hours and therefore more cytotoxic. Additionally, observing the internaliation of these peptides would also further add to our conclusions that a certain threshold must be reached to induce cytotoxicity. If no/little internalsation of the

peptides is seen, this would provide one explanation for the lack of cytotoxicity observed in the ReadyProbes assay.

In Chapter 5, we established the non-cytotoxic effects of AβSon. The next step would be to separate the mixture of assemblies by size using low speed centrifugation. This would separate the higher molecular weight assemblies present in the sample from the lower molecular weight assemblies, essentially providing an 'oligomer enriched' supernatent. Establishing the cytotoxicity of this would remove the possbility that significant cytotoxicity is not observed in AβSon incubated cells due to the lower concentration of oligomer-like species being added, compared to AβO. However, it would be expected that these fibrillar oligomer-like species or higher molecular weight fraction would not be cytotoxic due to their parallel β-sheet packing. One difficulty of this, however, would be establishing the correct concentration of the oligomer-enriched supernatent and higher molecular weight fraction. A possible way in which this could be overcome, would be by calculating the concentration of the supernatent using the A280nm intensity and subtracting this from the initial sample preparation concentration. Theoretically, this would provide the concentration of the higher molecular weight fraction of the centrifuged sample. Amino acid analysis would also be beneficial in establishing an accurate concentration.

It would also be an interesting direction to use similar characterisation of the Aβ sequence containing mutations found in FAD. This would provide us with a better understanding as to why some mutations cause rapid fibrillisation (e.g. the Dutch mutation) or why more oligomeric species are detected in other mutations (e.g. Iowa). It would also provide us with whether these mutations altered the kinetics of aggregation or simply produce a larger amount of Aβ42 and therefore more oligomers are detected.

As discussed in Chapter 5, analysis of the morphologyial changes that occur as a result of Aβ42 internalisation, would be an extremely interesting future direction. By intially increasing the n-number of cells imaged, analysis of factors such as the overall cell morphology and nuclei shape, would begin to indicate the consequences of internalised amyloid before cell death. Building on this, cryo X-ray

tomography would allow to view the ultra structure of cellular compartments and assess the morphological consequences of these as a result of internalised amyloid. Comparing the results of AβO, AβF and AβSon using these approaches, will allow us to further determine the effects of size, structure and internalisation in amyloid induced celluar dysfunction. Furthermore, an MTT assay to monitor cellular dysfunction would also investigate deleterious effects of AβSon and AβF, despite the ReadyProbes assay confirming it is not cytotoxic.

Interestingly, α-synuclein has been shown to be cytotoxic in its fibrillar form (Pieri et al., 2016). This may be due to the uptake of these fibrils and propagation to other cells in a prion-like mechanism (Freundt et al., 2012). Transmission of the amyloidogenic tau protein has also been demonstrated (Kfoury et al., 2012; Liu et al., 2012). It is therefore likely cell-to-cell transmission of amyloid proteins also play an important role in mediating toxicity (Braak & Del Tredici, 2011a; Guo & Lee, 2014; Jucker & Walker, 2013). Using technqiues such as microfluidic devices to mimic neuronal networks (Wu et al., 2016), we could establish the whether propagation is specific to certain primary sequences, size or conformation, or similar by-product of normal cell functioning.

Continuing to address factors that make pathogenic amyloid proteins deleterrious in this way, will advance our fundamental understanding of amyloid proteins as well as identify potential therapeutic targets.

References

Ader, C., Frey, S., Maas, W., Schmidt, H. B., Gorlich, D., & Baldus, M. (2010). Amyloid-like interactions within nucleoporin FG hydrogels. *Proc Natl Acad Sci U S A, 107*(14), 6281-6285. doi:10.1073/pnas.0910163107

Aggeli, A., Bell, M., Boden, N., Keen, J. N., Knowles, P. F., McLeish, T. C., . . . Radford, S. E. (1997). Responsive gels formed by the spontaneous self-assembly of peptides into polymeric beta-sheet tapes. *Nature, 386*(6622), 259-262. doi:10.1038/386259a0

Ahmed, E. M. (2015). Hydrogel: Preparation, characterization, and applications: A review. *J Adv Res, 6*(2), 105-121. doi:10.1016/j.jare.2013.07.006

Ahmed, M., Davis, J., Aucoin, D., Sato, T., Ahuja, S., Aimoto, S., . . . Smith, S. O. (2010). Structural conversion of neurotoxic amyloid-beta(1-42) oligomers to fibrils. *Nat Struct Mol Biol, 17*(5), 561-567. doi:10.1038/nsmb.1799

Ahn, M., Kang, S., Koo, H. J., Lee, J. H., Lee, Y. S., & Paik, S. R. (2010). Nanoporous protein matrix made of amyloid fibrils of beta2-microglobulin. *Biotechnol Prog, 26*(6), 1759-1764. doi:10.1002/btpr.466

Alavi Naini, S. M., & Soussi-Yanicostas, N. (2015). Tau Hyperphosphorylation and Oxidative Stress, a Critical Vicious Circle in Neurodegenerative Tauopathies? *Oxid Med Cell Longev, 2015*, 151979. doi:10.1155/2015/151979

Almeida, C. G., Takahashi, R. H., & Gouras, G. K. (2006). Beta-amyloid accumulation impairs multivesicular body sorting by inhibiting the ubiquitin-proteasome system. *J Neurosci, 26*(16), 4277-4288. doi:10.1523/JNEUROSCI.5078-05.2006

Anfinsen, C. B., Haber, E., Sela, M., & White, F. H., Jr. (1961). The kinetics of formation of native ribonuclease during oxidation of the reduced polypeptide chain. *Proc Natl Acad Sci U S A, 47*, 1309-1314.

Anfinsen, C. B. (1973). Principles that govern the folding of protein chains. *Science, 181*(4096), 223-230.

Arosio, P., Knowles, T. P., & Linse, S. (2015). On the lag phase in amyloid fibril formation. *Phys Chem Chem Phys, 17*(12), 7606-7618. doi:10.1039/c4cp05563b

Arranz, R., Mercado, G., Martin-Benito, J., Giraldo, R., Monasterio, O., Lagos, R., & Valpuesta, J. M. (2012). Structural characterization of microcin E492 amyloid formation: Identification of the precursors. *J Struct Biol, 178*(1), 54-60. doi:10.1016/j.jsb.2012.02.015

Asai, M., Hattori, C., Szabo, B., Sasagawa, N., Maruyama, K., Tanuma, S., & Ishiura, S. (2003). Putative function of ADAM9, ADAM10, and ADAM17 as APP alpha-secretase. *Biochem Biophys Res Commun, 301*(1), 231-235.

Audas, T. E., Audas, D. E., Jacob, M. D., Ho, J. J., Khacho, M., Wang, M., . . . Lee, S. (2016). Adaptation to Stressors by Systemic Protein Amyloidogenesis. *Dev Cell, 39*(2), 155-168. doi:10.1016/j.devcel.2016.09.002

Bacci, M., Vymetal, J., Mihajlovic, M., Caflisch, A., & Vitalis, A. (2017). Amyloid beta Fibril Elongation by Monomers Involves Disorder at the Tip. *J Chem Theory Comput, 13*(10), 5117-5130. doi:10.1021/acs.jctc.7b00662

Bachurin, S. O., Bovina, E. V., & Ustyugov, A. A. (2017). Drugs in Clinical Trials for Alzheimer's Disease: The Major Trends. *Med Res Rev, 37*(5), 1186-1225. doi:10.1002/med.21434

Bakota, E. L., Sensoy, O., Ozgur, B., Sayar, M., & Hartgerink, J. D. (2013). Self-assembling multidomain peptide fibers with aromatic cores. *Biomacromolecules, 14*(5), 1370-1378. doi:10.1021/bm4000019

Balbirnie, M., Grothe, R., & Eisenberg, D. S. (2001). An amyloid-forming peptide from the yeast prion Sup35 reveals a dehydrated beta-sheet structure for amyloid. *Proc Natl Acad Sci U S A, 98*(5), 2375-2380. doi:10.1073/pnas.041617698

Barrow, C. J., & Zagorski, M. G. (1991). Solution structures of beta peptide and its constituent fragments: relation to amyloid deposition. *Science, 253*(5016), 179-182.

Bartl, M. M., Luckenbach, T., Bergner, O., Ullrich, O., & Koch-Brandt, C. (2001). Multiple receptors mediate apoJ-dependent clearance of cellular debris into nonprofessional phagocytes. *Exp Cell Res, 271*(1), 130-141. doi:10.1006/excr.2001.5358

Bartolini, M., Bertucci, C., Bolognesi, M. L., Cavalli, A., Melchiorre, C., & Andrisano, V. (2007). Insight into the kinetic of amyloid beta (1-42) peptide self-aggregation: elucidation of inhibitors' mechanism of action. *Chembiochem, 8*(17), 2152-2161. doi:10.1002/cbic.200700427

Bayer, T. A., & Wirths, O. (2010). Intracellular accumulation of amyloid-Beta - a predictor for synaptic dysfunction and neuron loss in Alzheimer's disease. *Front Aging Neurosci, 2*, 8. doi:10.3389/fnagi.2010.00008

Benilova, I., Karran, E., & De Strooper, B. (2012). The toxic Abeta oligomer and Alzheimer's disease: an emperor in need of clothes. *Nat Neurosci, 15*(3), 349-357. doi:10.1038/nn.3028

Benseny-Cases, N., Cocera, M., & Cladera, J. (2007). Conversion of non-fibrillar beta-sheet oligomers into amyloid fibrils in Alzheimer's disease amyloid peptide aggregation. *Biochem Biophys Res Commun, 361*(4), 916-921. doi:10.1016/j.bbrc.2007.07.082

Berman, H. M., Westbrook, J., Feng, Z., Gilliland, G., Bhat, T. N., Weissig, H., . . . Bourne, P. E. (2000). The Protein Data Bank. *Nucleic Acids Res, 28*(1), 235-242.

Berson, J. F., Theos, A. C., Harper, D. C., Tenza, D., Raposo, G., & Marks, M. S. (2003). Proprotein convertase cleavage liberates a fibrillogenic fragment of a resident glycoprotein to initiate melanosome biogenesis. *J Cell Biol, 161*(3), 521-533. doi:10.1083/jcb.200302072

Berthelot, K., Lecomte, S., Coulary-Salin, B., Bentaleb, A., & Peruch, F. (2016). Hevea brasiliensis prohevein possesses a conserved C-terminal domain with amyloid-like properties in vitro. *Biochim Biophys Acta, 1864*(4), 388-399. doi:10.1016/j.bbapap.2016.01.006

Bertram, G., Innes, S., Minella, O., Richardson, J., & Stansfield, I. (2001). Endless possibilities: translation termination and stop codon recognition. *Microbiology, 147*(Pt 2), 255-269. doi:10.1099/00221287-147-2-255

Bertrand, S. J., Aksenova, M. V., Aksenov, M. Y., Mactutus, C. F., & Booze, R. M. (2011). Endogenous amyloidogenesis in long-term rat hippocampal cell cultures. *BMC Neurosci, 12*, 38. doi:10.1186/1471-2202-12-38

Bezprozvanny, I. (2009). Amyloid goes global. *Sci Signal, 2*(63), pe16. doi:10.1126/scisignal.263pe16

Bhak, G., Lee, S., Park, J. W., Cho, S., & Paik, S. R. (2010). Amyloid hydrogel derived from curly protein fibrils of alpha-synuclein. *Biomaterials, 31*(23), 5986-5995. doi:10.1016/j.biomaterials.2010.03.080

Biancalana, M., Makabe, K., Koide, A., & Koide, S. (2009). Molecular mechanism of thioflavin-T binding to the surface of beta-rich peptide self-assemblies. *J Mol Biol, 385*(4), 1052-1063. doi:10.1016/j.jmb.2008.11.006

Bishop, G. M., & Robinson, S. R. (2004). Physiological roles of amyloid-beta and implications for its removal in Alzheimer's disease. *Drugs Aging, 21*(10), 621-630.

Bissig, C., Rochin, L., & van Niel, G. (2016). PMEL Amyloid Fibril Formation: The Bright Steps of Pigmentation. *Int J Mol Sci, 17*(9). doi:10.3390/ijms17091438

Bitan, G., Kirkitadze, M. D., Lomakin, A., Vollers, S. S., Benedek, G. B., & Teplow, D. B. (2003). Amyloid beta -protein (Abeta) assembly: Abeta 40 and Abeta 42 oligomerize through distinct pathways. *Proc Natl Acad Sci U S A, 100*(1), 330-335. doi:10.1073/pnas.222681699

Bode, D. C., Baker, M. D., & Viles, J. H. (2017). Ion Channel Formation by Amyloid-beta42 Oligomers but Not Amyloid-beta40 in Cellular Membranes. *J Biol Chem, 292*(4), 1404-1413. doi:10.1074/jbc.M116.762526

Bothwell, M. (1996). p75NTR: a receptor after all. *Science, 272*(5261), 506-507.

Braak, H., & Braak, E. (1995). Staging of Alzheimer's disease-related neurofibrillary changes. *Neurobiol Aging, 16*(3), 271-278; discussion 278-284.

Braak, H., & Del Tredici, K. (2011a). Alzheimer's pathogenesis: is there neuron-to-neuron propagation? *Acta Neuropathol, 121*(5), 589-595. doi:10.1007/s00401-011-0825-z

Braak, H., & Del Tredici, K. (2011b). The pathological process underlying Alzheimer's disease in individuals under thirty. *Acta Neuropathol, 121*(2), 171-181. doi:10.1007/s00401-010-0789-4

Braakman, I., & Hebert, D. N. (2013). Protein folding in the endoplasmic reticulum. *Cold Spring Harb Perspect Biol, 5*(5), a013201. doi:10.1101/cshperspect.a013201

Brannstrom, K., Ohman, A., Nilsson, L., Pihl, M., Sandblad, L., & Olofsson, A. (2014). The N-terminal region of amyloid beta controls the aggregation rate and fibril stability at low pH through a gain of function mechanism. *J Am Chem Soc, 136*(31), 10956-10964. doi:10.1021/ja503535m

Brannstrom, K., Islam, T., Sandblad, L., & Olofsson, A. (2017). The role of histidines in amyloid beta fibril assembly. *FEBS Lett, 591*(8), 1167-1175. doi:10.1002/1873-3468.12616

Bremer, A., Henn, C., Engel, A., Baumeister, W., & Aebi, U. (1992). Has negative staining still a place in biomacromolecular electron microscopy? *Ultramicroscopy, 46*(1-4), 85-111.

Brockwell, D. J., & Radford, S. E. (2007). Intermediates: ubiquitous species on folding energy landscapes? *Curr Opin Struct Biol, 17*(1), 30-37. doi:10.1016/j.sbi.2007.01.003

Broersen, K., Rousseau, F., & Schymkowitz, J. (2010). The culprit behind amyloid beta peptide related neurotoxicity in Alzheimer's disease: oligomer size or conformation? *Alzheimers Res Ther, 2*(4), 12. doi:10.1186/alzrt36

Broersen, K., Jonckheere, W., Rozenski, J., Vandersteen, A., Pauwels, K., Pastore, A., . . . Schymkowitz, J. (2011). A standardized and biocompatible preparation of aggregate-free amyloid beta peptide for biophysical and biological studies of Alzheimer's disease. *Protein Eng Des Sel, 24*(9), 743-750. doi:10.1093/protein/gzr020

Bucciantini, M., Calloni, G., Chiti, F., Formigli, L., Nosi, D., Dobson, C. M., & Stefani, M. (2004). Prefibrillar amyloid protein aggregates share common features of cytotoxicity. *J Biol Chem, 279*(30), 31374-31382. doi:10.1074/jbc.M400348200

Buchete, N. V., & Hummer, G. (2007). Structure and dynamics of parallel beta-sheets, hydrophobic core, and loops in Alzheimer's A beta fibrils. *Biophys J, 92*(9), 3032-3039. doi:10.1529/biophysj.106.100404

Bulheller, B. M., Rodger, A., & Hirst, J. D. (2007). Circular and linear dichroism of proteins. *Phys Chem Chem Phys, 9*(17), 2020-2035. doi:10.1039/b615870f

Bulheller, B. M., & Hirst, J. D. (2009). DichroCalc--circular and linear dichroism online. *Bioinformatics, 25*(4), 539-540. doi:10.1093/bioinformatics/btp016

Burdick, D., Soreghan, B., Kwon, M., Kosmoski, J., Knauer, M., Henschen, A., . . . Glabe, C. (1992). Assembly and aggregation properties of synthetic Alzheimer's A4/beta amyloid peptide analogs. *J Biol Chem, 267*(1), 546-554.

Busciglio, J., Lorenzo, A., & Yankner, B. A. (1992). Methodological Variables in the Assessment of Beta-Amyloid Neurotoxicity. *Neurobiol Aging, 13*(5), 609-612. doi:Doi 10.1016/0197-4580(92)90065-6

Butterfield, D. A., & Boyd-Kimball, D. (2005). The critical role of methionine 35 in Alzheimer's amyloid beta-peptide (1-42)-induced oxidative stress and neurotoxicity. *Biochim Biophys Acta, 1703*(2), 149-156. doi:10.1016/j.bbapap.2004.10.014

Cai, H., Wang, Y., McCarthy, D., Wen, H., Borchelt, D. R., Price, D. L., & Wong, P. C. (2001). BACE1 is the major beta-secretase for generation of Abeta peptides by neurons. *Nat Neurosci, 4*(3), 233-234. doi:10.1038/85064

Caplan, M. R., Schwartzfarb, E. M., Zhang, S., Kamm, R. D., & Lauffenburger, D. A. (2002). Control of self-assembling oligopeptide matrix formation through systematic variation of amino acid sequence. *Biomaterials, 23*(1), 219-227.

Caputo, C. B., Sobel, I. R., Sygowski, L. A., Lampe, R. A., & Spreen, R. C. (1993). The influence of amino acid sequence on the fibrillogenicity and amyloidogenicity of the carboxy-terminus of beta-amyloid precursor protein. *Arch Biochem Biophys, 306*(2), 321-330. doi:10.1006/abbi.1993.1518

Carter, D. B. (2005). The interaction of amyloid-beta with ApoE. *Subcell Biochem, 38*, 255-272.

Carvalho, K. M., Franca, M. S., Camarao, G. C., & Ruchon, A. F. (1997). A new brain metalloendopeptidase which degrades the Alzheimer beta-amyloid 1-40 peptide producing soluble fragments without neurotoxic effects. *Braz J Med Biol Res, 30*(10), 1153-1156.

Caspersen, C., Wang, N., Yao, J., Sosunov, A., Chen, X., Lustbader, J. W., . . . Yan, S. D. (2005). Mitochondrial Abeta: a potential focal point for neuronal metabolic dysfunction in Alzheimer's disease. *FASEB J, 19*(14), 2040-2041. doi:10.1096/fj.05-3735fje

Castellani, R. J., Lee, H. G., Siedlak, S. L., Nunomura, A., Hayashi, T., Nakamura, M., . . . Smith, M. A. (2009). Reexamining Alzheimer's disease: evidence for a protective role for amyloid-beta protein precursor and amyloid-beta. *J Alzheimers Dis, 18*(2), 447-452. doi:10.3233/JAD-2009-1151

Cerf, E., Sarroukh, R., Tamamizu-Kato, S., Breydo, L., Derclaye, S., Dufrene, Y. F., . . . Raussens, V. (2009). Antiparallel beta-sheet: a signature structure of the oligomeric amyloid beta-peptide. *Biochem J, 421*(3), 415-423. doi:10.1042/BJ20090379

Chafekar, S. M., Baas, F., & Scheper, W. (2008). Oligomer-specific Abeta toxicity in cell models is mediated by selective uptake. *Biochim Biophys Acta, 1782*(9), 523-531. doi:10.1016/j.bbadis.2008.06.003

Chapman, M. R., Robinson, L. S., Pinkner, J. S., Roth, R., Heuser, J., Hammar, M., . . . Hultgren, S. J. (2002). Role of Escherichia coli curli operons in directing amyloid fiber formation. *Science, 295*(5556), 851-855. doi:10.1126/science.1067484

Chavez-Gutierrez, L., Bammens, L., Benilova, I., Vandersteen, A., Benurwar, M., Borgers, M., . . . De Strooper, B. (2012). The mechanism of gamma-Secretase dysfunction in familial Alzheimer disease. *EMBO J, 31*(10), 2261-2274. doi:10.1038/emboj.2012.79

Chen, B., Retzlaff, M., Roos, T., & Frydman, J. (2011). Cellular strategies of protein quality control. *Cold Spring Harb Perspect Biol, 3*(8), a004374. doi:10.1101/cshperspect.a004374

Chen, G. F., Xu, T. H., Yan, Y., Zhou, Y. R., Jiang, Y., Melcher, K., & Xu, H. E. (2017). Amyloid beta: structure, biology and structure-based therapeutic development. *Acta Pharmacol Sin, 38*(9), 1205-1235. doi:10.1038/aps.2017.28

Chen, X., Walker, D. G., Schmidt, A. M., Arancio, O., Lue, L. F., & Yan, S. D. (2007). RAGE: a potential target for Abeta-mediated cellular perturbation in Alzheimer's disease. *Curr Mol Med, 7*(8), 735-742.

Cheon, M., Chang, I., Mohanty, S., Luheshi, L. M., Dobson, C. M., Vendruscolo, M., & Favrin, G. (2007). Structural reorganisation and potential toxicity of oligomeric species formed during the assembly of amyloid fibrils. *PLoS Comput Biol, 3*(9), 1727-1738. doi:10.1371/journal.pcbi.0030173

Chiti, F., Webster, P., Taddei, N., Clark, A., Stefani, M., Ramponi, G., & Dobson, C. M. (1999). Designing conditions for in vitro formation of amyloid protofilaments and fibrils. *Proc Natl Acad Sci U S A, 96*(7), 3590-3594.

Chiti, F., & Dobson, C. M. (2006). Protein misfolding, functional amyloid, and human disease. *Annu Rev Biochem, 75*, 333-366. doi:10.1146/annurev.biochem.75.101304.123901

Chu, H., Pazgier, M., Jung, G., Nuccio, S. P., Castillo, P. A., de Jong, M. F., . . . Bevins, C. L. (2012). Human alpha-defensin 6 promotes mucosal innate immunity through self-assembled peptide nanonets. *Science, 337*(6093), 477-481. doi:10.1126/science.1218831

Cizas, P., Budvytyte, R., Morkuniene, R., Moldovan, R., Broccio, M., Losche, M., . . . Borutaite, V. (2010). Size-dependent neurotoxicity of beta-amyloid oligomers. *Arch Biochem Biophys, 496*(2), 84-92. doi:10.1016/j.abb.2010.02.001

Cohen, A. S., & Calkins, E. (1959). Electron microscopic observations on a fibrous component in amyloid of diverse origins. *Nature, 183*(4669), 1202-1203.

Cohen, F. E., & Kelly, J. W. (2003). Therapeutic approaches to protein-misfolding diseases. *Nature, 426*(6968), 905-909. doi:10.1038/nature02265

Cohen, S. I., Vendruscolo, M., Welland, M. E., Dobson, C. M., Terentjev, E. M., & Knowles, T. P. (2011). Nucleated polymerization with secondary pathways. I. Time evolution of the principal moments. *J Chem Phys, 135*(6), 065105. doi:10.1063/1.3608916

Cohen, S. I., Linse, S., Luheshi, L. M., Hellstrand, E., White, D. A., Rajah, L., . . . Knowles, T. P. (2013). Proliferation of amyloid-beta42 aggregates occurs through a secondary nucleation mechanism. *Proc Natl Acad Sci U S A, 110*(24), 9758-9763. doi:10.1073/pnas.1218402110

Cole, S. L., & Vassar, R. (2007). The Basic Biology of BACE1: A Key Therapeutic Target for Alzheimer's Disease. *Curr Genomics, 8*(8), 509-530. doi:10.2174/138920207783769512

Colletier, J. P., Laganowsky, A., Landau, M., Zhao, M., Soriaga, A. B., Goldschmidt, L., . . . Eisenberg, D. (2011). Molecular basis for amyloid-beta polymorphism. *Proc Natl Acad Sci U S A, 108*(41), 16938-16943. doi:10.1073/pnas.1112600108

Colquhoun, C., Draper, E. R., Schweins, R., Marcello, M., Vadukul, D., Serpell, L. C., & Adams, D. J. (2017). Controlling the network type in self-assembled dipeptide hydrogels. *Soft Matter, 13*(9), 1914-1919. doi:10.1039/c6sm02666d

Conboy, L., Murphy, K. J., & Regan, C. M. (2005). Amyloid precursor protein expression in the rat hippocampal dentate gyrus modulates during memory consolidation. *J Neurochem, 95*(6), 1677-1688. doi:10.1111/j.1471-4159.2005.03484.x

Conde, J., & Fink, G. R. (1976). A mutant of Saccharomyces cerevisiae defective for nuclear fusion. *Proc Natl Acad Sci U S A, 73*(10), 3651-3655.

Corder, E. H., Saunders, A. M., Strittmatter, W. J., Schmechel, D. E., Gaskell, P. C., Small, G. W., . . . Pericak-Vance, M. A. (1993). Gene dose of apolipoprotein E type 4 allele and the risk of Alzheimer's disease in late onset families. *Science, 261*(5123), 921-923.

Cordy, J. M., Hussain, I., Dingwall, C., Hooper, N. M., & Turner, A. J. (2003). Exclusively targeting beta-secretase to lipid rafts by GPI-anchor addition up-regulates beta-site processing of the amyloid precursor protein. *Proc Natl Acad Sci U S A, 100*(20), 11735-11740. doi:10.1073/pnas.1635130100

Coric, V., Salloway, S., van Dyck, C. H., Dubois, B., Andreasen, N., Brody, M., . . . Berman, R. M. (2015). Targeting Prodromal Alzheimer Disease With Avagacestat: A Randomized Clinical Trial. *JAMA Neurol, 72*(11), 1324-1333. doi:10.1001/jamaneurol.2015.0607

Costantini, C., Rossi, F., Formaggio, E., Bernardoni, R., Cecconi, D., & Della-Bianca, V. (2005). Characterization of the signaling pathway downstream p75 neurotrophin receptor involved in beta-amyloid peptide-dependent cell death. *J Mol Neurosci, 25*(2), 141-156. doi:10.1385/JMN:25:2:141

Couceiro, J. R., Gallardo, R., De Smet, F., De Baets, G., Baatsen, P., Annaert, W., . . . Rousseau, F. (2015). Sequence-dependent internalization of aggregating peptides. *J Biol Chem, 290*(1), 242-258. doi:10.1074/jbc.M114.586636

Coulson, D. T., Beyer, N., Quinn, J. G., Brockbank, S., Hellemans, J., Irvine, G. B., . . . Johnston, J. A. (2010). BACE1 mRNA expression in Alzheimer's disease postmortem brain tissue. *J Alzheimers Dis, 22*(4), 1111-1122. doi:10.3233/JAD-2010-101254

Coulson, E. J., Paliga, K., Beyreuther, K., & Masters, C. L. (2000). What the evolution of the amyloid protein precursor supergene family tells us about its function. *Neurochem Int, 36*(3), 175-184.

Crick, F. (1970). Central dogma of molecular biology. *Nature, 227*(5258), 561-563.

Crick, F. H. (1952). Is alpha-keratin a coiled coil? *Nature, 170*(4334), 882-883.

Crick, F. H. (1958). On protein synthesis. *Symp Soc Exp Biol, 12*, 138-163.

Cruz, L., Urbanc, B., Buldyrev, S. V., Christie, R., Gomez-Isla, T., Havlin, S., . . . Hyman, B. T. (1997). Aggregation and disaggregation of senile plaques in Alzheimer disease. *Proc Natl Acad Sci U S A, 94*(14), 7612-7616.

Cui, Y., Le, Y., Yazawa, H., Gong, W., & Wang, J. M. (2002). Potential role of the formyl peptide receptor-like 1 (FPRL1) in inflammatory aspects of Alzheimer's disease. *J Leukoc Biol, 72*(4), 628-635.

Cukalevski, R., Boland, B., Frohm, B., Thulin, E., Walsh, D., & Linse, S. (2012). Role of aromatic side chains in amyloid beta-protein aggregation. *ACS Chem Neurosci, 3*(12), 1008-1016. doi:10.1021/cn300073s

Cummings, J., Lee, G., Mortsdorf, T., Ritter, A., & Zhong, K. (2017). Alzheimer's disease drug development pipeline: 2017. *Alzheimers Dement (N Y), 3*(3), 367-384. doi:10.1016/j.trci.2017.05.002

Dahms, S. O., Hoefgen, S., Roeser, D., Schlott, B., Guhrs, K. H., & Than, M. E. (2010). Structure and biochemical analysis of the heparin-induced E1 dimer of the amyloid precursor protein. *Proc Natl Acad Sci U S A, 107*(12), 5381-5386. doi:10.1073/pnas.0911326107

Das, S., Zhou, K., Ghosh, D., Jha, N. N., Singh, P. K., Jacob, R. S., . . . Maji, S. K. (2016). Implantable amyloid hydrogels for promoting stem cell differentiation to neurons. *Npg Asia Materials, 8*. doi:ARTN e304

10.1038/am.2016.116

Daskalov, A., Dyrka, W., & Saupe, S. J. (2015). Theme and variations: evolutionary diversification of the HET-s functional amyloid motif. *Sci Rep, 5*, 12494. doi:10.1038/srep12494

Dawkins, E., & Small, D. H. (2014). Insights into the physiological function of the beta-amyloid precursor protein: beyond Alzheimer's disease. *J Neurochem, 129*(5), 756-769. doi:10.1111/jnc.12675

De Strooper, B., Iwatsubo, T., & Wolfe, M. S. (2012). Presenilins and gamma-secretase: structure, function, and role in Alzheimer Disease. *Cold Spring Harb Perspect Med, 2*(1), a006304. doi:10.1101/cshperspect.a006304

De Strooper, B., & Karran, E. (2016). The Cellular Phase of Alzheimer's Disease. *Cell, 164*(4), 603-615. doi:10.1016/j.cell.2015.12.056

Deane, R., Du Yan, S., Submamaryan, R. K., LaRue, B., Jovanovic, S., Hogg, E., . . . Zlokovic, B. (2003). RAGE mediates amyloid-beta peptide transport across the blood-brain barrier and accumulation in brain. *Nat Med, 9*(7), 907-913. doi:10.1038/nm890

Deshpande, A., Mina, E., Glabe, C., & Busciglio, J. (2006). Different conformations of amyloid beta induce neurotoxicity by distinct mechanisms in human cortical neurons. *J Neurosci, 26*(22), 6011-6018. doi:10.1523/JNEUROSCI.1189-06.2006

Desplats, P., Lee, H. J., Bae, E. J., Patrick, C., Rockenstein, E., Crews, L., . . . Lee, S. J. (2009). Inclusion formation and neuronal cell death through neuron-to-neuron transmission of alpha-synuclein. *Proc Natl Acad Sci U S A, 106*(31), 13010-13015. doi:10.1073/pnas.0903691106

Diaz-Avalos, R., Long, C., Fontano, E., Balbirnie, M., Grothe, R., Eisenberg, D., & Caspar, D. L. (2003). Cross-beta order and diversity in nanocrystals of an amyloid-forming peptide. *J Mol Biol, 330*(5), 1165-1175.

Dobson, C. M. (2003). Protein folding and misfolding. *Nature, 426*(6968), 884-890. doi:10.1038/nature02261

Dobson, C. M. (2004). Principles of protein folding, misfolding and aggregation. *Semin Cell Dev Biol, 15*(1), 3-16. doi:10.1016/j.semcdb.2003.12.008

Domanska, K., Vanderhaegen, S., Srinivasan, V., Pardon, E., Dupeux, F., Marquez, J. A., . . . Steyaert, J. (2011). Atomic structure of a nanobody-trapped domain-swapped dimer of an amyloidogenic beta2-microglobulin variant. *Proc Natl Acad Sci U S A, 108*(4), 1314-1319. doi:10.1073/pnas.1008560108

Domert, J., Rao, S. B., Agholme, L., Brorsson, A. C., Marcusson, J., Hallbeck, M., & Nath, S. (2014). Spreading of amyloid-beta peptides via neuritic cell-to-cell transfer is dependent on insufficient cellular clearance. *Neurobiol Dis, 65*, 82-92. doi:10.1016/j.nbd.2013.12.019

Doody, R. S., Raman, R., Farlow, M., Iwatsubo, T., Vellas, B., Joffe, S., . . . Semagacestat Study, G. (2013). A phase 3 trial of semagacestat for treatment of Alzheimer's disease. *N Engl J Med, 369*(4), 341-350. doi:10.1056/NEJMoa1210951

Dou, X. Q., & Feng, C. L. (2017). Amino Acids and Peptide-Based Supramolecular Hydrogels for Three-Dimensional Cell Culture. *Adv Mater, 29*(16). doi:10.1002/adma.201604062

Dzwolak, W., & Pecul, M. (2005). Chiral bias of amyloid fibrils revealed by the twisted conformation of Thioflavin T: an induced circular dichroism/DFT study. *FEBS Lett, 579*(29), 6601-6603. doi:10.1016/j.febslet.2005.10.048

Eckman, E. A., Reed, D. K., & Eckman, C. B. (2001). Degradation of the Alzheimer's amyloid beta peptide by endothelin-converting enzyme. *J Biol Chem, 276*(27), 24540-24548. doi:10.1074/jbc.M007579200

Eggert, S., Midthune, B., Cottrell, B., & Koo, E. H. (2009). Induced dimerization of the amyloid precursor protein leads to decreased amyloid-beta protein production. *J Biol Chem, 284*(42), 28943-28952. doi:10.1074/jbc.M109.038646

Eisenberg, D. S., & Sawaya, M. R. (2017). Structural Studies of Amyloid Proteins at the Molecular Level. *Annu Rev Biochem, 86*, 69-95. doi:10.1146/annurev-biochem-061516-045104

El-Agnaf, O. M., Mahil, D. S., Patel, B. P., & Austen, B. M. (2000). Oligomerization and toxicity of beta-amyloid-42 implicated in Alzheimer's disease. *Biochem Biophys Res Commun, 273*(3), 1003-1007. doi:10.1006/bbrc.2000.3051

Eliezer, D. (2012). Biochemistry. Visualizing amyloid assembly. *Science, 336*(6079), 308-309. doi:10.1126/science.1220356

Ellis, C. R., Tsai, C. C., Hou, X., & Shen, J. (2016). Constant pH Molecular Dynamics Reveals pH-Modulated Binding of Two Small-Molecule BACE1 Inhibitors. *J Phys Chem Lett, 7*(6), 944-949. doi:10.1021/acs.jpclett.6b00137

Ellis, R. J. (2001). Macromolecular crowding: an important but neglected aspect of the intracellular environment. *Curr Opin Struct Biol, 11*(1), 114-119.

Elsawy, M. A., Smith, A. M., Hodson, N., Squires, A., Miller, A. F., & Saiani, A. (2016). Modification of beta-Sheet Forming Peptide Hydrophobic Face: Effect on Self-Assembly and Gelation. *Langmuir, 32*(19), 4917-4923. doi:10.1021/acs.langmuir.5b03841

Esler, W. P., Stimson, E. R., Ghilardi, J. R., Lu, Y. A., Felix, A. M., Vinters, H. V., . . . Maggio, J. E. (1996). Point substitution in the central hydrophobic cluster of a human beta-amyloid congener disrupts peptide folding and abolishes plaque competence. *Biochemistry, 35*(44), 13914-13921. doi:10.1021/bi961302+

Esler, W. P., Stimson, E. R., Jennings, J. M., Vinters, H. V., Ghilardi, J. R., Lee, J. P., . . . Maggio, J. E. (2000). Alzheimer's disease amyloid propagation by a template-dependent dock-lock mechanism. *Biochemistry, 39*(21), 6288-6295.

Evin, G. (2016). Future Therapeutics in Alzheimer's Disease: Development Status of BACE Inhibitors. *BioDrugs, 30*(3), 173-194. doi:10.1007/s40259-016-0168-3

Extance, A. (2010). Alzheimer's failure raises questions about disease-modifying strategies. *Nat Rev Drug Discov, 9*(10), 749-751. doi:10.1038/nrd3288

Familia, C., Dennison, S. R., Quintas, A., & Phoenix, D. A. (2015). Prediction of Peptide and Protein Propensity for Amyloid Formation. *PLoS One, 10*(8), e0134679. doi:10.1371/journal.pone.0134679

Fandrich, M., & Dobson, C. M. (2002). The behaviour of polyamino acids reveals an inverse side chain effect in amyloid structure formation. *EMBO J, 21*(21), 5682-5690.

Fandrich, M., Meinhardt, J., & Grigorieff, N. (2009). Structural polymorphism of Alzheimer Abeta and other amyloid fibrils. *Prion, 3*(2), 89-93.

Farrer, L. A., Cupples, L. A., Haines, J. L., Hyman, B., Kukull, W. A., Mayeux, R., . . . van Duijn, C. M. (1997). Effects of age, sex, and ethnicity on the association between apolipoprotein E genotype and Alzheimer disease. A meta-analysis. APOE and Alzheimer Disease Meta Analysis Consortium. *JAMA, 278*(16), 1349-1356.

Ferrone, F. (1999). Analysis of protein aggregation kinetics. *Methods Enzymol, 309*, 256-274.

Finan, G. M., Okada, H., & Kim, T. W. (2011). BACE1 retrograde trafficking is uniquely regulated by the cytoplasmic domain of sortilin. *J Biol Chem, 286*(14), 12602-12616. doi:10.1074/jbc.M110.170217

Fioriti, L., Myers, C., Huang, Y. Y., Li, X., Stephan, J. S., Trifilieff, P., . . . Kandel, E. R. (2015). The Persistence of Hippocampal-Based Memory Requires Protein Synthesis Mediated by the Prion-like Protein CPEB3. *Neuron, 86*(6), 1433-1448. doi:10.1016/j.neuron.2015.05.021

Fitzpatrick, A. W. P., Falcon, B., He, S., Murzin, A. G., Murshudov, G., Garringer, H. J., . . . Scheres, S. H. W. (2017). Cryo-EM structures of tau filaments from Alzheimer's disease. *Nature, 547*(7662), 185-190. doi:10.1038/nature23002

Fonte, V., Dostal, V., Roberts, C. M., Gonzales, P., Lacor, P. N., Velasco, P. T., . . . Link, C. D. (2011). A glycine zipper motif mediates the formation of toxic beta-amyloid oligomers in vitro and in vivo. *Mol Neurodegener, 6*(1), 61. doi:10.1186/1750-1326-6-61

Fowler, D. M., Koulov, A. V., Alory-Jost, C., Marks, M. S., Balch, W. E., & Kelly, J. W. (2006). Functional amyloid formation within mammalian tissue. *PLoS Biol, 4*(1), e6. doi:10.1371/journal.pbio.0040006

Fowler, D. M., Koulov, A. V., Balch, W. E., & Kelly, J. W. (2007). Functional amyloid--from bacteria to humans. *Trends Biochem Sci, 32*(5), 217-224. doi:10.1016/j.tibs.2007.03.003

Fraser-Pitt, D., & O'Neil, D. (2015). Cystic fibrosis - a multiorgan protein misfolding disease. *Future Sci OA, 1*(2), FSO57. doi:10.4155/fso.15.57

Fraser, P. E., Nguyen, J. T., Surewicz, W. K., & Kirschner, D. A. (1991). pH-dependent structural transitions of Alzheimer amyloid peptides. *Biophys J, 60*(5), 1190-1201. doi:10.1016/S0006-3495(91)82154-3

Freedman, R. B., Brockway, B. E., & Lambert, N. (1984). Protein disulphide-isomerase and the formation of native disulphide bonds. *Biochem Soc Trans, 12*(6), 929-932.

Freundt, E. C., Maynard, N., Clancy, E. K., Roy, S., Bousset, L., Sourigues, Y., . . . Brahic, M. (2012). Neuron-to-neuron transmission of alpha-synuclein fibrils through axonal transport. *Ann Neurol, 72*(4), 517-524. doi:10.1002/ana.23747

Frousios, K. K., Iconomidou, V. A., Karletidi, C. M., & Hamodrakas, S. J. (2009). Amyloidogenic determinants are usually not buried. *BMC Struct Biol, 9*, 44. doi:10.1186/1472-6807-9-44

Fukumoto, H., Asami-Odaka, A., Suzuki, N., Shimada, H., Ihara, Y., & Iwatsubo, T. (1996). Amyloid beta protein deposition in normal aging has the same characteristics as that in Alzheimer's disease. Predominance of A beta 42(43) and association of A beta 40 with cored plaques. *Am J Pathol, 148*(1), 259-265.

Gadad, B. S., Britton, G. B., & Rao, K. S. (2011). Targeting oligomers in neurodegenerative disorders: lessons from alpha-synuclein, tau, and amyloid-beta peptide. *J Alzheimers Dis, 24 Suppl 2*, 223-232. doi:10.3233/JAD-2011-110182

Gamba, P., Leonarduzzi, G., Tamagno, E., Guglielmotto, M., Testa, G., Sottero, B., . . . Poli, G. (2011). Interaction between 24-hydroxycholesterol, oxidative stress, and amyloid-beta in amplifying neuronal damage in Alzheimer's disease: three partners in crime. *Aging Cell, 10*(3), 403-417. doi:10.1111/j.1474-9726.2011.00681.x

Gasset, M., Baldwin, M. A., Lloyd, D. H., Gabriel, J. M., Holtzman, D. M., Cohen, F., . . . Prusiner, S. B. (1992). Predicted alpha-helical regions of the prion protein when synthesized as peptides form amyloid. *Proc Natl Acad Sci U S A, 89*(22), 10940-10944.

Gazit, E. (2002). A possible role for pi-stacking in the self-assembly of amyloid fibrils. *FASEB J, 16*(1), 77-83. doi:10.1096/fj.01-0442hyp

Gazit, E. (2005). Mechanisms of amyloid fibril self-assembly and inhibition. Model short peptides as a key research tool. *FEBS J, 272*(23), 5971-5978. doi:10.1111/j.1742-4658.2005.05022.x

Gething, M. J., & Sambrook, J. (1992). Protein folding in the cell. *Nature, 355*(6355), 33-45. doi:10.1038/355033a0

Gimbel, D. A., Nygaard, H. B., Coffey, E. E., Gunther, E. C., Lauren, J., Gimbel, Z. A., & Strittmatter, S. M. (2010). Memory impairment in transgenic Alzheimer mice requires cellular prion protein. *J Neurosci, 30*(18), 6367-6374. doi:10.1523/JNEUROSCI.0395-10.2010

Glabe, C. G., & Kayed, R. (2006). Common structure and toxic function of amyloid oligomers implies a common mechanism of pathogenesis. *Neurology, 66*(2 Suppl 1), S74-78. doi:10.1212/01.wnl.0000192103.24796.42

Glabe, C. G. (2008). Structural classification of toxic amyloid oligomers. *J Biol Chem, 283*(44), 29639-29643. doi:10.1074/jbc.R800016200

Gras, S. L., Tickler, A. K., Squires, A. M., Devlin, G. L., Horton, M. A., Dobson, C. M., & MacPhee, C. E. (2008). Functionalised amyloid fibrils for roles in cell adhesion. *Biomaterials, 29*(11), 1553-1562. doi:10.1016/j.biomaterials.2007.11.028

Gras, S. L., Waddington, L. J., & Goldie, K. N. (2011). Transmission electron microscopy of amyloid fibrils. *Methods Mol Biol, 752*, 197-214. doi:10.1007/978-1-60327-223-0_13

Greenfield, N. J. (2006). Using circular dichroism spectra to estimate protein secondary structure. *Nat Protoc, 1*(6), 2876-2890. doi:10.1038/nprot.2006.202

Gremer, L., Scholzel, D., Schenk, C., Reinartz, E., Labahn, J., Ravelli, R. B. G., . . . Schroder, G. F. (2017). Fibril structure of amyloid-beta(1-42) by cryo-electron microscopy. *Science, 358*(6359), 116-119. doi:10.1126/science.aao2825

Groemer, T. W., Thiel, C. S., Holt, M., Riedel, D., Hua, Y., Huve, J., . . . Klingauf, J. (2011). Amyloid precursor protein is trafficked and secreted via synaptic vesicles. *PLoS One, 6*(4), e18754. doi:10.1371/journal.pone.0018754

Groenning, M., Olsen, L., van de Weert, M., Flink, J. M., Frokjaer, S., & Jorgensen, F. S. (2007). Study on the binding of Thioflavin T to beta-sheet-rich and non-beta-sheet cavities. *J Struct Biol, 158*(3), 358-369. doi:10.1016/j.jsb.2006.12.010

Groenning, M. (2010). Binding mode of Thioflavin T and other molecular probes in the context of amyloid fibrils-current status. *J Chem Biol, 3*(1), 1-18. doi:10.1007/s12154-009-0027-5

Gu, L., Liu, C., Stroud, J. C., Ngo, S., Jiang, L., & Guo, Z. (2014). Antiparallel triple-strand architecture for prefibrillar Abeta42 oligomers. *J Biol Chem, 289*(39), 27300-27313. doi:10.1074/jbc.M114.569004

Guo, J. L., & Lee, V. M. (2014). Cell-to-cell transmission of pathogenic proteins in neurodegenerative diseases. *Nat Med, 20*(2), 130-138. doi:10.1038/nm.3457

Guo, L., Giasson, B. I., Glavis-Bloom, A., Brewer, M. D., Shorter, J., Gitler, A. D., & Yang, X. (2014). A cellular system that degrades misfolded proteins and protects against neurodegeneration. *Mol Cell, 55*(1), 15-30. doi:10.1016/j.molcel.2014.04.030

Guyonnet, B., Egge, N., & Cornwall, G. A. (2014). Functional amyloids in the mouse sperm acrosome. *Mol Cell Biol, 34*(14), 2624-2634. doi:10.1128/MCB.00073-14

Habib, A., Sawmiller, D., & Tan, J. (2017). Restoring Soluble Amyloid Precursor Protein alpha Functions as a Potential Treatment for Alzheimer's Disease. *J Neurosci Res, 95*(4), 973-991. doi:10.1002/jnr.23823

Hamazaki, H. (1996). Cathepsin D is involved in the clearance of Alzheimer's beta-amyloid protein. *FEBS Lett, 396*(2-3), 139-142.

Hardy, J., & Selkoe, D. J. (2002). The amyloid hypothesis of Alzheimer's disease: progress and problems on the road to therapeutics. *Science, 297*(5580), 353-356. doi:10.1126/science.1072994

Hardy, J. A., & Higgins, G. A. (1992). Alzheimer's disease: the amyloid cascade hypothesis. *Science, 256*(5054), 184-185.

Harmeier, A., Wozny, C., Rost, B. R., Munter, L. M., Hua, H., Georgiev, O., . . . Multhaup, G. (2009). Role of amyloid-beta glycine 33 in oligomerization, toxicity, and neuronal plasticity. *J Neurosci, 29*(23), 7582-7590. doi:10.1523/JNEUROSCI.1336-09.2009

Harrison, P. M., Bamborough, P., Daggett, V., Prusiner, S. B., & Cohen, F. E. (1997). The prion folding problem. *Current Opinion in Structural Biology, 7*(1), 53-59. doi:Doi 10.1016/S0959-440x(97)80007-3

Harte, N. P., Klyubin, I., McCarthy, E. K., Min, S., Garrahy, S. A., Xie, Y., . . . Mok, K. H. (2015). Amyloid Oligomers and Mature Fibrils Prepared from an Innocuous Protein Cause Diverging Cellular Death Mechanisms. *J Biol Chem, 290*(47), 28343-28352. doi:10.1074/jbc.M115.676072

Hartl, F. U., & Hayer-Hartl, M. (2009). Converging concepts of protein folding in vitro and in vivo. *Nat Struct Mol Biol, 16*(6), 574-581. doi:10.1038/nsmb.1591

Hartl, F. U., Bracher, A., & Hayer-Hartl, M. (2011). Molecular chaperones in protein folding and proteostasis. *Nature, 475*(7356), 324-332. doi:10.1038/nature10317

Hasegawa, K., Ono, K., Yamada, M., & Naiki, H. (2002). Kinetic modeling and determination of reaction constants of Alzheimer's beta-amyloid fibril extension and dissociation using surface plasmon resonance. *Biochemistry, 41*(46), 13489-13498.

Hellstrand, E., Boland, B., Walsh, D. M., & Linse, S. (2010). Amyloid beta-protein aggregation produces highly reproducible kinetic data and occurs by a two-phase process. *ACS Chem Neurosci, 1*(1), 13-18. doi:10.1021/cn900015v

Higham, C. E., Jaikaran, E. T., Fraser, P. E., Gross, M., & Clark, A. (2000). Preparation of synthetic human islet amyloid polypeptide (IAPP) in a stable conformation to enable study of conversion to amyloid-like fibrils. *FEBS Lett, 470*(1), 55-60.

Hilbich, C., Kisters-Woike, B., Reed, J., Masters, C. L., & Beyreuther, K. (1991). Aggregation and secondary structure of synthetic amyloid beta A4 peptides of Alzheimer's disease. *J Mol Biol, 218*(1), 149-163.

Hilbich, C., Kisters-Woike, B., Reed, J., Masters, C. L., & Beyreuther, K. (1992). Substitutions of hydrophobic amino acids reduce the amyloidogenicity of Alzheimer's disease beta A4 peptides. *J Mol Biol, 228*(2), 460-473.

Hirota-Nakaoka, N., Hasegawa, K., Naiki, H., & Goto, Y. (2003). Dissolution of beta2-microglobulin amyloid fibrils by dimethylsulfoxide. *J Biochem, 134*(1), 159-164.

Hirst, A. R., Escuder, B., Miravet, J. F., & Smith, D. K. (2008). High-tech applications of self-assembling supramolecular nanostructured gel-phase materials: from regenerative medicine to electronic devices. *Angew Chem Int Ed Engl, 47*(42), 8002-8018. doi:10.1002/anie.200800022

Horii, A., Wang, X., Gelain, F., & Zhang, S. (2007). Biological designer self-assembling peptide nanofiber scaffolds significantly enhance osteoblast proliferation, differentiation and 3-D migration. *PLoS One, 2*(2), e190. doi:10.1371/journal.pone.0000190

Hu, K. N., McGlinchey, R. P., Wickner, R. B., & Tycko, R. (2011). Segmental polymorphism in a functional amyloid. *Biophys J, 101*(9), 2242-2250. doi:10.1016/j.bpj.2011.09.051

Hu, X., Zhou, X., He, W., Yang, J., Xiong, W., Wong, P., . . . Yan, R. (2010). BACE1 deficiency causes altered neuronal activity and neurodegeneration. *J Neurosci, 30*(26), 8819-8829. doi:10.1523/JNEUROSCI.1334-10.2010

Hung, L. W., Ciccotosto, G. D., Giannakis, E., Tew, D. J., Perez, K., Masters, C. L., . . . Barnham, K. J. (2008). Amyloid-beta peptide (Abeta) neurotoxicity is modulated by the rate of peptide aggregation: Abeta dimers and trimers correlate with neurotoxicity. *J Neurosci, 28*(46), 11950-11958. doi:10.1523/JNEUROSCI.3916-08.2008

Huotari, J., & Helenius, A. (2011). Endosome maturation. *EMBO J, 30*(17), 3481-3500. doi:10.1038/emboj.2011.286

Idicula-Thomas, S., & Balaji, P. V. (2005). Understanding the relationship between the primary structure of proteins and their amyloidogenic propensity: clues from inclusion body formation. *Protein Eng Des Sel, 18*(4), 175-180. doi:10.1093/protein/gzi022

Ivanova, M. I., Sawaya, M. R., Gingery, M., Attinger, A., & Eisenberg, D. (2004). An amyloid-forming segment of beta2-microglobulin suggests a molecular model for the fibril. *Proc Natl Acad Sci U S A, 101*(29), 10584-10589. doi:10.1073/pnas.0403756101

Iwata, N., Tsubuki, S., Takaki, Y., Shirotani, K., Lu, B., Gerard, N. P., . . . Saido, T. C. (2001). Metabolic regulation of brain Abeta by neprilysin. *Science, 292*(5521), 1550-1552. doi:10.1126/science.1059946

Izzo, N. J., Staniszewski, A., To, L., Fa, M., Teich, A. F., Saeed, F., . . . Catalano, S. M. (2014). Alzheimer's therapeutics targeting amyloid beta 1-42 oligomers I: Abeta 42 oligomer binding to specific neuronal receptors is displaced by drug candidates that improve cognitive deficits. *PLoS One, 9*(11), e111898. doi:10.1371/journal.pone.0111898

Jackson, M. P., & Hewitt, E. W. (2017). Why are Functional Amyloids Non-Toxic in Humans? *Biomolecules, 7*(4). doi:10.3390/biom7040071

Jacob, R. S., Ghosh, D., Singh, P. K., Basu, S. K., Jha, N. N., Das, S., . . . Maji, S. K. (2015). Self healing hydrogels composed of amyloid nano fibrils for cell culture and stem cell differentiation. *Biomaterials, 54*, 97-105. doi:10.1016/j.biomaterials.2015.03.002

Jahn, T. R., & Radford, S. E. (2005). The Yin and Yang of protein folding. *FEBS J, 272*(23), 5962-5970. doi:10.1111/j.1742-4658.2005.05021.x

Jahn, T. R., Makin, O. S., Morris, K. L., Marshall, K. E., Tian, P., Sikorski, P., & Serpell, L. C. (2010). The common architecture of cross-beta amyloid. *J Mol Biol, 395*(4), 717-727. doi:10.1016/j.jmb.2009.09.039

Jakhria, T., Hellewell, A. L., Porter, M. Y., Jackson, M. P., Tipping, K. W., Xue, W. F., . . . Hewitt, E. W. (2014). beta2-microglobulin amyloid fibrils are nanoparticles that disrupt lysosomal membrane protein trafficking and inhibit protein degradation by lysosomes. *J Biol Chem, 289*(52), 35781-35794. doi:10.1074/jbc.M114.586222

Jan, A., Adolfsson, O., Allaman, I., Buccarello, A. L., Magistretti, P. J., Pfeifer, A., . . . Lashuel, H. A. (2011). Abeta42 neurotoxicity is mediated by ongoing nucleated polymerization process rather than by discrete Abeta42 species. *J Biol Chem, 286*(10), 8585-8596. doi:10.1074/jbc.M110.172411

Jang, H., Arce, F. T., Mustata, M., Ramachandran, S., Capone, R., Nussinov, R., & Lal, R. (2011). Antimicrobial protegrin-1 forms amyloid-like fibrils with rapid kinetics suggesting a functional link. *Biophys J, 100*(7), 1775-1783. doi:10.1016/j.bpj.2011.01.072

Jarrett, J. T., Berger, E. P., & Lansbury, P. T., Jr. (1993). The carboxy terminus of the beta amyloid protein is critical for the seeding of amyloid formation: implications for the pathogenesis of Alzheimer's disease. *Biochemistry, 32*(18), 4693-4697.

Jean, Y. Y., Baleriola, J., Fa, M., Hengst, U., & Troy, C. M. (2015). Stereotaxic Infusion of Oligomeric Amyloid-beta into the Mouse Hippocampus. *J Vis Exp*(100), e52805. doi:10.3791/52805

Jiang, H., Burdick, D., Glabe, C. G., Cotman, C. W., & Tenner, A. J. (1994). beta-Amyloid activates complement by binding to a specific region of the collagen-like domain of the C1q A chain. *J Immunol, 152*(10), 5050-5059.

Jolly, C., & Morimoto, R. I. (2000). Role of the heat shock response and molecular chaperones in oncogenesis and cell death. *J Natl Cancer Inst, 92*(19), 1564-1572.

Jucker, M., & Walker, L. C. (2013). Self-propagation of pathogenic protein aggregates in neurodegenerative diseases. *Nature, 501*(7465), 45-51. doi:10.1038/nature12481

Kaden, D., Munter, L. M., Joshi, M., Treiber, C., Weise, C., Bethge, T., . . . Multhaup, G. (2008). Homophilic interactions of the amyloid precursor protein (APP) ectodomain are regulated by the loop region and affect beta-secretase cleavage of APP. *J Biol Chem, 283*(11), 7271-7279. doi:10.1074/jbc.M708046200

Kahler, A., Sticht, H., & Horn, A. H. (2013). Conformational stability of fibrillar amyloid-beta oligomers via protofilament pair formation - a systematic computational study. *PLoS One, 8*(7), e70521. doi:10.1371/journal.pone.0070521

Kandalepas, P. C., & Vassar, R. (2014). The normal and pathologic roles of the Alzheimer's beta-secretase, BACE1. *Curr Alzheimer Res, 11*(5), 441-449.

Kang, J., Lemaire, H. G., Unterbeck, A., Salbaum, J. M., Masters, C. L., Grzeschik, K. H., . . . Muller-Hill, B. (1987). The precursor of Alzheimer's disease amyloid A4 protein resembles a cell-surface receptor. *Nature, 325*(6106), 733-736. doi:10.1038/325733a0

Kang, J., & Muller-Hill, B. (1990). Differential splicing of Alzheimer's disease amyloid A4 precursor RNA in rat tissues: PreA4(695) mRNA is predominantly produced in rat and human brain. *Biochem Biophys Res Commun, 166*(3), 1192-1200.

Karran, E., Mercken, M., & De Strooper, B. (2011). The amyloid cascade hypothesis for Alzheimer's disease: an appraisal for the development of therapeutics. *Nat Rev Drug Discov, 10*(9), 698-712. doi:10.1038/nrd3505

Karran, E., & Hardy, J. (2014). A critique of the drug discovery and phase 3 clinical programs targeting the amyloid hypothesis for Alzheimer disease. *Ann Neurol, 76*(2), 185-205. doi:10.1002/ana.24188

Kaufman, R. J. (2002). Orchestrating the unfolded protein response in health and disease. *J Clin Invest, 110*(10), 1389-1398. doi:10.1172/JCI16886

Kayed, R., Head, E., Thompson, J. L., McIntire, T. M., Milton, S. C., Cotman, C. W., & Glabe, C. G. (2003). Common structure of soluble amyloid oligomers implies common mechanism of pathogenesis. *Science, 300*(5618), 486-489. doi:10.1126/science.1079469

Kayed, R., Sokolov, Y., Edmonds, B., McIntire, T. M., Milton, S. C., Hall, J. E., & Glabe, C. G. (2004). Permeabilization of lipid bilayers is a common conformation-dependent activity of soluble amyloid oligomers in protein misfolding diseases. *J Biol Chem, 279*(45), 46363-46366. doi:10.1074/jbc.C400260200

Kayed, R., & Glabe, C. G. (2006). Conformation-dependent anti-amyloid oligomer antibodies. *Methods Enzymol, 413*, 326-344. doi:10.1016/S0076-6879(06)13017-7

Kayed, R., Head, E., Sarsoza, F., Saing, T., Cotman, C. W., Necula, M., . . . Glabe, C. G. (2007). Fibril specific, conformation dependent antibodies recognize a generic epitope common to amyloid fibrils and fibrillar oligomers that is absent in prefibrillar oligomers. *Mol Neurodegener, 2*, 18. doi:10.1186/1750-1326-2-18

Kayed, R., Canto, I., Breydo, L., Rasool, S., Lukacsovich, T., Wu, J., . . . Glabe, C. (2010). Conformation dependent monoclonal antibodies distinguish different replicating strains or conformers of prefibrillar Abeta oligomers. *Mol Neurodegener, 5*, 57. doi:10.1186/1750-1326-5-57

Kayed, R., & Lasagna-Reeves, C. A. (2013). Molecular mechanisms of amyloid oligomers toxicity. *J Alzheimers Dis, 33 Suppl 1*, S67-78. doi:10.3233/JAD-2012-129001

Kenney, J. M., Knight, D., Wise, M. J., & Vollrath, F. (2002). Amyloidogenic nature of spider silk. *Eur J Biochem, 269*(16), 4159-4163.

Kepp, K. P. (2017). Ten Challenges of the Amyloid Hypothesis of Alzheimer's Disease. *Journal of Alzheimers Disease, 55*(2), 447-457. doi:10.3233/Jad-160550

Kerje, S., Sharma, P., Gunnarsson, U., Kim, H., Bagchi, S., Fredriksson, R., . . . Andersson, L. (2004). The Dominant white, Dun and Smoky color variants in chicken are associated with insertion/deletion polymorphisms in the PMEL17 gene. *Genetics, 168*(3), 1507-1518. doi:10.1534/genetics.104.027995

Kfoury, N., Holmes, B. B., Jiang, H., Holtzman, D. M., & Diamond, M. I. (2012). Trans-cellular propagation of Tau aggregation by fibrillar species. *J Biol Chem, 287*(23), 19440-19451. doi:10.1074/jbc.M112.346072

Khalifa, N. B., Van Hees, J., Tasiaux, B., Huysseune, S., Smith, S. O., Constantinescu, S. N., . . . Kienlen-Campard, P. (2010). What is the role of amyloid precursor protein dimerization? *Cell Adh Migr, 4*(2), 268-272.

Khurana, R., Coleman, C., Ionescu-Zanetti, C., Carter, S. A., Krishna, V., Grover, R. K., . . . Singh, S. (2005). Mechanism of thioflavin T binding to amyloid fibrils. *J Struct Biol, 151*(3), 229-238. doi:10.1016/j.jsb.2005.06.006

Kido, H., Fukutomi, A., Schilling, J., Wang, Y., Cordell, B., & Katunuma, N. (1990). Protease-specificity of Kunitz inhibitor domain of Alzheimer's disease amyloid protein precursor. *Biochem Biophys Res Commun, 167*(2), 716-721.

Kim, H. J., Chae, S. C., Lee, D. K., Chromy, B., Lee, S. C., Park, Y. C., . . . Hong, S. T. (2003). Selective neuronal degeneration induced by soluble oligomeric amyloid beta protein. *FASEB J, 17*(1), 118-120. doi:10.1096/fj.01-0987fje

Kim, S., Jeon, T. J., Oberai, A., Yang, D., Schmidt, J. J., & Bowie, J. U. (2005). Transmembrane glycine zippers: physiological and pathological roles in membrane proteins. *Proc Natl Acad Sci U S A, 102*(40), 14278-14283. doi:10.1073/pnas.0501234102

Kisiday, J., Jin, M., Kurz, B., Hung, H., Semino, C., Zhang, S., & Grodzinsky, A. J. (2002). Self-assembling peptide hydrogel fosters chondrocyte extracellular matrix production and cell division: implications for cartilage tissue repair. *Proc Natl Acad Sci U S A, 99*(15), 9996-10001. doi:10.1073/pnas.142309999

Knowles, T. P., Shu, W., Devlin, G. L., Meehan, S., Auer, S., Dobson, C. M., & Welland, M. E. (2007). Kinetics and thermodynamics of amyloid formation from direct measurements of fluctuations in fibril mass. *Proc Natl Acad Sci U S A, 104*(24), 10016-10021. doi:10.1073/pnas.0610659104

Knowles, T. P., Waudby, C. A., Devlin, G. L., Cohen, S. I., Aguzzi, A., Vendruscolo, M., . . . Dobson, C. M. (2009). An analytical solution to the kinetics of breakable filament assembly. *Science, 326*(5959), 1533-1537. doi:10.1126/science.1178250

Knowles, T. P., Oppenheim, T. W., Buell, A. K., Chirgadze, D. Y., & Welland, M. E. (2010). Nanostructured films from hierarchical self-assembly of amyloidogenic proteins. *Nat Nanotechnol, 5*(3), 204-207. doi:10.1038/nnano.2010.26

Knowles, T. P., Vendruscolo, M., & Dobson, C. M. (2014). The amyloid state and its association with protein misfolding diseases. *Nat Rev Mol Cell Biol, 15*(6), 384-396. doi:10.1038/nrm3810

Kok, W. M., Scanlon, D. B., Karas, J. A., Miles, L. A., Tew, D. J., Parker, M. W., . . . Hutton, C. A. (2009). Solid-phase synthesis of homodimeric peptides: preparation of covalently-linked dimers of amyloid beta peptide. *Chem Commun (Camb)*(41), 6228-6230. doi:10.1039/b912784d

Krebs, M. R., Bromley, E. H., & Donald, A. M. (2005). The binding of thioflavin-T to amyloid fibrils: localisation and implications. *J Struct Biol, 149*(1), 30-37. doi:10.1016/j.jsb.2004.08.002

Krysmann, M. J., Castelletto, V., Kelarakis, A., Hamley, I. W., Hule, R. A., & Pochan, D. J. (2008). Self-assembly and hydrogelation of an amyloid peptide fragment. *Biochemistry, 47*(16), 4597-4605. doi:10.1021/bi8000616

Kurochkin, I. V., & Goto, S. (1994). Alzheimer's beta-amyloid peptide specifically interacts with and is degraded by insulin degrading enzyme. *FEBS Lett, 345*(1), 33-37.

Kurt, T. D., Aguilar-Calvo, P., Jiang, L., Rodriguez, J. A., Alderson, N., Eisenberg, D. S., & Sigurdson, C. J. (2017). Asparagine and glutamine ladders promote cross-species prion conversion. *J Biol Chem*. doi:10.1074/jbc.M117.794107

Kushnirov, V. V., Kochneva-Pervukhova, N. V., Chechenova, M. B., Frolova, N. S., & Ter-Avanesyan, M. D. (2000). Prion properties of the Sup35 protein of yeast Pichia methanolica. *EMBO J, 19*(3), 324-331. doi:10.1093/emboj/19.3.324

Kusumoto, Y., Lomakin, A., Teplow, D. B., & Benedek, G. B. (1998). Temperature dependence of amyloid beta-protein fibrillization. *Proc Natl Acad Sci U S A, 95*(21), 12277-12282.

Ladiwala, A. R., Litt, J., Kane, R. S., Aucoin, D. S., Smith, S. O., Ranjan, S., . . . Tessier, P. M. (2012). Conformational differences between two amyloid beta oligomers of similar size and dissimilar toxicity. *J Biol Chem, 287*(29), 24765-24773. doi:10.1074/jbc.M111.329763

Lakshmanan, A., Cheong, D. W., Accardo, A., Di Fabrizio, E., Riekel, C., & Hauser, C. A. (2013). Aliphatic peptides show similar self-assembly to amyloid core sequences, challenging the importance of aromatic interactions in amyloidosis. *Proc Natl Acad Sci U S A, 110*(2), 519-524. doi:10.1073/pnas.1217742110

Lambert, M. P., Barlow, A. K., Chromy, B. A., Edwards, C., Freed, R., Liosatos, M., . . . Klein, W. L. (1998). Diffusible, nonfibrillar ligands derived from Abeta1-42 are potent central nervous system neurotoxins. *Proc Natl Acad Sci U S A, 95*(11), 6448-6453.

Lambert, M. P., Velasco, P. T., Chang, L., Viola, K. L., Fernandez, S., Lacor, P. N., . . . Klein, W. L. (2007). Monoclonal antibodies that target pathological assemblies of Abeta. *J Neurochem, 100*(1), 23-35. doi:10.1111/j.1471-4159.2006.04157.x

Landreh, M., Sawaya, M. R., Hipp, M. S., Eisenberg, D. S., Wuthrich, K., & Hartl, F. U. (2016). The formation, function and regulation of amyloids: insights from structural biology. *J Intern Med, 280*(2), 164-176. doi:10.1111/joim.12500

Langkilde, A. E., & Vestergaard, B. (2009). Methods for structural characterization of prefibrillar intermediates and amyloid fibrils. *FEBS Lett, 583*(16), 2600-2609. doi:10.1016/j.febslet.2009.05.040

Langkilde, A. E., Morris, K. L., Serpell, L. C., Svergun, D. I., & Vestergaard, B. (2015). The architecture of amyloid-like peptide fibrils revealed by X-ray scattering, diffraction and electron microscopy. *Acta Crystallogr D Biol Crystallogr, 71*(Pt 4), 882-895. doi:10.1107/S1399004715001674

Larson, M. E., & Lesne, S. E. (2012). Soluble Abeta oligomer production and toxicity. *J Neurochem, 120 Suppl 1*, 125-139. doi:10.1111/j.1471-4159.2011.07478.x

Lauer, D., Reichenbach, A., & Birkenmeier, G. (2001). Alpha 2-macroglobulin-mediated degradation of amyloid beta 1--42: a mechanism to enhance amyloid beta catabolism. *Exp Neurol, 167*(2), 385-392. doi:10.1006/exnr.2000.7569

Lee, E. B., Skovronsky, D. M., Abtahian, F., Doms, R. W., & Lee, V. M. (2003). Secretion and intracellular generation of truncated Abeta in beta-site amyloid-beta precursor protein-cleaving enzyme expressing human neurons. *J Biol Chem, 278*(7), 4458-4466. doi:10.1074/jbc.M210105200

Lee, Y. J., Savtchenko, R., Ostapchenko, V. G., Makarava, N., & Baskakov, I. V. (2011). Molecular structure of amyloid fibrils controls the relationship between fibrillar size and toxicity. *PLoS One, 6*(5), e20244. doi:10.1371/journal.pone.0020244

Lesne, S. E., Sherman, M. A., Grant, M., Kuskowski, M., Schneider, J. A., Bennett, D. A., & Ashe, K. H. (2013). Brain amyloid-beta oligomers in ageing and Alzheimer's disease. *Brain, 136*(Pt 5), 1383-1398. doi:10.1093/brain/awt062

Leung, C., Hodel, A. W., Brennan, A. J., Lukoyanova, N., Tran, S., House, C. M., . . . Hoogenboom, B. W. (2017). Real-time visualization of perforin nanopore assembly. *Nat Nanotechnol, 12*(5), 467-473. doi:10.1038/nnano.2016.303

Li, J., McQuade, T., Siemer, A. B., Napetschnig, J., Moriwaki, K., Hsiao, Y. S., . . . Wu, H. (2012). The RIP1/RIP3 necrosome forms a functional amyloid signaling complex required for programmed necrosis. *Cell, 150*(2), 339-350. doi:10.1016/j.cell.2012.06.019

Liebman, S. W., & Derkatch, I. L. (1999). The yeast [PSI+] prion: making sense of nonsense. *J Biol Chem, 274*(3), 1181-1184.

Lin, M. S., Chen, L. Y., Tsai, H. T., Wang, S. S., Chang, Y., Higuchi, A., & Chen, W. Y. (2008). Investigation of the mechanism of beta-amyloid fibril formation by kinetic and thermodynamic analyses. *Langmuir, 24*(11), 5802-5808. doi:10.1021/la703369b

Lindgren, M., Sorgjerd, K., & Hammarstrom, P. (2005). Detection and characterization of aggregates, prefibrillar amyloidogenic oligomers, and protofibrils using fluorescence spectroscopy. *Biophys J, 88*(6), 4200-4212. doi:10.1529/biophysj.104.049700

Linse, S. (2017). Monomer-dependent secondary nucleation in amyloid formation. *Biophys Rev, 9*(4), 329-338. doi:10.1007/s12551-017-0289-z

Liu, L., Drouet, V., Wu, J. W., Witter, M. P., Small, S. A., Clelland, C., & Duff, K. (2012). Trans-synaptic spread of tau pathology in vivo. *PLoS One, 7*(2), e31302. doi:10.1371/journal.pone.0031302

Lomakin, A., Chung, D. S., Benedek, G. B., Kirschner, D. A., & Teplow, D. B. (1996). On the nucleation and growth of amyloid beta-protein fibrils: detection of nuclei and quantitation of rate constants. *Proc Natl Acad Sci U S A, 93*(3), 1125-1129.

Lopez de la Paz, M., & Serrano, L. (2004). Sequence determinants of amyloid fibril formation. *Proc Natl Acad Sci U S A, 101*(1), 87-92. doi:10.1073/pnas.2634884100

Maddelein, M. L., Dos Reis, S., Duvezin-Caubet, S., Coulary-Salin, B., & Saupe, S. J. (2002). Amyloid aggregates of the HET-s prion protein are infectious. *Proc Natl Acad Sci U S A, 99*(11), 7402-7407. doi:10.1073/pnas.072199199

Madine, J., Jack, E., Stockley, P. G., Radford, S. E., Serpell, L. C., & Middleton, D. A. (2008). Structural insights into the polymorphism of amyloid-like fibrils formed by region 20-29 of amylin revealed by solid-state NMR and X-ray fiber diffraction. *J Am Chem Soc, 130*(45), 14990-15001. doi:10.1021/ja802483d

Magdesian, M. H., Carvalho, M. M., Mendes, F. A., Saraiva, L. M., Juliano, M. A., Juliano, L., . . . Ferreira, S. T. (2008). Amyloid-beta binds to the extracellular cysteine-rich domain of Frizzled and inhibits Wnt/beta-catenin signaling. *J Biol Chem, 283*(14), 9359-9368. doi:10.1074/jbc.M707108200

Magliani, W., Conti, S., Ciociola, T., Giovati, L., Zanello, P. P., Pertinhez, T., . . . Polonelli, L. (2011). Killer peptide: a novel paradigm of antimicrobial, antiviral and immunomodulatory auto-delivering drugs. *Future Med Chem, 3*(9), 1209-1231. doi:10.4155/fmc.11.71

Mahler, H. C., Friess, W., Grauschopf, U., & Kiese, S. (2009). Protein aggregation: pathways, induction factors and analysis. *J Pharm Sci, 98*(9), 2909-2934. doi:10.1002/jps.21566

Maji, S. K., Schubert, D., Rivier, C., Lee, S., Rivier, J. E., & Riek, R. (2008). Amyloid as a depot for the formulation of long-acting drugs. *PLoS Biol, 6*(2), e17. doi:10.1371/journal.pbio.0060017

Maji, S. K., Perrin, M. H., Sawaya, M. R., Jessberger, S., Vadodaria, K., Rissman, R. A., . . . Riek, R. (2009). Functional amyloids as natural storage of peptide hormones in pituitary secretory granules. *Science, 325*(5938), 328-332. doi:10.1126/science.1173155

Makin, O. S., & Serpell, L. C. (2005). Structures for amyloid fibrils. *FEBS J, 272*(23), 5950-5961. doi:10.1111/j.1742-4658.2005.05025.x

Makin, O. S., Atkins, E., Sikorski, P., Johansson, J., & Serpell, L. C. (2005). Molecular basis for amyloid fibril formation and stability. *Proc Natl Acad Sci U S A, 102*(2), 315-320. doi:10.1073/pnas.0406847102

Mangialasche, F., Solomon, A., Winblad, B., Mecocci, P., & Kivipelto, M. (2010). Alzheimer's disease: clinical trials and drug development. *Lancet Neurol, 9*(7), 702-716. doi:10.1016/S1474-4422(10)70119-8

Mankar, S., Anoop, A., Sen, S., & Maji, S. K. (2011). Nanomaterials: amyloids reflect their brighter side. *Nano Rev, 2*. doi:10.3402/nano.v2i0.6032

Marshall, G. A., Kaufer, D. I., Lopez, O. L., Rao, G. R., Hamilton, R. L., & DeKosky, S. T. (2004). Right prosubiculum amyloid plaque density correlates with anosognosia in Alzheimer's disease. *J Neurol Neurosurg Psychiatry, 75*(10), 1396-1400. doi:10.1136/jnnp.2003.030007

Marshall, K. E., & Serpell, L. C. (2009). Structural integrity of beta-sheet assembly. *Biochem Soc Trans, 37*(Pt 4), 671-676. doi:10.1042/BST0370671

Marshall, K. E., Hicks, M. R., Williams, T. L., Hoffmann, S. V., Rodger, A., Dafforn, T. R., & Serpell, L. C. (2010). Characterizing the assembly of the Sup35 yeast prion fragment, GNNQQNY: structural changes accompany a fiber-to-crystal switch. *Biophys J, 98*(2), 330-338. doi:10.1016/j.bpj.2009.10.020

Marshall, K. E., Morris, K. L., Charlton, D., O'Reilly, N., Lewis, L., Walden, H., & Serpell, L. C. (2011). Hydrophobic, aromatic, and electrostatic interactions play a central role in amyloid fibril formation and stability. *Biochemistry, 50*(12), 2061-2071. doi:10.1021/bi101936c

Marshall, K. E., Marchante, R., Xue, W. F., & Serpell, L. C. (2014). The relationship between amyloid structure and cytotoxicity. *Prion, 8*(2).

Marshall, K. E., Vadukul, D. M., Dahal, L., Theisen, A., Fowler, M. W., Al-Hilaly, Y., . . . Serpell, L. C. (2016). A critical role for the self-assembly of Amyloid-beta1-42 in neurodegeneration. *Sci Rep, 6*, 30182. doi:10.1038/srep30182

Martin, S. R., & Schilstra, M. J. (2008). Circular dichroism and its application to the study of biomolecules. *Methods Cell Biol, 84*, 263-293. doi:10.1016/S0091-679X(07)84010-6

Martins, I. C., Kuperstein, I., Wilkinson, H., Maes, E., Vanbrabant, M., Jonckheere, W., . . . Rousseau, F. (2008). Lipids revert inert Abeta amyloid fibrils to neurotoxic protofibrils that affect learning in mice. *EMBO J, 27*(1), 224-233. doi:10.1038/sj.emboj.7601953

Masuda, Y., Uemura, S., Nakanishi, A., Ohashi, R., Takegoshi, K., Shimizu, T., . . . Irie, K. (2008). Verification of the C-terminal intramolecular beta-sheet in Abeta42 aggregates using solid-state NMR: implications for potent neurotoxicity through the formation of radicals. *Bioorg Med Chem Lett, 18*(11), 3206-3210. doi:10.1016/j.bmcl.2008.04.060

Mattson, M. P., Cheng, B., Davis, D., Bryant, K., Lieberburg, I., & Rydel, R. E. (1992). beta-Amyloid peptides destabilize calcium homeostasis and render human cortical neurons vulnerable to excitotoxicity. *J Neurosci, 12*(2), 376-389.

Maurer-Stroh, S., Debulpaep, M., Kuemmerer, N., Lopez de la Paz, M., Martins, I. C., Reumers, J., . . . Rousseau, F. (2010). Exploring the sequence determinants of amyloid structure using position-specific scoring matrices. *Nat Methods, 7*(3), 237-242. doi:10.1038/nmeth.1432

McKhann, G. M., Knopman, D. S., Chertkow, H., Hyman, B. T., Jack, C. R., Jr., Kawas, C. H., . . . Phelps, C. H. (2011). The diagnosis of dementia due to Alzheimer's disease: recommendations from the National Institute on Aging-Alzheimer's Association workgroups on diagnostic guidelines for Alzheimer's disease. *Alzheimers Dement, 7*(3), 263-269. doi:10.1016/j.jalz.2011.03.005

McLean, C. A., Cherny, R. A., Fraser, F. W., Fuller, S. J., Smith, M. J., Beyreuther, K., . . . Masters, C. L. (1999). Soluble pool of Abeta amyloid as a determinant of severity of neurodegeneration in Alzheimer's disease. *Ann Neurol, 46*(6), 860-866.

Meleleo, D., Galliani, A., & Notarachille, G. (2013). AbetaP1-42 incorporation and channel formation in planar lipid membranes: the role of cholesterol and its oxidation products. *J Bioenerg Biomembr, 45*(4), 369-381. doi:10.1007/s10863-013-9513-0

Menendez-Gonzalez, M., Perez-Pinera, P., Martinez-Rivera, M., Calatayud, M. T., & Blazquez Menes, B. (2005). APP processing and the APP-KPI domain involvement in the amyloid cascade. *Neurodegener Dis, 2*(6), 277-283. doi:10.1159/000092315

Meyer-Luehmann, M., Spires-Jones, T. L., Prada, C., Garcia-Alloza, M., de Calignon, A., Rozkalne, A., . . . Hyman, B. T. (2008). Rapid appearance and local toxicity of amyloid-beta plaques in a mouse model of Alzheimer's disease. *Nature, 451*(7179), 720-724. doi:10.1038/nature06616

Miller, Y., Ma, B., Tsai, C. J., & Nussinov, R. (2010). Hollow core of Alzheimer's Abeta42 amyloid observed by cryoEM is relevant at physiological pH. *Proc Natl Acad Sci U S A, 107*(32), 14128-14133. doi:10.1073/pnas.1004704107

Milto, K., Botyriute, A., & Smirnovas, V. (2013). Amyloid-like fibril elongation follows michaelis-menten kinetics. *PLoS One, 8*(7), e68684. doi:10.1371/journal.pone.0068684

Mizushima, N. (2007). Autophagy: process and function. *Genes Dev, 21*(22), 2861-2873. doi:10.1101/gad.1599207

Mockett, B. G., Richter, M., Abraham, W. C., & Muller, U. C. (2017). Therapeutic Potential of Secreted Amyloid Precursor Protein APPsalpha. *Front Mol Neurosci, 10*, 30. doi:10.3389/fnmol.2017.00030

Morris, K. L., & Serpell, L. C. (2012). X-ray fibre diffraction studies of amyloid fibrils. *Methods Mol Biol, 849*, 121-135. doi:10.1007/978-1-61779-551-0_9

Morris, K. L., Rodger, A., Hicks, M. R., Debulpaep, M., Schymkowitz, J., Rousseau, F., & Serpell, L. C. (2013). Exploring the sequence-structure relationship for amyloid peptides. *Biochem J, 450*(2), 275-283. doi:10.1042/BJ20121773

Morris, O., Elsawy, M. A., Fairclough, M., Williams, K. J., McMahon, A., Grigg, J., . . . Prenant, C. (2017). In vivo characterisation of a therapeutically relevant self-assembling (18) F-labelled beta-sheet forming peptide and its hydrogel using positron emission tomography. *J Labelled Comp Radiopharm, 60*(10), 481-488. doi:10.1002/jlcr.3534

Morris, V. K., & Sunde, M. (2013). Formation of amphipathic amyloid monolayers from fungal hydrophobin proteins. *Methods Mol Biol, 996*, 119-129. doi:10.1007/978-1-62703-354-1_7

Mostaert, A. S., Higgins, M. J., Fukuma, T., Rindi, F., & Jarvis, S. P. (2006). Nanoscale mechanical characterisation of amyloid fibrils discovered in a natural adhesive. *J Biol Phys, 32*(5), 393-401. doi:10.1007/s10867-006-9023-y

Muller, U. C., Deller, T., & Korte, M. (2017). Not just amyloid: physiological functions of the amyloid precursor protein family. *Nat Rev Neurosci, 18*(5), 281-298. doi:10.1038/nrn.2017.29

Munter, L. M., Voigt, P., Harmeier, A., Kaden, D., Gottschalk, K. E., Weise, C., . . . Multhaup, G. (2007). GxxxG motifs within the amyloid precursor protein transmembrane sequence are critical for the etiology of Abeta42. *EMBO J, 26*(6), 1702-1712. doi:10.1038/sj.emboj.7601616

Murakami, K., Irie, K., Ohigashi, H., Hara, H., Nagao, M., Shimizu, T., & Shirasawa, T. (2005). Formation and stabilization model of the 42-mer Abeta radical: implications for the long-lasting oxidative stress in Alzheimer's disease. *J Am Chem Soc, 127*(43), 15168-15174. doi:10.1021/ja054041c

Murray, M. M., Bernstein, S. L., Nyugen, V., Condron, M. M., Teplow, D. B., & Bowers, M. T. (2009). Amyloid beta protein: Abeta40 inhibits Abeta42 oligomerization. *J Am Chem Soc, 131*(18), 6316-6317. doi:10.1021/ja8092604

Nath, S., Agholme, L., Kurudenkandy, F. R., Granseth, B., Marcusson, J., & Hallbeck, M. (2012). Spreading of neurodegenerative pathology via neuron-to-neuron transmission of beta-amyloid. *J Neurosci, 32*(26), 8767-8777. doi:10.1523/JNEUROSCI.0615-12.2012

Nelson, R., Sawaya, M. R., Balbirnie, M., Madsen, A. O., Riekel, C., Grothe, R., & Eisenberg, D. (2005). Structure of the cross-beta spine of amyloid-like fibrils. *Nature, 435*(7043), 773-778. doi:10.1038/nature03680

Nichols, M. R., Moss, M. A., Reed, D. K., Hoh, J. H., & Rosenberry, T. L. (2005). Amyloid-beta aggregates formed at polar-nonpolar interfaces differ from amyloid-beta protofibrils produced in aqueous buffers. *Microsc Res Tech, 67*(3-4), 164-174. doi:10.1002/jemt.20189

Nixon, R. A. (2007). Autophagy, amyloidogenesis and Alzheimer disease. *J Cell Sci, 120*(Pt 23), 4081-4091. doi:10.1242/jcs.019265

Nolting, B., Golbik, R., Neira, J. L., Soler-Gonzalez, A. S., Schreiber, G., & Fersht, A. R. (1997). The folding pathway of a protein at high resolution from microseconds to seconds. *Proc Natl Acad Sci U S A, 94*(3), 826-830.

O'Nuallain, B., & Wetzel, R. (2002). Conformational Abs recognizing a generic amyloid fibril epitope. *Proc Natl Acad Sci U S A, 99*(3), 1485-1490. doi:10.1073/pnas.022662599

Okada, H., Zhang, W., Peterhoff, C., Hwang, J. C., Nixon, R. A., Ryu, S. H., & Kim, T. W. (2010). Proteomic identification of sorting nexin 6 as a negative regulator of BACE1-mediated APP processing. *FASEB J, 24*(8), 2783-2794. doi:10.1096/fj.09-146357

Olsson, F., Schmidt, S., Althoff, V., Munter, L. M., Jin, S., Rosqvist, S., . . . Lundkvist, J. (2014). Characterization of intermediate steps in amyloid beta (Abeta) production under near-native conditions. *J Biol Chem, 289*(3), 1540-1550. doi:10.1074/jbc.M113.498246

Oltersdorf, T., Fritz, L. C., Schenk, D. B., Lieberburg, I., Johnson-Wood, K. L., Beattie, E. C., . . . Sinha, S. (1989). The secreted form of the Alzheimer's amyloid precursor protein with the Kunitz domain is protease nexin-II. *Nature, 341*(6238), 144-147. doi:10.1038/341144a0

Ono, K., Condron, M. M., & Teplow, D. B. (2009). Structure-neurotoxicity relationships of amyloid beta-protein oligomers. *Proc Natl Acad Sci U S A, 106*(35), 14745-14750. doi:10.1073/pnas.0905127106

Otoo, H. N., Lee, K. G., Qiu, W., & Lipke, P. N. (2008). Candida albicans Als adhesins have conserved amyloid-forming sequences. *Eukaryot Cell, 7*(5), 776-782. doi:10.1128/EC.00309-07

Pachahara, S. K., & Nagaraj, R. (2015). Probing the role of aromatic residues in the self-assembly of Abeta(16-22) in fluorinated alcohols and their aqueous mixtures. *Biochem Biophys Rep, 2*, 1-13. doi:10.1016/j.bbrep.2015.04.005

Pauling, L., Corey, R. B., & Branson, H. R. (1951). The structure of proteins; two hydrogen-bonded helical configurations of the polypeptide chain. *Proc Natl Acad Sci U S A, 37*(4), 205-211.

Pauling, L., & Corey, R. B. (1951). The pleated sheet, a new layer configuration of polypeptide chains. *Proc Natl Acad Sci U S A, 37*(5), 251-256.

Paushkin, S. V., Kushnirov, V. V., Smirnov, V. N., & Ter-Avanesyan, M. D. (1996). Propagation of the yeast prion-like [psi+] determinant is mediated by oligomerization of the SUP35-encoded polypeptide chain release factor. *EMBO J, 15*(12), 3127-3134.

Pauwels, K., Williams, T. L., Morris, K. L., Jonckheere, W., Vandersteen, A., Kelly, G., . . . Broersen, K. (2012). Structural basis for increased toxicity of pathological abeta42:abeta40 ratios in Alzheimer disease. *J Biol Chem, 287*(8), 5650-5660. doi:10.1074/jbc.M111.264473

Petkova, A. T., Yau, W. M., & Tycko, R. (2006). Experimental constraints on quaternary structure in Alzheimer's beta-amyloid fibrils. *Biochemistry, 45*(2), 498-512. doi:10.1021/bi051952q

Pham, C. L., Kwan, A. H., & Sunde, M. (2014). Functional amyloid: widespread in Nature, diverse in purpose. *Essays Biochem, 56*, 207-219. doi:10.1042/bse0560207

Pieri, L., Madiona, K., & Melki, R. (2016). Structural and functional properties of prefibrillar alpha-synuclein oligomers. *Sci Rep, 6*, 24526. doi:10.1038/srep24526

Pike, C. J., Walencewicz, A. J., Glabe, C. G., & Cotman, C. W. (1991). In vitro aging of beta-amyloid protein causes peptide aggregation and neurotoxicity. *Brain Res, 563*(1-2), 311-314.

Pike, C. J., Burdick, D., Walencewicz, A. J., Glabe, C. G., & Cotman, C. W. (1993). Neurodegeneration induced by beta-amyloid peptides in vitro: the role of peptide assembly state. *J Neurosci, 13*(4), 1676-1687.

Platt, G. W., Routledge, K. E., Homans, S. W., & Radford, S. E. (2008). Fibril growth kinetics reveal a region of beta2-microglobulin important for nucleation and elongation of aggregation. *J Mol Biol, 378*(1), 251-263. doi:10.1016/j.jmb.2008.01.092

Porat, Y., Abramowitz, A., & Gazit, E. (2006). Inhibition of amyloid fibril formation by polyphenols: structural similarity and aromatic interactions as a common inhibition mechanism. *Chem Biol Drug Des, 67*(1), 27-37. doi:10.1111/j.1747-0285.2005.00318.x

Preece, P., Virley, D. J., Costandi, M., Coombes, R., Moss, S. J., Mudge, A. W., . . . Cairns, N. J. (2004). Amyloid precursor protein mRNA levels in Alzheimer's disease brain. *Brain Res Mol Brain Res, 122*(1), 1-9. doi:10.1016/j.molbrainres.2003.08.022

Puchtler, H., & Sweat, F. (1965). Congo red as a stain for fluorescence microscopy of amyloid. *J Histochem Cytochem, 13*(8), 693-694. doi:10.1177/13.8.693

Qi, X., Hong, L., & Zhang, Y. (2012). A variational model for oligomer-formation process of GNNQQNY peptide from yeast prion protein Sup35. *Biophys J, 102*(3), 597-605. doi:10.1016/j.bpj.2011.12.036

Qiang, W., Yau, W. M., Luo, Y., Mattson, M. P., & Tycko, R. (2012). Antiparallel beta-sheet architecture in Iowa-mutant beta-amyloid fibrils. *Proc Natl Acad Sci U S A, 109*(12), 4443-4448. doi:10.1073/pnas.1111305109

Rambaran, R. N., & Serpell, L. C. (2008). Amyloid fibrils: abnormal protein assembly. *Prion, 2*(3), 112-117.

Reynolds, N. P., Charnley, M., Mezzenga, R., & Hartley, P. G. (2014). Engineered lysozyme amyloid fibril networks support cellular growth and spreading. *Biomacromolecules, 15*(2), 599-608. doi:10.1021/bm401646x

Riek, R., & Eisenberg, D. S. (2016). The activities of amyloids from a structural perspective. *Nature, 539*(7628), 227-235. doi:10.1038/nature20416

Rikhvanov, E. G., Romanova, N. V., & Chernoff, Y. O. (2007). Chaperone effects on prion and nonprion aggregates. *Prion, 1*(4), 217-222.

Rohan de Silva, H. A., Jen, A., Wickenden, C., Jen, L. S., Wilkinson, S. L., & Patel, A. J. (1997). Cell-specific expression of beta-amyloid precursor protein isoform mRNAs and proteins in neurons and astrocytes. *Brain Res Mol Brain Res, 47*(1-2), 147-156.

Roher, A. E., Chaney, M. O., Kuo, Y. M., Webster, S. D., Stine, W. B., Haverkamp, L. J., . . . Emmerling, M. R. (1996). Morphology and toxicity of Abeta-(1-42) dimer derived from neuritic and vascular amyloid deposits of Alzheimer's disease. *J Biol Chem, 271*(34), 20631-20635.

Romanova, N. V., & Chernoff, Y. O. (2009). Hsp104 and prion propagation. *Protein Pept Lett, 16*(6), 598-605.

Roper, R. J., & Reeves, R. H. (2006). Understanding the basis for Down syndrome phenotypes. *PLoS Genet, 2*(3), e50. doi:10.1371/journal.pgen.0020050

Roychaudhuri, R., Yang, M., Hoshi, M. M., & Teplow, D. B. (2009). Amyloid beta-protein assembly and Alzheimer disease. *J Biol Chem, 284*(8), 4749-4753. doi:10.1074/jbc.R800036200

Saavedra, L., Mohamed, A., Ma, V., Kar, S., & de Chaves, E. P. (2007). Internalization of beta-amyloid peptide by primary neurons in the absence of apolipoprotein E. *J Biol Chem, 282*(49), 35722-35732. doi:10.1074/jbc.M701823200

Sakono, M., & Zako, T. (2010). Amyloid oligomers: formation and toxicity of Abeta oligomers. *FEBS J, 277*(6), 1348-1358. doi:10.1111/j.1742-4658.2010.07568.x

Salazar, S. V., & Strittmatter, S. M. (2017). Cellular prion protein as a receptor for amyloid-beta oligomers in Alzheimer's disease. *Biochem Biophys Res Commun, 483*(4), 1143-1147. doi:10.1016/j.bbrc.2016.09.062

Sandbrink, R., Masters, C. L., & Beyreuther, K. (1996). APP gene family. Alternative splicing generates functionally related isoforms. *Ann N Y Acad Sci, 777*, 281-287.

Sarroukh, R., Cerf, E., Derclaye, S., Dufrene, Y. F., Goormaghtigh, E., Ruysschaert, J. M., & Raussens, V. (2011). Transformation of amyloid beta(1-40) oligomers into fibrils is characterized by a major change in secondary structure. *Cell Mol Life Sci, 68*(8), 1429-1438. doi:10.1007/s00018-010-0529-x

Sato, C., Morohashi, Y., Tomita, T., & Iwatsubo, T. (2006a). Structure of the catalytic pore of gamma-secretase probed by the accessibility of substituted cysteines. *J Neurosci, 26*(46), 12081-12088. doi:10.1523/JNEUROSCI.3614-06.2006

Sato, T., Kienlen-Campard, P., Ahmed, M., Liu, W., Li, H., Elliott, J. I., . . . Smith, S. O. (2006b). Inhibitors of amyloid toxicity based on beta-sheet packing of Abeta40 and Abeta42. *Biochemistry, 45*(17), 5503-5516. doi:10.1021/bi052485f

Sawaya, M. R., Sambashivan, S., Nelson, R., Ivanova, M. I., Sievers, S. A., Apostol, M. I., . . . Eisenberg, D. (2007). Atomic structures of amyloid cross-beta spines reveal varied steric zippers. *Nature, 447*(7143), 453-457. doi:10.1038/nature05695

Scheuermann, S., Hambsch, B., Hesse, L., Stumm, J., Schmidt, C., Beher, D., . . . Multhaup, G. (2001). Homodimerization of amyloid precursor protein and its implication in the amyloidogenic pathway of Alzheimer's disease. *J Biol Chem, 276*(36), 33923-33929. doi:10.1074/jbc.M105410200

Schmidt, M., Sachse, C., Richter, W., Xu, C., Fandrich, M., & Grigorieff, N. (2009). Comparison of Alzheimer Abeta(1-40) and Abeta(1-42) amyloid fibrils reveals similar protofilament structures. *Proc Natl Acad Sci U S A, 106*(47), 19813-19818. doi:10.1073/pnas.0905007106

Schmidt, M., Rohou, A., Lasker, K., Yadav, J. K., Schiene-Fischer, C., Fandrich, M., & Grigorieff, N. (2015). Peptide dimer structure in an Abeta(1-42) fibril visualized with cryo-EM. *Proc Natl Acad Sci U S A, 112*(38), 11858-11863. doi:10.1073/pnas.1503455112

Schneider, J. P., Pochan, D. J., Ozbas, B., Rajagopal, K., Pakstis, L., & Kretsinger, J. (2002). Responsive hydrogels from the intramolecular folding and self-assembly of a designed peptide. *J Am Chem Soc, 124*(50), 15030-15037.

Selkoe, D. J. (1994). Alzheimer's disease: a central role for amyloid. *J Neuropathol Exp Neurol, 53*(5), 438-447.

Selkoe, D. J., & Hardy, J. (2016). The amyloid hypothesis of Alzheimer's disease at 25 years. *EMBO Mol Med, 8*(6), 595-608. doi:10.15252/emmm.201606210

Serpell, L. C., Fraser, P. E., & Sunde, M. (1999). X-ray fiber diffraction of amyloid fibrils. *Methods Enzymol, 309*, 526-536.

Serpell, L. C. (2000). Alzheimer's amyloid fibrils: structure and assembly. *Biochim Biophys Acta, 1502*(1), 16-30.

Serpell, L. C., Berriman, J., Jakes, R., Goedert, M., & Crowther, R. A. (2000). Fiber diffraction of synthetic alpha-synuclein filaments shows amyloid-like cross-beta conformation. *Proc Natl Acad Sci U S A, 97*(9), 4897-4902.

Serra-Batiste, M., Ninot-Pedrosa, M., Bayoumi, M., Gairi, M., Maglia, G., & Carulla, N. (2016). Abeta42 assembles into specific beta-barrel pore-forming oligomers in membrane-mimicking environments. *Proc Natl Acad Sci U S A, 113*(39), 10866-10871. doi:10.1073/pnas.1605104113

Shankar, G. M., Bloodgood, B. L., Townsend, M., Walsh, D. M., Selkoe, D. J., & Sabatini, B. L. (2007). Natural oligomers of the Alzheimer amyloid-beta protein induce reversible synapse loss by modulating an NMDA-type glutamate receptor-dependent signaling pathway. *J Neurosci, 27*(11), 2866-2875. doi:10.1523/JNEUROSCI.4970-06.2007

Shankar, G. M., Li, S., Mehta, T. H., Garcia-Munoz, A., Shepardson, N. E., Smith, I., . . . Selkoe, D. J. (2008). Amyloid-beta protein dimers isolated directly from Alzheimer's brains impair synaptic plasticity and memory. *Nat Med, 14*(8), 837-842. doi:10.1038/nm1782

Sharma, J., Wisniewski, B. T., Paulson, E., Obaoye, J. O., Merrill, S. J., & Manogaran, A. L. (2017). De novo [PSI (+)] prion formation involves multiple pathways to form infectious oligomers. *Sci Rep, 7*(1), 76. doi:10.1038/s41598-017-00135-6

Shen, C. L., & Murphy, R. M. (1995). Solvent effects on self-assembly of beta-amyloid peptide. *Biophys J, 69*(2), 640-651. doi:10.1016/S0006-3495(95)79940-4

Shi, Q., Ge, Y., He, W., Hu, X., & Yan, R. (2017). RTN1 and RTN3 protein are differentially associated with senile plaques in Alzheimer's brains. *Sci Rep, 7*(1), 6145. doi:10.1038/s41598-017-05504-9

Shimizu, H., Tosaki, A., Kaneko, K., Hisano, T., Sakurai, T., & Nukina, N. (2008). Crystal structure of an active form of BACE1, an enzyme responsible for amyloid beta protein production. *Mol Cell Biol, 28*(11), 3663-3671. doi:10.1128/MCB.02185-07

Shruster, A., Eldar-Finkelman, H., Melamed, E., & Offen, D. (2011). Wnt signaling pathway overcomes the disruption of neuronal differentiation of neural progenitor cells induced by oligomeric amyloid beta-peptide. *J Neurochem, 116*(4), 522-529. doi:10.1111/j.1471-4159.2010.07131.x

Silva, R. F., Araujo, D. R., Silva, E. R., Ando, R. A., & Alves, W. A. (2013). L-diphenylalanine microtubes as a potential drug-delivery system: characterization, release kinetics, and cytotoxicity. *Langmuir, 29*(32), 10205-10212. doi:10.1021/la4019162

Sipe, J. D., & Cohen, A. S. (2000). Review: history of the amyloid fibril. *J Struct Biol, 130*(2-3), 88-98. doi:10.1006/jsbi.2000.4221

Sipe, J. D., Benson, M. D., Buxbaum, J. N., Ikeda, S., Merlini, G., Saraiva, M. J., & Westermark, P. (2014). Nomenclature 2014: Amyloid fibril proteins and clinical classification of the amyloidosis. *Amyloid, 21*(4), 221-224. doi:10.3109/13506129.2014.964858

Sipe, J. D., Benson, M. D., Buxbaum, J. N., Ikeda, S. I., Merlini, G., Saraiva, M. J., & Westermark, P. (2016). Amyloid fibril proteins and amyloidosis: chemical identification and clinical classification International Society of Amyloidosis 2016 Nomenclature Guidelines. *Amyloid, 23*(4), 209-213. doi:10.1080/13506129.2016.1257986

Skovronsky, D. M., Doms, R. W., & Lee, V. M. (1998). Detection of a novel intraneuronal pool of insoluble amyloid beta protein that accumulates with time in culture. *J Cell Biol, 141*(4), 1031-1039.

Slotta, U., Hess, S., Spiess, K., Stromer, T., Serpell, L., & Scheibel, T. (2007). Spider silk and amyloid fibrils: a structural comparison. *Macromol Biosci, 7*(2), 183-188. doi:10.1002/mabi.200600201

Smith, J. F., Knowles, T. P., Dobson, C. M., Macphee, C. E., & Welland, M. E. (2006). Characterization of the nanoscale properties of individual amyloid fibrils. *Proc Natl Acad Sci U S A, 103*(43), 15806-15811. doi:10.1073/pnas.0604035103

Snyder, S. W., Ladror, U. S., Wade, W. S., Wang, G. T., Barrett, L. W., Matayoshi, E. D., . . . Holzman, T. F. (1994). Amyloid-beta aggregation: selective inhibition of aggregation in mixtures of amyloid with different chain lengths. *Biophys J, 67*(3), 1216-1228. doi:10.1016/S0006-3495(94)80591-0

Soba, P., Eggert, S., Wagner, K., Zentgraf, H., Siehl, K., Kreger, S., . . . Beyreuther, K. (2005). Homo- and heterodimerization of APP family members promotes intercellular adhesion. *EMBO J, 24*(20), 3624-3634. doi:10.1038/sj.emboj.7600824

Soldi, G., Bemporad, F., Torrassa, S., Relini, A., Ramazzotti, M., Taddei, N., & Chiti, F. (2005). Amyloid formation of a protein in the absence of initial unfolding and destabilization of the native state. *Biophys J, 89*(6), 4234-4244. doi:10.1529/biophysj.105.067538

Somavarapu, A. K., & Kepp, K. P. (2016). The dynamic mechanism of presenilin-1 function: Sensitive gate dynamics and loop unplugging control protein access. *Neurobiol Dis, 89*, 147-156. doi:10.1016/j.nbd.2016.02.008

Sommer, B. (2002). Alzheimer's disease and the amyloid cascade hypothesis: ten years on. *Curr Opin Pharmacol, 2*(1), 87-92.

Soscia, S. J., Kirby, J. E., Washicosky, K. J., Tucker, S. M., Ingelsson, M., Hyman, B., . . . Moir, R. D. (2010). The Alzheimer's disease-associated amyloid beta-protein is an antimicrobial peptide. *PLoS One, 5*(3), e9505. doi:10.1371/journal.pone.0009505

Soura, V., Stewart-Parker, M., Williams, T. L., Ratnayaka, A., Atherton, J., Gorringe, K., . . . Serpell, L. C. (2012). Visualization of co-localization in Abeta42-administered neuroblastoma cells reveals lysosome damage and autophagosome accumulation related to cell death. *Biochem J, 441*(2), 579-590. doi:10.1042/BJ20110749

Sreerama, N., Manning, M. C., Powers, M. E., Zhang, J. X., Goldenberg, D. P., & Woody, R. W. (1999). Tyrosine, phenylalanine, and disulfide contributions to the circular dichroism of proteins: circular dichroism spectra of wild-type and mutant bovine pancreatic trypsin inhibitor. *Biochemistry, 38*(33), 10814-10822. doi:10.1021/bi990516z

Sreerama, N., & Woody, R. W. (2004). Computation and analysis of protein circular dichroism spectra. *Methods Enzymol, 383*, 318-351. doi:10.1016/S0076-6879(04)83013-1

Strodel, B., Whittleston, C. S., & Wales, D. J. (2007). Thermodynamics and kinetics of aggregation for the GNNQQNY peptide. *J Am Chem Soc, 129*(51), 16005-16014. doi:10.1021/ja075346p

Stroud, J. C., Liu, C., Teng, P. K., & Eisenberg, D. (2012). Toxic fibrillar oligomers of amyloid-beta have cross-beta structure. *Proc Natl Acad Sci U S A, 109*(20), 7717-7722. doi:10.1073/pnas.1203193109

Su, Y., & Chang, P. T. (2001). Acidic pH promotes the formation of toxic fibrils from beta-amyloid peptide. *Brain Res, 893*(1-2), 287-291.

Sumner Makin, O., & Serpell, L. C. (2004). Structural characterisation of islet amyloid polypeptide fibrils. *J Mol Biol, 335*(5), 1279-1288.

Swasthi, H. M., & Mukhopadhyay, S. (2017). Electrostatic lipid-protein interactions sequester the curli amyloid fold on the lipopolysaccharide membrane surface. *J Biol Chem, 292*(48), 19861-19872. doi:10.1074/jbc.M117.815522

Szkolar, L., Guilbaud, J. B., Miller, A. F., Gough, J. E., & Saiani, A. (2014). Enzymatically triggered peptide hydrogels for 3D cell encapsulation and culture. *J Pept Sci, 20*(7), 578-584. doi:10.1002/psc.2666

Taglialegna, A., Navarro, S., Ventura, S., Garnett, J. A., Matthews, S., Penades, J. R., . . . Valle, J. (2016). Staphylococcal Bap Proteins Build Amyloid Scaffold Biofilm Matrices in Response to Environmental Signals. *PLoS Pathog, 12*(6), e1005711. doi:10.1371/journal.ppat.1005711

Takami, M., Nagashima, Y., Sano, Y., Ishihara, S., Morishima-Kawashima, M., Funamoto, S., & Ihara, Y. (2009). gamma-Secretase: successive tripeptide and tetrapeptide release from the transmembrane domain of beta-carboxyl terminal fragment. *J Neurosci, 29*(41), 13042-13052. doi:10.1523/JNEUROSCI.2362-09.2009

Tang, C., Miller, A. F., & Saiani, A. (2014). Peptide hydrogels as mucoadhesives for local drug delivery. *Int J Pharm, 465*(1-2), 427-435. doi:10.1016/j.ijpharm.2014.02.039

Taylor, B. M., Sarver, R. W., Fici, G., Poorman, R. A., Lutzke, B. S., Molinari, A., . . . Epps, D. E. (2003). Spontaneous aggregation and cytotoxicity of the beta-amyloid Abeta1-40: a kinetic model. *J Protein Chem, 22*(1), 31-40.

Tenidis, K., Waldner, M., Bernhagen, J., Fischle, W., Bergmann, M., Weber, M., . . . Kapurniotu, A. (2000). Identification of a penta- and hexapeptide of islet amyloid polypeptide (IAPP) with amyloidogenic and cytotoxic properties. *J Mol Biol, 295*(4), 1055-1071. doi:10.1006/jmbi.1999.3422

Thomas, P. D., & Dill, K. A. (1993). Local and nonlocal interactions in globular proteins and mechanisms of alcohol denaturation. *Protein Sci, 2*(12), 2050-2065. doi:10.1002/pro.5560021206

Tiiman, A., Noormagi, A., Friedemann, M., Krishtal, J., Palumaa, P., & Tougu, V. (2013). Effect of agitation on the peptide fibrillization: Alzheimer's amyloid-beta peptide 1-42 but not amylin and insulin fibrils can grow under quiescent conditions. *J Pept Sci, 19*(6), 386-391. doi:10.1002/psc.2513

Tiiman, A., Krishtal, J., Palumaa, P., & Tougu, V. (2015). In vitro fibrillization of Alzheimer's amyloid-beta peptide (1-42). *Aip Advances, 5*(9). doi:Artn 092401

10.1063/1.4921071

Tipping, K. W., Karamanos, T. K., Jakhria, T., Iadanza, M. G., Goodchild, S. C., Tuma, R., . . . Radford, S. E. (2015). pH-induced molecular shedding drives the formation of amyloid fibril-derived oligomers. *Proc Natl Acad Sci U S A, 112*(18), 5691-5696. doi:10.1073/pnas.1423174112

Tjernberg, L. O., Naslund, J., Lindqvist, F., Johansson, J., Karlstrom, A. R., Thyberg, J., . . . Nordstedt, C. (1996). Arrest of beta-amyloid fibril formation by a pentapeptide ligand. *J Biol Chem, 271*(15), 8545-8548.

Tjernberg, L. O., Callaway, D. J., Tjernberg, A., Hahne, S., Lilliehook, C., Terenius, L., . . . Nordstedt, C. (1999). A molecular model of Alzheimer amyloid beta-peptide fibril formation. *J Biol Chem, 274*(18), 12619-12625.

Tominaga, A., Cai, T., Takagi-Niidome, S., Iwatsubo, T., & Tomita, T. (2016). Conformational Changes in Transmembrane Domain 4 of Presenilin 1 Are Associated with Altered Amyloid-beta 42 Production. *J Neurosci, 36*(4), 1362-1372. doi:10.1523/JNEUROSCI.5090-14.2016

Townsend, M., Shankar, G. M., Mehta, T., Walsh, D. M., & Selkoe, D. J. (2006). Effects of secreted oligomers of amyloid beta-protein on hippocampal synaptic plasticity: a potent role for trimers. *J Physiol, 572*(Pt 2), 477-492. doi:10.1113/jphysiol.2005.103754

Trinh, C. H., Smith, D. P., Kalverda, A. P., Phillips, S. E., & Radford, S. E. (2002). Crystal structure of monomeric human beta-2-microglobulin reveals clues to its amyloidogenic properties. *Proc Natl Acad Sci U S A, 99*(15), 9771-9776. doi:10.1073/pnas.152337399

Troy, C. M., Rabacchi, S. A., Friedman, W. J., Frappier, T. F., Brown, K., & Shelanski, M. L. (2000). Caspase-2 mediates neuronal cell death induced by beta-amyloid. *J Neurosci, 20*(4), 1386-1392.

Tsai, H. H., Gunasekaran, K., & Nussinov, R. (2006). Sequence and structure analysis of parallel beta helices: implication for constructing amyloid structural models. *Structure, 14*(6), 1059-1072. doi:10.1016/j.str.2006.03.015

Tsemekhman, K., Goldschmidt, L., Eisenberg, D., & Baker, D. (2007). Cooperative hydrogen bonding in amyloid formation. *Protein Sci, 16*(4), 761-764. doi:10.1110/ps.062609607

Tycko, R. (2011). Solid-state NMR studies of amyloid fibril structure. *Annu Rev Phys Chem, 62*, 279-299. doi:10.1146/annurev-physchem-032210-103539

Uversky, V. N., & Fink, A. L. (2004). Conformational constraints for amyloid fibrillation: the importance of being unfolded. *Biochim Biophys Acta, 1698*(2), 131-153. doi:10.1016/j.bbapap.2003.12.008

Vadukul, D. M., Gbajumo, O., Marshall, K. E., & Serpell, L. C. (2017). Amyloidogenicity and toxicity of the reverse and scrambled variants of amyloid-beta 1-42. *FEBS Lett, 591*(5), 822-830. doi:10.1002/1873-3468.12590

Valastyan, J. S., & Lindquist, S. (2014). Mechanisms of protein-folding diseases at a glance. *Dis Model Mech, 7*(1), 9-14. doi:10.1242/dmm.013474

van Bommel, K. J., van der Pol, C., Muizebelt, I., Friggeri, A., Heeres, A., Meetsma, A., . . . van Esch, J. (2004). Responsive cyclohexane-based low-molecular-weight hydrogelators with modular architecture. *Angew Chem Int Ed Engl, 43*(13), 1663-1667. doi:10.1002/anie.200352396

Vassar, P. S., & Culling, C. F. (1959). Fluorescent stains, with special reference to amyloid and connective tissues. *Arch Pathol, 68*, 487-498.

Verdier, Y., & Penke, B. (2004). Binding sites of amyloid beta-peptide in cell plasma membrane and implications for Alzheimer's disease. *Curr Protein Pept Sci, 5*(1), 19-31.

Verghese, P. B., Castellano, J. M., Garai, K., Wang, Y., Jiang, H., Shah, A., . . . Holtzman, D. M. (2013). ApoE influences amyloid-beta (Abeta) clearance despite minimal apoE/Abeta association in physiological conditions. *Proc Natl Acad Sci U S A, 110*(19), E1807-1816. doi:10.1073/pnas.1220484110

Verma, M., Vats, A., & Taneja, V. (2015). Toxic species in amyloid disorders: Oligomers or mature fibrils. *Ann Indian Acad Neurol, 18*(2), 138-145. doi:10.4103/0972-2327.144284

Vetrivel, K. S., Meckler, X., Chen, Y., Nguyen, P. D., Seidah, N. G., Vassar, R., . . . Thinakaran, G. (2009). Alzheimer disease Abeta production in the absence of S-palmitoylation-dependent targeting of BACE1 to lipid rafts. *J Biol Chem, 284*(6), 3793-3803. doi:10.1074/jbc.M808920200

Villmow, M., Baumann, M., Malesevic, M., Sachs, R., Hause, G., Fandrich, M., . . . Schiene-Fischer, C. (2016). Inhibition of Abeta(1-40) fibril formation by cyclophilins. *Biochem J, 473*(10), 1355-1368. doi:10.1042/BCJ20160098

von Einem, B., Wahler, A., Schips, T., Serrano-Pozo, A., Proepper, C., Boeckers, T. M., . . . von Arnim, C. A. (2015). The Golgi-Localized gamma-Ear-Containing ARF-Binding (GGA) Proteins Alter Amyloid-beta Precursor Protein (APP) Processing through Interaction of Their GAE Domain with the Beta-Site APP Cleaving Enzyme 1 (BACE1). *PLoS One, 10*(6), e0129047. doi:10.1371/journal.pone.0129047

Walsh, D. M., Klyubin, I., Fadeeva, J. V., Cullen, W. K., Anwyl, R., Wolfe, M. S., . . . Selkoe, D. J. (2002a). Naturally secreted oligomers of amyloid beta protein potently inhibit hippocampal long-term potentiation in vivo. *Nature, 416*(6880), 535-539. doi:10.1038/416535a

Walsh, D. M., Klyubin, I., Fadeeva, J. V., Rowan, M. J., & Selkoe, D. J. (2002b). Amyloid-beta oligomers: their production, toxicity and therapeutic inhibition. *Biochem Soc Trans, 30*(4), 552-557. doi:10.1042/

Wan, S., Borland, S., Richardson, S. M., Merry, C. L. R., Saiani, A., & Gough, J. E. (2016). Self-assembling peptide hydrogel for intervertebral disc tissue engineering. *Acta Biomater, 46*, 29-40. doi:10.1016/j.actbio.2016.09.033

Wang, X., Smith, D. R., Jones, J. W., & Chapman, M. R. (2007). In vitro polymerization of a functional Escherichia coli amyloid protein. *J Biol Chem, 282*(6), 3713-3719. doi:10.1074/jbc.M609228200

Wang, X., Zhou, Y., Ren, J. J., Hammer, N. D., & Chapman, M. R. (2010). Gatekeeper residues in the major curlin subunit modulate bacterial amyloid fiber biogenesis. *Proc Natl Acad Sci U S A, 107*(1), 163-168. doi:10.1073/pnas.0908714107

Wang, Y., & Ha, Y. (2004). The X-ray structure of an antiparallel dimer of the human amyloid precursor protein E2 domain. *Mol Cell, 15*(3), 343-353. doi:10.1016/j.molcel.2004.06.037

Wasmer, C., Lange, A., Van Melckebeke, H., Siemer, A. B., Riek, R., & Meier, B. H. (2008). Amyloid fibrils of the HET-s(218-289) prion form a beta solenoid with a triangular hydrophobic core. *Science, 319*(5869), 1523-1526. doi:10.1126/science.1151839

Watanabe-Nakayama, T., Ono, K., Itami, M., Takahashi, R., Teplow, D. B., & Yamada, M. (2016). High-speed atomic force microscopy reveals structural dynamics of amyloid beta1-42 aggregates. *Proc Natl Acad Sci U S A, 113*(21), 5835-5840. doi:10.1073/pnas.1524807113

Watt, B., Tenza, D., Lemmon, M. A., Kerje, S., Raposo, G., Andersson, L., & Marks, M. S. (2011). Mutations in or near the transmembrane domain alter PMEL amyloid formation from functional to pathogenic. *PLoS Genet, 7*(9), e1002286. doi:10.1371/journal.pgen.1002286

Weidemann, A., Konig, G., Bunke, D., Fischer, P., Salbaum, J. M., Masters, C. L., & Beyreuther, K. (1989). Identification, biogenesis, and localization of precursors of Alzheimer's disease A4 amyloid protein. *Cell, 57*(1), 115-126.

Wetzel, R. (2006). Kinetics and thermodynamics of amyloid fibril assembly. *Acc Chem Res, 39*(9), 671-679. doi:10.1021/ar050069h

Wilcock, G. K., & Esiri, M. M. (1982). Plaques, tangles and dementia. A quantitative study. *J Neurol Sci, 56*(2-3), 343-356.

Willem, M., Garratt, A. N., Novak, B., Citron, M., Kaufmann, S., Rittger, A., . . . Haass, C. (2006). Control of peripheral nerve myelination by the beta-secretase BACE1. *Science, 314*(5799), 664-666. doi:10.1126/science.1132341

Williams, T. L., & Serpell, L. C. (2011). Membrane and surface interactions of Alzheimer's Abeta peptide--insights into the mechanism of cytotoxicity. *FEBS J, 278*(20), 3905-3917. doi:10.1111/j.1742-4658.2011.08228.x

Winey, M., Meehl, J. B., O'Toole, E. T., & Giddings, T. H., Jr. (2014). Conventional transmission electron microscopy. *Mol Biol Cell, 25*(3), 319-323. doi:10.1091/mbc.E12-12-0863

Wood, S. J., Maleeff, B., Hart, T., & Wetzel, R. (1996). Physical, morphological and functional differences between ph 5.8 and 7.4 aggregates of the Alzheimer's amyloid peptide Abeta. *J Mol Biol, 256*(5), 870-877. doi:10.1006/jmbi.1996.0133

Wu, C., Scott, J., & Shea, J. E. (2012). Binding of Congo red to amyloid protofibrils of the Alzheimer Abeta(9-40) peptide probed by molecular dynamics simulations. *Biophys J, 103*(3), 550-557. doi:10.1016/j.bpj.2012.07.008

Wu, F., & Yao, P. J. (2009). Clathrin-mediated endocytosis and Alzheimer's disease: an update. *Ageing Res Rev, 8*(3), 147-149. doi:10.1016/j.arr.2009.03.002

Wu, J. W., Hussaini, S. A., Bastille, I. M., Rodriguez, G. A., Mrejeru, A., Rilett, K., . . . Duff, K. E. (2016). Neuronal activity enhances tau propagation and tau pathology in vivo. *Nat Neurosci, 19*(8), 1085-1092. doi:10.1038/nn.4328

Wurth, C., Guimard, N. K., & Hecht, M. H. (2002). Mutations that reduce aggregation of the Alzheimer's Abeta42 peptide: an unbiased search for the sequence determinants of Abeta amyloidogenesis. *J Mol Biol, 319*(5), 1279-1290. doi:10.1016/S0022-2836(02)00399-6

Xue, C., Lin, T. Y., Chang, D., & Guo, Z. (2017). Thioflavin T as an amyloid dye: fibril quantification, optimal concentration and effect on aggregation. *R Soc Open Sci, 4*(1), 160696. doi:10.1098/rsos.160696

Xue, W. F., Homans, S. W., & Radford, S. E. (2008). Systematic analysis of nucleation-dependent polymerization reveals new insights into the mechanism of amyloid self-assembly. *Proc Natl Acad Sci U S A, 105*(26), 8926-8931. doi:10.1073/pnas.0711664105

Xue, W. F., Hellewell, A. L., Gosal, W. S., Homans, S. W., Hewitt, E. W., & Radford, S. E. (2009). Fibril fragmentation enhances amyloid cytotoxicity. *J Biol Chem, 284*(49), 34272-34282. doi:10.1074/jbc.M109.049809

Xue, Y., Lee, S., Wang, Y., & Ha, Y. (2011). Crystal structure of the E2 domain of amyloid precursor protein-like protein 1 in complex with sucrose octasulfate. *J Biol Chem, 286*(34), 29748-29757. doi:10.1074/jbc.M111.219659

Yamamoto, N., Matsubara, E., Maeda, S., Minagawa, H., Takashima, A., Maruyama, W., . . . Yanagisawa, K. (2007). A ganglioside-induced toxic soluble Abeta assembly. Its enhanced formation from Abeta bearing the Arctic mutation. *J Biol Chem, 282*(4), 2646-2655. doi:10.1074/jbc.M606202200

Yamin, G. (2009). NMDA receptor-dependent signaling pathways that underlie amyloid beta-protein disruption of LTP in the hippocampus. *J Neurosci Res, 87*(8), 1729-1736. doi:10.1002/jnr.21998

Yan, R. (2017). Physiological Functions of the beta-Site Amyloid Precursor Protein Cleaving Enzyme 1 and 2. *Front Mol Neurosci, 10*, 97. doi:10.3389/fnmol.2017.00097

Yan, S. D., Chen, X., Fu, J., Chen, M., Zhu, H., Roher, A., . . . Schmidt, A. M. (1996). RAGE and amyloid-beta peptide neurotoxicity in Alzheimer's disease. *Nature, 382*(6593), 685-691. doi:10.1038/382685a0

Yan, S. D., Stern, D., Kane, M. D., Kuo, Y. M., Lampert, H. C., & Roher, A. E. (1998). RAGE-Abeta interactions in the pathophysiology of Alzheimer's disease. *Restor Neurol Neurosci, 12*(2-3), 167-173.

Yan, S. D., Bierhaus, A., Nawroth, P. P., & Stern, D. M. (2009). RAGE and Alzheimer's disease: a progression factor for amyloid-beta-induced cellular perturbation? *J Alzheimers Dis, 16*(4), 833-843. doi:10.3233/JAD-2009-1030

Yatin, S. M., Varadarajan, S., Link, C. D., & Butterfield, D. A. (1999). In vitro and in vivo oxidative stress associated with Alzheimer's amyloid beta-peptide (1-42). *Neurobiol Aging, 20*(3), 325-330; discussion 339-342.

Yin, W., He, J., Yu, Z., & Wang, J. (2011). [Mechanism and application of molecular self-assembly in Sup35 prion domain of Saccharomyces cerevisiae]. *Sheng Wu Gong Cheng Xue Bao, 27*(10), 1401-1407.

Young, L. J., Kaminski Schierle, G. S., & Kaminski, C. F. (2017). Imaging Abeta(1-42) fibril elongation reveals strongly polarised growth and growth incompetent states. *Phys Chem Chem Phys, 19*(41), 27987-27996. doi:10.1039/c7cp03412a

Yu, C., Nwabuisi-Heath, E., Laxton, K., & Ladu, M. J. (2010). Endocytic pathways mediating oligomeric Abeta42 neurotoxicity. *Mol Neurodegener, 5*, 19. doi:10.1186/1750-1326-5-19

Yu, L., Edalji, R., Harlan, J. E., Holzman, T. F., Lopez, A. P., Labkovsky, B., . . . Olejniczak, E. T. (2009). Structural characterization of a soluble amyloid beta-peptide oligomer. *Biochemistry, 48*(9), 1870-1877. doi:10.1021/bi802046n

Yu, X., Zou, J., Ye, Z., Hammond, H., Chen, G., Tokunaga, A., . . . Cheng, L. (2008). Notch signaling activation in human embryonic stem cells is required for embryonic, but not trophoblastic, lineage commitment. *Cell Stem Cell, 2*(5), 461-471. doi:10.1016/j.stem.2008.03.001

Yu, X., & Zheng, J. (2011). Polymorphic structures of Alzheimer's beta-amyloid globulomers. *PLoS One, 6*(6), e20575. doi:10.1371/journal.pone.0020575

Yue, T., & Zhang, X. (2012). Cooperative effect in receptor-mediated endocytosis of multiple nanoparticles. *ACS Nano, 6*(4), 3196-3205. doi:10.1021/nn205125e

Yuyama, K., Yamamoto, N., & Yanagisawa, K. (2008). Accelerated release of exosome-associated GM1 ganglioside (GM1) by endocytic pathway abnormality: another putative pathway for GM1-induced amyloid fibril formation. *J Neurochem, 105*(1), 217-224. doi:10.1111/j.1471-4159.2007.05128.x

Zagorski, M. G., Yang, J., Shao, H., Ma, K., Zeng, H., & Hong, A. (1999). Methodological and chemical factors affecting amyloid beta peptide amyloidogenicity. *Methods Enzymol, 309*, 189-204.

Zhang, R., Hu, X., Khant, H., Ludtke, S. J., Chiu, W., Schmid, M. F., . . . Lee, J. M. (2009). Interprotofilament interactions between Alzheimer's Abeta1-42 peptides in amyloid fibrils revealed by cryoEM. *Proc Natl Acad Sci U S A, 106*(12), 4653-4658. doi:10.1073/pnas.0901085106

Zhang, S., Wang, Z., Cai, F., Zhang, M., Wu, Y., Zhang, J., & Song, W. (2017). BACE1 Cleavage Site Selection Critical for Amyloidogenesis and Alzheimer's Pathogenesis. *J Neurosci, 37*(29), 6915-6925. doi:10.1523/JNEUROSCI.0340-17.2017

Zhang, Z., Chen, H., Bai, H., & Lai, L. (2007). Molecular dynamics simulations on the oligomer-formation process of the GNNQQNY peptide from yeast prion protein Sup35. *Biophys J, 93*(5), 1484-1492. doi:10.1529/biophysj.106.100537

Zhao, X., & Yang, J. (2010). Amyloid-beta peptide is a substrate of the human 20S proteasome. *ACS Chem Neurosci, 1*(10), 655-660. doi:10.1021/cn100067e

Zheng, H., & Koo, E. H. (2011). Biology and pathophysiology of the amyloid precursor protein. *Mol Neurodegener, 6*(1), 27. doi:10.1186/1750-1326-6-27

Zheng, W., Schafer, N. P., & Wolynes, P. G. (2013). Frustration in the energy landscapes of multidomain protein misfolding. *Proc Natl Acad Sci U S A, 110*(5), 1680-1685. doi:10.1073/pnas.1222130110

Zheng, Y., Joo, H. S., Nair, V., Le, K. Y., & Otto, M. (2017). Do amyloid structures formed by Staphylococcus aureus phenol-soluble modulins have a biological function? *Int J Med Microbiol*. doi:10.1016/j.ijmm.2017.08.010

Zheng, Y. J., & Ornstein, R. L. (1996). A molecular dynamics study of the effect of carbon tetrachloride on enzyme structure and dynamics: subtilisin. *Protein Eng, 9*(6), 485-492.

Zoltowska, K. M., & Berezovska, O. (2017). Dynamic Nature of presenilin1/gamma-Secretase: Implication for Alzheimer's Disease Pathogenesis. *Mol Neurobiol*. doi:10.1007/s12035-017-0487-5